CHAPTER 5.
ELECTRON AND POSITRON SOURCES

5. ELECTRON AND POSITRON SOURCES

5.1 THE ELECTRON SOURCE

The electron source for the collider is required to provide two intense single bunches for each cycle of collider operation. One of these bunches is used to create the positrons for the next cycle of collider operation, while one provides the electrons to interact with the existing positrons in the same cycle of collider operation. Each of these bunches must result in 5×10^{10} electrons being captured and damped in the damping ring. Normally, longitudinally polarized electrons will be delivered by a photoemission electron gun. This polarization is transformed into transverse polarization (parallel to the damping ring magnetic field) in the linac-to-ring beamline, and back to longitudinal polarization for re-injection into the linac in the ring-to-linac beamline. Alternatively, unpolarized electrons may be delivered by a thermionic gun.

5.1.1 The Laser Gun for Polarized Electron Beams

This gun utilizes photoemission from a semiconductor cathode to produce a longitudinally polarized electron beam. The short optical pulses which cause the photoemission are chopped by a Pockels cell optical pulse chopper from a much longer optical pulse provided by a flashlamp pumped dye laser. The laser operates at a wavelength corresponding to the energy of the minimum direct bandgap of the semiconductor. The chopped optical pulses are circularly polarized by a pulsed Pockels cell optical retarder, and this circular polarization, responsible for the longitudinal polarization of the electrons, may be reversed randomly on a pulse-to-pulse basis, providing considerable reduction in potential polarization dependent systematic effects.

The semiconductor cathode is activated by exposure to monolayer quantities of cesium and oxygen. This activated surface requires a good UHV environment for long lifetime, typically 10^{-10} torr or better.

SLAC has considerable experience operating polarized electron guns of this type on the linac.[1] An electron gun suitable for use on the collider has been built and is operational in a laboratory setup. Considerable developmental work has been done to simplify the operational aspects of this gun. Current photocathodes of GaAs provide a maximum polarization of only 50%. A program is underway to develop alternate photocathodes to deliver much higher beam polarizations, with a goal of $\geq$ 90%. We anticipate that such photoemitters could be incorporated into the existing gun structure without significant change.

Figure 5.1.1.1

Overall Schematic of Photocathode Gun Showing Side View and Down-beam View

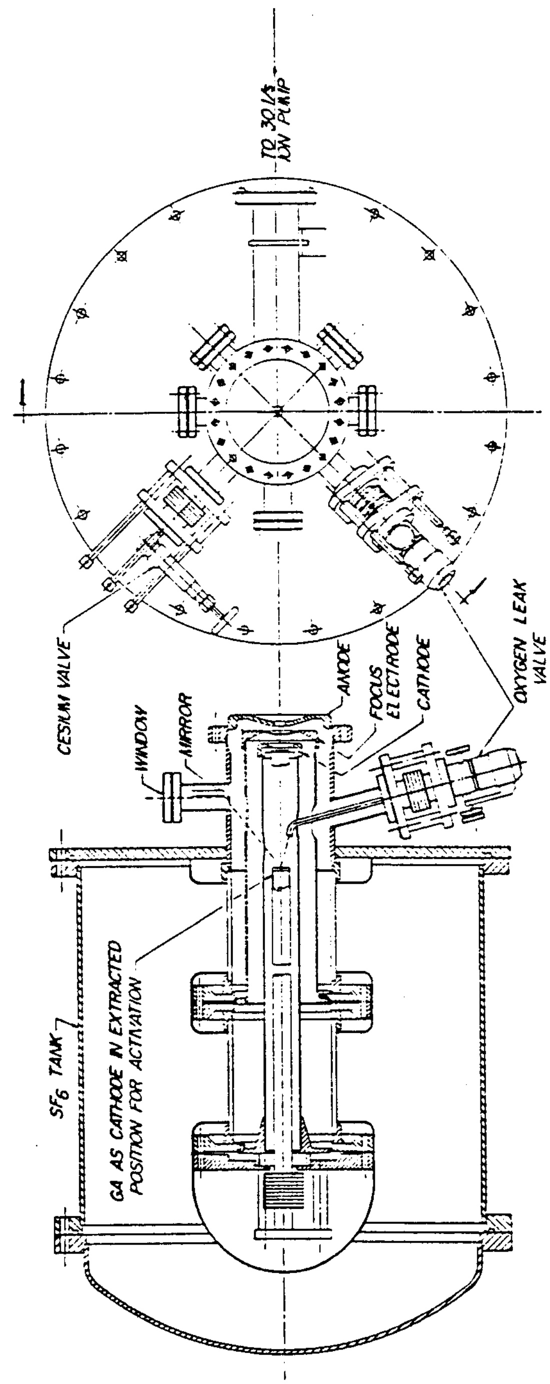

Table 5.1.1.1 Laser Gun Specifications	
Electrons (charge) per pulse	1×10^{11} (16 nC)
Repetition Rate	180 Hz
Pulse width	2.5 ns FWHM
Cathode voltage	200 kV
Anode voltage	Ground
Gun insulation	Low pressure SF_6
Cathode area (diameter)	1.8 cm^2 (1.5 cm)
Electron pulse time stability w.r.t. RF zero crossing	$\sigma = 10$ ps
Cathode material	Cesium activated GaAs
Cathode current	Space charge limited to 15 A peak
Pulse-to-pulse amplitude stability	$\sigma \leq 0.5\%$
Electron polarization	50%
Calculated invariant emittance area	$1 \times 10^{-3}\pi\, m_0 c$ cm

5.1.2 The Thermionic Gun[2]

While thermionic emission does not provide the polarized electrons, guns of this type are far less complex than photoemission guns, and thus could provide a high reliability backup gun for the polarized guns. A high current thermionic gun has been constructed, based upon a dispenser cathode–grid assembly developed by EIMAC for use in high power planar triodes. This gun has delivered 20 ampere pulses at 175 kV during tests with a 20 nsec pulser. Using an avalanche transistor pulser, the gun can deliver 8 amp pulses with a FWHM of 2 nsec. The calculated gun emittance is 3×10^{-3} πm_0c-cm. This gun has been in routine single pulse operation at 150 kV on the collider injector development project for over 18 months without any major difficulty. Recently the pulser was modified[3] to provide two single bunches per cycle.

Figure 5.1.2.1 Side View of Thermionic Gun

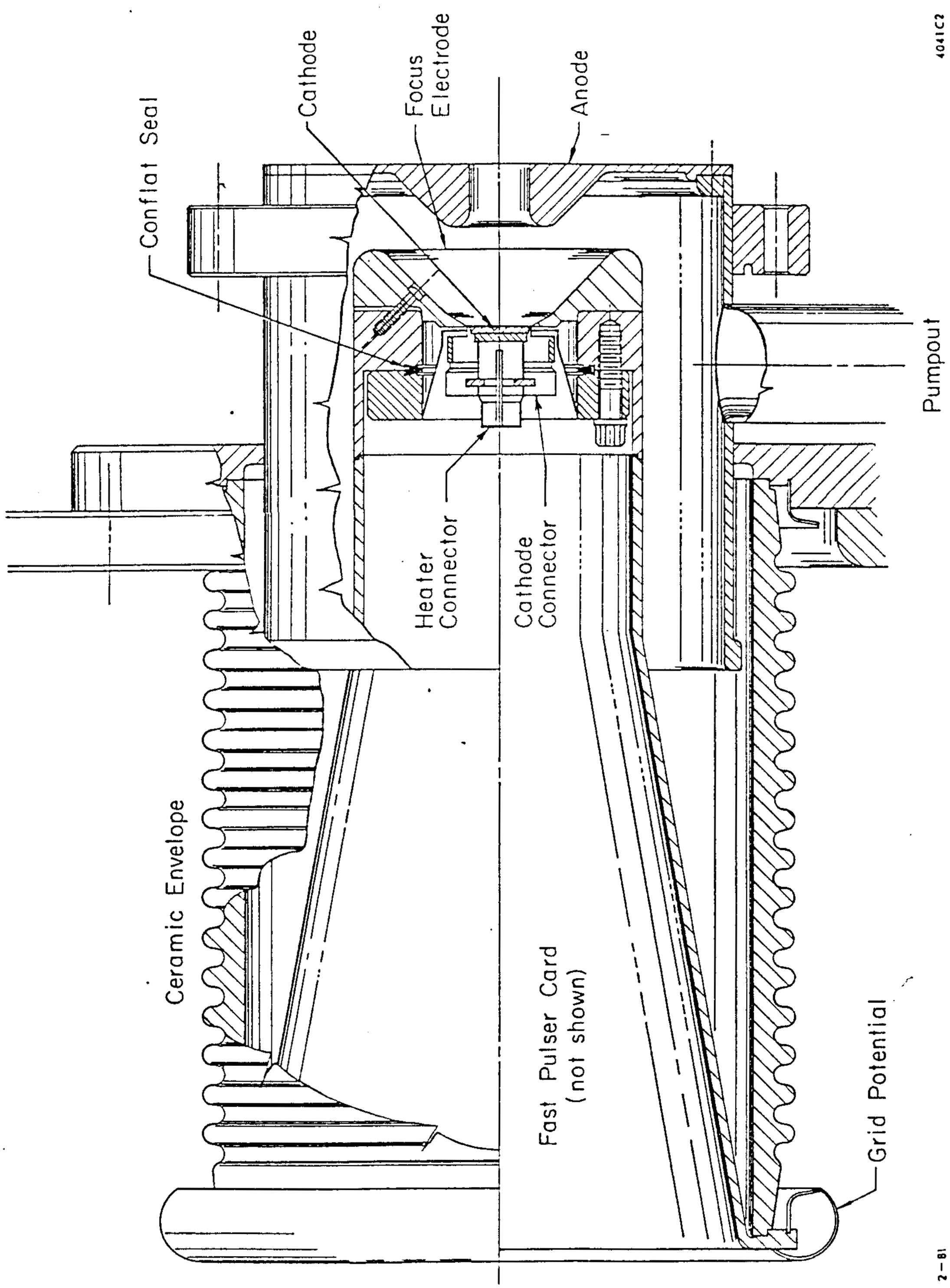

Table 5.1.2.1 Thermionic Gun Specifications	
Type	Triode with intercepting mesh control grid
Electrons per pulse (charge)	1×10^{11} (16 nC)
Repetition rate	360 Hz
Pulse width	2.5 ns FWHM
Cathode voltage	175 kV
Anode voltage	Ground
Gun insulation	Air
Cathode area (diameter)	2 cm^2 (1.6 cm)
Cathode-to-grid-spacing	150 μm
Grid pulse height	500 V
Electron pulse time stability w.r.t. RF zero crossing	$\sigma = 10$ ps
Cathode material	Dispenser type
Cathode current	Space charge limited to 20 A peak; Maximum of 9 A peak for 2.5 ns pulse
Pulse-to-pulse amplitude stability	$\sigma \leq 0.5\%$
Calculated invariant Emittance area	$3 \times 10^{-3} \pi m_0 c$ cm

5.1.3 The Buncher[4]

While it appears likely that photoemission cathodes could directly generate an electron pulse containing 5×10^{10} electrons lasting only about 100 psec, computer simulations indicate that the transient and space-charge phenomena associated with such a bunch are so severe that it might not be possible to bunch and capture 100% of this charge into a single S-band bunch in the linac. Since these problems decrease significantly as the electron bunch becomes longer, we have decided to employ a subharmonic buncher consisting of two cavities located between the electron gun and the S-band linac. In the present scheme, initial bunching is accomplished at the 16th subharmonic (178.5 MHz) of the linac RF frequency. This allows the electron pulse from the gun to be several nsec long, thus eliminating most of the ill effects associated with the higher charge density of the 100 psec bunch. The subharmonic buncher will deliver an electron pulse of approximately 150 psec length at 150 kV to a standard SLAC injector section. Subharmonic bunching with 178.5 MHz cavities has been used at SLAC to achieve single S-band bunches containing more than 1×10^{11} electrons.

Figure 5.1.3.1

Schematic of Existing 178.5 MHz Subharmonic Buncher System

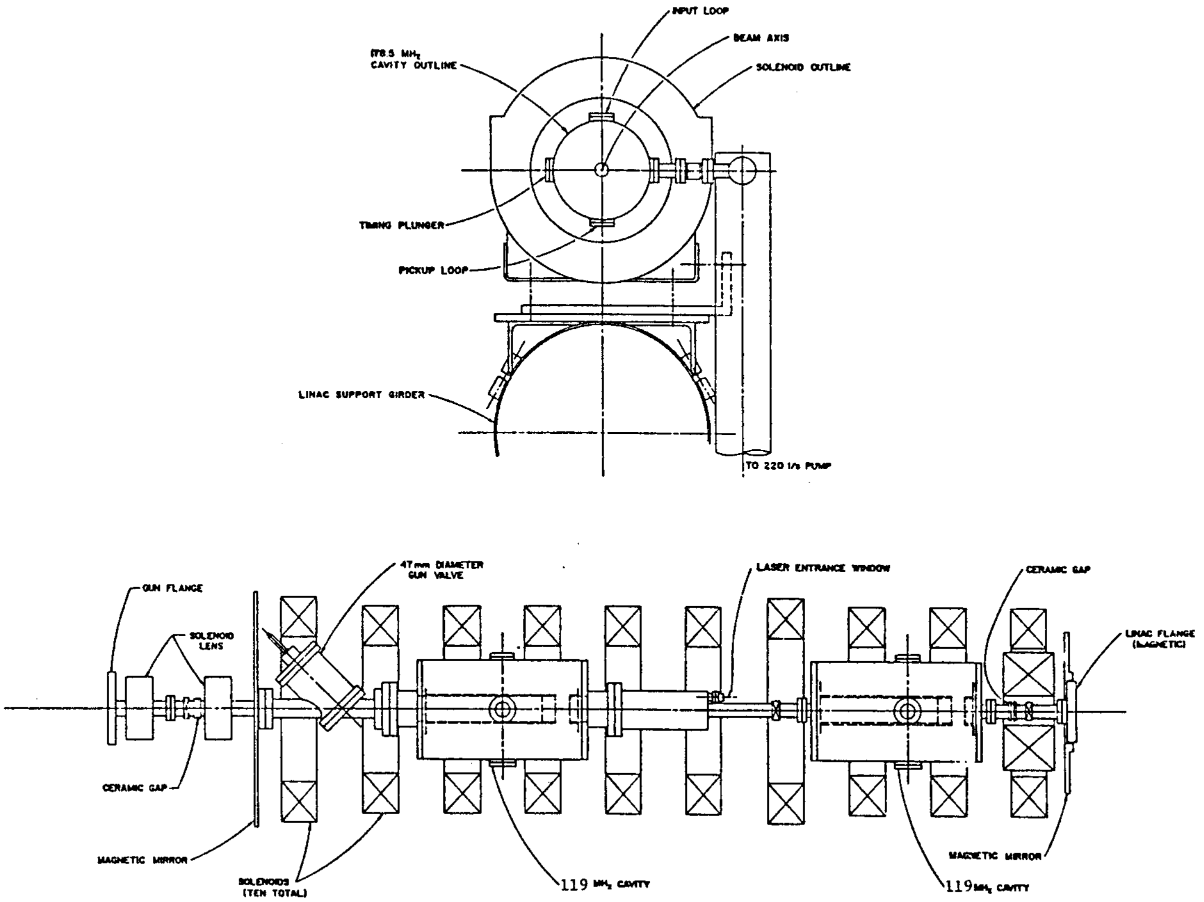

5.1.4 The Injector[5]

The bunch from the subharmonic bunching section enters a standard SLAC injector section. This section is composed of a standard 3-meter accelerator section with an attached 10-cm traveling-wave buncher. At the output of this section, the beam has a 30-psec bunch length and an energy of about 50 MeV. The beam then enters an achromatic bending system which can be used to alter the longitudinal bunch shape. Further acceleration will then attain the energy spectrum necessary for damping ring injection. Solenoidal focusing is used along the entire length of the subharmonic buncher and the injector section. The cathode itself will be in a magnetic-field-free region in order to avoid emittance degradation. For injection into Section 1-2 along with the positrons, the electron beam is accelerated to about 200 MeV by four conventional accelerator sections interspersed with instrumentation. A quadrupole F0D0 array with a β of four m beginning at the injector accelerator section is used to focus this beam.

Table 5.1.4.1 Specifications for New Injector	
Assumptions concerning gun beam	
Peak current	15 A
Pulse shape	Gaussian
Pulse width	$\sigma = 1.0$ ns
Energy	200 keV
$\Delta E/E$	$\pm0.2\%$ or less
Emittance area	$5 \times 10^{-3}\pi\ m_0c$-cm or less
Cathode area	1.8 cm^2
Repetition rate	up to 180 pps
Gun lenses	
Focal length	11.5 cm
Peak field	586 gauss
Sub-harmonic buncher	
Frequency	178.5 MHz
Type	re-entrant cylindrical cavity
Gap length	3.8 cm
Bore	5 cm
Q_L	4×10^3
Shunt impedance	Rs$-V^2/2P = 2.2M\Omega$
Pulse length	30 μs
Drive power (typical)	2 kW
Gap voltage	60 kV
Drift distances	1 m and 40 cm
Solenoid field	200 to 600 Gauss
Matching solenoid field	$\sim$ 1 kG
S-band Buncher	
Type	Travelling wave DLWG
Length	10.5 cm
Field strength	20 kV/cm
Buncher solenoid field	1.2 kG
Accelerator Section	
Gap to buncher	2 cm
Length of accelerator section	3 m
Accelerating field	150 keV/cm
Solenoid field	1 to 2 kG
Beam injected into sector 1-2	
Current	5×10^{10} electrons/bunch (8 nCoulomb/bunch)
Bunch length (σ_z)	2 mm
Energy	200 MeV (at BAS I)
Emittance area	$3 \times 10^{-2}\pi\ m_0c$ cm

5.1.5 State of Development[6]

A complete single-bunch injection system composed of the thermionic gun (Fig. 5.1.5.1), two subharmonic bunchers operating at 178.5 MHz (Fig. 5.1.5.2), the standard injection section, and the instrument section, has been in operation at the front end of the linac since spring, 1981. This injection system meets the SLC specifications for intensity and emittance.

Figure 5.1.5.1 The Thermionic Gun

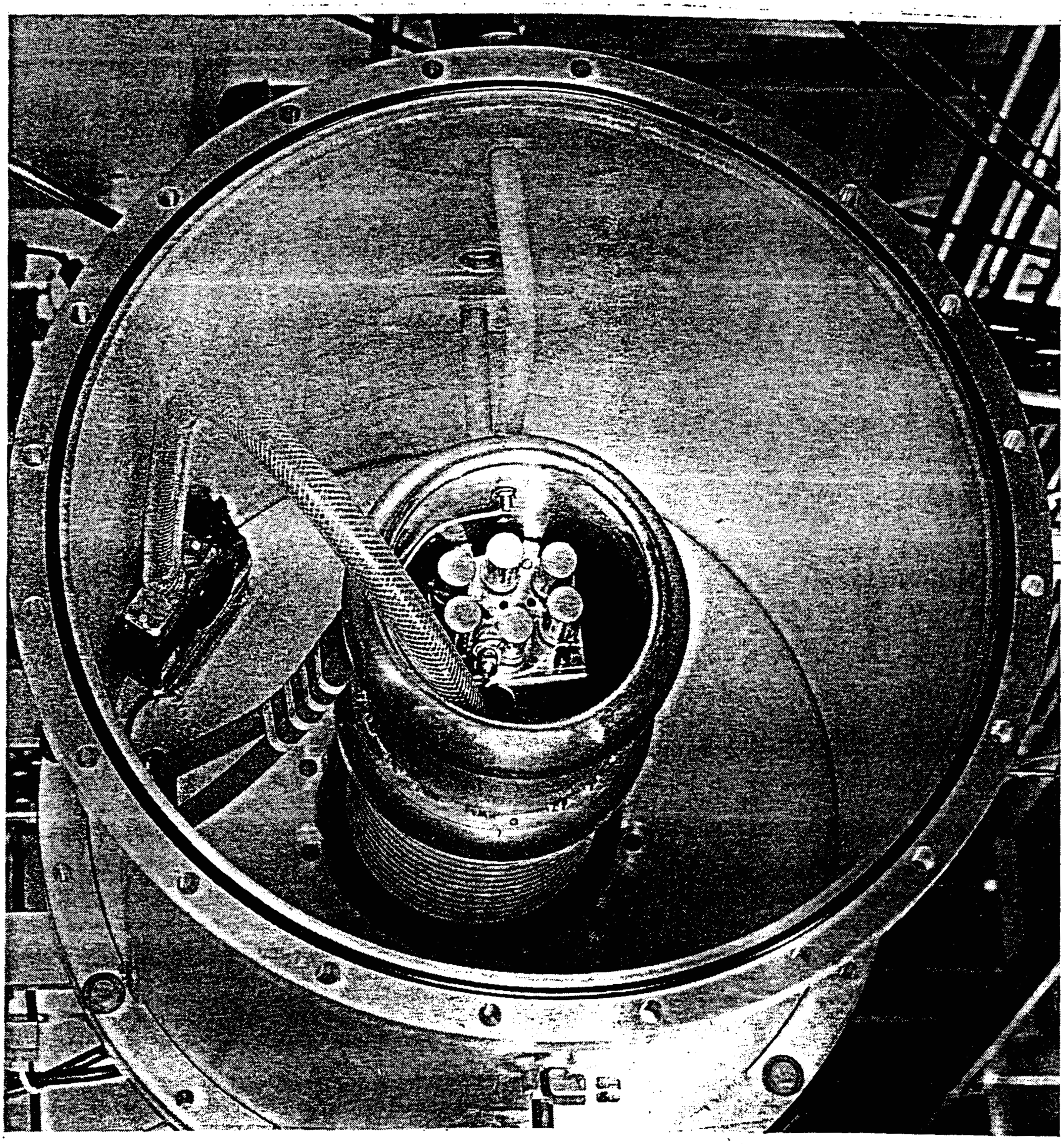

Figure 5.1.5.2: Subharmonic Buncher

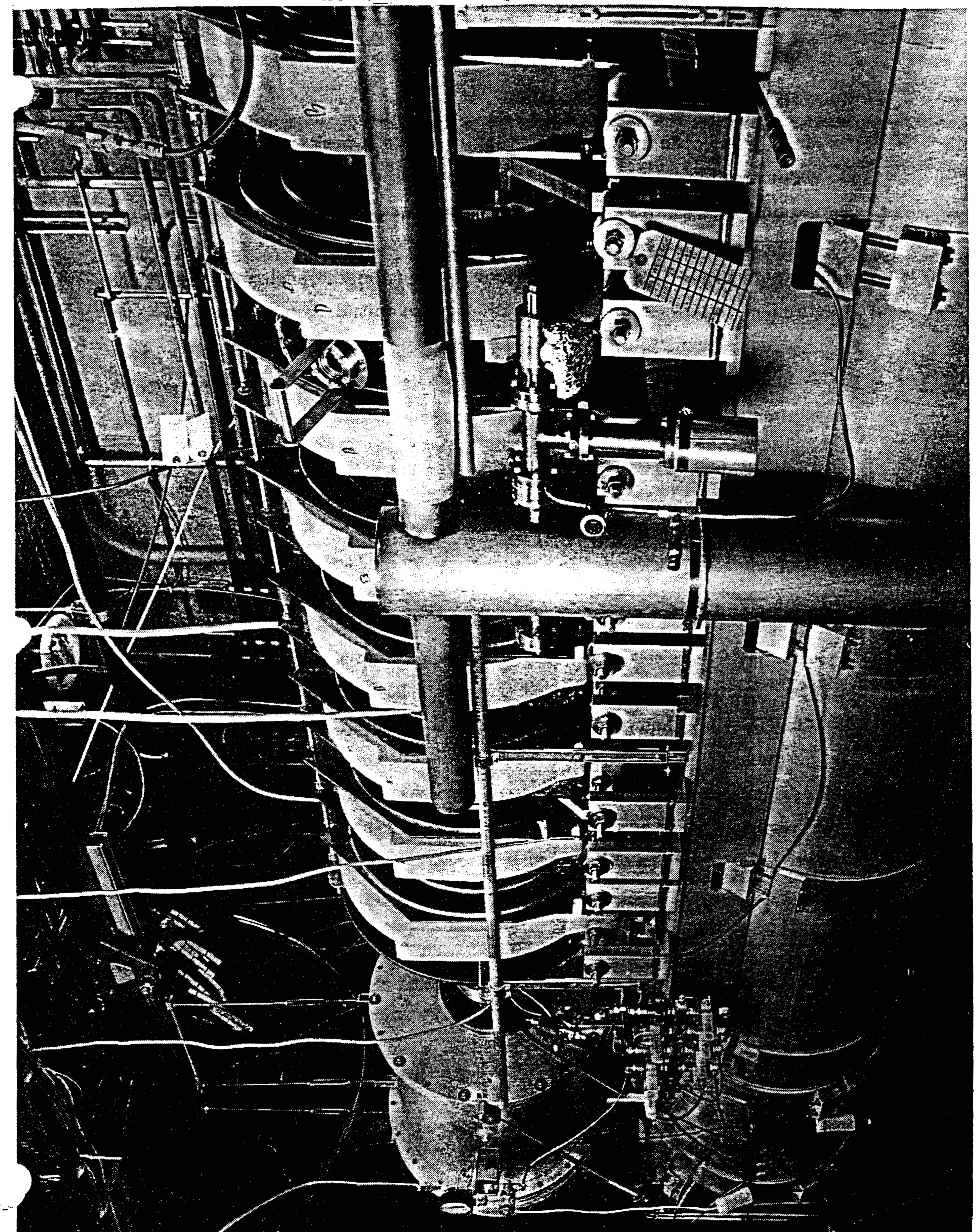

5.2 THE POSITRON SOURCE

In order to optimize the collider luminosity, the positron source is required to produce sufficient numbers of positrons to saturate the intensity capability of the linac. Since the intensity of the scavenger pulse is subject to the same linac capability, the positron system is required to deliver at least one positron into the damping ring for each electron incident on the positron target. This requirement implies more than an order-of-magnitude improvement over the existing source which, at 7 GeV incident electron energy, normally has a yield of 7% but, under optimum conditions, has been tuned to 15%. The needed improvement will result from (a) increasing the incident electron energy to 33 GeV, and (b) using a collection system with a larger admittance.

The overall positron production system is shown in Figs. 5.2.0.1–3. and component parameters are summarized in Table 5.2.0.1. A single bunch of electrons (the scavenger pulse) is extracted from the linac at the 2/3 point by means of a fast kicker magnet and a pair of septum magnets. The extracted electron beam is transported through a 24° bend and into the positron vault where it is focused to the desired beam spot size at the target. Positrons are collected and accelerated up to 200 MeV in a 35-ft length of linac accelerator section. They are then transported back to the beginning of the linac for further acceleration to 1.2 GeV, whereupon they are sent to the damping ring. Achieving the desired number of positrons depends on the efficiency of the collection and transport systems. The optimization of the yield is constrained by the minimum allowable beam size as determined by the target strength.

Table 5.2.0.1 Positron Source Specifications

EXTRACTION	
Electron Scavenger Pulse	
Energy	33 GeV
Intensity	5.0×10^{10} e^-/pulse
Size (1 σ)	0.6 mm
Pulse energy	264 Joules/pulse
Pulse rate	180 Hz
Power	47 kW
Target	
Material	90% Ta – 10% W
Length	6 radiation lengths = 24 mm
Energy deposited in target	53 J/pulse
Pulse temperature rise	380°C
Max. pulse temp.	580°C
Max. compressive stress	32,000 psi
Power deposition	9 kW
Steady-state temp.	200°C
Positron Beam at Target	
Energy range	2 – 20 MeV
Transverse emittance (Invariant)	2 mm × 2.5 MeV/c = 0.01 m-radians
Yield (e^+/e^- in.)	2.5
Beam Properties at End of Sector 1	
Energy	1.21 GeV
Energy spread	2% full
Transverse emittance	4.2×10^{-6} m-radians

Figure 5.2.0.1

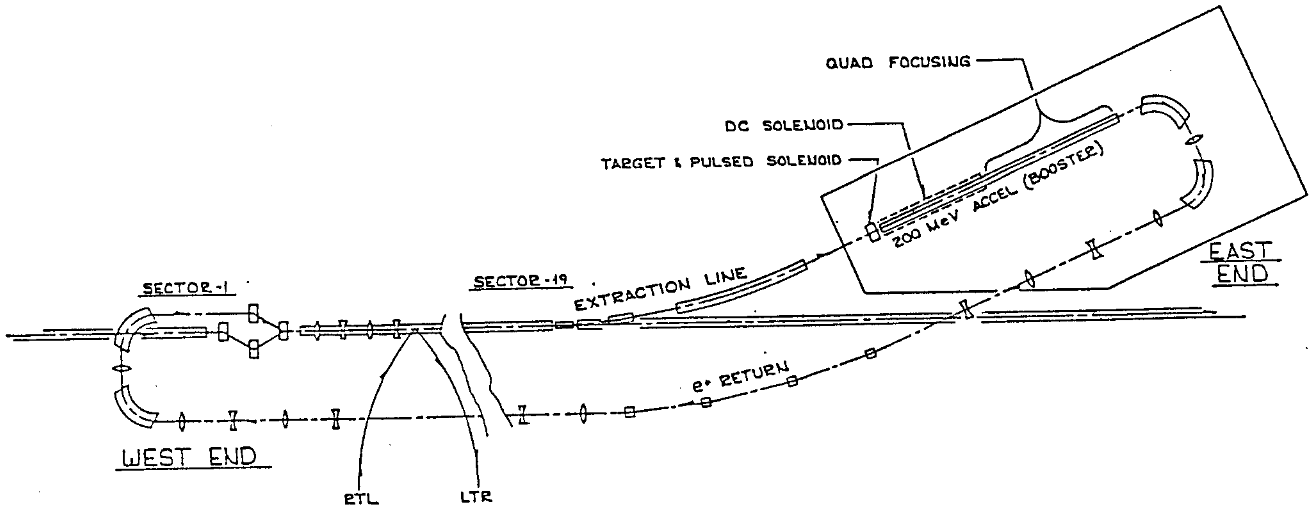
QUAD FOCUSING
DC SOLENOID
TARGET & PULSED SOLENOID
200 MeV ACCEL (BOOSTER)
EAST END
SECTOR-1
SECTOR-19
EXTRACTION LINE
e+ RETURN
WEST END
RTL
LTR

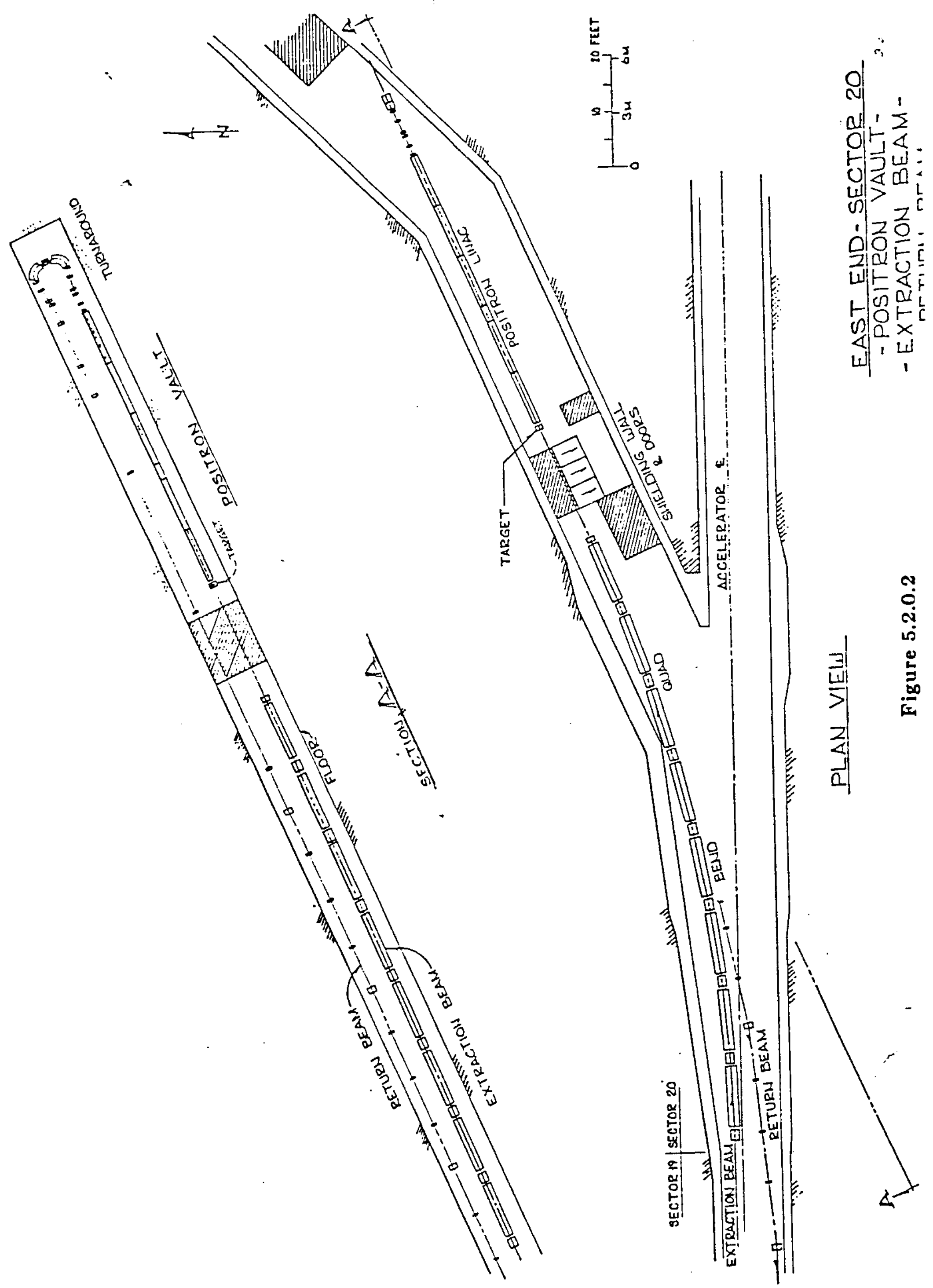
EAST END- SECTOR 20
- POSITRON VAULT -
- EXTRACTION BEAM -
PLAN VIEW
SECTION A-A
POSITRON VAULT
TURNAROUND
TARGET
FLOOR
RETURN BEAM
EXTRACTION BEAM
POSITRON LINAC
SHIELDING WALL & DOORS
ACCELERATOR ℄
QUAD
BEND
SECTOR 19
SECTOR 20
0
10
20 FEET
3M
6M

Figure 5.2.0.2

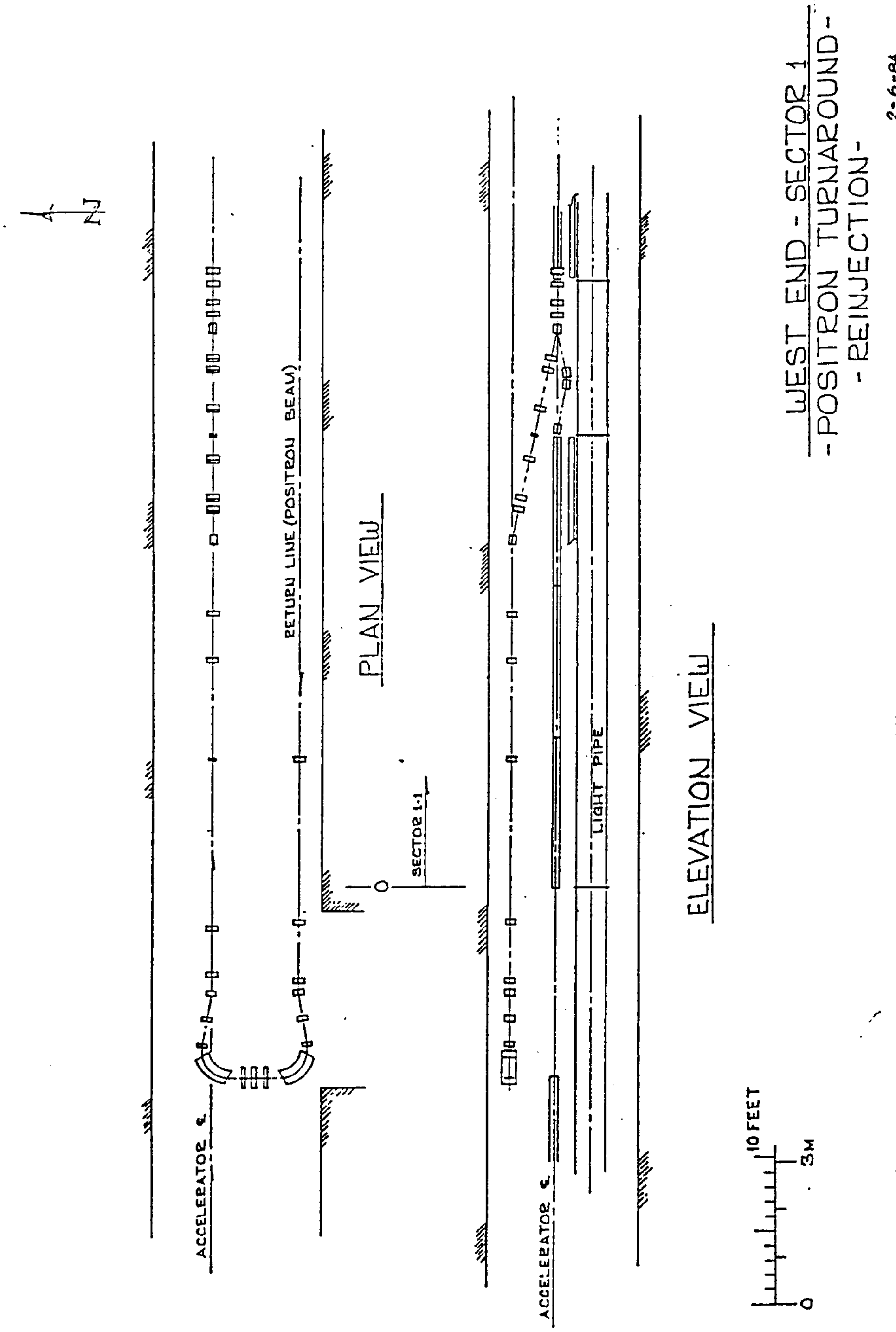
WEST END - SECTOR 1
- POSITRON TURNAROUND -
- REINJECTION -
2-6-84
PLAN VIEW
RETURN LINE (POSITRON BEAM)
SECTOR 1-1
ACCELERATOR ℄
ELEVATION VIEW
LIGHT PIPE
ACCELERATOR ℄
10 FEET
3M
0
N

Figure 5.2.0.3

5.2.1. Yield Calculations

It is important to determine where gains in positron yield can be made and what the limits are due to the nature of the electromagnetic cascade. Yields have been calculated for various beam energies and target materials using the EGS computer program,[7] and some of the results are shown in Fig. 5.2.1.1. The following conclusions have been drawn from these studies: (a) Materials with large atomic number are more efficient. For example, tungsten gives twice the yield of copper under the same conditions at their shower maxima. (b) Denser materials localize the shower to a smaller region. This results in a smaller emittance and hence better collection efficiency, but it also produces higher physical stress and pulse temperature rise. (c) Positrons are produced preferentially in the 2-20 MeV range. (d) In dense materials, the positrons come from a small spot, typically 0.5 mm radius, but with large angles, typically $\pm 20°$. (e) The yield is nearly proportional to the incident electron energy. (f) The number of positrons produced is more than sufficient, provided they can be captured and accelerated as desired. Using the parameters for the collection optics of the existing SLAC source, we calculate a yield of 15%, in good agreement with the measured yield. The intended factor of 3 increase in admittance in each transverse plane of the collecting optics, and the higher incident electron energy, result in a total calculated yield of 2.5 e^+/incident e^-.

Figure 5.2.1.1

Positron yield vs depth. The longitudinal distribution of positrons in a tungsten target per incident 33 GeV electron is shown for maximum positron energies of 5, 10, 20, 50 and 100 MeV.

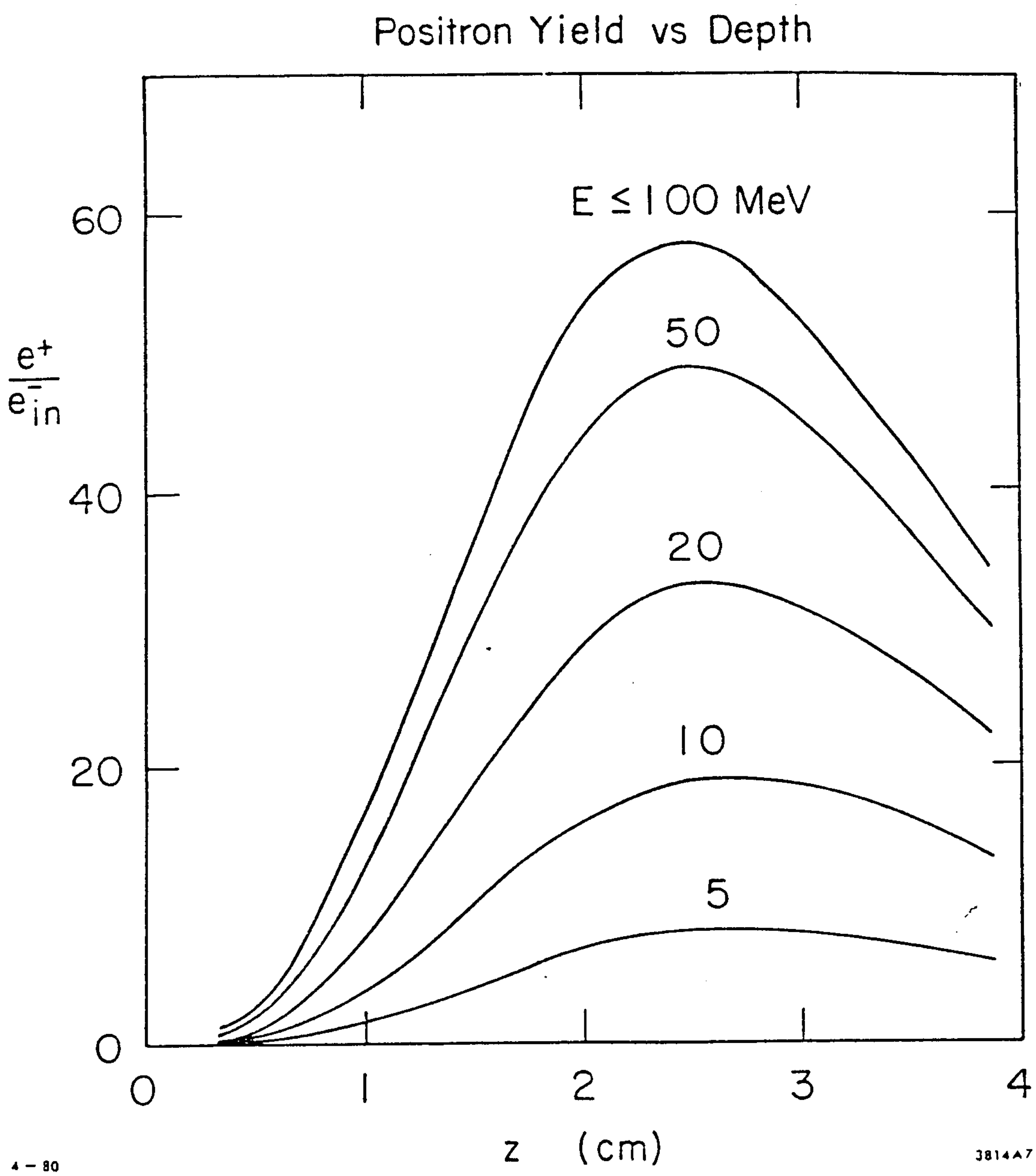

Figure 5.2.1.2

A schematic representation of positron source

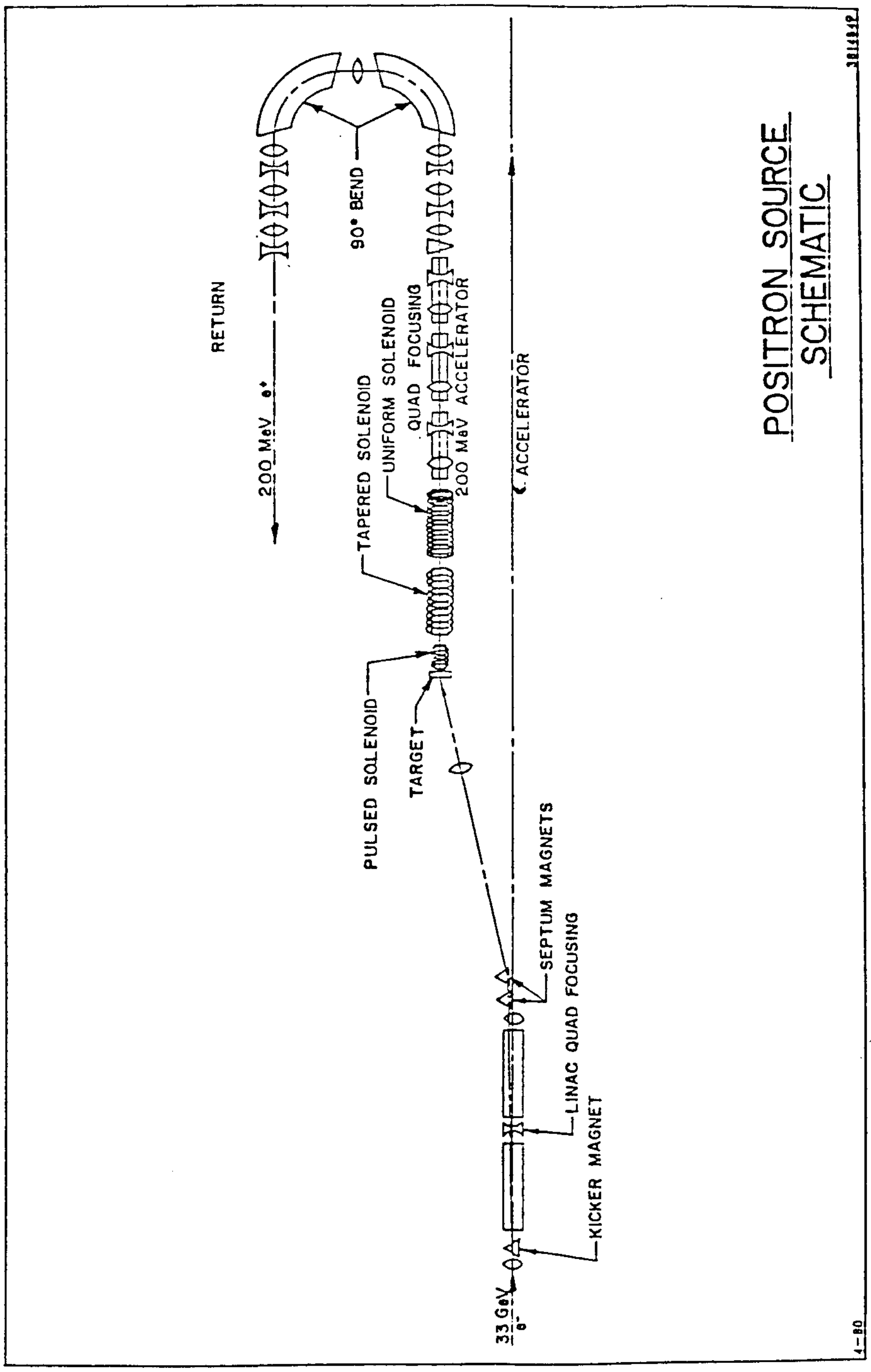

5.2.2 Target

Beam tests indicated that a target composed of either W-26Re (tungsten – 26% rhenium) or Ta-10W (tantalum - 10% tungsten) material would be suitable for our application. Both materials were analyzed on an engineering basis using their basic material properties and how these would affect pulse temperature rise, heat transfer, and thermal stress. The stress was compared to the material's tensile strength and fatigue strength. A slight advantage for Ta-10W over W-26Re was found. In as much as Ta-10W is also more readily available, less expensive and easier to work with, it is the obvious material of choice. Ta-10W material properties are shown in Table 5.2.2.1.

Calculations indicate that the single pulse temperature rise will be 380°C for a 0.6 mm incident beam radius (1.3 mm at shower peak). This, when added to the expected steady state temperature, results in a peak temperature of 580°C. The resulting stress from each thermal pulse will be $\approx$ 32,000 psi which is well below the expected yield strength of 60,000 psi. Fatigue characteristics for pure tantalum indicate an infinite number of cycles at 34000 psi. To avoid interaction between adjacent pulses and the resulting compounding of stress, the target will be rotated, thus distributing the power deposited over a larger area. Figure 5.2.2.2 shows the prototype target assembly. The target wheel, inside a vacuum chamber, is spun at about 2 Hz to distribute the power. The rotating motion is attained utilizing a commercially available feedthrough which uses a ferromagnetic fluid to seal the drive shaft. The target is cooled by water passages in the drive shaft.

Table 5.2.2.1	
TARGET MATERIAL PROPERTIES	
TANTALUM - 10% TUNGSTEN	
Atomic Number	73/74
Density, gm/cm^3	16.9
Specific Heat, cal/gm°C	0.035
Radiation Length, gm/cm^2	6.814
Thermal Conductivity cal/s-cm-°C	0.185
Tensile Strength, lb/in^2	71000
Melt Temperature, °C	3035

Figure 5.2.2.1

Positron target energy deposition. The radial distribution of energy deposition from an electromagnetic shower cascade is shown at 6 radiation lengths in tungsten for 33 GeV incident electrons. The left-hand scale is the energy density normalized to the incident beam energy. The right-hand scale shows the pulse temperature rise for 3.7×10^{10} incident electrons, corresponding to 194 Joules of beam energy. The histogram is the Monte Carlo calculation for a point incident beam. The curves are for Gaussian incident beam with $\sigma = 0.4$ and 0.8 mm.

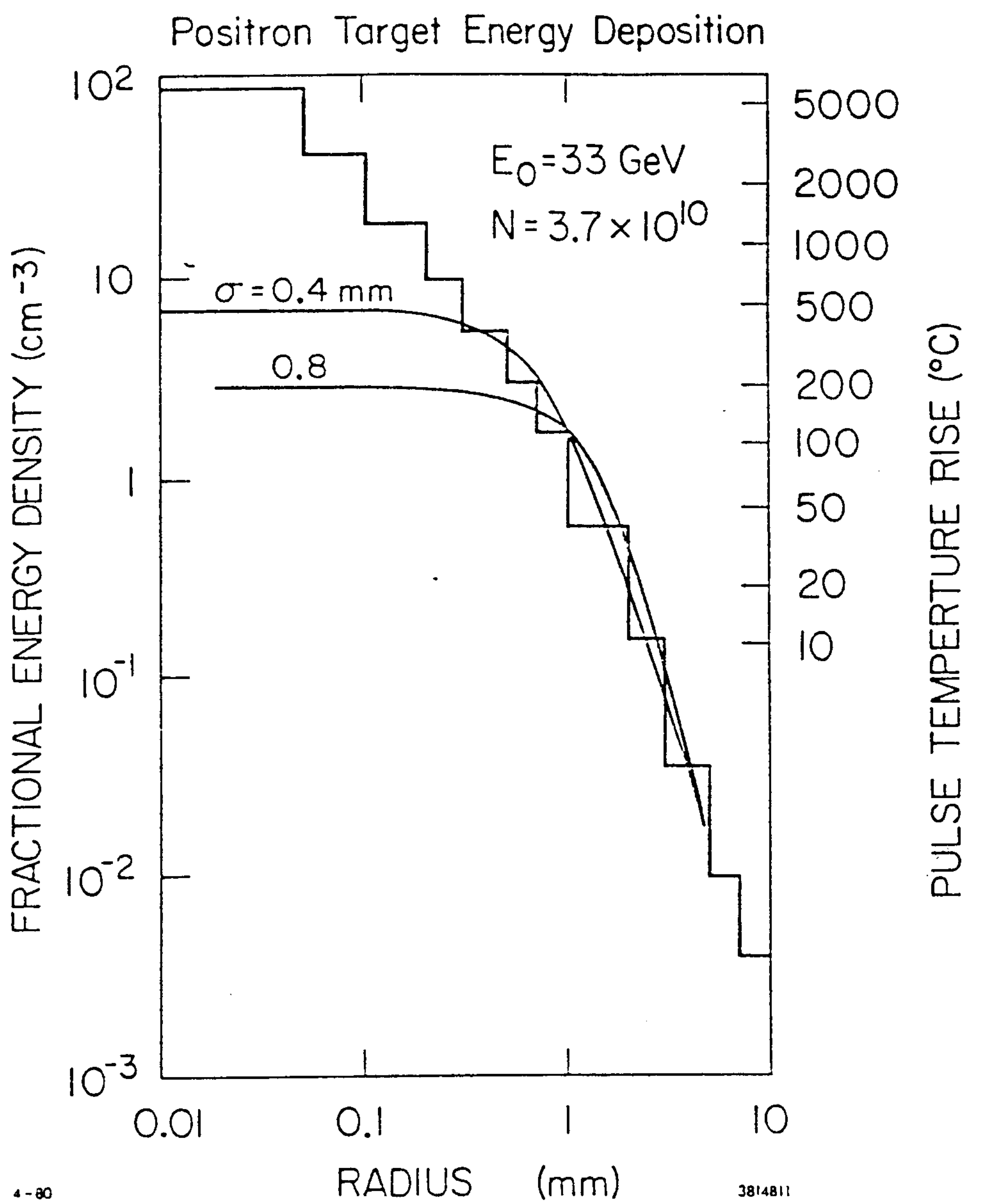

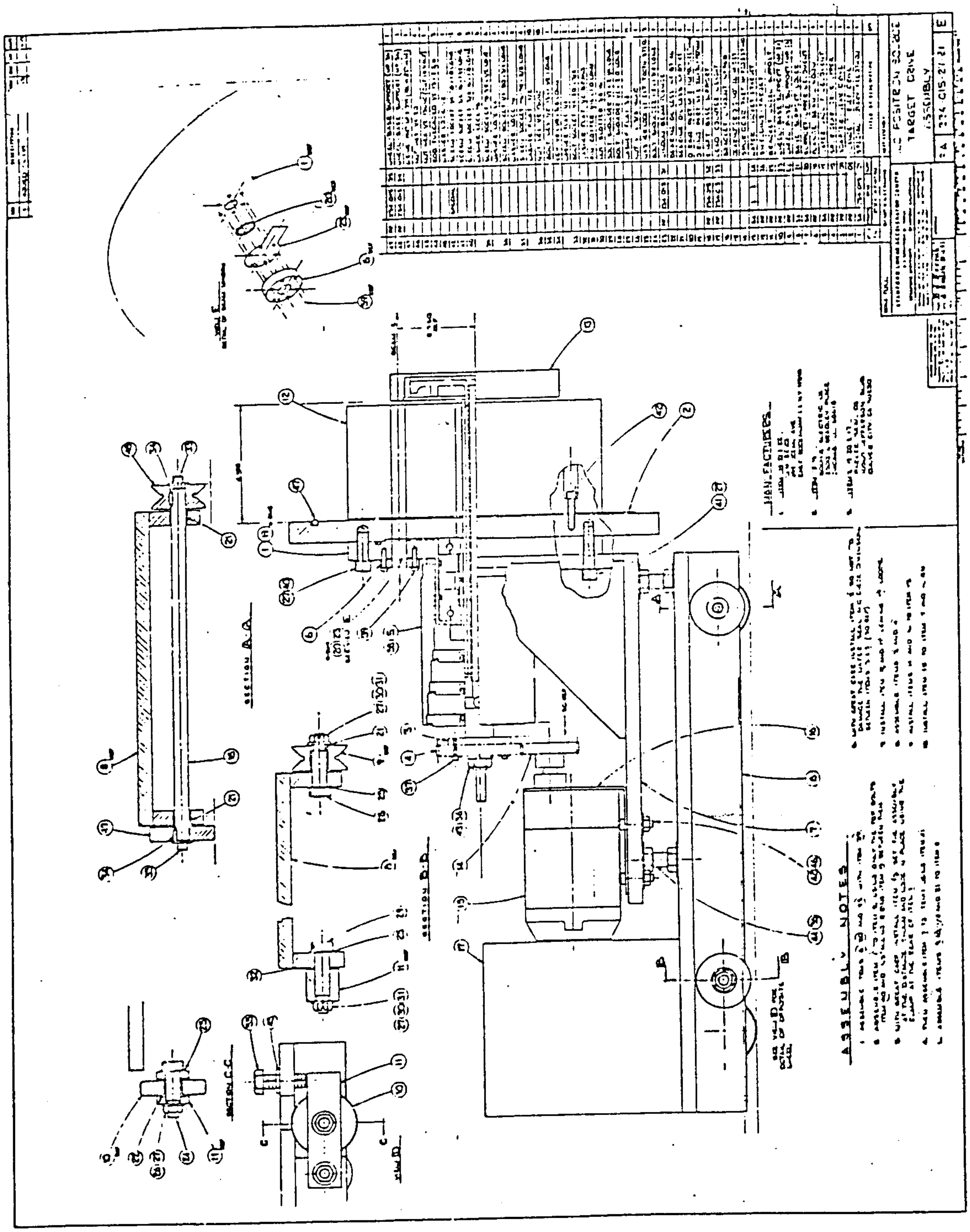
SECTION A-A
SECTION B-B
SECTION C-C
ASSEMBLY NOTES
TARGET DRIVE
ASSEMBLY

Figure 5.2.2.2

5.2.3 Transverse and Longitudinal Acceptance

The positron beam emerging from the target will enter a focusing solenoid system. The goal is to transform a 2 mm $\times$ 2.5 MeV $\sigma_x \times \sigma_{p_x}$ transverse emittance into a 8 mm $\times$ 0.6 MeV emittance, which corresponds to the accelerator aperture with a superimposed 5 kG solenoidal field. This is accomplished with a pseudo-adiabatically changing solenoidal field where the initial-to-final field ratio is the square of the radii ratio.[8] Thus a 80 kG initial field is desired. We believe fields approaching this can be achieved with a pulsed magnetic field utilizing a flux concentrator.[9] The flux concentrator can conveniently be made to produce the desired field taper; it produces field only where needed for the particle orbits, and provides to some extent, a correctly shaped collimator to stop unwanted shower particles.

The positrons emerging from the target have a longitudinal spatial extent which is nearly identical to the extent of the incident electron bunch, which is roughly 2 mm long. The emergent positrons have a large spread in energy from roughly 2 to 20 MeV with most concentrated at low energies. At the lower energies the positrons are sufficiently non-relativistic that they slip in phase, so that after the positrons have been accelerated in the booster to about 200 MeV there is a distinct energy-phase angle correlation, with the positrons that emerged from the target with low energies lagging in phase. Additional phase slip occurs for positrons that leave the target with non-zero transverse momentum because the resulting helical motion has a longer path length than straight motion down the axis.

Two design considerations for the positron source have been incorporated to minimize the phase slip. The first is to minimize drift regions before acceleration and the second is to accelerate initially with a high field accelerator section. A 1.5 m accelerator section with acceleration at 50 MeV/m will be used.

The positron capture efficiency has been calculated by ray tracing positrons through a target solenoidal field of 10 kG, the pulsed solenoidal field "flux concentrator" magnet, and into a solenoid of 5 kG axial field enclosing the RF accelerating cavity. Positrons were taken from the output of EGS for an incident 33 GeV electron beam having a nominal beam radius of 0.6 mm standard deviation both vertically and horizontally. Figure 5.2.3.1(a) shows the momentum spectrum $(1/N_{e-})\, dN_{e+}/dp$ of positrons produced where N_{e-} is the number of electrons incident on the target, and N_{e+} is the number of positrons produced. Because of bandwidth limitation in the later transport system, only positrons below 20 MeV/c momentum are considered; the integral of this plot is 31 e^+ per incident e^-. Figure 5.2.3.1(b) shows the momentum spectrum of positrons accepted by the geometrical aperture of 18 mm diameter; the integral of this spectrum is 5.5 e^+/e^-. Figure 5.2.3.2 shows the distribution $(1/N_{e-})dN_{e+}/dp_t$ where p_t is the momentum transverse to the nominal beam direction at the exit of the target.The curves show the yield for all positrons and positrons accepted geometrically. The primary loss at high p_t is due to the limited transverse acceptance.

The effect of the phase slip is illustrated in Figure 5.2.3.3 where the geometrically accepted positrons have their final momentum plotted against the phase lag Δt, which is the difference between the time a positron reaches the end of the accelerator section and that of a relativistic positron with straight motion down the axis. The momentum acceptance of the damping ring (2%) will limit Δt to less than 22 ps. Wake fields or beam loading may further reduce Δt. For the present study, we have assumed a total width of $\Delta t = 15$ ps which corresponds to the positrons in the first three columns of Fig. 5.2.3.3. This additional requirement reduces the positron efficiency. The in-phase positrons within $\Delta t = 15$ ps are shown in Figure 5.2.3.1 and 5.2.3.2. The integral of this system is 2.5 e^+ per incident e^-.

Many studies[10] have been made varying magnetic field, drift spaces, and accelerating fields to other values which design and operating criteria may require. For these studies the acceptance for in-phase positrons varies between 2 and 3.4 positrons per incident electron. These studies do not take into account effects due to space charge and wake fields. Longitudinal wake fields in the 1.5 m, section have been estimated[11] to cause 2 MeV lower energy of the tail of the positron bunch than at the head. Transverse wakes are on the order of 0.1 MeV/c per mm offset of the bunch centroid.

This scheme does not use deceleration followed by acceleration which is known to lead to a more compact $E_f - \psi_f$ distribution in phase space and to the capture of lower E_i particles.[11] In the deceleration mode many of the particles spend some time in the booster accelerator at low energies where they are more susceptible to the adverse effects of space charge and wake field forces. More detailed calculations are needed to identify an optimum capture strategy. Eventually the optimum operation will be based on experimental tests. We will try to make the hardware compatible with operation in higher acceleration or deceleration mode.

Figure 5.2.3.1

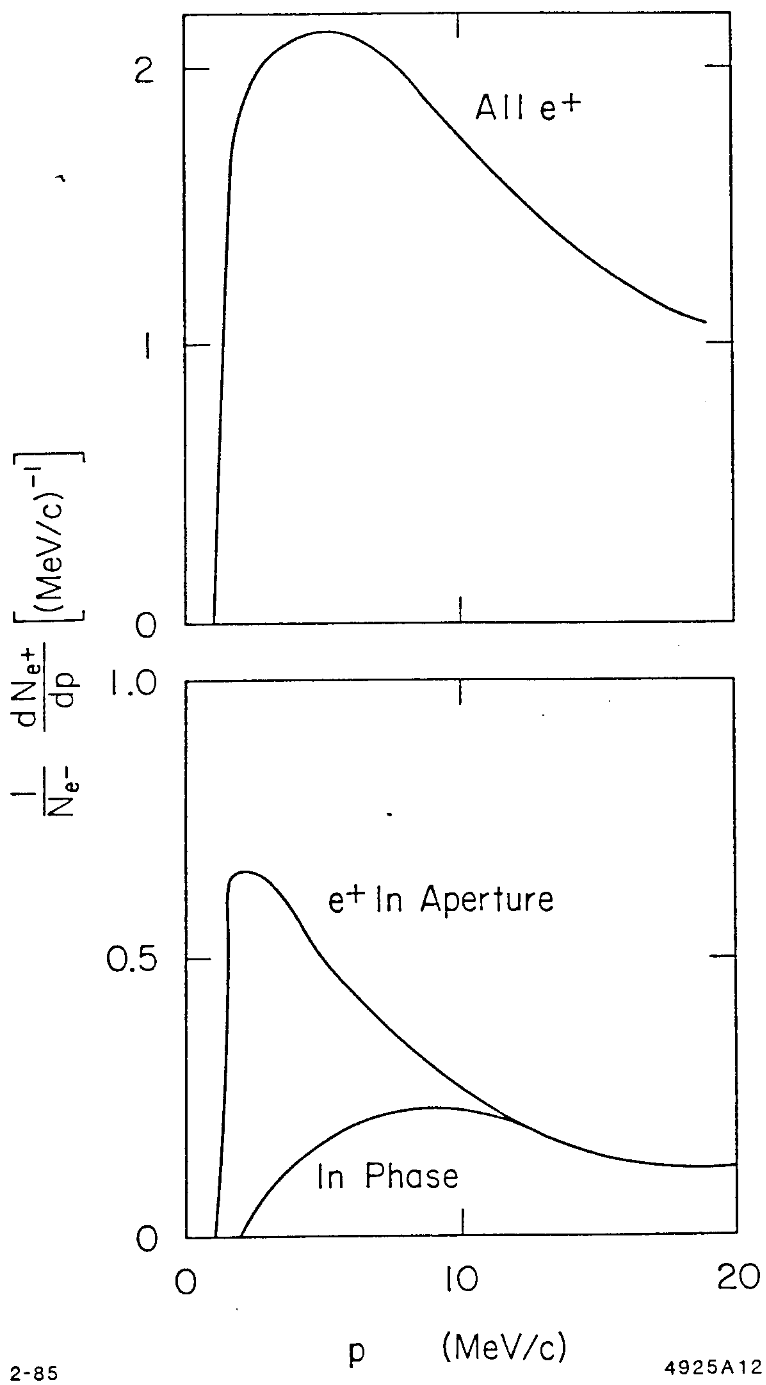
2
All e+
1
0
1.0
e+ In Aperture
0.5
In Phase
0
0
10
20
p (MeV/c)
2-85
4925A12

Figure 5.2.3.2

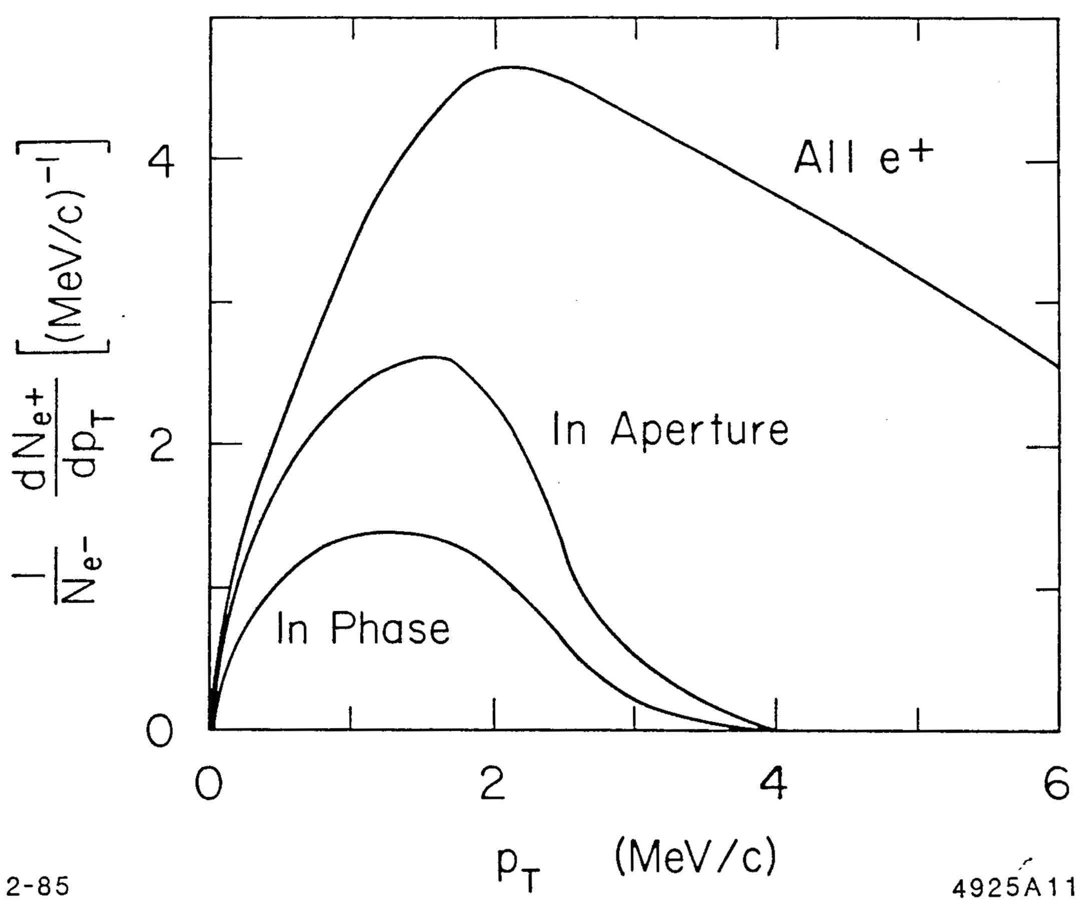

All e+
In Aperture
In Phase
0
2
4
6
0
2
4
$\frac{1}{N_{e^-}} \frac{dN_{e^+}}{dp_T} \left[(MeV/c)^{-1}\right]$
p_T (MeV/c)
2-85
4925A11

Figure 5.2.3.3

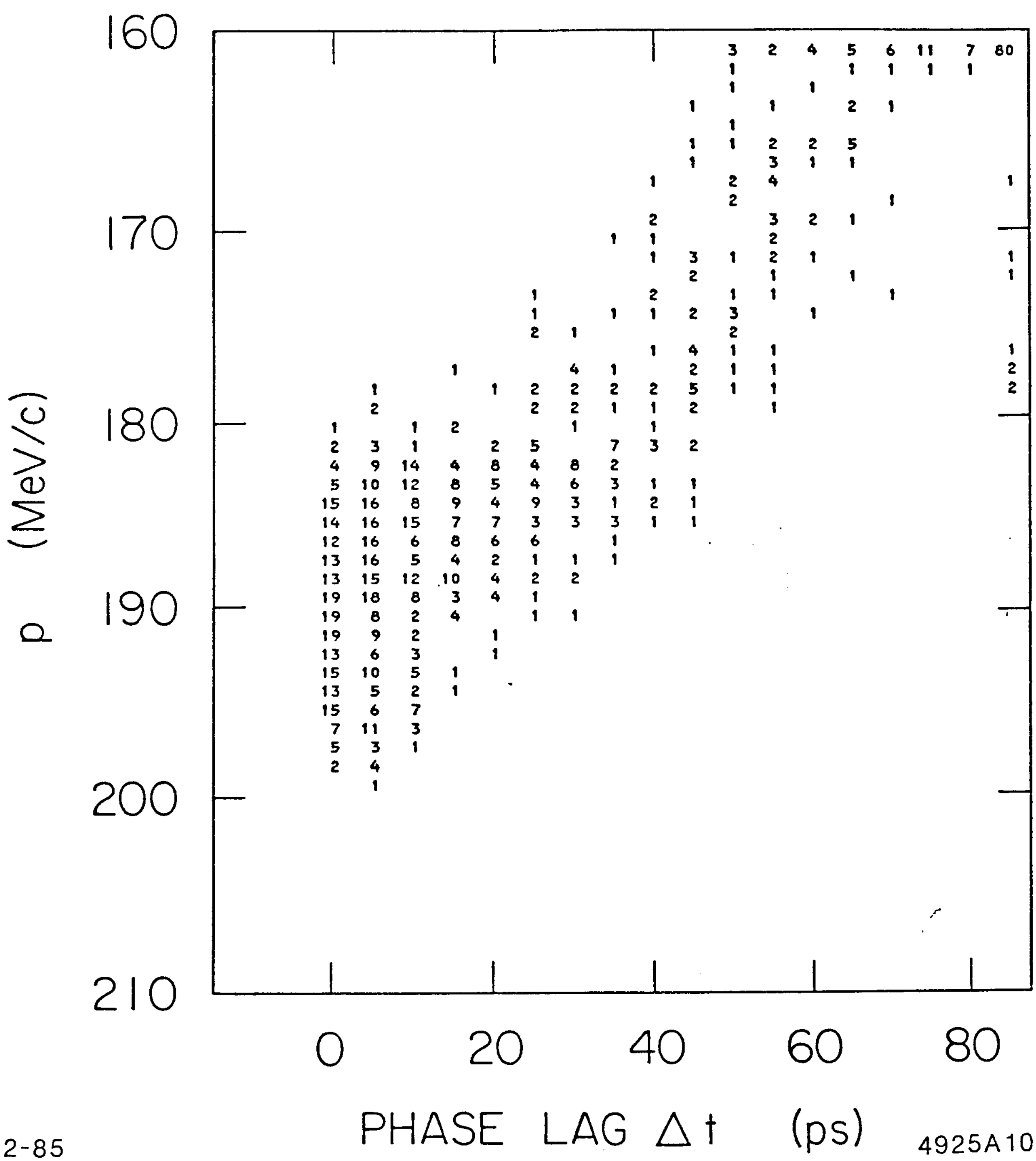
p (MeV/c)
160
170
180
190
200
210
0
20
40
60
80
PHASE LAG Δt (ps)
2-85
4925A10

5.2.4 High Gradient Accelerator

5.2.4.1 Design Parameters for the Capture Accelerator Section:

Choice of Structure and Iris Diameter: A preliminary study was made to compare the predicted performances of uniformly periodic Constant Gradient and Constant Impedance Disk Loaded Waveguide Structures, operated Traveling-Wave with SLED, and Standing-Wave and Recirculating (no SLED). The results of this study, reported in CN-282 dated 17 Oct' 84, showed that, for a given iris aperture diameter, the Constant Impedance (CI) Disk Loaded Waveguide (DLWG) structure would give the highest energy gain, and would also be simpler to build and operate. The expected energy gain increased rapidly as the iris aperture diameter decreased. However, separate calculations showed that the beam-induced wake-field effects increased even more rapidly with decreasing aperture diameter. As a compromise, it was decided to set the iris aperture to 23 mm diameter.

Choice of Length: The length of DLWG was initially taken to be 1 m. However, increasing the iris diameter to 23 mm lowered the expected energy gain to 60 MeV for a 1 m section. After looking at the tradeoffs involved in using a longer section (especially the decrease in input cavity field at beam time, due to the increased time-decay of the incoming SLED pulse), it was decided to increase the length to 1.5 m.

Parameters:

Length	1.5	m
Iris Aperture diameter	23.0	mm
Number of Cavities (including couplers)	42	
Normalized group velocity, v_g/c	0.0124	
Shunt Impedance	57.0	M Ω/m
Q	13600	
Attenuation per unit length	0.177	nepers
Total attenuation	0.266	nepers
Filling Time	403	ns
Energy (assuming 50 MW klystron, SLEDed in with 0.97 db waveguide feed loss)	82.8	MeV
Peak SLED Power into First Cavity	256	MW
Peak Axial Field in First Cavity	71.9	MV/m
Axial Field in First Cavity at Beam Time	54.3	MV/m
Axial Field in Last Cavity at Beam Time	55.1	MV/m
Average Axial Field at Beam Time	55.2	MV/m

Description of RF Feed to Capture Section: The layout of the RF System feeding the SLC Positron Source is shown in Fig. 5.2.4.1. Power from a SLEDed 50 MW klystron installed at Station 20-3C travels through approximately 131 ft of waveguide to the 1.5 m section. The attenuation is about 0.97 db. Some system parameters follow. Average power values assume 120 pps operation.

Klystron average RF power output	30.0	kW
Power dissipation in SLED cavities	9.1	kW
SLED Power Gain Factor	6.4	
SLED Accelerator Voltage Gain Factor		
(for 1.5 m section with 403 ns filling time)	2.21	
Power into rectangular waveguide	20.9	kW
Power into 1.5 m DLWG section	16.7	kW
Power dissipation (RF) in 1.5 m section	7.9	kW
Power dissipation in first cavity of section	210	W
Power dissipation in last cavity of section	125	W
Power dissipation in each of two output loads	4.9	kW

5.2.4.2 Note on Radiation Power Dissipation in 1.5 m Section: EGS computations have shown that radiation generated in the positron target will deposit 12.6 kW of power in the 1.5 m section. The radial temperature drop across the first disk in the section (which can be water–cooled only at its outer periphery, and absorbs a total of 0.51 kW from radiation and RF losses) will be about 40°F. Preliminary calculations[3] indicate that the radial and hoop stresses will be well below the yield values for annealed copper, and disk 'dishing' will not be a problem. Detuning due to an increase in the iris aperture diameter will be offset to first order by the effect of an increase in the disk wall thickness. More detailed calculations are in progress.

With a total flow of 27.4 gpm in 12 parallel circuits, the output water temperature will be 4.9°F above the input. A feedback system will set the inlet water temperature so that the average metal temperature is held at 113°F.

5.2.4.3 The Constant Gradient Sections: The 1.5 m capture section will be followed by three standard 3.05 m constant gradient sections, mounted on a standard girder. The first section will be about 0.5 m downbeam of the capture section. The space normally occupied by the second section on a standard girder will be used for instrumentation. The arrangement, including the waveguide feed from a second 50 MW SLEDed klystron at station 20-4A is also shown in Fig. 5.2.4.1. Half the klystron power goes to the first section, and one fourth the power goes to each of the second and third sections. The length of rectangular waveguide run to each section is about 200 ft, introducing an attenuation of about 1.5 db. Parameters are as follows:

Power dissipation in SLED cavities	7.2	kW
SLED Power Gain Factor	6.2	
SLED Accelerating Voltage Gain Factor (for 3.05 m section with 830 ns filling time)	1.78	
Power dissipation in rectangular waveguide	6.7	kW
Power dissipation in first CG DLWG section	5.5	kW
Power dissipation in each of 2nd and 3rd CG DLWG sections	2.7	kW
Power dissipation in each load for these sections	1.3	kW
Peak SLED power into first section	110	MW
Energy gain in first section	81	MeV
Energy gain in each of 2nd and 3rd sections	57	MeV

Figure 5.2.4.1:

Waveguide Layout for SLC Positron Source

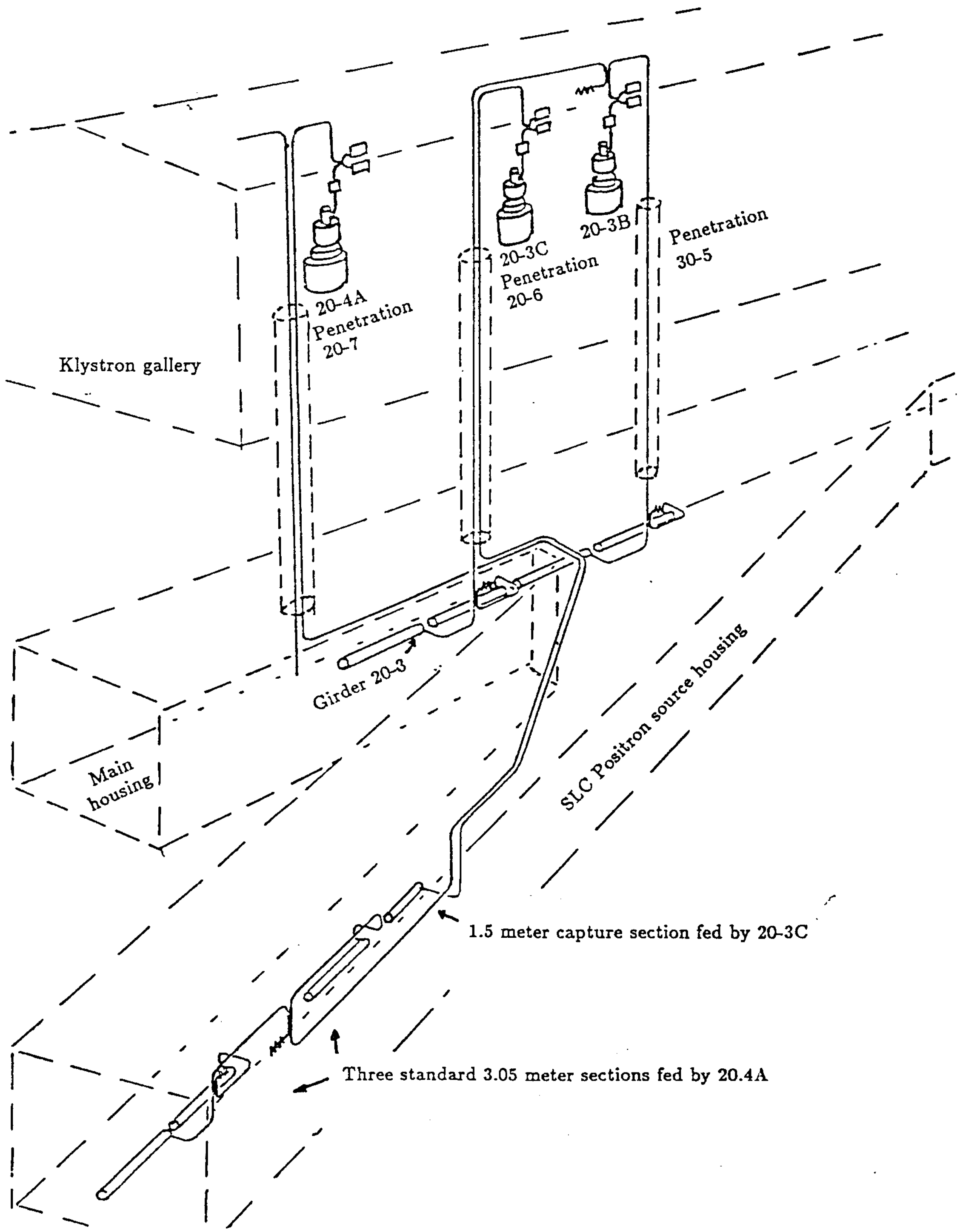

5.2.5 Transport Systems

The beam transport systems consist of an extraction line to bring the 33-GeV e^- scavenger pulse from the linac to the target, the east turn which takes the output of the booster accelerator to the return line in the linac housing, the return line, the west turn and reinjector, and the Sector 1 focusing array. Each of these systems must be sufficiently isochronous so to not spread the S-band bunch unduly. In addition, the total path length of the system from the scavenger extraction kicker in the e^- damping ring to the injection kicker in the e^+ ring must be a multiple of the damping ring circumference in order to place the positrons in the correct bucket of the e^+ ring. The east turn will be built as a movable "trombone" to allow small adjustments ($\pm$ 8 cm) to be made.

5.2.5.1 Extraction Line: The extracted beam is first deflected down by a kicker at Sector 19, girder 4d. At girder 7 of Sector 19, a horizontal and vertical pair of Lambertson septum dipoles deflect the beam down and to the north. The main portion of the 24° bend is provided by a F0D0 array of 9 quadrupoles and 8 bend magnets. In order to match the desired elevation and slope of the e^+ systems, the plane of the bending arc is rolled by about 4.4° and an additional vertical bend magnet just ahead of the arc provides the correct initial pitch angle. Two additional quadrupoles midway between the Lambertson septa and the vertical bend aid in matching the beam optics.

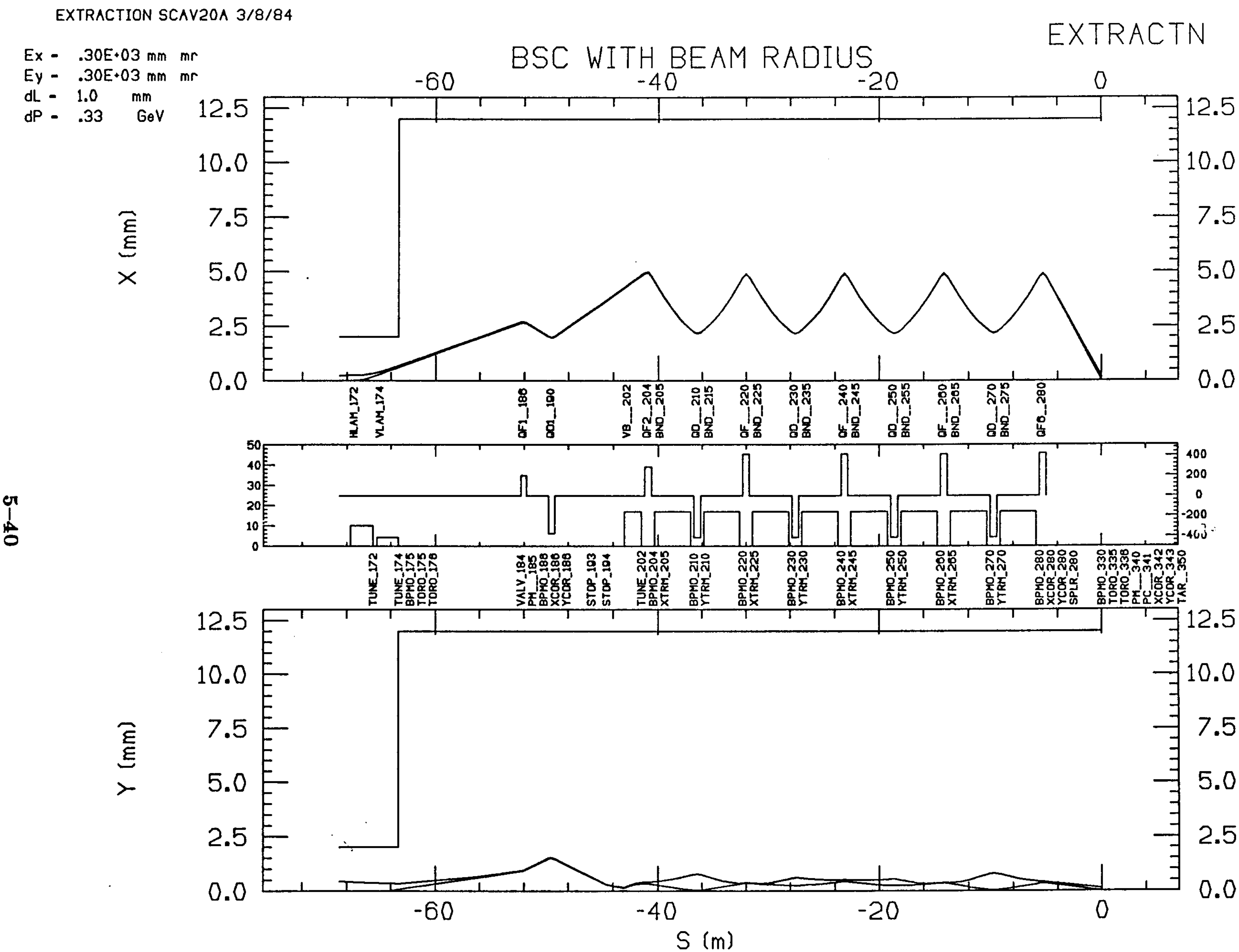

Figure 5.2.5.1.1

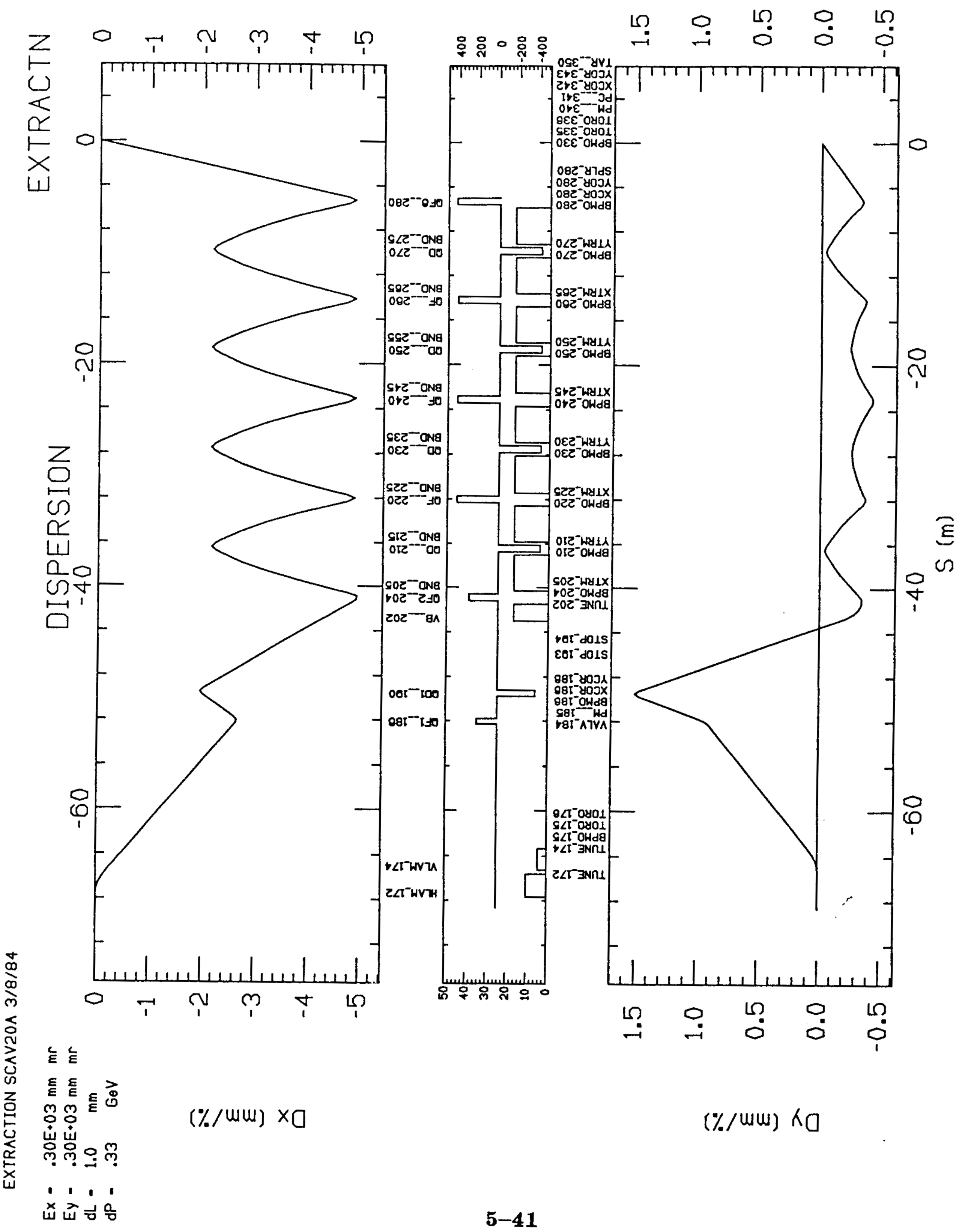

Figure 5.2.5.1.2

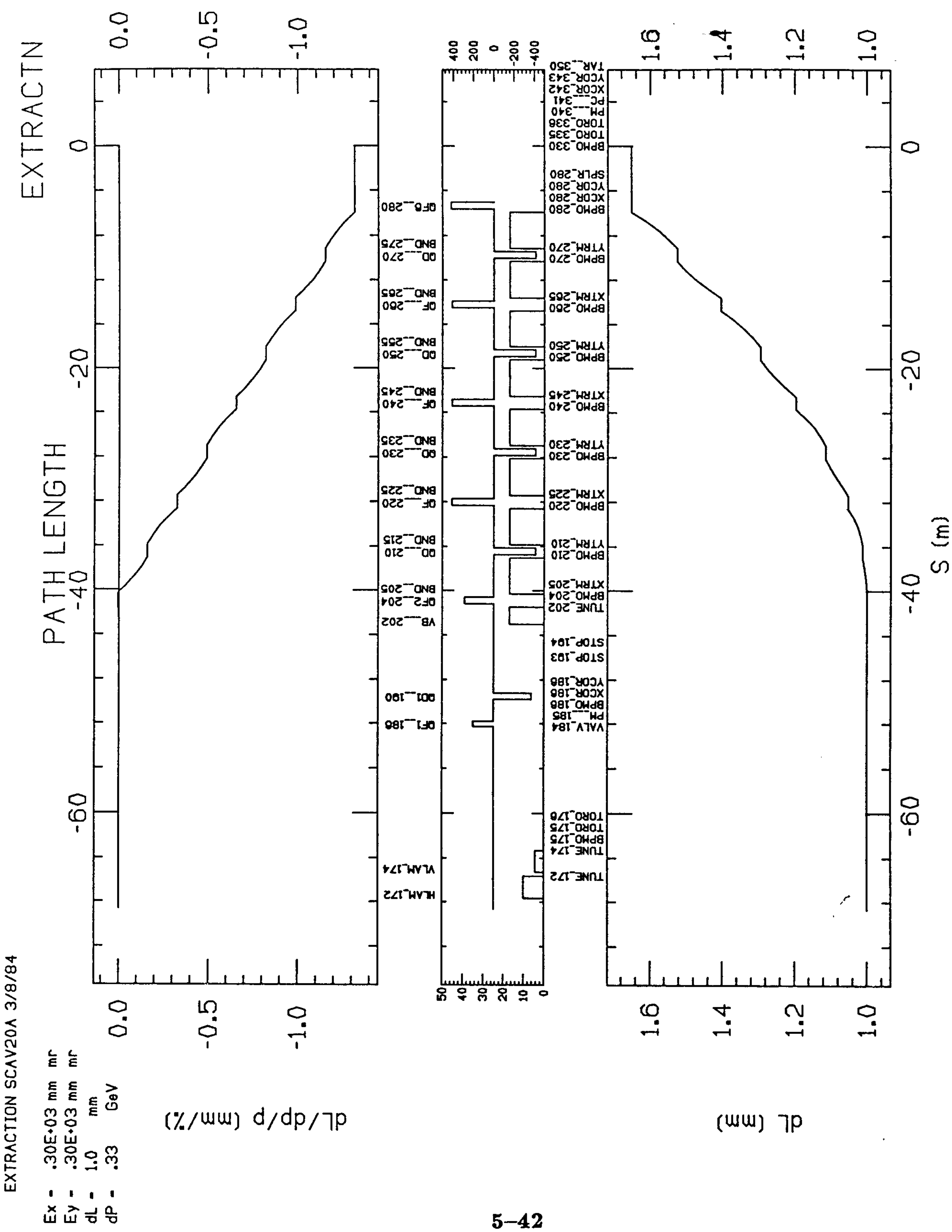

Figure 5.2.5.1.3

Figure 5.2.5.1.4 TURTLE plots for the Extraction Line. The initial particle distribution was generated by K. Bane( ) for a case in which blowup of the beam by transverse wake-fields was suppressed by Landau damping resulting from the introduction of energy spread. Energy = 33 GeV. No aberrations in magnets.

Figure 5.2.5.1.4.1 Horizontal phase plot at beginning of Extraction Line.

```
        TWO DIMENSIONAL PLOT OF   X' (mr) VS    X (mm)

                     -1.000    -0.000     1.000 TOTALS
                       I**---**---**---**---**I--------
  -0.050 TO  -0.045 I                         I      0
  -0.045 TO  -0.040 I                         I      0
  -0.040 TO  -0.035 I                         I      0
  -0.035 TO  -0.030 I                         I      0
  -0.030 TO  -0.025 I                         I      0
  -0.025 TO  -0.020 I                         I      0
  -0.020 TO  -0.015 I                         I      0
  -0.015 TO  -0.010 I                         I      0
  -0.010 TO  -0.005 I         136 1           I     11
  -0.005 TO  -0.000 I        8$$$$$0511       I    494
  -0.000 TO   0.005 I       2CS$$$$ND1        I    485
   0.005 TO   0.010 I          13222          I     10
   0.010 TO   0.015 I                         I      0
   0.015 TO   0.020 I                         I      0
   0.020 TO   0.025 I                         I      0
   0.025 TO   0.030 I                         I      0
   0.030 TO   0.035 I                         I      0
   0.035 TO   0.040 I                         I      0
   0.040 TO   0.045 I                         I      0
   0.045 TO   0.050 I                         I      0
                    I**---**---**---**---**I--------
                    I                         I
                    I                         I
                    I          1221           I
                    I        27881441         I
            TOTALS  I 00000202964798210000 I   1000

        TOTAL NUMBER OF ENTRIES =       1000 INCLUDING UNDERFLOW AND OVERFLOW

                               UNDERFLOW      OVERFLOW
                   ACROSS              0             0
                   DOWN                0             0

  SUM OF SQUARES =    93070.

        CENTER =    -0.017  RMS HALF WIDTH =     0.146

        CENTER =     0.000  RMS HALF WIDTH =     0.002
        CORRELATION =     0.0268
NO    1 TWO DIMENSIONAL PLOT OF
           X IN MM       0.0   M    FROM THE TARGET
          X' IN MR       0.0   M    FROM THE TARGET
```

Figure 5.2.5.1.4.2 Vertical phase plot at beginning of Extraction Line.

```
         TWO DIMENSIONAL PLOT OF    Y' (mr) VS    Y (mm)

                        -1.000     -0.000     1.000 TOTALS
                        I**---**----**----**----**I--------
 -0.050 TO  -0.045 I                          I     0
 -0.045 TO  -0.040 I                          I     0
 -0.040 TO  -0.035 I                          I     0
 -0.035 TO  -0.030 I                          I     0
 -0.030 TO  -0.025 I                          I     0
 -0.025 TO  -0.020 I           1              I     1
 -0.020 TO  -0.015 I          157             I    13
 -0.015 TO  -0.010 I          2YK4            I    60
 -0.010 TO  -0.005 I          2$$2            I   160
 -0.005 TO  -0.000 I          6$$2            I   284
 -0.000 TO   0.005 I          3$$6            I   253
  0.005 TO   0.010 I          6$$3            I   165
  0.010 TO   0.015 I           OX1            I    58
  0.015 TO   0.020 I           41             I     5
  0.020 TO   0.025 I            1             I     1
  0.025 TO   0.030 I                          I     0
  0.030 TO   0.035 I                          I     0
  0.035 TO   0.040 I                          I     0
  0.040 TO   0.045 I                          I     0
  0.045 TO   0.050 I                          I     0
                        I**---**----**----**----**I--------
                        I                         I
                        I                         I
                        I          44             I
                        I         2871            I
              TOTALS    I 00000000084800000000 I   1000

         TOTAL NUMBER OF ENTRIES =       1000 INCLUDING UNDERFLOW AND OVERFLOW

                              UNDERFLOW       OVERFLOW
                  ACROSS              0              0
                  DOWN                0              0

    SUM OF SQUARES =     95908.

         CENTER =     -0.000   RMS HALF WIDTH =      0.047

         CENTER =     -0.000   RMS HALF WIDTH =      0.007
         CORRELATION =     0.0396
 NO   2 TWO DIMENSIONAL PLOT OF
            Y IN MM         0.0    M    FROM THE TARGET
            Y' IN MR        0.0    M    FROM THE TARGET
```

Figure 5.2.5.1.4.3 Longitudinal phase plot at beginning of Extraction Line.

```
                 TWO DIMENSIONAL PLOT OF DP/P (%)  VS   DL (mm)

                         -4.000     -2.000     -0.000     2.000      4.000 TOTALS
                          I**---**---**---**---**---**---**---**---**I--------
    -1.000 TO  -0.900 I                                          I       0
    -0.900 TO  -0.800 I                                          I       0
    -0.800 TO  -0.700 I                                          I       0
    -0.700 TO  -0.600 I                                          I       0
    -0.600 TO  -0.500 I                                          I       0
    -0.500 TO  -0.400 I                                  1       I       1
    -0.400 TO  -0.300 I                                          I       0
    -0.300 TO  -0.200 I                                 2        I       2
    -0.200 TO  -0.100 I                 V                        I      31
    -0.100 TO  -0.000 I              JUZH               1        I     102
    -0.000 TO   0.100 I             2TC $$             1         I     177
     0.100 TO   0.200 I              I     9                     I      27
     0.200 TO   0.300 I            8A      $           2         I      89
     0.300 TO   0.400 I             E     GR          4          I      61
     0.400 TO   0.500 I           83       $          1          I      52
     0.500 TO   0.600 I            9        F         2          I      26
     0.600 TO   0.700 I          94         $        2           I      61
     0.700 TO   0.800 I           7        FM       28           I      54
     0.800 TO   0.900 I         32          Y       3            I      42
     0.900 TO   1.000 I          2         D$       4            I      58
     1.000 TO   1.100 I          4          V9     J             I      63
     1.100 TO   1.200 I                      $Y M3               I      99
     1.200 TO   1.300 I                       95$                I      53
     1.300 TO   1.400 I                                          I       0
     1.400 TO   1.500 I                                          I       0
                      I**---**---**---**---**---**---**---**---**I--------
                      I                                          I
                      I                                          I
                      I                                          I
                      I          1223446779676753322 1           I
               TOTALS I 0000000009815082673476908992290733100000 I     998

         TOTAL NUMBER OF ENTRIES =        1000 INCLUDING UNDERFLOW AND OVERFLOW

                                 UNDERFLOW       OVERFLOW
                      ACROSS             0              0
                      DOWN               2              0

 SUM OF SQUARES =    34402.

         CENTER =       0.038   RMS HALF WIDTH =      0.970

         CENTER =       0.497   RMS HALF WIDTH =      0.457
         CORRELATION =     0.6248
NO    3 TWO DIMENSIONAL PLOT OF
           DL IN MM        0.0    M    FROM THE TARGET
         DP/P IN PC        0.0    M    FROM THE TARGET
```

Figure 5.2.5.1.4.4 Horizontal phase plot at Positron Target.

```
   TWO DIMENSIONAL PLOT OF    X' (mr) VS    X (mm)

                   -0.500     0.000     0.500 TOTALS
                    I**----**----**----**----**I--------
 -2.000 TO  -1.800 I                        I       0
 -1.800 TO  -1.600 I                        I       0
 -1.600 TO  -1.400 I                        I       0
 -1.400 TO  -1.200 I                        I       0
 -1.200 TO  -1.000 I        1               I       1
 -1.000 TO  -0.800 I         1              I       1
 -0.800 TO  -0.600 I                        I       0
 -0.600 TO  -0.400 I         1              I       1
 -0.400 TO  -0.200 I       1   1            I       2
 -0.200 TO   0.000 I      16B$$J761         I     151
  0.000 TO   0.200 I       58V$$ZA   1      I     200
  0.200 TO   0.400 I       3C$$$G51         I     157
  0.400 TO   0.600 I       1CNTA73          I      85
  0.600 TO   0.800 I       6KY$A61          I     115
  0.800 TO   1.000 I     12BTW0531          I     108
  1.000 TO   1.200 I      2S$$$B            I     170
  1.200 TO   1.400 I        126             I       9
  1.400 TO   1.600 I                        I       0
  1.600 TO   1.800 I                        I       0
  1.800 TO   2.000 I                        I       0
                    I**----**----**----**----**I--------
                   I                        I
                   I                        I
                   I        1221            I
                   I       6368572          I
            TOTALS I 00001511144462010000 I    1000

       TOTAL NUMBER OF ENTRIES =       1000 INCLUDING UNDERFLOW AND OVERFLOW

                              UNDERFLOW        OVERFLOW
                   ACROSS             0               0
                   DOWN               0               0

  SUM OF SQUARES =     33414.

        CENTER =     -0.041   RMS HALF WIDTH =      0.071

        CENTER =      0.464   RMS HALF WIDTH =      0.433
        CORRELATION =   -0.3722
NO    7 TWO DIMENSIONAL PLOT OF
           X IN MM       68.625 M     FROM THE TARGET
           X' IN MR      68.625 M     FROM THE TARGET
```

Figure 5.2.5.1.4.5 Vertical phase plot at Positron Target.

```
        TWO DIMENSIONAL PLOT OF    Y' (mr) VS    Y (mm)

                         -1.000    -0.000     1.000 TOTALS
                         I**---**---**---**---**I--------
  -0.200 TO  -0.180 I                       I       0
  -0.180 TO  -0.160 I                       I       0
  -0.160 TO  -0.140 I                       I       0
  -0.140 TO  -0.120 I                       I       0
  -0.120 TO  -0.100 I                       I       0
  -0.100 TO  -0.080 I          2            I       2
  -0.080 TO  -0.060 I                       I       0
  -0.060 TO  -0.040 I          1            I       1
  -0.040 TO  -0.020 I          L3           I      24
  -0.020 TO   0.000 I          $$           I     138
   0.000 TO   0.020 I          $$           I     222
   0.020 TO   0.040 I          $$1          I     169
   0.040 TO   0.060 I          $$1          I     144
   0.060 TO   0.080 I          $$3          I     194
   0.080 TO   0.100 I          $$1          I     103
   0.100 TO   0.120 I          3            I       3
   0.120 TO   0.140 I                       I       0
   0.140 TO   0.160 I                       I       0
   0.160 TO   0.180 I                       I       0
   0.180 TO   0.200 I                       I       0
                    I**---**---**---**---**I--------
                    I                       I
                    I                       I
                    I          45           I
                    I          53           I
            TOTALS  I 00000000095600000000 I   1000

        TOTAL NUMBER OF ENTRIES =      1000 INCLUDING UNDERFLOW AND OVERFLOW

                            UNDERFLOW       OVERFLOW
                  ACROSS            0              0
                  DOWN              0              0

  SUM OF SQUARES =    87442.

        CENTER =      0.005    RMS HALF WIDTH =      0.035

        CENTER =      0.035    RMS HALF WIDTH =      0.034
        CORRELATION =    0.2248
NO   8 TWO DIMENSIONAL PLOT OF
           Y IN MM       68.625 M     FROM THE TARGET
          Y' IN MR       68.625 M     FROM THE TARGET
```

Figure 5.2.5.1.4.6 Longitudinal phase plot at Positron Target.

```
        TWO DIMENSIONAL PLOT OF DP/P (%)  VS   DL (mm)

                 -4.000    -2.000    -0.000     2.000     4.000 TOTALS
                  I**---**---**---**---**---**---**---**---**I--------
-1.000 TO  -0.900 I                                          I      0
-0.900 TO  -0.800 I                                          I      0
-0.800 TO  -0.700 I                                          I      0
-0.700 TO  -0.600 I                                          I      0
-0.600 TO  -0.500 I                                          I      0
-0.500 TO  -0.400 I                                      1   I      1
-0.400 TO  -0.300 I                                          I      0
-0.300 TO  -0.200 I                                    2     I      2
-0.200 TO  -0.100 I                  V                       I     31
-0.100 TO  -0.000 I               BUTV               1       I    102
-0.000 TO   0.100 I              LCA $$             1        I    177
 0.100 TO   0.200 I             F3   9                       I     27
 0.200 TO   0.300 I           3F     $            2          I     89
 0.300 TO   0.400 I          59      $           4           I     61
 0.400 TO   0.500 I         56       $          1            I     52
 0.500 TO   0.600 I        54        F         2             I     26
 0.600 TO   0.700 I       A3         $        2              I     61
 0.700 TO   0.800 I     16          6V      46               I     54
 0.800 TO   0.900 I     5           X1     12                I     42
 0.900 TO   1.000 I    2            $1    31                 I     58
 1.000 TO   1.100 I   4             $   3G                   I     63
 1.100 TO   1.200 I                 $Y AF                    I     99
 1.200 TO   1.300 I                 9KO                      I     53
 1.300 TO   1.400 I                                          I      0
 1.400 TO   1.500 I                                          I      0
                  I**---**---**---**---**---**---**---**---**I--------
                  I                                          I
                  I                                          I
                  I                 24                       I
                  I       1  1111224047111                   I
          TOTALS  I 0042660891255430899086326622142011020100 I    998

        TOTAL NUMBER OF ENTRIES =       1000 INCLUDING UNDERFLOW AND OVERFLOW

                                 UNDERFLOW       OVERFLOW
                  ACROSS               0               2
                  DOWN                 0               0

 SUM OF SQUARES =    35872.

        CENTER =    -0.627   RMS HALF WIDTH =     0.755

        CENTER =     0.497   RMS HALF WIDTH =     0.457
        CORRELATION =   -0.0122
NO   9 TWO DIMENSIONAL PLOT OF
          DL IN MM      68.625 M    FROM THE TARGET
        DP/P IN PC      68.625 M    FROM THE TARGET
```

Figure 5.2.5.1.5 TURTLE plots showing effects of sextupole fields induced by dipole excitation of the QD quadrupoles. The sextupole field is assumed to be induced by dipole excitation to correct for vertical misalignments of magnitude |dy| = 1 mm. Cases (a) and (b) show the extreme effects for different distributions of the sign of the sextupole in the four QD's. Compare to Figure 5.2.5.1.4.5 which is the case of no sextupole. The effects on horizontal and longitudinal phase space is minimal.

Figure 5.2.5.1.5.1 Signs of the sextupoles in the QD's is +--+.

```
          TWO DIMENSIONAL PLOT OF    Y' (mr) VS    Y (mm)

                      -1.000    -0.000     1.000 TOTALS
                       I**----**----**----**----**I--------
 -0.200 TO  -0.180 I                       I      0
 -0.180 TO  -0.160 I                       I      0
 -0.160 TO  -0.140 I                       I      0
 -0.140 TO  -0.120 I                       I      0
 -0.120 TO  -0.100 I                       I      0
 -0.100 TO  -0.080 I                       I      0
 -0.080 TO  -0.060 I                       I      0
 -0.060 TO  -0.040 I                       I      0
 -0.040 TO  -0.020 I          P            I     25
 -0.020 TO   0.000 I          $$1 11       I    136
  0.000 TO   0.020 I          $$           I    198
  0.020 TO   0.040 I          9$8          I    129
  0.040 TO   0.060 I          2$R          I     78
  0.060 TO   0.080 I           6$E         I     64
  0.080 TO   0.100 I           3JV8        I     61
  0.100 TO   0.120 I            3NK2       I     48
  0.120 TO   0.140 I             4$K6      I     69
  0.140 TO   0.160 I              6$T2     I     75
  0.160 TO   0.180 I               F$0     I     90
  0.180 TO   0.200 I                1FA1   I     27
                   I**----**----**----**I--------
                   I                       I
                   I                       I
                   I          131   1      I
                   I          85077703     I
            TOTALS I 0000000034224716100 I   1000

          TOTAL NUMBER OF ENTRIES =        1000 INCLUDING UNDERFLOW AND OVERFLOW

                               UNDERFLOW        OVERFLOW
                   ACROSS              0               0
                   DOWN                0               0

   SUM OF SQUARES =    61804.

          CENTER =      0.181   RMS HALF WIDTH =      0.211

          CENTER =      0.064   RMS HALF WIDTH =      0.064
          CORRELATION =    0.9613
NO   8 TWO DIMENSIONAL PLOT OF
              Y IN MM       68.625 M    FROM THE TARGET
             Y' IN MR       68.625 M    FROM THE TARGET
```

Figure 5.2.5.1.5.2 Signs of the sextupoles in the QD's is -++-.

```
        TWO DIMENSIONAL PLOT OF    Y' (mr) VS    Y (mm)

                       -1.000     -0.000     1.000 TOTALS
                       I**---**---**---**---**I--------
 -0.200 TO  -0.180 I     1                 I     1
 -0.180 TO  -0.160 I                       I     0
 -0.160 TO  -0.140 I      1                I     1
 -0.140 TO  -0.120 I                       I     0
 -0.120 TO  -0.100 I                       I     0
 -0.100 TO  -0.080 I                       I     0
 -0.080 TO  -0.060 I                       I     0
 -0.060 TO  -0.040 I           1           I     1
 -0.040 TO  -0.020 I     42    M1          I    29
 -0.020 TO   0.000 I    D$$D44$$           I   278
  0.000 TO   0.020 I    30$$$$$$           I   491
  0.020 TO   0.040 I     11CV$$$2          I   189
  0.040 TO   0.060 I        136            I    10
  0.060 TO   0.080 I                       I     0
  0.080 TO   0.100 I                       I     0
  0.100 TO   0.120 I                       I     0
  0.120 TO   0.140 I                       I     0
  0.140 TO   0.160 I                       I     0
  0.160 TO   0.180 I                       I     0
  0.180 TO   0.200 I                       I     0
                   I**---**---**---**---**I--------
                   I                       I
                   I                       I
                   I      1   32           I
                   I    17079930           I
            TOTALS I 00067136735200000000 I   1000

        TOTAL NUMBER OF ENTRIES =       1000 INCLUDING UNDERFLOW AND OVERFLOW

                            UNDERFLOW       OVERFLOW
                   ACROSS           0              0
                   DOWN             0              0

  SUM OF SQUARES =    71206.

        CENTER =    -0.169   RMS HALF WIDTH =     0.199

        CENTER =     0.007   RMS HALF WIDTH =     0.017
        CORRELATION =    0.2244
NO   8 TWO DIMENSIONAL PLOT OF
           Y IN MM       68.625 M    FROM THE TARGET
          Y' IN MR       68.625 M    FROM THE TARGET
```

5.2.5.2 Booster: The beam transport system around the booster accelerator consists of solenoid and then quadrupole focusing. A uniform 5 kG solenoidal field extends from the target through the high gradient 1.5 m section to the end of the first normal gradient 3 m section. There a transition is made to a F0D0 quadrupole array. The 3 m section following the solenoid is devoted to instrumentation and a magnetic charge separator to stop the electrons.

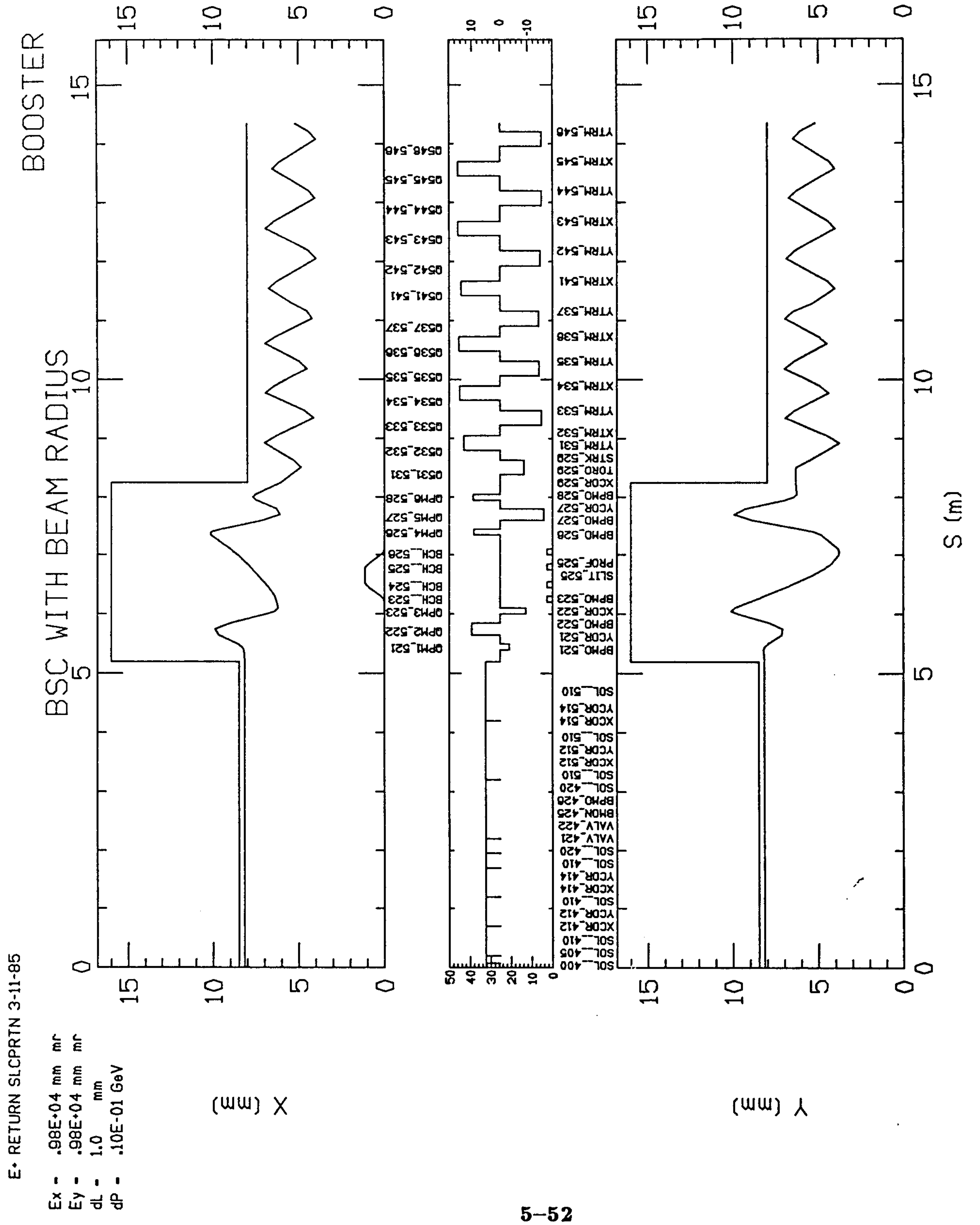

Figure 5.2.5.2.1

Figure 5.2.5.2.2 TURTLE plots at end of first 10-ft accelerator section in positron booster. Initial number of electrons on target = 327. Relative yield = 2.7 e+/e-.

Figure 5.2.5.2.2.1 Horizontal phase plane.

```
         TWO DIMENSIONAL PLOT OF    X' (mr) VS    X (mm)

                        -10.000     0.000     10.000 TOTALS
                          I**---**---**---**---**I--------
 -10.000 TO  -9.000 I                      I       0
  -9.000 TO  -8.000 I                      I       0
  -8.000 TO  -7.000 I                      I       0
  -7.000 TO  -6.000 I                      I       0
  -6.000 TO  -5.000 I                      I       0
  -5.000 TO  -4.000 I    1  2  321         I       9
  -4.000 TO  -3.000 I  21384466563312      I      54
  -3.000 TO  -2.000 I 2214366A7AA7223      I      75
  -2.000 TO  -1.000 I 3356BDGEIE865241     I     129
  -1.000 TO   0.0   I2123AIJJLGSMAA341     I     189
   0.0   TO   1.000 I 316ADBENVTFB8583     I     191
   1.000 TO   2.000 I114355GBAG9H55932     I     122
   2.000 TO   3.000 I 21353969AC764113     I      82
   3.000 TO   4.000 I  121523653331        I      35
   4.000 TO   5.000 I    1 3 1111  1       I       9
   5.000 TO   6.000 I                      I       0
   6.000 TO   7.000 I                      I       0
   7.000 TO   8.000 I                      I       0
   8.000 TO   9.000 I                      I       0
   9.000 TO  10.000 I                      I       0
                    I**---**---**---**---**I--------
                    I                      I
                    I                      I
                    I        111           I
                    I  1124688011953221    I
             TOTALS I 03264663100412845000 I     895

        TOTAL NUMBER OF ENTRIES =          895 INCLUDING UNDERFLOW AND OVERFLOW

                                 UNDERFLOW       OVERFLOW
                   ACROSS                0              0
                   DOWN                  0              0

  SUM OF SQUARES =      11193.

        CENTER =        0.009    RMS HALF WIDTH =       3.222

        CENTER =       -0.070    RMS HALF WIDTH =       1.842
        CORRELATION =       0.0036
NO    1 TWO DIMENSIONAL PLOT OF
             X IN MM          5.200 M     FROM THE TARGET
             X' IN MR         5.200 M     FROM THE TARGET
```

Figure 5.2.5.2.2.2 Vertical phase plane.

```
         TWO DIMENSIONAL PLOT OF    Y' (mr) VS    Y (mm)

                  -10.000      0.000     10.000 TOTALS
                    I**---**---**---**---**I--------
-10.000 TO  -9.000 I                      I      0
 -9.000 TO  -8.000 I                      I      0
 -8.000 TO  -7.000 I                      I      0
 -7.000 TO  -6.000 I                      I      0
 -6.000 TO  -5.000 I                      I      0
 -5.000 TO  -4.000 I      1214 32         I     13
 -4.000 TO  -3.000 I   1 61446746611      I     47
 -3.000 TO  -2.000 I  213218C8A888B74     I     93
 -2.000 TO  -1.000 I 12426DBIBJDED65421   I    145
 -1.000 TO   0.0   I  1153BDKLRLED7354    I    169
  0.0   TO   1.000 I  1 8AABJLFMCA98131   I    161
  1.000 TO   2.000 I  43256ECACABH66131   I    123
  2.000 TO   3.000 I  3 2378796C9A8122    I     89
  3.000 TO   4.000 I    222514534242      I     36
  4.000 TO   5.000 I     12141513 1       I     19
  5.000 TO   6.000 I                      I      0
  6.000 TO   7.000 I                      I      0
  7.000 TO   8.000 I                      I      0
  8.000 TO   9.000 I                      I      0
  9.000 TO  10.000 I                      I      0
                    I**---**---**---**---**I--------
                    I                      I
                    I                      I
                    I          1           I
                    I  1123579909875311    I
             TOTALS I 01304847856739337430 I    895

         TOTAL NUMBER OF ENTRIES =        895 INCLUDING UNDERFLOW AND OVERFLOW

                              UNDERFLOW       OVERFLOW
                    ACROSS            0              0
                    DOWN              0              0

  SUM OF SQUARES =     10073.

         CENTER =      0.338   RMS HALF WIDTH =     3.247

         CENTER =     -0.053   RMS HALF WIDTH =     1.959
         CORRELATION =   -0.0147
NO   2 TWO DIMENSIONAL PLOT OF
            Y IN MM        5.200 M    FROM THE TARGET
           Y' IN MR        5.200 M    FROM THE TARGET
```

Figure 5.2.5.2.2.3 Longitudinal phase plane.

```
              TWO DIMENSIONAL PLOT OF DP/P (%)  VS   DL (mm)

                   -10.000    -5.000    -0.000     5.000 TOTALS
                    I**---**---**---**---**---**---**I--------
-10.000 TO  -9.000 I                                I       0
 -9.000 TO  -8.000 I                                I       0
 -8.000 TO  -7.000 I                                I       0
 -7.000 TO  -6.000 I                                I       0
 -6.000 TO  -5.000 I                                I       0
 -5.000 TO  -4.000 I               11               I       2
 -4.000 TO  -3.000 I            7463 22             I      24
 -3.000 TO  -2.000 I            E9AEHC74            I      87
 -2.000 TO  -1.000 I            8DAFMJH2            I     106
 -1.000 TO   0.000 I            B9CBABDJ1           I      97
  0.000 TO   1.000 I            4A98HAJF            I      92
  1.000 TO   2.000 I            69ACIBKI            I     104
  2.000 TO   3.000 I            64A58IGR2           I      96
  3.000 TO   4.000 I            23BBADDQ6           I      95
  4.000 TO   5.000 I            133588BE6           I      59
  5.000 TO   6.000 I              535ACP4           I      64
  6.000 TO   7.000 I            2 1345868           I      37
  7.000 TO   8.000 I               111945           I      21
  8.000 TO   9.000 I                12611           I      11
  9.000 TO  10.000 I                                I       0
                   I**---**---**---**---**---**---**I--------
                   I                                I
                   I                                I
                   I                1111            I
                   I            668922563           I
            TOTALS I 0000000000001472223130000000000 I     895

          TOTAL NUMBER OF ENTRIES =        895 INCLUDING UNDERFLOW AND OVERFLOW

                             UNDERFLOW        OVERFLOW
                    ACROSS           0               0
                    DOWN             0               0

 SUM OF SQUARES =    11687.

         CENTER =    -2.052   RMS HALF WIDTH =      1.124

         CENTER =     1.540   RMS HALF WIDTH =      2.923
         CORRELATION =    0.3931
NO   3 TWO DIMENSIONAL PLOT OF
           DL IN MM        5.200 M    FROM THE TARGET
         DP/P IN PC        5.200 M    FROM THE TARGET
```

5.2.5.3 East Turn & 24° Bend: Two 90° dipoles turn the positron beam around 180° in a vertical plane and back along the 24° housing. In order to satisfy the isochronous condition, the integral of the dispersion must average to zero in the bend dipoles. This is accomplished by two small 10° bends on each side of the main 180° bend. A weak quadrupole between each of the 10° bends permits adjustment of the isochronism. Four 6° dipoles are used to bring the beam into the return line. This system is also made isochronous, by quadrupoles which suitably control the dispersion function. A sextupole at the symmetry point of the 180° turn corrects the second order non-isochronism.

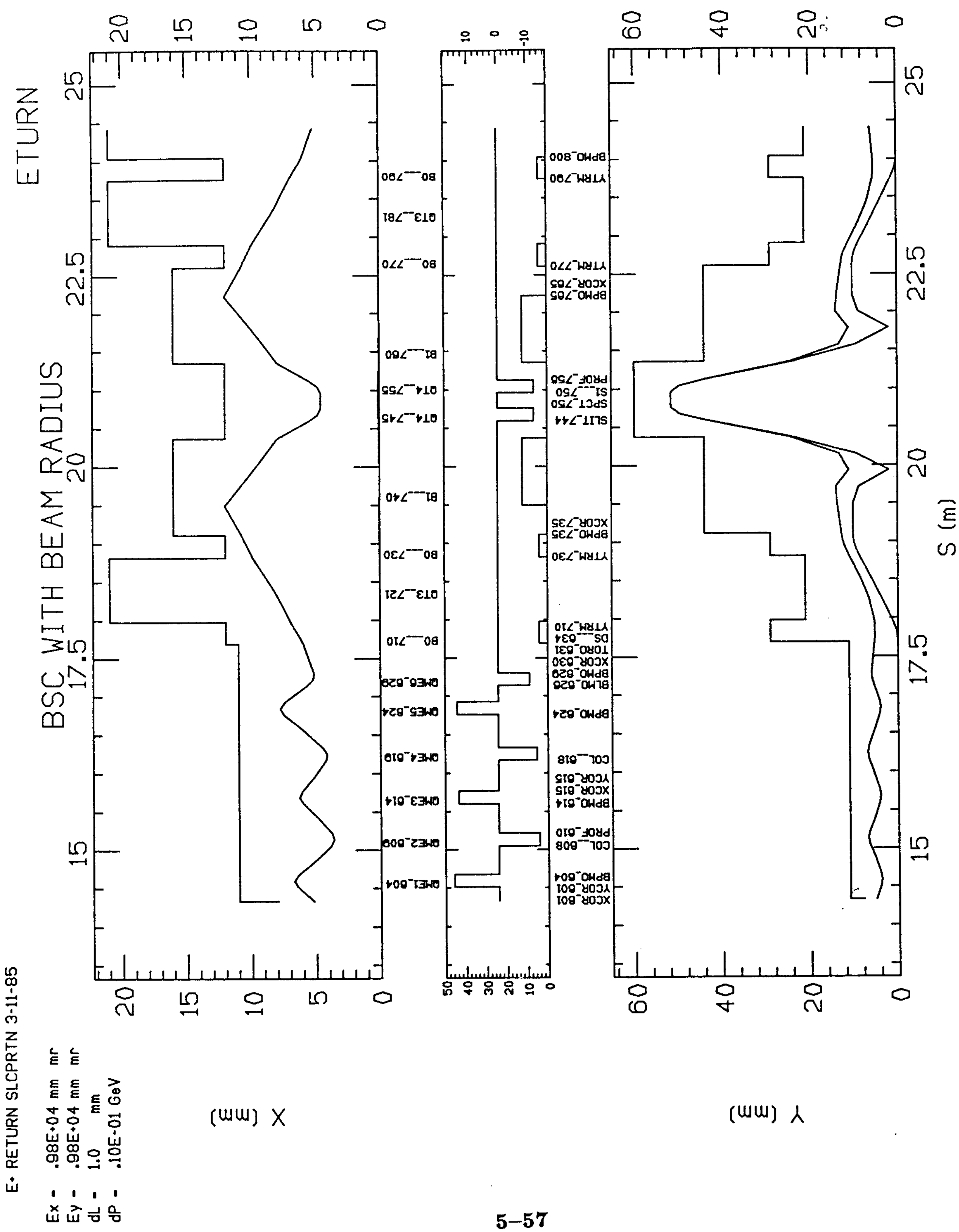

Figure 5.2.5.3.1

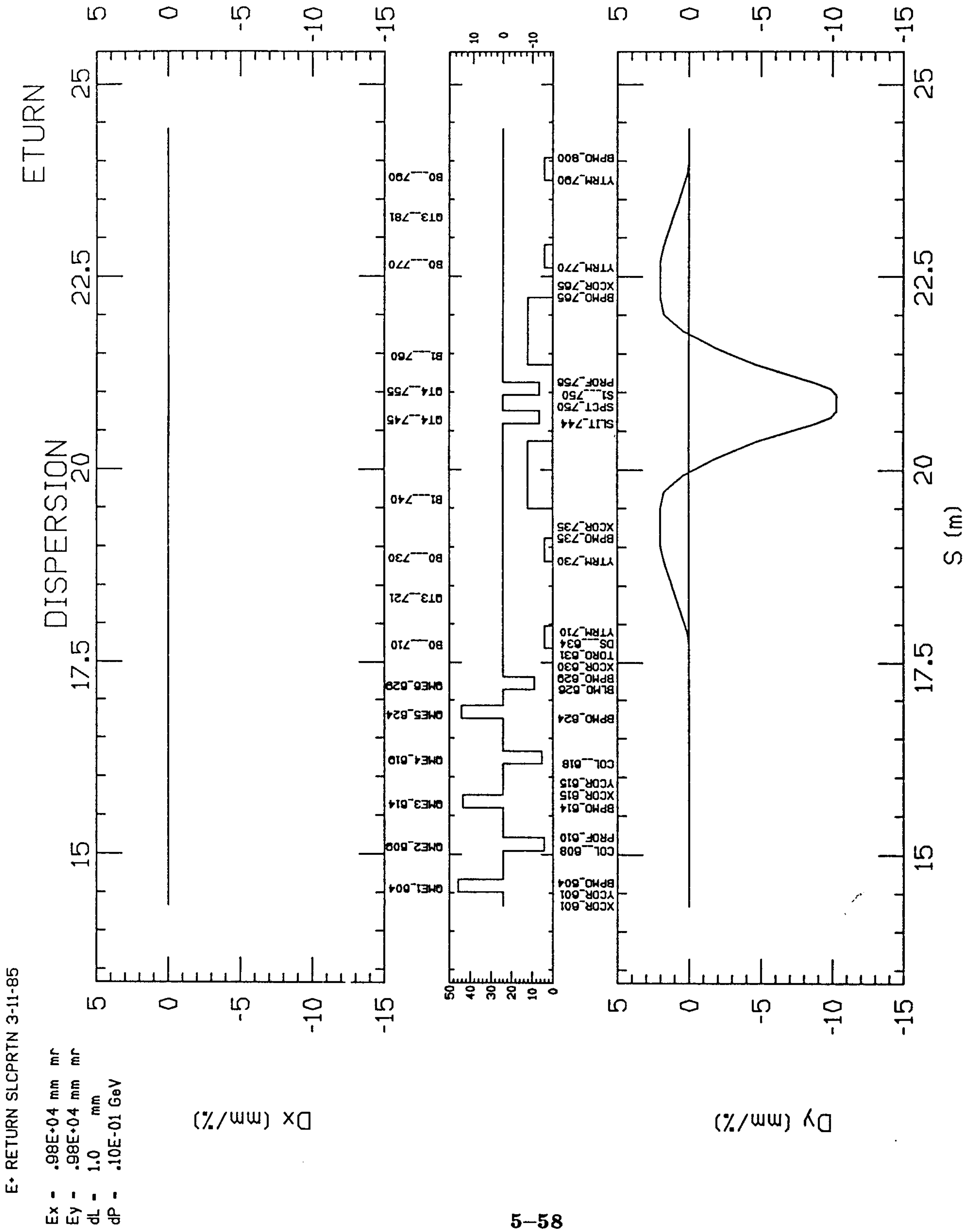

Figure 5.2.5.3.2

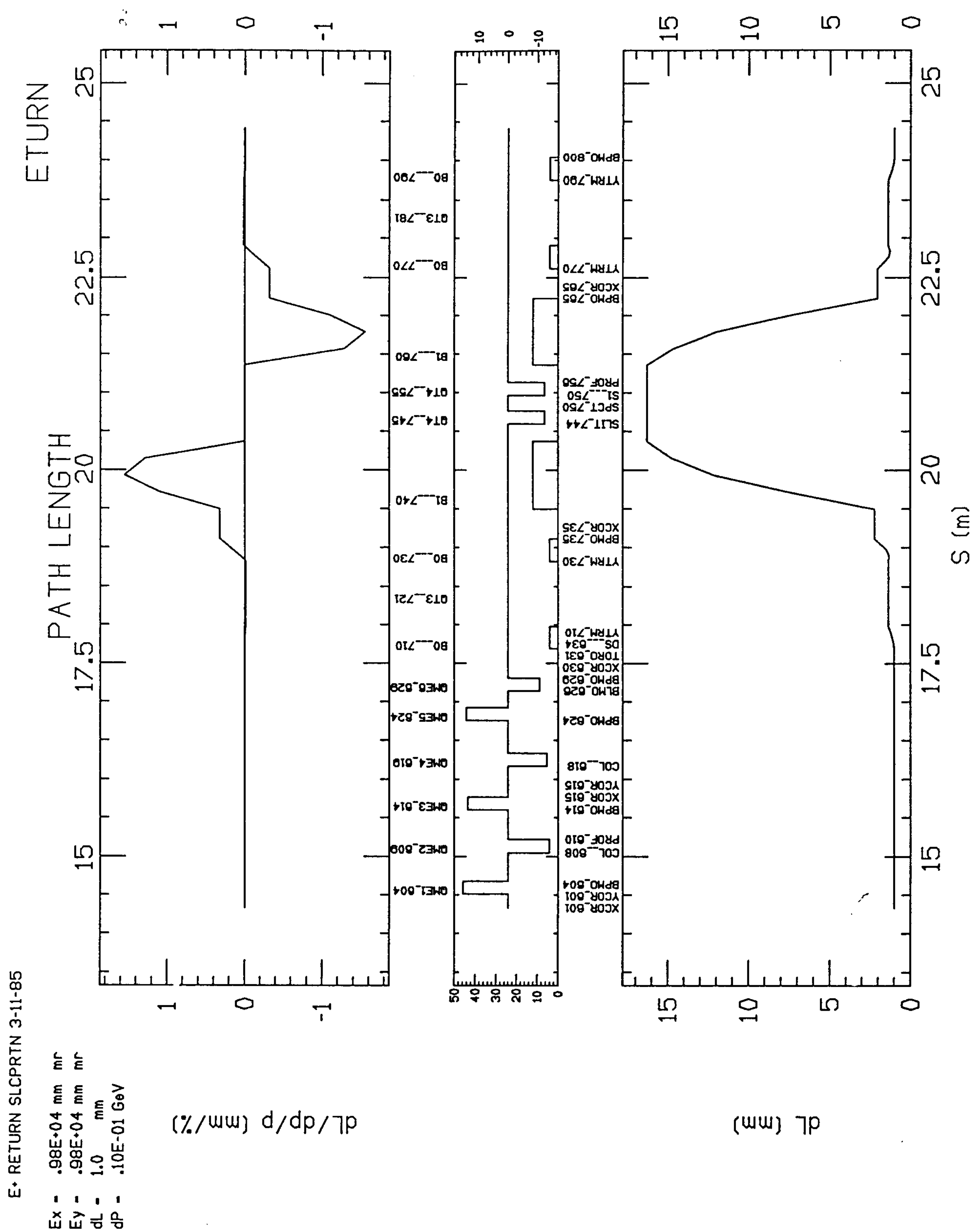

Figure 5.2.5.3.3

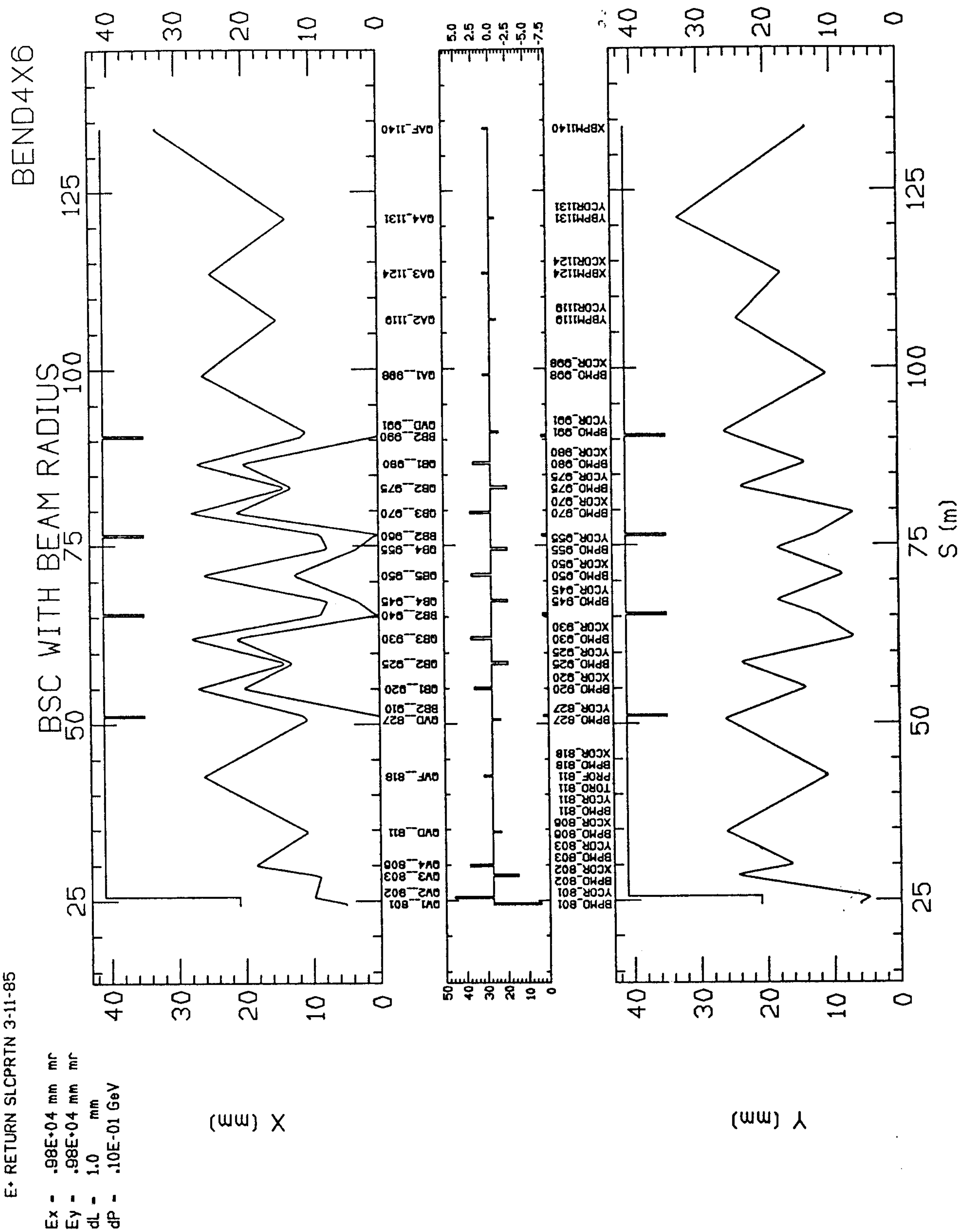

Figure 5.2.5.3.4

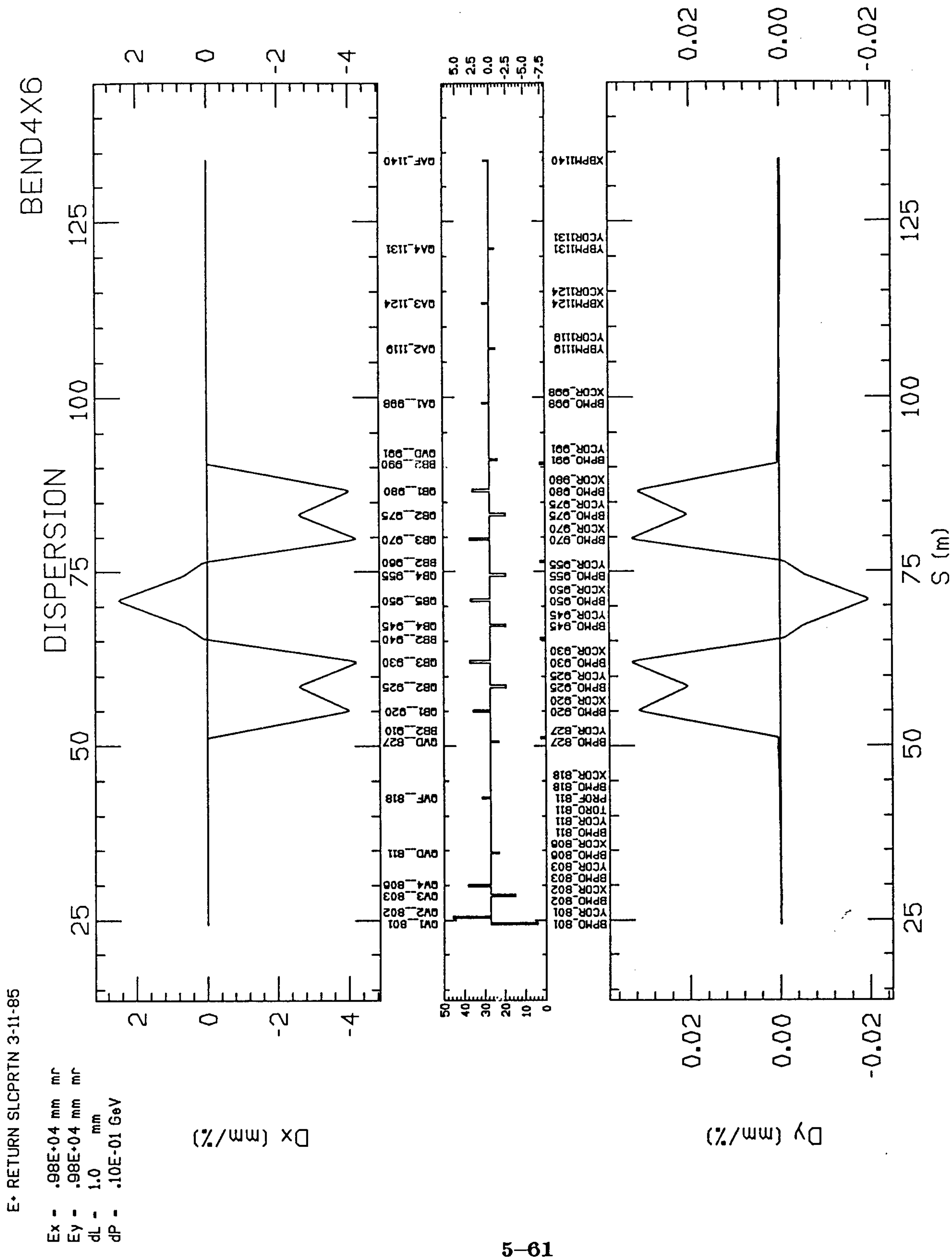

Figure 5.2.5.3.5

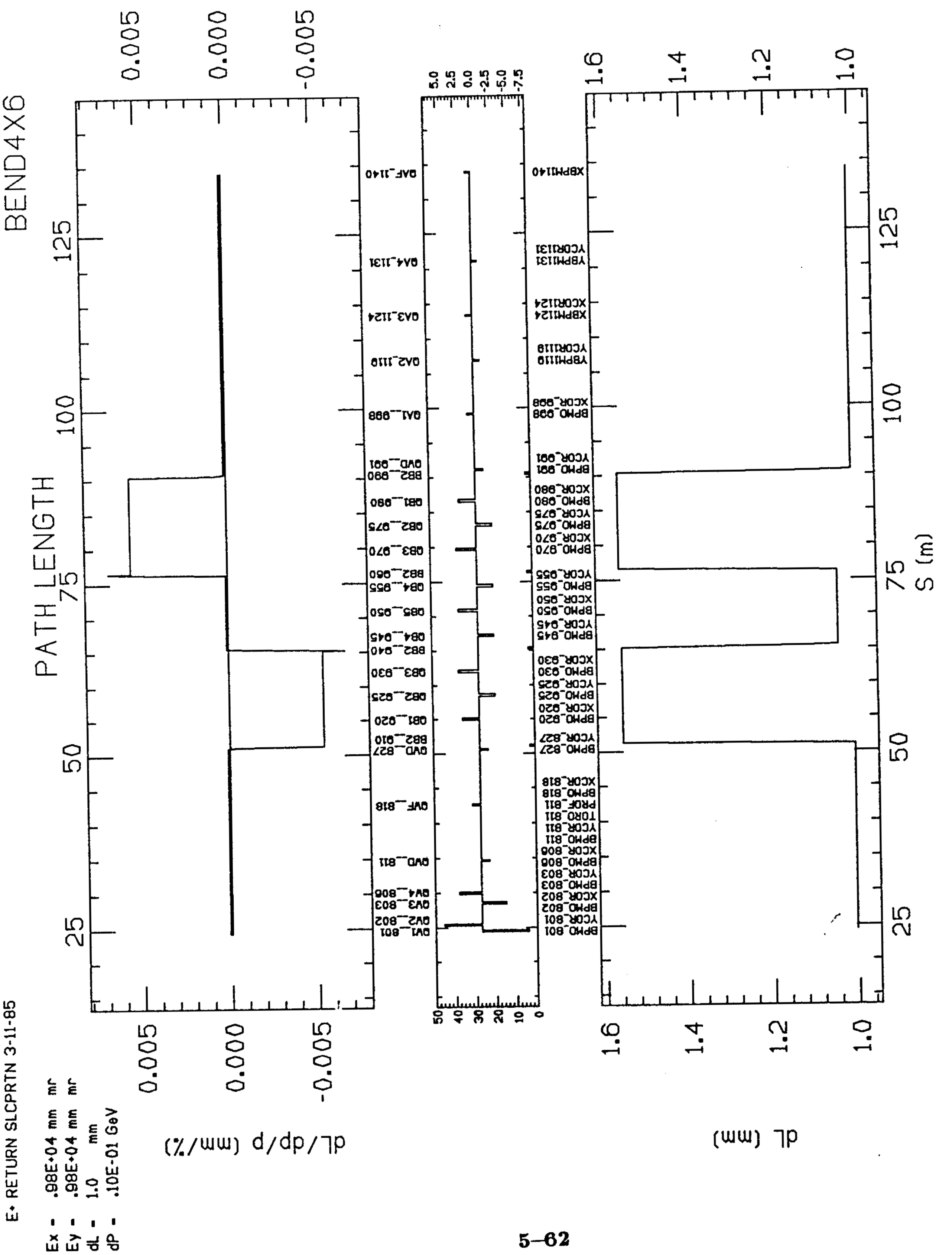

Figure 5.2.5.3.6

<u>5.2.5.4 **Return Line:**</u> The transport from Sector 19 to Sector 1 is done with a F0D0 array of eight quadrupoles per sector of nominal phase advance of 90°/cell. Dipole correctors, 4 vertical and 4 horizontal per sector, are located at respective maxima in the β function to provide steering and compensation for the deflection due to the earth's magnetic field or other stray fields.

Figure 5.2.5.4.1

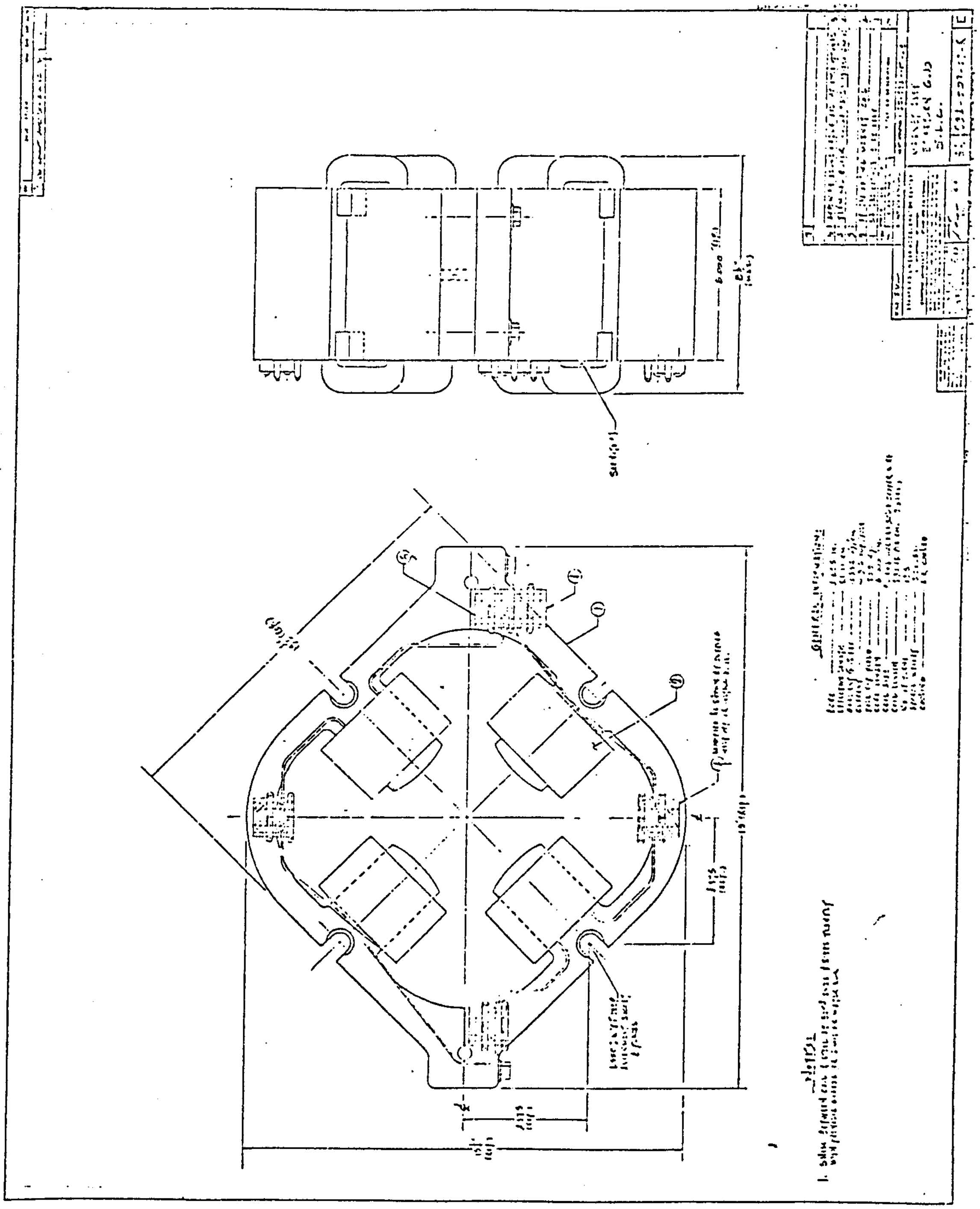

Figure 5.2.5.4.2

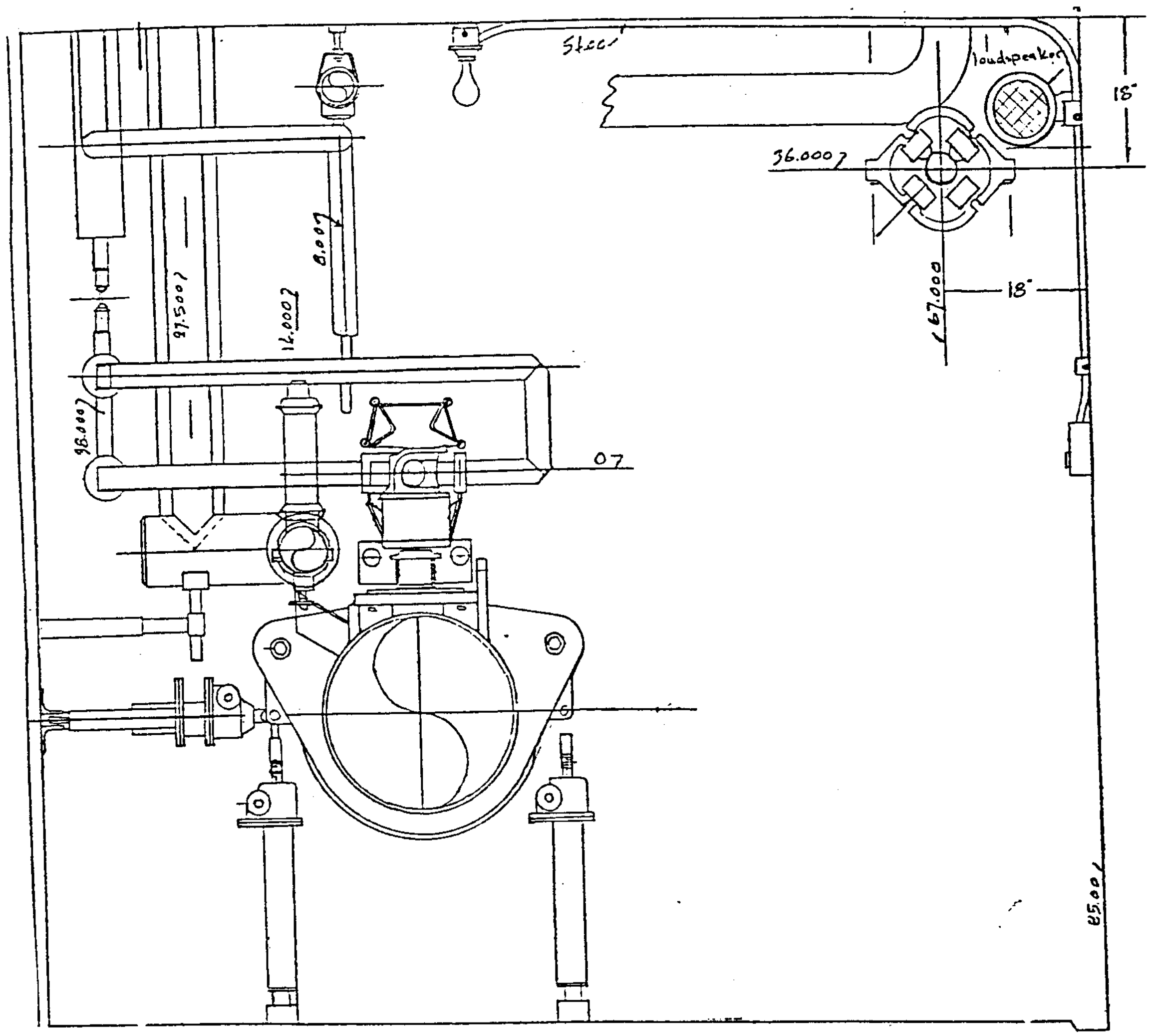

5.2.5.5 West Turn and Inflector: This transport matches from the return line to a 180° turn similar to the east turn but in the horizontal plane. The e^+ beam is brought down to the linac by a 12° bend and recombined with the e^- beam by an upward 12° bend. The combined west turn and inflection system is made isochronous by slightly over compensating the path length dispersion of the west turn.

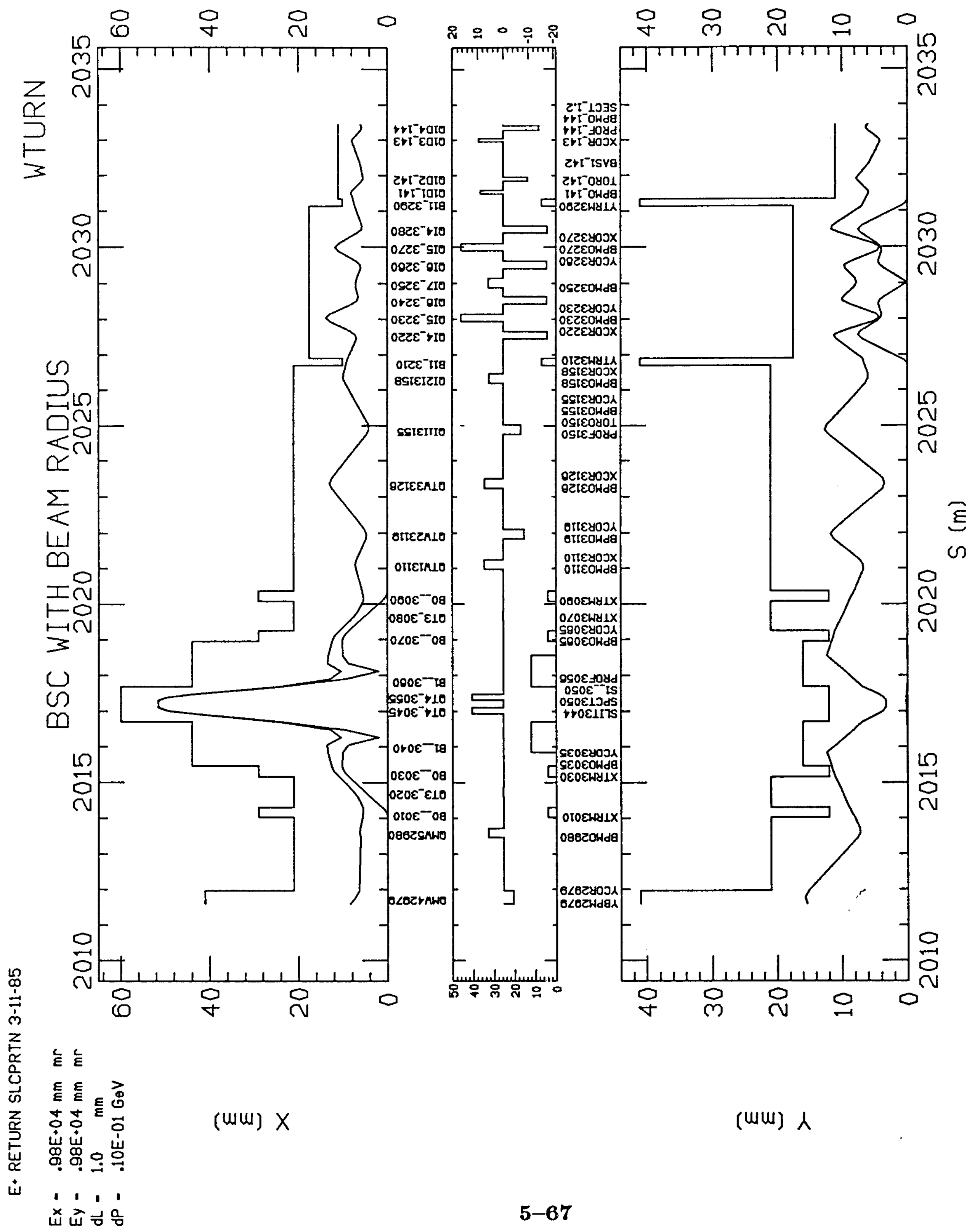

Figure 5.2.5.5.1

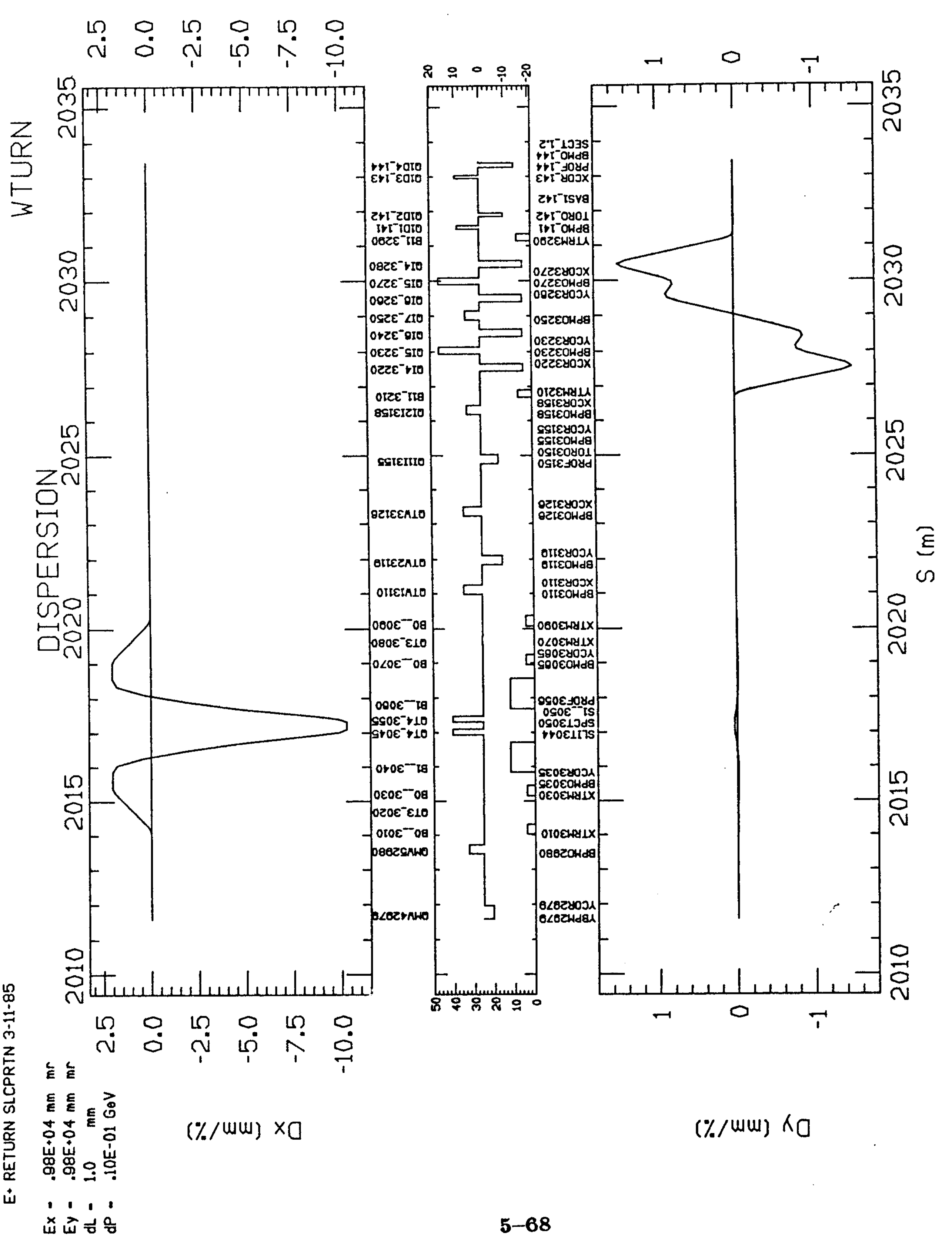

Figure 5.2.5.5.2

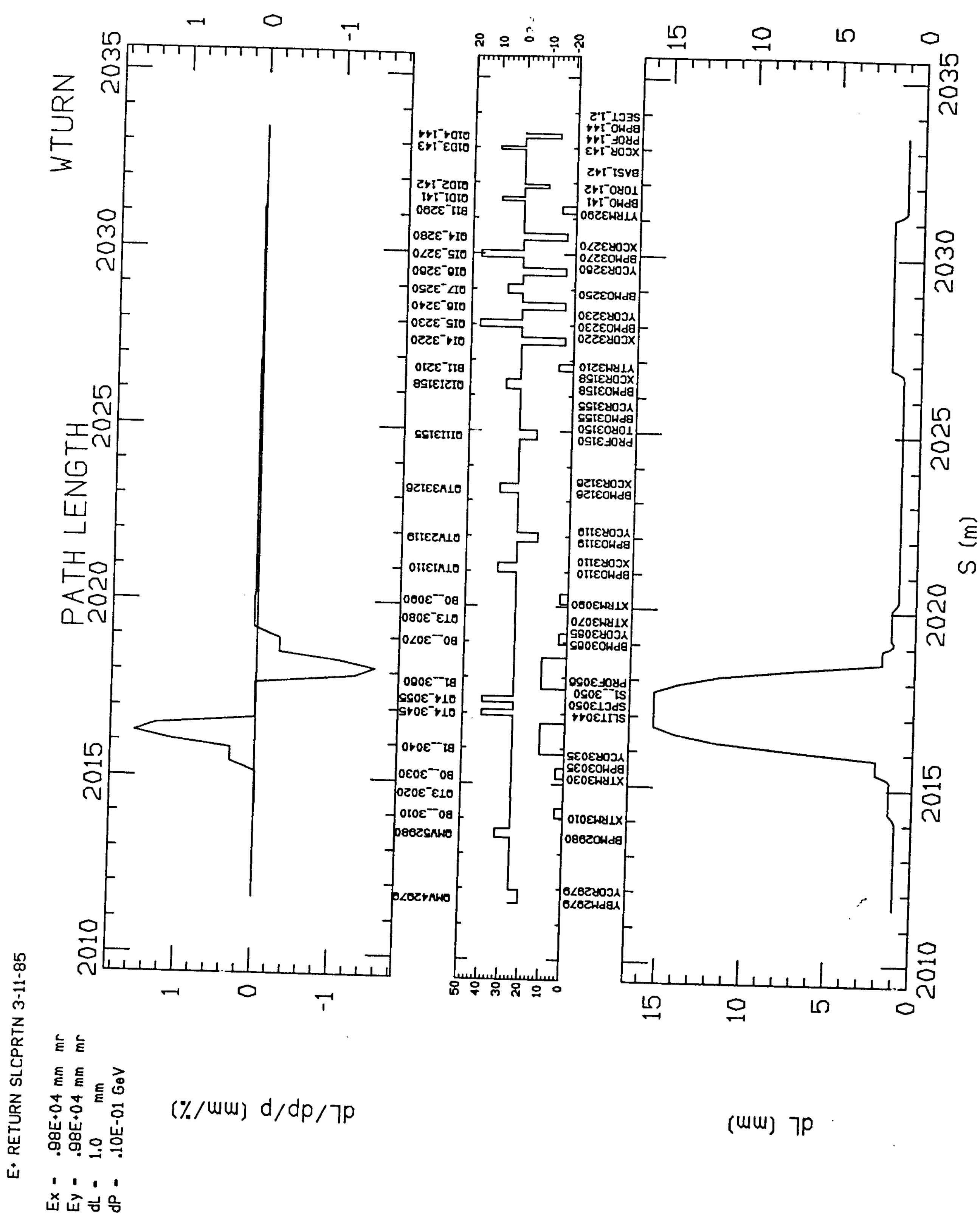

Figure 5.2.5.5.3

Figure 5.2.5.5.4 TURTLE plots at reinjection into Sector 1. Initial number of electrons on target = 327. Relative yield = 2.2 e+/e-. Transmission through Return Line = 81 %.

Figure 5.2.5.5.4.1 Horizontal phase plane.

```
           TWO DIMENSIONAL PLOT OF    X' (mr) VS    X (mm)

                       -10.000      0.000     10.000 TOTALS
                          I**---**---**---**---**I--------
 -5.000 TO  -4.500 I                1        I       1
 -4.500 TO  -4.000 I            1  121       I       5
 -4.000 TO  -3.500 I             11231221    I      13
 -3.500 TO  -3.000 I            1 1 551 2    I      15
 -3.000 TO  -2.500 I             1153656     I      27
 -2.500 TO  -2.000 I           1217A38241    I      39
 -2.000 TO  -1.500 I            233626B2     I      35
 -1.500 TO  -1.000 I          1151ACF624     I      57
 -1.000 TO  -0.500 I          466ACG98442    I      81
 -0.500 TO  -0.000 I          146AAI89941    I      80
 -0.000 TO   0.500 I         2 27GFAD911     I      76
  0.500 TO   1.000 I           345CKK9342    I      82
  1.000 TO   1.500 I           156DA7922     I      55
  1.500 TO   2.000 I         1217B992612     I      51
  2.000 TO   2.500 I         244769643       I      45
  2.500 TO   3.000 I           2267323 1     I      26
  3.000 TO   3.500 I           12133411      I      16
  3.500 TO   4.000 I           2131412       I      14
  4.000 TO   4.500 I             3 2 1       I       6
  4.500 TO   5.000 I           1             I       1
                          I**---**---**---**---**I--------
                          I                      I
                          I                      I
                          I          11          I
                          I       2369129743     I
                   TOTALS I 00005174989257170000 I     725

      TOTAL NUMBER OF ENTRIES =         729 INCLUDING UNDERFLOW AND OVERFLOW

                              UNDERFLOW        OVERFLOW
                   ACROSS          0               0
                   DOWN            3               1

  SUM OF SQUARES =       6155.

      CENTER =        0.167    RMS HALF WIDTH =       2.256

      CENTER =        0.049    RMS HALF WIDTH =       1.817
      CORRELATION =    -0.4230
 NO  22 TWO DIMENSIONAL PLOT OF
              X IN MM     2033.382 M    FROM THE TARGET
             X' IN MR     2033.382 M    FROM THE TARGET
```

Figure 5.2.5.5.4.2 Vertical phase plane.

```
        TWO DIMENSIONAL PLOT OF    Y' (mr) VS    Y (mm)

                 -10.000     0.000     10.000 TOTALS
                  I**---**---**---**---**I--------
-10.000 TO  -9.000 I                       I     0
 -9.000 TO  -8.000 I                       I     0
 -8.000 TO  -7.000 I                       I     0
 -7.000 TO  -6.000 I                       I     0
 -6.000 TO  -5.000 I                       I     0
 -5.000 TO  -4.000 I                       I     0
 -4.000 TO  -3.000 I      12 7524151       I    28
 -3.000 TO  -2.000 I    22446655746211     I    55
 -2.000 TO  -1.000 I    2287F7CBF96641     I   105
 -1.000 TO   0.0   I    137GBQWKDF97311    I   165
  0.0   TO   1.000 I    347EEHUMLQD45      I   180
  1.000 TO   2.000 I     528GGF8FB953      I   113
  2.000 TO   3.000 I     23774787745       I    61
  3.000 TO   4.000 I      23343211 1       I    20
  4.000 TO   5.000 I          2            I     2
  5.000 TO   6.000 I                       I     0
  6.000 TO   7.000 I                       I     0
  7.000 TO   8.000 I                       I     0
  8.000 TO   9.000 I                       I     0
  9.000 TO  10.000 I                       I     0
                  I**---**---**---**---**I--------
                  I                       I
                  I                       I
                  I          1            I
                  I     136781787531      I
          TOTALS  I 00088412718342163100 I   729

        TOTAL NUMBER OF ENTRIES =        729 INCLUDING UNDERFLOW AND OVERFLOW

                            UNDERFLOW       OVERFLOW
                 ACROSS             0              0
                 DOWN               0              0

 SUM OF SQUARES =      9779.

        CENTER =     -0.140   RMS HALF WIDTH =       2.752

        CENTER =      0.014   RMS HALF WIDTH =       1.598
        CORRELATION =     -0.0391
NO  23 TWO DIMENSIONAL PLOT OF
            Y IN MM     2033.382 M    FROM THE TARGET
           Y' IN MR     2033.382 M    FROM THE TARGET
```

Figure 5.2.5.5.4.3 Longitudinal phase plane.

```
         TWO DIMENSIONAL PLOT OF DP/P (%)  VS   DL (mm)

                   -10.000    -5.000    -0.000     5.000 TOTALS
                    I**---**---**---**---**---**---**I--------
-10.000 TO  -9.000 I                                 I       0
 -9.000 TO  -8.000 I                                 I       0
 -8.000 TO  -7.000 I                                 I       0
 -7.000 TO  -6.000 I                                 I       0
 -6.000 TO  -5.000 I                                 I       0
 -5.000 TO  -4.000 I                                 I       0
 -4.000 TO  -3.000 I              1                  I       1
 -3.000 TO  -2.000 I       11112331  11              I      15
 -2.000 TO  -1.000 I  1   36367ADHAEFD63             I     127
 -1.000 TO   0.000 I       2589DEEIEGAC93            I     147
  0.000 TO   1.000 I      1249DAAB98HB885            I     126
  1.000 TO   2.000 I       256CCBCGE8CCA4            I     136
  2.000 TO   3.000 I      13426G8AAE56753            I     100
  3.000 TO   4.000 I       11342595A5911             I      56
  4.000 TO   5.000 I        1  2422323               I      19
  5.000 TO   6.000 I         1  1                    I       2
  6.000 TO   7.000 I                                 I       0
  7.000 TO   8.000 I                                 I       0
  8.000 TO   9.000 I                                 I       0
  9.000 TO  10.000 I                                 I       0
                   I**---**---**---**---**---**---**I--------
                   I                                 I
                   I                                 I
                   I                                 I
                   I       12356677766431            I
            TOTALS I 01005746279817957650000000000  I     729

        TOTAL NUMBER OF ENTRIES =        729 INCLUDING UNDERFLOW AND OVERFLOW

                               UNDERFLOW       OVERFLOW
                   ACROSS             0              0
                   DOWN               0              0

  SUM OF SQUARES =      7495.

        CENTER =     -3.940   RMS HALF WIDTH =      1.640

        CENTER =      0.680   RMS HALF WIDTH =      1.694
        CORRELATION =     0.0392
NO  24 TWO DIMENSIONAL PLOT OF
           DL IN MM     2033.473 M     FROM THE TARGET
        DP/P IN PC      2033.473 M     FROM THE TARGET
```

5.2.5.6 Sector 1 Focusing: In order to constrain the large e^+ emittance to the available aperture and overpower transverse wake fields, an energy-graded F0D0 array is used. Seventy-two quadrupoles of maximum strength 15 kG (gradient $\times$ length) have been placed around the linac structure. In order to minimize interference with existing structures, the spacings of quadrupoles deviate slightly from that of an ideal graded F0D0 array due to linac physical constraints.

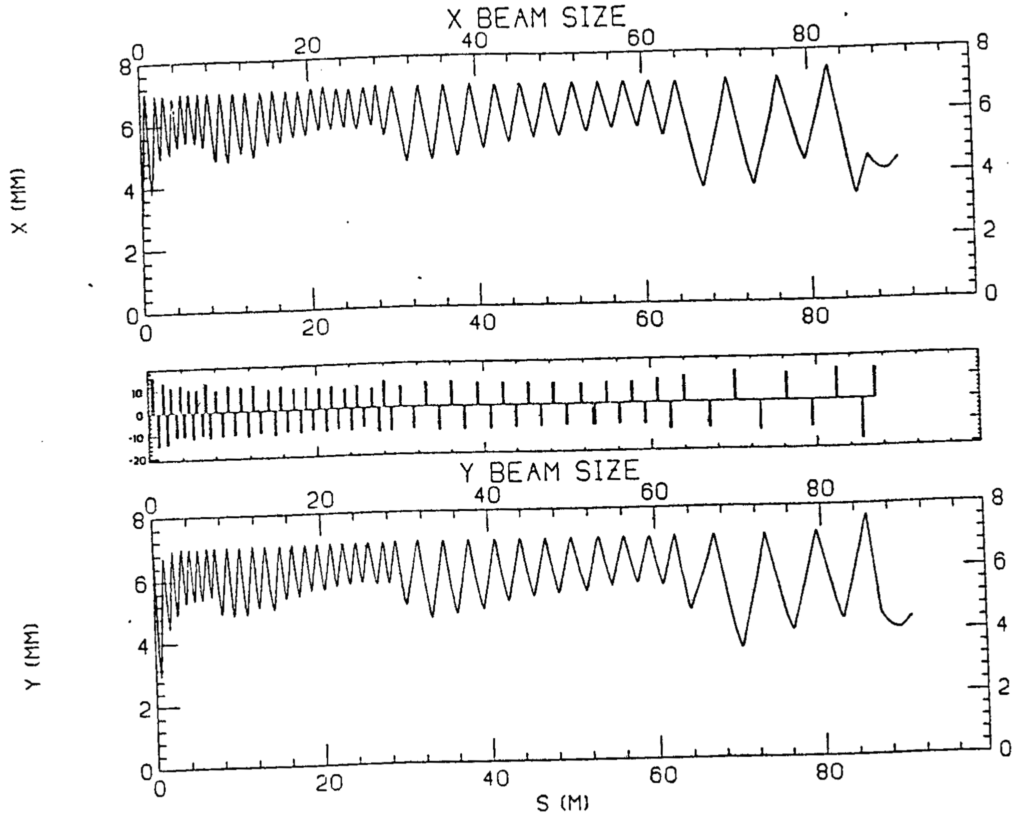

Figure 5.2.5.6.1

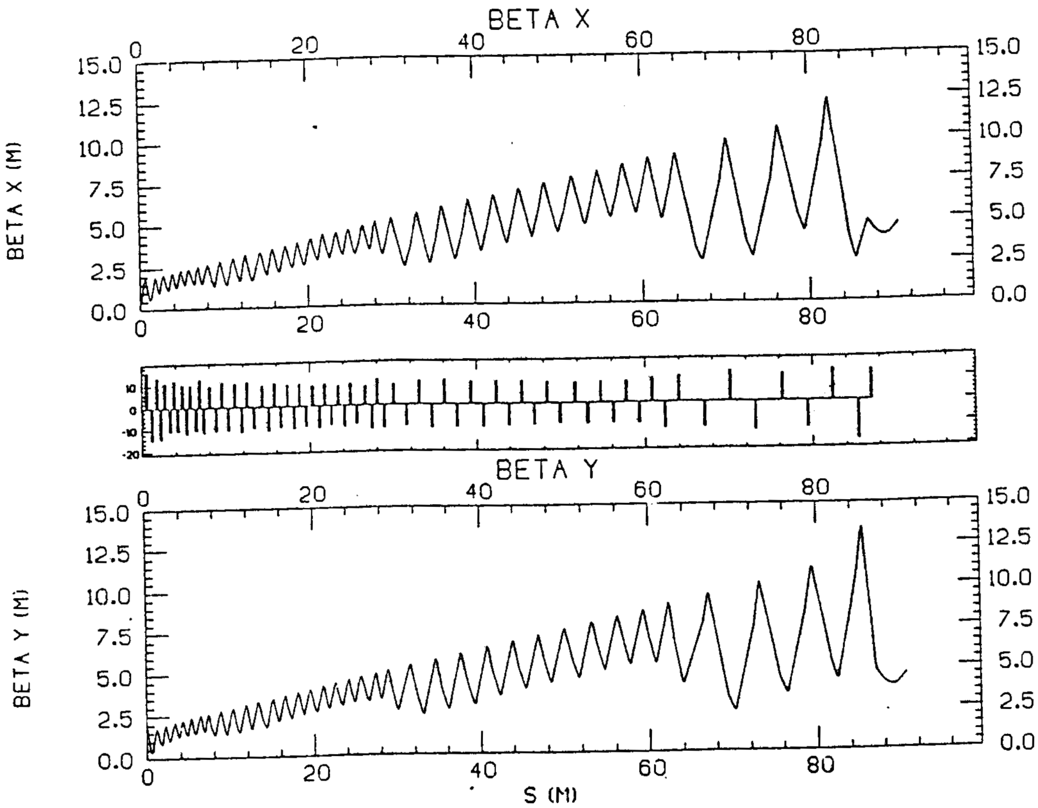

Figure 5.2.5.6.2

5.2.6 Flux Concentrator:

The flux concentrator is a pulsed magnet producing an axially tapered magnetic field with a maximum value of 6 T. The magnet immediately follows the target and acts as a short focal length lens in order to collect the highly divergent positrons.

A cross section of the magnet is shown schematically in Fig. 5.2.6.1. The body of the magnet core is a copper slug 120 mm long with a radius of 37 mm. The throat of the core tapers from a radius of 3.5 mm with a slope of 0.233 to about 31 mm. The coil consists of a total of 13 turns of water cooled copper conductor, and is wound in two halves so that both the outside ends remain at ground potential while the high voltage is applied at the center. This is done to reduce breakdown problems as well as to reduce the length of the water passage.

The magnet is powered by a resonant, pulsed supply; the resonant frequency of the charging capacitor and the magnet is of the order of 15 kHz. The supply delivers a half sine-wave at a repetition rate of 180 Hz with a peak current of 32 kA and a peak potential of 2 kV for a total input power to the magnet of about 80 kW. For test purposes a SLAC test lab klystron modulator will be modified to power the magnet. Design for a normal pulsed supply is under way.

The power dissipated in the magnet is estimated to about 50 kW of electrical power plus a significant fraction of the beam power. The electrical dissipation has been estimated from measurements of the Q of a prototype magnet. Estimates of the beam power dissipation are still in progress; we have assumed 25 kW for design purposes, which should be conservative.

Removing the total amount of heat from the magnet by water cooling presents no particular problems; the main concern is in local heating of the magnet core. It is estimated that about 4 kW due to eddy current heating will be dissipated in the first 5 mm of the throat of the core throat.

Instantaneous temperature rise in the coil is of the order of 1°C, and exterior of the core is of the order of 5° and present no problem. The throat of the core is estimated to have a maximum instantaneous temperature rise of 40°C. This may present long term fatigue problems; tests are required.

Prototype magnets operating at reduced current and repetition rate have been constructed to measure magnetic fields and make general design tests. A full scale prototype magnet is being built to test the design at full current. These will be especially useful to measure heat dissipation in the core.

The coil is mechanically constrained by a surrounding band to contain the radial force per unit length of coil of 5×10^4 nt/m at full current. The mechanical constraint poses no particular problems, but it must not form a shorted turn which would decrease the magnetic field in the concentrator. A mechanical design for this exists.

SLC Positron Source
Flux Concentrator and Clamp

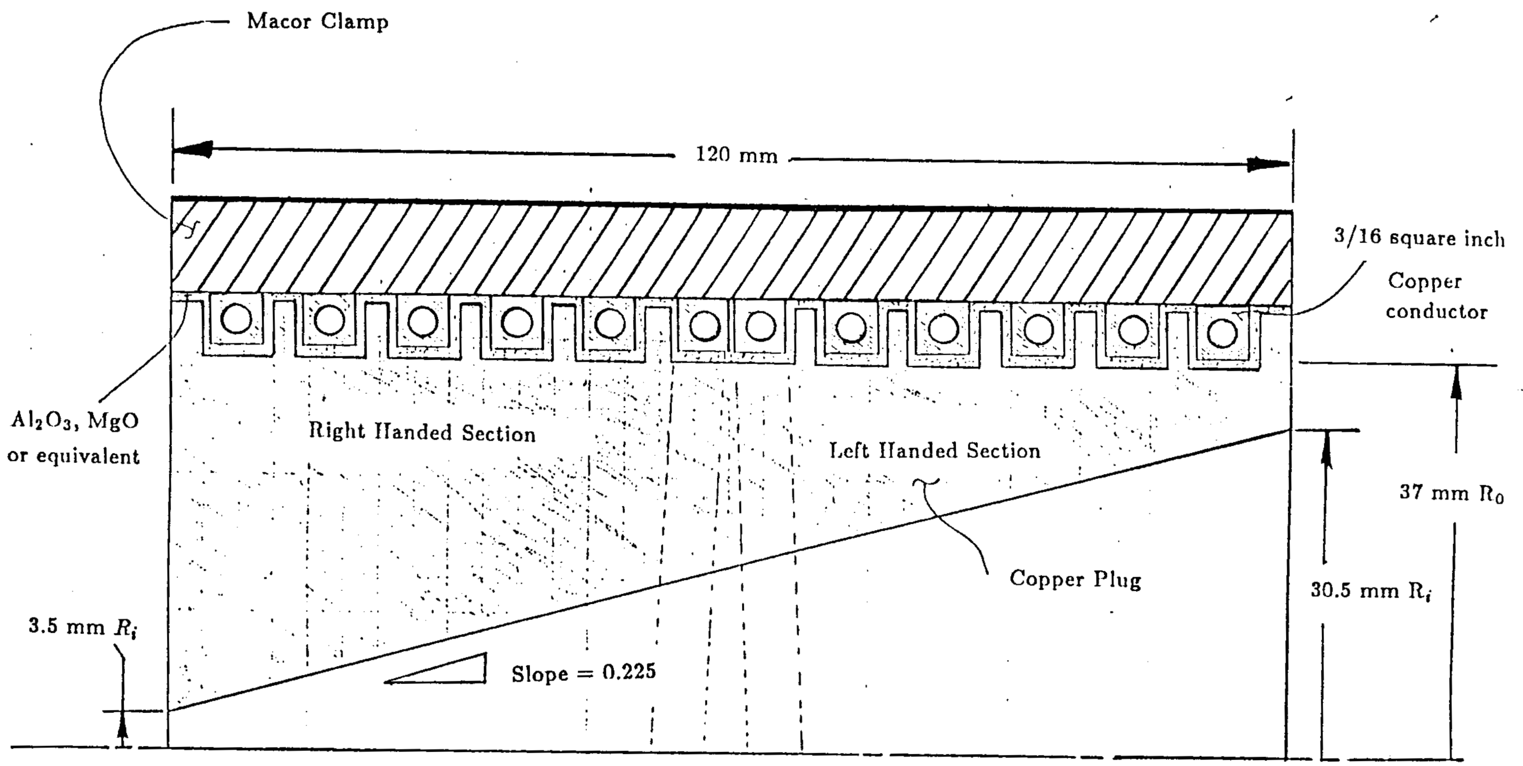

Figure 5.2.6.1

5.2.7 Index of SLAC Linear Collider Notes Relating to the e^+ Source

21	Temperature Calculations for the Positron Target	H. DeStaebler	03-31-80
22	Tapered Solenoid for SPC Positron Source	D. Sherden	05-08-80
23	Calculations for Positron Target Test in ESA	H. DeStaebler	05-15-80
24	More Calculations for Positron Target Test in ESA	H. DeStaebler	06-04-80
25	Considerations with Respect to e^+ Emittance	S. Ecklund	09-11-80
128	Positron Target Materials Tests	S. Ecklund	10-20-81
135	Energy Deposition and Thermal Heating in Materials due to low Emittance Electron Beams	S. Ecklund/ R. Nelson	12-08-83
221	A Note on Shielding the SLC Positron Source	T. Jenkins	04-21-83
226	Radioactive Air & Ozone in the Positron Source Tunnel	T. Jenkins	05-28-83
250	Engineering Basis for Selection of Positron Source Material	B. Feerick	10-10-83
253	Positron Acceleration to 200 MeV	H. Leboutet	11-11-83
262	Temperature Rise in Lambertsen Septum Magnet Assoc with Positron Target	W. Nelson/ T. Jenkins	01-06-84
268	Positron Source: First 50 Nanoseconds	K. Moffeit	05-22-84
277	The Positron Flux Consentrator and update	F. Bulos	08-09-84
282	Notes on RF System for SLC e+ Source	H. Hoag	09-20-84
295	Additional Muon Calculations for the SLC Positron Source	W.R. Nelson/ R.C. McCall	04-23-85

REFERENCES

1. C.K. Sinclair and R.H. Miller, "A High Current, Short Pulse, RF Synchronized Electron Gun for the Stanford Linear Accelerator," IEEE Trans. Nucl. Sci., **NS-28** (1981), 2649 (SLAC-PUB-2705).
2. R.F. Koontz, "CID Thermionic Gun System," Proc. of the 1981 Linear Acc. Conf., Santa Fe (1981), 62. (SLAC-PUB-2824).
3. M.J. Browne, J.E. Clendenin, P.L. Corredoura, et al., "A Multi-Channel Pulser for the SLC Thermionic Electron Source," to be published. (SLAC-PUB-3546).
4. M.B. James and R.H. Miller, "A High Current Injector for the Proposed SLAC Linear Collider," IEEE Trans. Nucl. Sci., **NS-28** (1981), 3461. (SLAC-PUB-2701).
5. M.B. James, J.E. Clendenin, S.D. Ecklund, et al., "Update on the High-Current Injector for the Stanford Linear Collider," IEEE Trans. Nucl. Sci., **NS-30** (1983), 2992. (SLAC-PUB-3085).
6. J.E. Clendenin, S.D. Ecklund, M.B. James, et al., "Making Electron Beams for the SLC Linac," Proc. of the 1984 Linear Acc. Conf., Seeheim (1984), 457. (SLAC-PUB-3285).
7. R.L. Ford, W.R. Nelson, "The EGS Code System: Computer Programs for the Monte Carlo Simulation of Electromagnetic Cascade Showers," (1978), SLAC Report No. 210.
8. R.B. Neal, ed., **The Stanford Two-Mile Accelerator**, W.A. Benjamin, Inc., New York (1968), pp. 551-560; R. Helm, SLAC Report No. 4.
9. Y.B. Kim, and E.D. Platner, Rev. Sci. Instrum. **30**, 524 (1959); M.N. Wilson, K.D. Srivasta, Rev. Sci. Instrum. **36**, 1096 (1965).
10. K. Moffeit, "Positron Source: first 50 nanoseconds," Collider Note 268, May, 1984.
11. B. Aune, R.H. Miller, Proceedings of 1979 Linear Accelerator Conference. BNL-51134; (SLAC-PUB-2393).

CHAPTER 6.
DAMPING RING AND BUNCH COMPRESSOR

6. DAMPING RING AND BUNCH COMPRESSOR

6.1 INTRODUCTION

The primary purpose[1] of damping rings is to reduce the transverse phase spaces of positron and electron beams to suitably small values at the injection end of a linear collider such that their bunches, when accelerated to high energies, can be made to collide with high luminosity. Further, longitudinal bunch length control must be provided to minimize wake field effects in the accelerator. Finally, it is desirable to provide a means of preserving and manipulating the spin polarization of the electron beam.

The following description pertains primarily to the first SLC damping ring which was made operational in 1983. the second ring is identical in concept and major features, but differs in some details. These dissimilarities are due to differing requirements for the two beams and some improvements that were indicated by experience with the first ring.

6.1.1 Choice of Ring Parameters

Taking as given[2] that positrons are created at the converter with an invariant emittance of about $\epsilon = 5\pi$ (MeV/c) mm, and that the design luminosity requires (before certain emittance growths are accounted for) an invariant emittance of 0.015π (MeV/c) mm, a transverse phase space reduction of about 300 is needed. The damping time must be in the millisecond region, since the Collider will operate at 180 Hz. The interplay between damping ring energy E_D, bending radius r_D, field B_D, the number of bunches per ring n_B, the number of rings n_M, the time between bunches t_B, the total beam current i_D (assuming 5×10^{10} particles/bunch) has been parameterized[3] as a function of bending magnet length for a separated function lattice and is shown in Fig. 6.1.1.

Combining this parameterization with the physically realizable values of magnetic fields, gradients and practical rise and fall times for injection and extraction kickers leads to the ring parameters shown in Table 6.1.1. Two bunches circulate in each ring in diametrically opposite buckets. For the positron case,

the two buckets are filled and emptied on alternating accelerator pulses. Hence, the positrons spend 11.1 ms or 3.6 damping times in the ring. For the electron case, less damping is required, so two bunches are simultaneously injected and extracted each 5.6 ms, the second bunch being used to subsequently generate positrons for refilling the emptied positron bucket.

Figure 6.1.1 Parameterization for Design

ρ:	bending radius	t_B:	time between bunches
E_D:	energy	$n_D = n_B n_m$:	total number of bunches
B_D:	bending field	n_B:	number of bunches per damping ring
i_D:	total beam current (5 × 10^{10} particles/bunch)	n_m:	number of damping rings

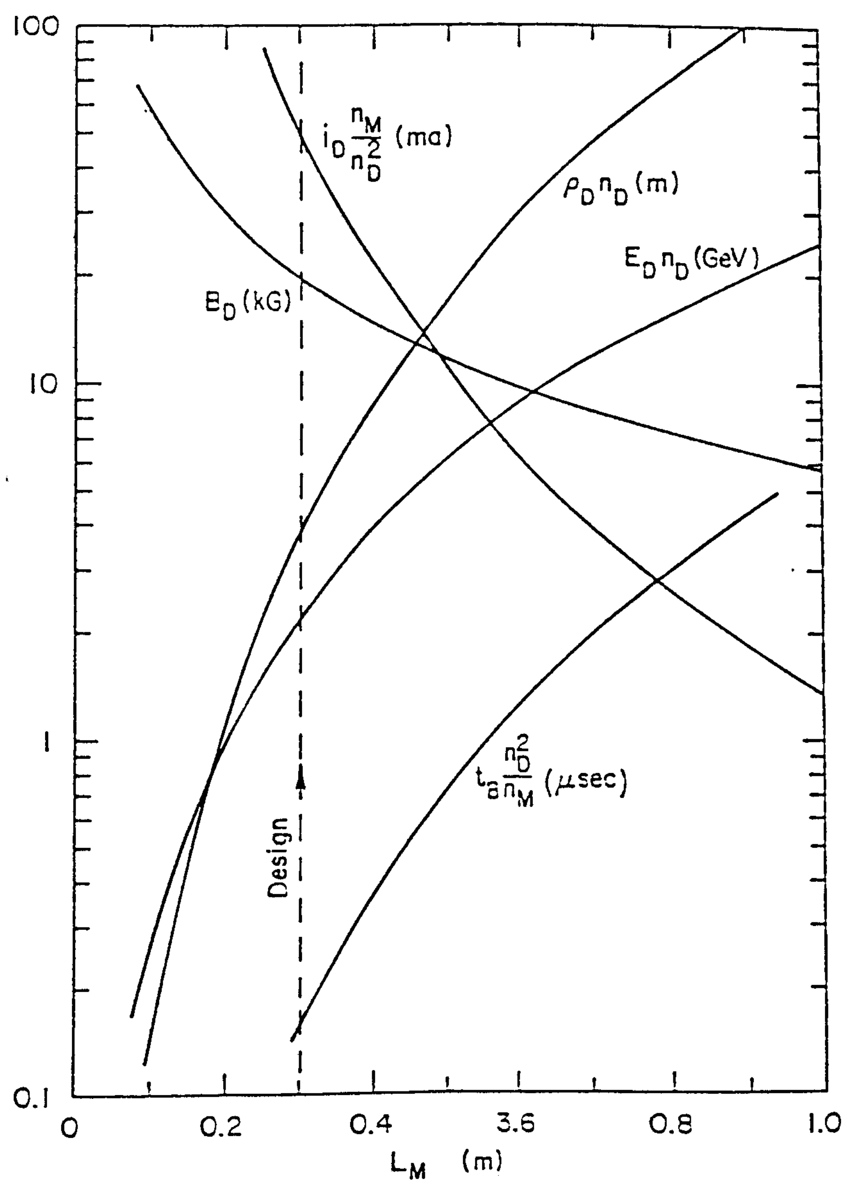

Table 6.1.1 General Design Parameters for the Damping Rings		
Energy	1.210	GeV
Circumference	35.270	m
Revolution Frequency	8.5	MHz
RF Frequency	714.000	MHz
Harmonic Number	84	
Transverse Damping Time	3.059	msec
Equilibrium Emittance		
(with full coupling)	9.1×10^{-9}	π rad m
Equilibrium rel. Energy spread	7.3×10^{-4}	
Momentum Comp. Factor	.01814	
Energy loss/Turn	93.1	keV
Bending Radius	2.0372	m
Bending Field	19.812	k gauss
CELL - Structure	1/2 FODO 1/2 F	
ν_x	~ 7.25	variable
ν_y	~ 3.25	variable
Acceptance		
in phase space	$\geq 4.13 \times 10^{-6}$	π rad m
in energy	$\geq \pm 1\%$	
RF System and Related Parameter		
RF - voltage	800	kV
phase	6.7°	
Synchrotron Frequency	107.3	kHz
tune	.0126	
Equilibrium Bunch length	5.9	mm
$\epsilon_c =$	1.9283	keV
I (2 bunches)	136.2	ma
P (synchrotron rad.)	12.68	kW

6.1.2 General Features and Layout

The first damping ring is located on the south side of the west end of the linac near the juncture of Sector 1 and Sector 2. The geometry of this complex is shown in Figure 6.1.2.1. A second ring, now under construction and not shown in the figure, will lie on the north side of the linac. The plan view of this second ring will be almost a perfect mirror image of the south ring with the linac beam line being the axis of symmetry. The insert in the figure depicts how particles of opposite charge are extracted and reinjected into the accelerator in the presently limited space between linac sectors. The scheme employs two horizontally bending dipole magnets. The upstream magnet is the extraction dipole which bends electrons (positrons) to the south (north) into the entrance of the linac-to-Ring (LTR) transport line. For stability during collider operation this magnet will operate dc, but for ring tests it is pulsed to provide interlacing with beams for the other linac programs. The downstream or reinjection magnet is designed for dc operation only. It, again, bends returning beams of opposite charge in opposite directions so that they both exit in a direction collinear with the center line of the linac wave guide. When this magnet is operating the the damping rings become the only sources of beams for the linac sectors downstream of Sector 1.

The south ring and those parts of its transport lines outside of the linac housing lie in a common level plane at an elevation 36 cm below the elevation defined by the height of the undeflected linac beam at the center of the extraction-reinjection region. This elevation for the intial design was chosen to allow the option of building the second ring above the first. The north ring and its corresponding transport lines will also lie in a common level plane, but at an elevation 4 cm above the previously defined point, an optimal height for minimizing vertical deflections in the second order optical design of the return line.

Both rings reside in concrete vaults some 35 ft. below grade. The south transport lines are housed in eight-ft diameter corrugated steel tunnels, while those on the north are hosed in ten-ft square concrete tunnels.

Figure 6.1.2

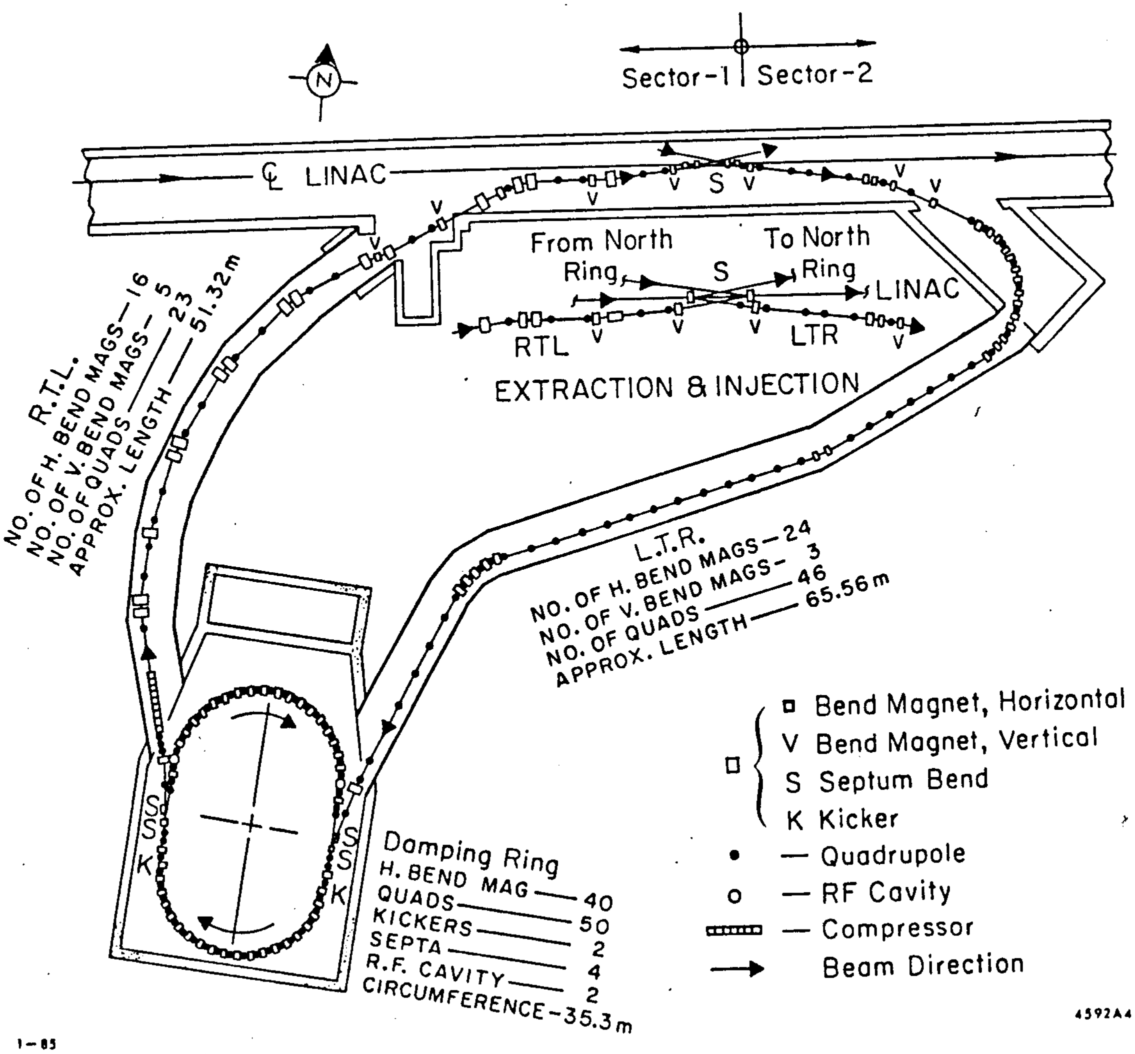

Sector-1
Sector-2
N
℄ LINAC
From North Ring
To North Ring
LINAC
S
RTL
LTR
EXTRACTION & INJECTION
R.T.L.
NO. OF H. BEND MAGS—16
NO. OF V. BEND MAGS—5
NO. OF QUADS—23
APPROX. LENGTH—51.32m
L.T.R.
NO. OF H. BEND MAGS—24
NO. OF V. BEND MAGS—3
NO. OF QUADS—46
APPROX. LENGTH—65.56m
Damping Ring
H. BEND MAG—40
QUADS—50
KICKERS—2
SEPTA—4
R.F. CAVITY—2
CIRCUMFERENCE—35.3m
Bend Magnet, Horizontal
V Bend Magnet, Vertical
S Septum Bend
K Kicker
— Quadrupole
— RF Cavity
— Compressor
Beam Direction
1-85
4592A4

6.2 DAMPING RING

The global design parameters for the damping ring have been previously given in Table 6.1.1. Figure 6.2.1 shows the ring and important components in greater detail. In this figure the two injection and two extraction septa magnets are labeled with the prefix SB, the two kicker magnets with the prefix K, and the two RF cavities with prefix RFC. The nominal design betatron and dispersion functions of the ring are shown in Figure 6.2.2. A complete listing of the Twiss parameters at the exit of each element as generated by the machine modeling code COMFORT[4] is given in Table 6.2.1. The position of all orbit correctors[5–6] and beam position monitors are included in this deck for the purpose of modeling closed orbit corrections. The bend magnet cross section is shown in Figure 6.2.3. The field in the 2 cm gap is 19.8 kG and the effective length is 32 cm. The good field region where $|\delta B/B| < 0.1\%$ extends over ± 1.0 cm in the horizontal plane.

Quadrupoles which bear a common name in the COMFORT deck are bussed in six families so that their strengths can be varied to change tunes and the optical properties of the insertion. It is intended to run the machine on the coupling resonance $\nu_x - \nu_y = 4$ to minimize the beam emittance. The cross section of a typical laminated quadrupole is shown in Figure 6.2.4. The bore of the quadrupoles in the arc lattice is 25.8 mm. The bore of the four insertion quadrupoles and the four matching quadrupoles is 51.5 mm and 35.4 mm, respectively.

Sextupoles are introduced at the ends of each bending magnet by pole face shaping to correct the natural chromaticities from ≈ -9 to $\approx +0.5$. In addition, four discrete sextupoles ($S_F \approx S_D \leq 25\, m^{-2}$) powered in pairs are used to trim the chromaticity.

Figure 6.2.1 Damping Ring Components

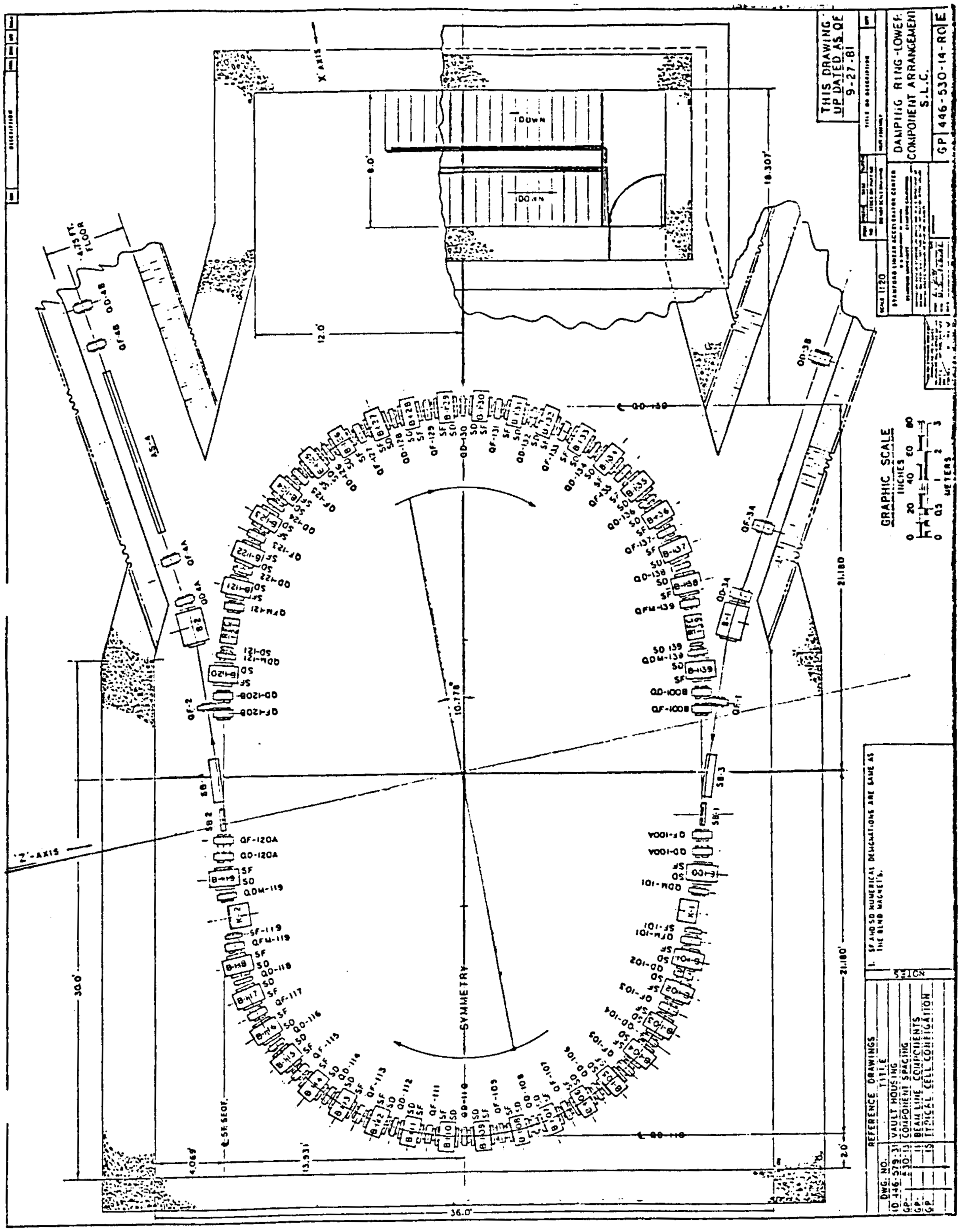

Figure 6.2.2 Nominal Betatron and Dispersion Functions

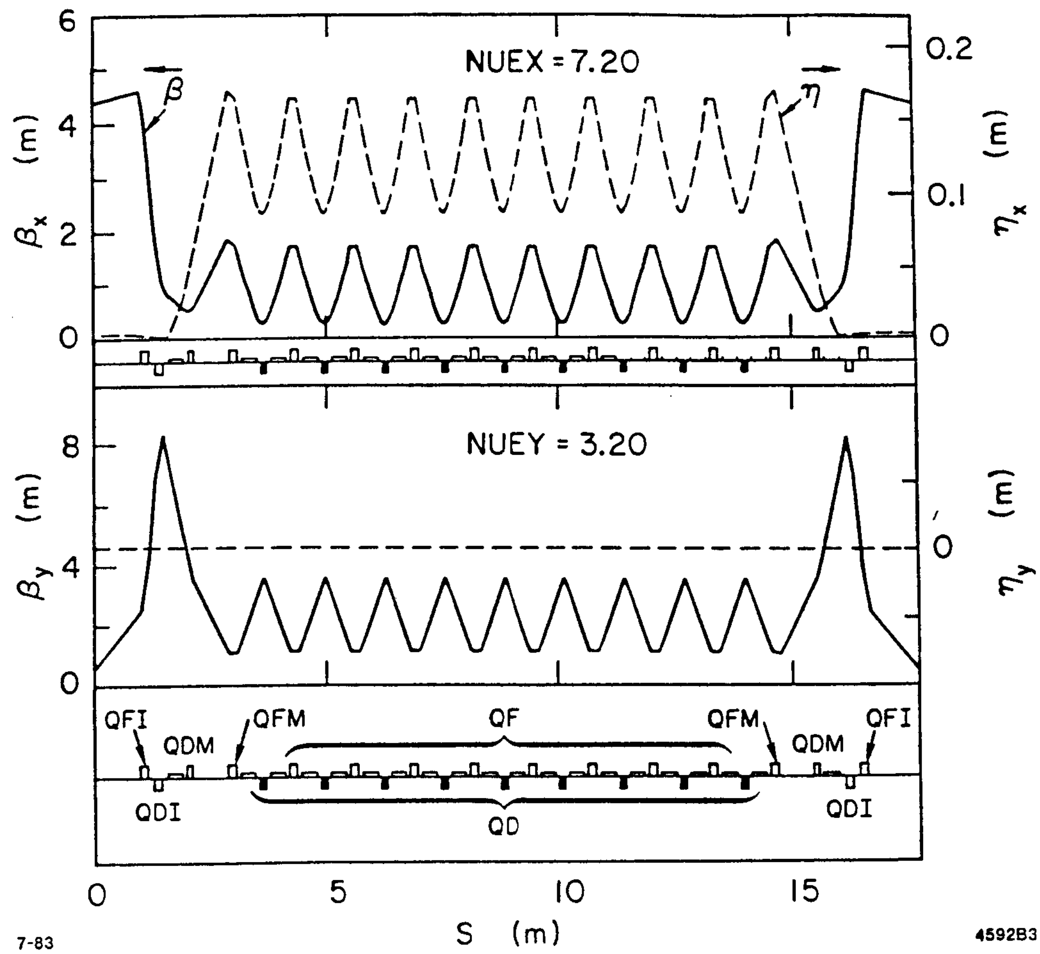

Table 6.2.1

```
C
C                   "COMFORT" INPUT DECK --> "MIZANEWP.DAT"
C                   ---------------------------------------
C
C                   Damping Ring: With new effective magnet lengths and
C                   bend endfield corrections as per H. Wiedemann
C                   (3-9-83); quads at new design lattice values for
C                   E=0.957822 GeV.
C
C-----------------------------------------------------------------------
C
      NUM           NSTP CIJ
                    0    1
          *         P0
                    0.957822
      DRF *         D0        D1        D2        D3        D4A
                    1.0267    0.1473    0.1516    0.1067    0.3337
          *         D4B       D4C       D4D       D5        DQD
                    0.4302    0.4147    0.3492    0.0962    0.0977
          *         DQF       SYMM      KICK      LTR       CELL
                    0.0962    0.0000    0.0000    0.0000    0.0000
          *         RTL       RFCW
                    0.0000    0.0000
C
      BBX *         B         BH
                    0.0000    0.0000
                    0.3200    0.1600
                    9.0000    4.5000
C
      EDG *         E         EH
                    -4.44516  -4.44516
C
      QUA *         QFH       QDH       QFIH      QDIH      QFMH
                    -15.52592 18.32565  -10.48429 15.39309  -12.90218
                    0.0828    0.0493    0.0843    0.0684    0.0828
          *         QDMH
                    -0.74350
                    0.0493
C
      RPL  EHBH     EH   BH
           BHEH     BH   EH
           EBE      E    B    E
C
      MON X         BPMX
      MON Y         BPMY
      COR X         XCOR
      COR Y         YCOR
      SEX           SF   SD
C
C                   This beamline represents the complete Damping Ring
C                   as found in CN-184. (NOTE: all quadrupoles have
C                   been split in half.)
C
      CEL           SYMM D0   QFIH BPMX BPMY XCOR QFIH D1   QDIH YCOR
                    QDIH D2   EHBH XCOR BHEH D3   QDMH QDMH D4A  KICK
                    D4B  SF   LTR  QFMH BPMX BPMY QFMH D5   EBE  DQD
                    QDH  BPMX BPMY YCOR CELL
                    QDH  DQD  EHBH XCOR BHEH DQF  QFH  QFH
                    DQF  EBE  DQD  QDH  BPMX BPMY
```

Table 6.2.1 Continued

```
QDH  DQD  EHBH XCOR BHEH DQF  QFH  QFH
DQF  EBE  DQD  QDH  BPMX BPMY YCOR
QDH  DQD  EHBH XCOR BHEH DQF  QFH  QFH
DQF  EBE  DQD  QDH  BPMX BPMY
QDH  DQD  EHBH XCOR BHEH DQF  QFH  QFH
DQF  EBE  DQD  QDH  BPMX BPMY YCOR
----------------------------------------------------
QDH  DQD  EHBH XCOR BHEH DQF  QFH  QFH
DQF  EBE  DQD  QDH  BPMX BPMY
QDH  DQD  EHBH XCOR BHEH DQF  QFH  QFH
DQF  EBE  DQD  QDH  BPMX BPMY YCOR
QDH  DQD  EHBH XCOR BHEH DQF  QFH  QFH
DQF  EBE  DQD  QDH  BPMX BPMY
QDH  DQD  EHBH XCOR BHEH DQF  QFH  QFH
DQF  EBE  DQD  QDH  BPMX BPMY YCOR
QDH  DQD  EHBH XCOR BHEH D5   QFMH QFMH RTL  SF
D4B  KICK D4A  QDMH BPMX BPMY QDMH D3   EHBH XCOR
BHEH D2   QDIH YCOR QDIH D1   QFIH BPMX BPMY XCOR
QFIH D0
----------------------------------------------------
SYMM D0   QFIH BPMX BPMY XCOR QFIH D1   QDIH YCOR
QDIH D2   EHBH XCOR BHEH D3   QDMH QDMH SD   D4C
RFCW D4D  QFMH BPMX BPMY QFMH D5   EBE  DQD  QDH
BPMX BPMY YCOR
QDH  DQD  EHBH XCOR BHEH DQF  QFH  QFH
DQF  EBE  DQD  QDH  BPMX BPMY
QDH  DQD  EHBH XCOR BHEH DQF  QFH  QFH
DQF  EBE  DQD  QDH  BPMX BPMY YCOR
QDH  DQD  EHBH XCOR BHEH DQF  QFH  QFH
DQF  EBE  DQD  QDH  BPMX BPMY
QDH  DQD  EHBH XCOR BHEH DQF  QFH  QFH
DQF  EBE  DQD  QDH  BPMX BPMY YCOR
----------------------------------------------------
QDH  DQD  EHBH XCOR BHEH DQF  QFH  QFH
DQF  EBE  DQD  QDH  BPMX BPMY
QDH  DQD  EHBH XCOR BHEH DQF  QFH  QFH
DQF  EBE  DQD  QDH  BPMX BPMY YCOR
QDH  DQD  EHBH XCOR BHEH DQF  QFH  QFH
DQF  EBE  DQD  QDH  BPMX BPMY
QDH  DQD  EHBH XCOR BHEH DQF  QFH  QFH
DQF  EBE  DQD  QDH  BPMX BPMY YCOR
QDH  DQD  EHBH XCOR BHEH D5   QFMH QFMH D4D  RFCW
D4C  SD   QDMH BPMX BPMY QDMH D3   EHBH XCOR BHEH
D2   QDIH YCOR QDIH D1   QFIH BPMX BPMY XCOR QFIH
D0
```

*VALUE OF ...ISS PARAMETERS AT THE EXIT OF EACH ELEMENT:

ELEM	S[M]	PHI[DEG]	K[1/M2]	NUX	NUY	BX[M]	BY[M]	EX[M]	EY[M]	AX	AY	EX'	EY'
BEG	0.0000	0.0000	0.000000	0.00000	0.00000	4.39997	0.53288	0.00434	0.000	0.00000	0.00000	0.00000	0.000
SYMM	0.0000	0.0000	0.000000	0.00000	0.00000	4.39997	0.53288	0.00434	0.000	0.00000	0.00000	0.00000	0.000
D0	1.0267	0.0000	0.000000	0.03648	0.17380	4.63954	2.51101	0.00434	0.000	-0.23334	-1.92669	0.00000	0.000
QFIH	1.1110	0.0000	-10.484290	0.03944	0.17871	4.34136	3.05768	0.00418	0.000	3.68223	-4.71835	-0.00379	0.000
BPMX	1.1110	0.0000	0.000000	0.03944	0.17871	4.34136	3.05768	0.00418	0.000	3.68223	-4.71835	-0.00379	0.000
BPMY	1.1110	0.0000	0.000000	0.03944	0.17871	4.34136	3.05768	0.00418	0.000	3.68223	-4.71835	-0.00379	0.000
XCOR	1.1110	0.0000	0.000000	0.03944	0.17871	4.34136	3.05768	0.00418	0.000	3.68223	-4.71835	-0.00379	0.000
QFIH	1.1953	0.0000	-10.484290	0.04286	0.18251	3.45866	4.18226	0.00371	0.000	6.52739	-8.95148	-0.00730	0.000
D1	1.3426	0.0000	0.000000	0.05223	0.18677	1.80924	7.24026	0.00264	0.000	4.67023	-11.80886	-0.00730	0.000
QDIH	1.4110	0.0000	15.393090	0.05933	0.18815	1.33311	8.35883	0.00223	0.000	2.45710	-4.15006	-0.00476	0.000
YCOR	1.4110	0.0000	0.000000	0.05933	0.18815	1.33311	8.35883	0.00223	0.000	2.45710	-4.15006	-0.00476	0.000
QDIH	1.4794	0.0000	15.393090	0.06842	0.18944	1.10424	8.32198	0.00198	0.000	0.96894	4.67582	-0.00256	0.000
D2	1.6310	0.0000	0.000000	0.09341	0.19261	0.85081	6.96741	0.00159	0.000	0.70276	4.25932	-0.00256	0.000
EH	1.6310	-4.4452	0.000000	0.09341	0.19261	0.85081	6.96741	0.00159	0.000	0.73522	3.99345	-0.00262	0.000
BH	1.7910	0.0785	0.000000	0.12769	0.19663	0.65753	5.75177	0.00745	0.000	0.47032	3.60426	0.07579	0.000
XCOR	1.7910	0.0000	0.000000	0.12769	0.19663	0.65753	5.75177	0.00745	0.000	0.47032	3.60426	0.07579	0.000
BH	1.9510	0.0785	0.000000	0.17046	0.20155	0.55104	4.66068	0.02582	0.000	0.19383	3.21508	0.15373	0.000
EH	1.9510	-4.4452	0.000000	0.17046	0.20155	0.55104	4.66068	0.02582	0.000	0.21486	3.03722	0.15274	0.000
D3	2.0577	0.0000	0.000000	0.20219	0.20547	0.52681	4.03751	0.04212	0.000	0.01229	2.80314	0.15274	0.000
QDMH	2.1070	0.0000	-0.743500	0.21707	0.20748	0.52926	3.77343	0.04961	0.000	-0.06196	2.55682	0.15106	0.000
QDMH	2.1563	0.0000	-0.743500	0.23177	0.20963	0.53901	3.53270	0.05701	0.000	-0.13575	2.32899	0.14911	0.000
D4A	2.4900	0.0000	0.000000	0.31436	0.22881	0.84001	2.18083	0.10676	0.000	-0.76626	1.72216	0.14911	0.000
KICK	2.4900	0.0000	0.000000	0.31436	0.22881	0.84001	2.18083	0.10676	0.000	-0.76626	1.72216	0.14911	0.000
D4B	2.9202	0.0000	0.000000	0.37045	0.27501	1.84898	1.03564	0.17091	0.000	-1.57910	0.93984	0.14911	0.000
SF	2.9202	0.0000	0.000000	0.37045	0.27501	1.84898	1.03564	0.17091	0.000	-1.57910	0.93984	0.14911	0.000
LTR	2.9202	0.0000	0.000000	0.37045	0.27501	1.84898	1.03564	0.17091	0.000	-1.57910	0.93984	0.14911	0.000
QFMH	3.0030	0.0000	-12.902180	0.37729	0.28832	1.94912	0.97784	0.17557	0.000	0.40557	-0.22132	-0.03734	0.000
BPMX	3.0030	0.0000	0.000000	0.37729	0.28832	1.94912	0.97784	0.17557	0.000	0.40557	-0.22132	-0.03734	0.000
BPMY	3.0030	0.0000	0.000000	0.37729	0.28832	1.94912	0.97784	0.17557	0.000	0.40557	-0.22132	-0.03734	0.000
QFMH	3.0858	0.0000	-12.902180	0.38438	0.30115	1.72244	1.11333	0.16482	0.000	2.25091	-1.46311	-0.22051	0.000
D5	3.1820	0.0000	0.000000	0.39454	0.31333	1.32196	1.42094	0.14360	0.000	1.91209	-1.73449	-0.22051	0.000
E	3.1820	-4.4452	0.000000	0.39454	0.31333	1.32196	1.42094	0.14360	0.000	1.96253	-1.78872	-0.22599	0.000
B	3.5020	0.1571	0.000000	0.46427	0.33867	0.42687	2.86836	0.09490	0.000	0.81158	-2.73446	-0.07780	0.000
E	3.5020	-4.4452	0.000000	0.46427	0.33867	0.42687	2.86836	0.09490	0.000	0.82787	-2.84391	-0.08142	0.000
DQD	3.5997	0.0000	0.000000	0.50807	0.34361	0.30279	3.45430	0.08694	0.000	0.44213	-3.15346	-0.08142	0.000
QDH	3.6490	0.0000	18.325650	0.53528	0.34581	0.28132	3.61209	0.08484	0.000	-0.00013	0.00067	-0.00411	0.000
BPMX	3.6490	0.0000	0.000000	0.53528	0.34581	0.28132	3.61209	0.08484	0.000	-0.00013	0.00067	-0.00411	0.000
BPMY	3.6490	0.0000	0.000000	0.53528	0.34581	0.28132	3.61209	0.08484	0.000	-0.00013	0.00067	-0.00411	0.000
YCOR	3.6490	0.0000	0.000000	0.53528	0.34581	0.28132	3.61209	0.08484	0.000	-0.00013	0.00067	-0.00411	0.000
CELL	3.6490	0.0000	0.000000	0.53528	0.34581	0.28132	3.61209	0.08484	0.000	-0.00013	0.00067	-0.00411	0.000
QDH	3.6983	0.0000	18.325650	0.56250	0.34802	0.30282	3.45418	0.08653	0.000	-0.44241	3.15468	0.07302	0.000
DQD	3.7960	0.0000	0.000000	0.60630	0.35296	0.42695	2.86802	0.09367	0.000	-0.82820	2.84490	0.07302	0.000
EH	3.7960	-4.4452	0.000000	0.60630	0.35296	0.42695	2.86802	0.09367	0.000	-0.81191	2.73546	0.06944	0.000
BH	3.9560	0.0785	0.000000	0.65089	0.36342	0.78235	2.06839	0.11076	0.000	-1.40474	2.26223	0.14408	0.000
XCOR	3.9560	0.0000	0.000000	0.65089	0.36342	0.78235	2.06839	0.11076	0.000	-1.40474	2.26223	0.14408	0.000
BH	4.1160	0.0785	0.000000	0.67601	0.37830	1.32230	1.42019	0.13973	0.000	-1.96299	1.78900	0.21783	0.000
EH	4.1160	-4.4452	0.000000	0.67601	0.37830	1.32230	1.42019	0.13973	0.000	-1.91253	1.73480	0.21250	0.000
DQF	4.2122	0.0000	0.000000	0.68616	0.39049	1.72286	1.11254	0.16017	0.000	-2.25139	1.46321	0.21250	0.000
QFH	4.2950	0.0000	-15.525920	0.69328	0.40325	1.91613	0.99541	0.16900	0.000	0.00070	0.00131	-0.00098	0.000
QFH	4.3778	0.0000	-15.525920	0.70041	0.41601	1.72265	1.11208	0.16001	0.000	2.25250	-1.46002	-0.21436	0.000
DQF	4.4740	0.0000	0.000000	0.71057	0.42821	1.32190	1.41905	0.13939	0.000	1.91332	-1.73092	-0.21436	0.000
E	4.4740	-4.4452	0.000000	0.71057	0.42821	1.32190	1.41905	0.13939	0.000	1.96376	-1.78507	-0.21968	0.000
B	4.7940	0.1571	0.000000	0.78033	0.45359	0.42642	2.86360	0.09275	0.000	0.81154	-2.72914	-0.07124	0.000
E	4.7940	-4.4452	0.000000	0.78033	0.45359	0.42642	2.86360	0.09275	0.000	0.82781	-2.83842	-0.07478	0.000
DQD	4.8917	0.0000	0.000000	0.82419	0.45854	0.30239	3.44841	0.08544	0.000	0.44169	-3.14741	-0.07478	0.000

QDH	4.9410	0.0000	18.325650	0.85144	0.46074	0.28096	3.60586	0.08364	0.000	-0.00043	0.00129	0.00131	0.000
BPMX	4.9410	0.0000	0.000000	0.85144	0.46074	0.28096	3.60586	0.08364	0.000	-0.00043	0.00129	0.00131	0.000
BPMY	4.9410	0.0000	0.000000	0.85144	0.46074	0.28096	3.60586	0.08364	0.000	-0.00043	0.00129	0.00131	0.000
QDH	4.9903	0.0000	18.325650	0.87869	0.46295	0.30248	3.44816	0.08557	0.000	-0.44264	3.14976	0.07747	0.000
DQD	5.0880	0.0000	0.000000	0.92252	0.46790	0.42671	2.86293	0.09314	0.000	-0.82892	2.84033	0.07747	0.000
EH	5.0880	-4.4452	0.000000	0.92252	0.46790	0.42671	2.86293	0.09314	0.000	-0.81263	2.73108	0.07391	0.000
BH	5.2480	0.0785	0.000000	0.96713	0.47838	0.78247	2.06463	0.11094	0.000	-1.40626	2.25834	0.14856	0.000
XCOR	5.2480	0.0000	0.000000	0.96713	0.47838	0.78247	2.06463	0.11094	0.000	-1.40626	2.25834	0.14856	0.000
BH	5.4080	0.0785	0.000000	0.99224	0.49329	1.32302	1.41759	0.14063	0.000	-1.96526	1.78561	0.22228	0.000
EH	5.4080	-4.4452	0.000000	0.99224	0.49329	1.32302	1.41759	0.14063	0.000	-1.91478	1.73151	0.21692	0.000
DQF	5.5042	0.0000	0.000000	1.00238	0.50551	1.72407	1.11055	0.16150	0.000	-2.25408	1.46019	0.21692	0.000
QFH	5.5870	0.0000	-15.525920	1.00950	0.51829	1.91765	0.99371	0.17062	0.000	-0.00035	0.00063	0.00153	0.000
QFH	5.6698	0.0000	-15.525920	1.01662	0.53107	1.72418	1.11033	0.16174	0.000	2.25352	-1.45866	-0.21402	0.000
DQF	5.7660	0.0000	0.000000	1.02677	0.54329	1.32322	1.41704	0.14116	0.000	1.91438	-1.72965	-0.21402	0.000
E	5.7660	-4.4452	0.000000	1.02677	0.54329	1.32322	1.41704	0.14116	0.000	1.96488	-1.78372	-0.21941	0.000
B	6.0860	0.1571	0.000000	1.09645	0.56869	0.42698	2.86080	0.09458	0.000	0.81282	-2.72803	-0.07111	0.000
E	6.0860	-4.4452	0.000000	1.09645	0.56869	0.42698	2.86080	0.09458	0.000	0.82911	-2.83720	-0.07472	0.000
DQD	6.1837	0.0000	0.000000	1.14025	0.57365	0.30269	3.44539	0.08728	0.000	0.44300	-3.14626	-0.07472	0.000
QDH	6.2330	0.0000	18.325650	1.16748	0.57586	0.28114	3.60286	0.08552	0.000	0.00072	-0.00035	0.00305	0.000
BPMX	6.2330	0.0000	0.000000	1.16748	0.57586	0.28114	3.60286	0.08552	0.000	0.00072	-0.00035	0.00305	0.000
BPMY	6.2330	0.0000	0.000000	1.16748	0.57586	0.28114	3.60286	0.08552	0.000	0.00072	-0.00035	0.00305	0.000
YCOR	6.2330	0.0000	0.000000	1.16748	0.57586	0.28114	3.60286	0.08552	0.000	0.00072	-0.00035	0.00305	0.000
QDH	6.2823	0.0000	18.325650	1.19472	0.57807	0.30255	3.44545	0.08758	0.000	-0.44144	3.14563	0.08095	0.000
DQD	6.3800	0.0000	0.000000	1.23856	0.58302	0.42650	2.86098	0.09549	0.000	-0.82729	2.83669	0.08095	0.000
EH	6.3800	-4.4452	0.000000	1.23856	0.58302	0.42650	2.86098	0.09549	0.000	-0.81101	2.72751	0.07731	0.000
BH	6.5400	0.0785	0.000000	1.28320	0.59351	0.78163	2.06369	0.11383	0.000	-1.40399	2.25554	0.15185	0.000
XCOR	6.5400	0.0000	0.000000	1.28320	0.59351	0.78163	2.06369	0.11383	0.000	-1.40399	2.25554	0.15185	0.000
BH	6.7000	0.0785	0.000000	1.30834	0.60842	1.32136	1.41743	0.14403	0.000	-1.96240	1.78358	0.22546	0.000
EH	6.7000	-4.4452	0.000000	1.30834	0.60842	1.32136	1.41743	0.14403	0.000	-1.91198	1.72949	0.21996	0.000
DQF	6.7962	0.0000	0.000000	1.31849	0.62063	1.72184	1.11074	0.16519	0.000	-2.25092	1.45861	0.21996	0.000
QFH	6.8790	0.0000	-15.525920	1.32563	0.63341	1.91514	0.99417	0.17437	0.000	-0.00023	-0.00115	-0.00026	0.000
QFH	6.9618	0.0000	-15.525920	1.33276	0.64619	1.72191	1.11114	0.16515	0.000	2.25056	-1.46141	-0.22044	0.000
DQF	7.0580	0.0000	0.000000	1.34291	0.65839	1.32150	1.41844	0.14394	0.000	1.91172	-1.73290	-0.22044	0.000
E	7.0580	-4.4452	0.000000	1.34291	0.65839	1.32150	1.41844	0.14394	0.000	1.96214	-1.78702	-0.22594	0.000
B	7.3780	0.1571	0.000000	1.41267	0.68377	0.42668	2.86487	0.09525	0.000	0.81113	-2.73307	-0.07777	0.000
E	7.3780	-4.4452	0.000000	1.41267	0.68377	0.42668	2.86487	0.09525	0.000	0.82741	-2.84239	-0.08141	0.000
DQD	7.4757	0.0000	0.000000	1.45649	0.68871	0.30269	3.45052	0.08729	0.000	0.44167	-3.15202	-0.08141	0.000
QDH	7.5250	0.0000	18.325650	1.48372	0.69092	0.28125	3.60833	0.08520	0.000	-0.00053	-0.00138	-0.00378	0.000
BPMX	7.5250	0.0000	0.000000	1.48372	0.69092	0.28125	3.60833	0.08520	0.000	-0.00053	-0.00138	-0.00378	0.000
BPMY	7.5250	0.0000	0.000000	1.48372	0.69092	0.28125	3.60833	0.08520	0.000	-0.00053	-0.00138	-0.00378	0.000
QDH	7.5743	0.0000	18.325650	1.51094	0.69313	0.30279	3.45078	0.08692	0.000	-0.44283	3.14951	0.07369	0.000
DQD	7.6720	0.0000	0.000000	1.55473	0.69807	0.42703	2.86557	0.09412	0.000	-0.82877	2.84035	0.07369	0.000
EH	7.6720	-4.4452	0.000000	1.55473	0.69807	0.42703	2.86557	0.09412	0.000	-0.81247	2.73100	0.07010	0.000
BH	7.8320	0.0785	0.000000	1.59931	0.70854	0.78264	2.06722	0.11131	0.000	-1.40553	2.25873	0.14472	0.000
XCOR	7.8320	0.0000	0.000000	1.59931	0.70854	0.78264	2.06722	0.11131	0.000	-1.40553	2.25873	0.14472	0.000
BH	7.9920	0.0785	0.000000	1.62442	0.72343	1.32287	1.41999	0.14038	0.000	-1.96398	1.78645	0.21844	0.000
EH	7.9920	-4.4452	0.000000	1.62442	0.72343	1.32287	1.41999	0.14038	0.000	-1.91350	1.73227	0.21309	0.000
DQF	8.0882	0.0000	0.000000	1.63456	0.73562	1.72364	1.11277	0.16088	0.000	-2.25249	1.46123	0.21309	0.000
QFH	8.1710	0.0000	-15.525920	1.64169	0.74837	1.91700	0.99598	0.16973	0.000	0.00066	-0.00092	-0.00132	0.000
QFH	8.2538	0.0000	-15.525920	1.64881	0.76113	1.72344	1.11310	0.16066	0.000	2.25353	-1.46346	-0.21559	0.000
DQF	8.3500	0.0000	0.000000	1.65896	0.77331	1.32250	1.42079	0.13992	0.000	1.91425	-1.73499	-0.21559	0.000
E	8.3500	-4.4452	0.000000	1.65896	0.77331	1.32250	1.42079	0.13992	0.000	1.96471	-1.78921	-0.22093	0.000
B	8.6700	0.1571	0.000000	1.72870	0.79865	0.42653	2.86868	0.09287	0.000	0.81213	-2.73544	-0.07252	0.000
E	8.6700	-4.4452	0.000000	1.72870	0.79865	0.42653	2.86868	0.09287	0.000	0.82840	-2.84491	-0.07607	0.000
DQD	8.7677	0.0000	0.000000	1.77255	0.80359	0.30240	3.45483	0.08544	0.000	0.44215	-3.15461	-0.07607	0.000
QDH	8.8170	0.0000	18.325650	1.79981	0.80579	0.28092	3.61271	0.08357	0.000	0.00000	0.00000	0.00000	0.000
BPMX	8.8170	0.0000	0.000000	1.79981	0.80579	0.28092	3.61271	0.08357	0.000	0.00000	0.00000	0.00000	0.000
BPMY	8.8170	0.0000	0.000000	1.79981	0.80579	0.28092	3.61271	0.08357	0.000	0.00000	0.00000	0.00000	0.000
YCOR	8.8170	0.0000	0.000000	1.79981	0.80579	0.28092	3.61271	0.08357	0.000	0.00000	0.00000	0.00000	0.000
QDH	8.8663	0.0000	18.325650	1.82706	0.80800	0.30240	3.45483	0.08544	0.000	-0.44215	3.15461	0.07607	0.000

DQD	8.9640	0.0000	0.000000	1.87091	0.81294	0.42653	2.86868	0.09287	0.000	-0.82840	2.84491	0.07607	0.000
EH	8.9640	-4.4452	0.000000	1.87091	0.81294	0.42653	2.86868	0.09287	0.000	-0.81213	2.73544	0.07252	0.000
BH	9.1240	0.0785	0.000000	1.91554	0.82340	0.78212	2.06904	0.11046	0.000	-1.40573	2.26232	0.14718	0.000
XCOR	9.1240	0.0000	0.000000	1.91554	0.82340	0.78212	2.06904	0.11046	0.000	-1.40573	2.26232	0.14718	0.000
BH	9.2840	0.0785	0.000000	1.94065	0.83827	1.32250	1.42079	0.13992	0.000	-1.96471	1.78921	0.22093	0.000
EH	9.2840	-4.4452	0.000000	1.94065	0.83827	1.32250	1.42079	0.13992	0.000	-1.91425	1.73499	0.21559	0.000
DQF	9.3802	0.0000	0.000000	1.95080	0.85046	1.72344	1.11310	0.16066	0.000	-2.25353	1.46346	0.21559	0.000
QFH	9.4630	0.0000	-15.525920	1.95793	0.86321	1.91700	0.99598	0.16973	0.000	-0.00066	0.00092	0.00132	0.000
QFH	9.5458	0.0000	-15.525920	1.96505	0.87596	1.72364	1.11277	0.16088	0.000	2.25249	-1.46123	-0.21309	0.000
DQF	9.6420	0.0000	0.000000	1.97520	0.88816	1.32287	1.41999	0.14038	0.000	1.91350	-1.73227	-0.21309	0.000
E	9.6420	-4.4452	0.000000	1.97520	0.88816	1.32287	1.41999	0.14038	0.000	1.96398	-1.78645	-0.21844	0.000
B	9.9620	0.1571	0.000000	2.04489	0.91351	0.42703	2.86557	0.09412	0.000	0.81247	-2.73100	-0.07010	0.000
E	9.9620	-4.4452	0.000000	2.04489	0.91351	0.42703	2.86557	0.09412	0.000	0.82877	-2.84035	-0.07369	0.000
DQD	10.0597	0.0000	0.000000	2.08868	0.91846	0.30279	3.45078	0.08692	0.000	0.44283	-3.14951	-0.07369	0.000
QDH	10.1090	0.0000	18.325650	2.11590	0.92066	0.28125	3.60833	0.08520	0.000	0.00053	0.00138	0.00378	0.000
BPMX	10.1090	0.0000	0.000000	2.11590	0.92066	0.28125	3.60833	0.08520	0.000	0.00053	0.00138	0.00378	0.000
BPMY	10.1090	0.0000	0.000000	2.11590	0.92066	0.28125	3.60833	0.08520	0.000	0.00053	0.00138	0.00378	0.000
QDH	10.1583	0.0000	18.325650	2.14312	0.92287	0.30269	3.45052	0.08729	0.000	-0.44167	3.15202	0.08141	0.000
DQD	10.2560	0.0000	0.000000	2.18694	0.92782	0.42668	2.86487	0.09525	0.000	-0.82741	2.84239	0.08141	0.000
EH	10.2560	-4.4452	0.000000	2.18694	0.92782	0.42668	2.86487	0.09525	0.000	-0.81113	2.73307	0.07777	0.000
BH	10.4160	0.0785	0.000000	2.23157	0.93829	0.78181	2.06597	0.11367	0.000	-1.40392	2.26005	0.15233	0.000
XCOR	10.4160	0.0000	0.000000	2.23157	0.93829	0.78181	2.06597	0.11367	0.000	-1.40392	2.26005	0.15233	0.000
BH	10.5760	0.0785	0.000000	2.25670	0.95319	1.32150	1.41844	0.14394	0.000	-1.96214	1.78702	0.22594	0.000
EH	10.5760	-4.4452	0.000000	2.25670	0.95319	1.32150	1.41844	0.14394	0.000	-1.91172	1.73290	0.22044	0.000
DQF	10.6722	0.0000	0.000000	2.26686	0.96540	1.72191	1.11114	0.16515	0.000	-2.25056	1.46141	0.22044	0.000
QFH	10.7550	0.0000	-15.525920	2.27399	0.97817	1.91514	0.99417	0.17437	0.000	0.00023	0.00115	0.00026	0.000
QFH	10.8378	0.0000	-15.525920	2.28112	0.99095	1.72184	1.11074	0.16519	0.000	2.25092	-1.45861	-0.21996	0.000
DQF	10.9340	0.0000	0.000000	2.29128	1.00316	1.32136	1.41743	0.14403	0.000	1.91198	-1.72949	-0.21996	0.000
E	10.9340	-4.4452	0.000000	2.29128	1.00316	1.32136	1.41743	0.14403	0.000	1.96240	-1.78358	-0.22546	0.000
B	11.2540	0.1571	0.000000	2.36105	1.02856	0.42650	2.86098	0.09549	0.000	0.81101	-2.72751	-0.07731	0.000
E	11.2540	-4.4452	0.000000	2.36105	1.02856	0.42650	2.86098	0.09549	0.000	0.82729	-2.83669	-0.08095	0.000
DQD	11.3517	0.0000	0.000000	2.40489	1.03352	0.30255	3.44545	0.08758	0.000	0.44144	-3.14563	-0.08095	0.000
QDH	11.4010	0.0000	18.325650	2.43213	1.03573	0.28114	3.60286	0.08552	0.000	-0.00072	0.00035	-0.00305	0.000
BPMX	11.4010	0.0000	0.000000	2.43213	1.03573	0.28114	3.60286	0.08552	0.000	-0.00072	0.00035	-0.00305	0.000
BPMY	11.4010	0.0000	0.000000	2.43213	1.03573	0.28114	3.60286	0.08552	0.000	-0.00072	0.00035	-0.00305	0.000
YCOR	11.4010	0.0000	0.000000	2.43213	1.03573	0.28114	3.60286	0.08552	0.000	-0.00072	0.00035	-0.00305	0.000
QDH	11.4503	0.0000	18.325650	2.45936	1.03794	0.30269	3.44539	0.08728	0.000	-0.44300	3.14626	0.07472	0.000
DQD	11.5480	0.0000	0.000000	2.50316	1.04289	0.42698	2.86080	0.09458	0.000	-0.82911	2.83720	0.07472	0.000
EH	11.5480	-4.4452	0.000000	2.50316	1.04289	0.42698	2.86080	0.09458	0.000	-0.81282	2.72803	0.07111	0.000
BH	11.7080	0.0785	0.000000	2.54775	1.05338	0.78275	2.06338	0.11193	0.000	-1.40616	2.25588	0.14571	0.000
XCOR	11.7080	0.0000	0.000000	2.54775	1.05338	0.78275	2.06338	0.11193	0.000	-1.40616	2.25588	0.14571	0.000
BH	11.8680	0.0785	0.000000	2.57285	1.06829	1.32322	1.41704	0.14116	0.000	-1.96488	1.78372	0.21941	0.000
EH	11.8680	-4.4452	0.000000	2.57285	1.06829	1.32322	1.41704	0.14116	0.000	-1.91438	1.72965	0.21402	0.000
DQF	11.9642	0.0000	0.000000	2.58299	1.08051	1.72418	1.11033	0.16174	0.000	-2.25352	1.45866	0.21402	0.000
QFH	12.0470	0.0000	-15.525920	2.59011	1.09329	1.91765	0.99371	0.17062	0.000	0.00035	-0.00063	-0.00153	0.000
QFH	12.1298	0.0000	-15.525920	2.59723	1.10608	1.72407	1.11055	0.16150	0.000	2.25408	-1.46019	-0.21692	0.000
DQF	12.2260	0.0000	0.000000	2.60738	1.11829	1.32302	1.41759	0.14063	0.000	1.91478	-1.73151	-0.21692	0.000
E	12.2260	-4.4452	0.000000	2.60738	1.11829	1.32302	1.41759	0.14063	0.000	1.96526	-1.78561	-0.22228	0.000
B	12.5460	0.1571	0.000000	2.67709	1.14368	0.42671	2.86293	0.09314	0.000	0.81263	-2.73108	-0.07391	0.000
E	12.5460	-4.4452	0.000000	2.67709	1.14368	0.42671	2.86293	0.09314	0.000	0.82892	-2.84033	-0.07747	0.000
DQD	12.6437	0.0000	0.000000	2.72092	1.14863	0.30248	3.44816	0.08557	0.000	0.44264	-3.14976	-0.07747	0.000
QDH	12.6930	0.0000	18.325650	2.74817	1.15084	0.28096	3.60586	0.08364	0.000	0.00043	-0.00129	-0.00131	0.000
BPMX	12.6930	0.0000	0.000000	2.74817	1.15084	0.28096	3.60586	0.08364	0.000	0.00043	-0.00129	-0.00131	0.000
BPMY	12.6930	0.0000	0.000000	2.74817	1.15084	0.28096	3.60586	0.08364	0.000	0.00043	-0.00129	-0.00131	0.000
QDH	12.7423	0.0000	18.325650	2.77542	1.15305	0.30239	3.44841	0.08544	0.000	-0.44169	3.14741	0.07478	0.000
DQD	12.8400	0.0000	0.000000	2.81928	1.15800	0.42642	2.86360	0.09275	0.000	-0.82781	2.83842	0.07478	0.000
EH	12.8400	-4.4452	0.000000	2.81928	1.15800	0.42642	2.86360	0.09275	0.000	-0.81154	2.72914	0.07124	0.000
BH	13.0000	0.0785	0.000000	2.86392	1.16847	0.78179	2.06580	0.11013	0.000	-1.40495	2.25711	0.14591	0.000
XCOR	13.0000	0.0000	0.000000	2.86392	1.16847	0.78179	2.06580	0.11013	0.000	-1.40495	2.25711	0.14591	0.000
BH	13.1600	0.0785	0.000000	2.88905	1.18337	1.32190	1.41905	0.13939	0.000	-1.96376	1.78507	0.21968	0.000

EH	13.[illegible]00	-4.4452	0.000000	2.88905	1.18337	1.32190	1.41905	0.13939	0.000	-1.91332	1.73092	0.21436	0.000
DQF	13.2562	0.0000	0.000000	2.89920	1.19557	1.72265	1.11208	0.16001	0.000	-2.25250	1.46002	0.21436	0.000
QFH	13.3390	0.0000	-15.525920	2.90633	1.20833	1.91613	0.99541	0.16900	0.000	-0.00070	-0.00131	0.00098	0.000
QFH	13.4218	0.0000	-15.525920	2.91346	1.22109	1.72286	1.11254	0.16017	0.000	2.25139	-1.46321	-0.21250	0.000
DQF	13.5180	0.0000	0.000000	2.92361	1.23328	1.32230	1.42019	0.13973	0.000	1.91253	-1.73480	-0.21250	0.000
E	13.5180	-4.4452	0.000000	2.92361	1.23328	1.32230	1.42019	0.13973	0.000	1.96299	-1.78900	-0.21783	0.000
B	13.8380	0.1571	0.000000	2.99332	1.25862	0.42695	2.86802	0.09367	0.000	0.81191	-2.73546	-0.06944	0.000
E	13.8380	-4.4452	0.000000	2.99332	1.25862	0.42695	2.86802	0.09367	0.000	0.82820	-2.84490	-0.07302	0.000
DQD	13.9357	0.0000	0.000000	3.03711	1.26356	0.30282	3.45418	0.08653	0.000	0.44241	-3.15468	-0.07302	0.000
QDH	13.9850	0.0000	18.325650	3.06433	1.26577	0.28132	3.61209	0.08484	0.000	0.00013	-0.00067	0.00411	0.000
BPMX	13.9850	0.0000	0.000000	3.06433	1.26577	0.28132	3.61209	0.08484	0.000	0.00013	-0.00067	0.00411	0.000
BPMY	13.9850	0.0000	0.000000	3.06433	1.26577	0.28132	3.61209	0.08484	0.000	0.00013	-0.00067	0.00411	0.000
YCOR	13.9850	0.0000	0.000000	3.06433	1.26577	0.28132	3.61209	0.08484	0.000	0.00013	-0.00067	0.00411	0.000
QDH	14.0343	0.0000	18.325650	3.09155	1.26797	0.30279	3.45430	0.08694	0.000	-0.44213	3.15346	0.08142	0.000
DQD	14.1320	0.0000	0.000000	3.13535	1.27292	0.42687	2.86836	0.09490	0.000	-0.82787	2.84391	0.08142	0.000
EH	14.1320	-4.4452	0.000000	3.13535	1.27292	0.42687	2.86836	0.09490	0.000	-0.81158	2.73446	0.07780	0.000
BH	14.2920	0.0785	0.000000	3.17996	1.28338	0.78215	2.06899	0.11332	0.000	-1.40434	2.26159	0.15236	0.000
XCOR	14.2920	0.0000	0.000000	3.17996	1.28338	0.78215	2.06899	0.11332	0.000	-1.40434	2.26159	0.15236	0.000
BH	14.4520	0.0785	0.000000	3.20508	1.29825	1.32196	1.42094	0.14360	0.000	-1.96253	1.78872	0.22599	0.000
EH	14.4520	-4.4452	0.000000	3.20508	1.29825	1.32196	1.42094	0.14360	0.000	-1.91209	1.73449	0.22051	0.000
D5	14.5482	0.0000	0.000000	3.21523	1.31043	1.72244	1.11333	0.16482	0.000	-2.25091	1.46311	0.22051	0.000
QFMH	14.6310	0.0000	-12.902180	3.22232	1.32326	1.94912	0.97784	0.17557	0.000	-0.40557	0.22132	0.03734	0.000
QFMH	14.7138	0.0000	-12.902180	3.22916	1.33657	1.84898	1.03564	0.17091	0.000	1.57910	-0.93984	-0.14911	0.000
RTL	14.7138	0.0000	0.000000	3.22916	1.33657	1.84898	1.03564	0.17091	0.000	1.57910	-0.93984	-0.14911	0.000
SF	14.7138	0.0000	0.000000	3.22916	1.33657	1.84898	1.03564	0.17091	0.000	1.57910	-0.93984	-0.14911	0.000
D4B	15.1440	0.0000	0.000000	3.28525	1.38277	0.84001	2.18083	0.10676	0.000	0.76626	-1.72216	-0.14911	0.000
KICK	15.1440	0.0000	0.000000	3.28525	1.38277	0.84001	2.18083	0.10676	0.000	0.76626	-1.72216	-0.14911	0.000
D4A	15.4777	0.0000	0.000000	3.36784	1.40196	0.53901	3.53270	0.05701	0.000	0.13575	-2.32899	-0.14911	0.000
QDMH	15.5270	0.0000	-0.743500	3.38255	1.40411	0.52926	3.77343	0.04961	0.000	0.06196	-2.55682	-0.15106	0.000
BPMX	15.5270	0.0000	0.000000	3.38255	1.40411	0.52926	3.77343	0.04961	0.000	0.06196	-2.55682	-0.15106	0.000
BPMY	15.5270	0.0000	0.000000	3.38255	1.40411	0.52926	3.77343	0.04961	0.000	0.06196	-2.55682	-0.15106	0.000
QDMH	15.5763	0.0000	-0.743500	3.39742	1.40612	0.52681	4.03751	0.04212	0.000	-0.01229	-2.80314	-0.15274	0.000
D3	15.6830	0.0000	0.000000	3.42915	1.41003	0.55104	4.66068	0.02582	0.000	-0.21486	-3.03722	-0.15274	0.000
EH	15.6830	-4.4452	0.000000	3.42915	1.41003	0.55104	4.66068	0.02582	0.000	-0.19383	-3.21508	-0.15373	0.000
BH	15.8430	0.0785	0.000000	3.47193	1.41495	0.65753	5.75177	0.00745	0.000	-0.47032	-3.60426	-0.07579	0.000
XCOR	15.8430	0.0000	0.000000	3.47193	1.41495	0.65753	5.75177	0.00745	0.000	-0.47032	-3.60426	-0.07579	0.000
BH	16.0030	0.0785	0.000000	3.50620	1.41897	0.85081	6.96741	0.00159	0.000	-0.73522	-3.99345	0.00262	0.000
EH	16.0030	-4.4452	0.000000	3.50620	1.41897	0.85081	6.96741	0.00159	0.000	-0.70276	-4.25932	0.00256	0.000
D2	16.1546	0.0000	0.000000	3.53120	1.42214	1.10424	8.32198	0.00198	0.000	-0.96894	-4.67582	0.00256	0.000
QDIH	16.2230	0.0000	15.393090	3.54028	1.42343	1.33311	8.35883	0.00223	0.000	-2.45710	4.15006	0.00476	0.000
YCOR	16.2230	0.0000	0.000000	3.54028	1.42343	1.33311	8.35883	0.00223	0.000	-2.45710	4.15006	0.00476	0.000
QDIH	16.2914	0.0000	15.393090	3.54738	1.42481	1.80924	7.24026	0.00264	0.000	-4.67023	11.80886	0.00730	0.000
D1	16.4387	0.0000	0.000000	3.55676	1.42908	3.45866	4.18226	0.00371	0.000	-6.52739	8.95148	0.00730	0.000
QFIH	16.5230	0.0000	-10.484290	3.56018	1.43287	4.34136	3.05768	0.00418	0.000	-3.68223	4.71835	0.00379	0.000
BPMX	16.5230	0.0000	0.000000	3.56018	1.43287	4.34136	3.05768	0.00418	0.000	-3.68223	4.71835	0.00379	0.000
BPMY	16.5230	0.0000	0.000000	3.56018	1.43287	4.34136	3.05768	0.00418	0.000	-3.68223	4.71835	0.00379	0.000
XCOR	16.5230	0.0000	0.000000	3.56018	1.43287	4.34136	3.05768	0.00418	0.000	-3.68223	4.71835	0.00379	0.000
QFIH	16.6073	0.0000	-10.484290	3.56313	1.43778	4.63954	2.51101	0.00434	0.000	0.23334	1.92669	0.00000	0.000
D0	17.6340	0.0000	0.000000	3.59961	1.61158	4.39997	0.53288	0.00434	0.000	0.00000	0.00000	0.00000	0.000
SYMM	17.6340	0.0000	0.000000	3.59961	1.61158	4.39997	0.53288	0.00434	0.000	0.00000	0.00000	0.00000	0.000
D0	18.6607	0.0000	0.000000	3.63610	1.78539	4.63954	2.51101	0.00434	0.000	-0.23334	-1.92669	0.00000	0.000
QFIH	18.7450	0.0000	-10.484290	3.63905	1.79029	4.34136	3.05768	0.00418	0.000	3.68223	-4.71835	-0.00379	0.000
BPMX	18.7450	0.0000	0.000000	3.63905	1.79029	4.34136	3.05768	0.00418	0.000	3.68223	-4.71835	-0.00379	0.000
BPMY	18.7450	0.0000	0.000000	3.63905	1.79029	4.34136	3.05768	0.00418	0.000	3.68223	-4.71835	-0.00379	0.000
XCOR	18.7450	0.0000	0.000000	3.63905	1.79029	4.34136	3.05768	0.00418	0.000	3.68223	-4.71835	-0.00379	0.000
QFIH	18.8293	0.0000	-10.484290	3.64247	1.79409	3.45866	4.18226	0.00371	0.000	6.52739	-8.95148	-0.00730	0.000
D1	18.9766	0.0000	0.000000	3.65185	1.79835	1.80924	7.24026	0.00264	0.000	4.67023	-11.80886	-0.00730	0.000
QDIH	19.0450	0.0000	15.393090	3.65895	1.79973	1.33311	8.35883	0.00223	0.000	2.45710	-4.15006	-0.00476	0.000
YCOR	19.0450	0.0000	0.000000	3.65895	1.79973	1.33311	8.35883	0.00223	0.000	2.45710	-4.15006	-0.00476	0.000
QDIH	19.1134	0.0000	15.393090	3.66803	1.80102	1.10424	8.32198	0.00198	0.000	0.96894	4.67582	-0.00256	0.000

D2	19.1650	0.0000	0.000000	3.69303	1.80419	0.85081	6.96741	0.00159	0.000	0.70276	4.25932	-0.00256	0.000
EH	19.2650	-4.4452	0.000000	3.69303	1.80419	0.85081	6.96741	0.00159	0.000	0.73522	3.99345	-0.00262	0.000
BH	19.4250	0.0785	0.000000	3.72730	1.80821	0.65753	5.75177	0.00745	0.000	0.47032	3.60426	0.07579	0.000
XCOR	19.4250	0.0000	0.000000	3.72730	1.80821	0.65753	5.75177	0.00745	0.000	0.47032	3.60426	0.07579	0.000
BH	19.5850	0.0785	0.000000	3.77008	1.81313	0.55104	4.66068	0.02582	0.000	0.19383	3.21508	0.15373	0.000
EH	19.5850	-4.4452	0.000000	3.77008	1.81313	0.55104	4.66068	0.02582	0.000	0.21486	3.03722	0.15274	0.000
D3	19.6917	0.0000	0.000000	3.80180	1.81705	0.52681	4.03751	0.04212	0.000	0.01229	2.80314	0.15274	0.000
QDMH	19.7410	0.0000	-0.743500	3.81668	1.81906	0.52926	3.77343	0.04961	0.000	-0.06196	2.55682	0.15106	0.000
QDMH	19.7903	0.0000	-0.743500	3.83139	1.82121	0.53901	3.53270	0.05701	0.000	-0.13575	2.32899	0.14911	0.000
SD	19.7903	0.0000	0.000000	3.83139	1.82121	0.53901	3.53270	0.05701	0.000	-0.13575	2.32899	0.14911	0.000
D4C	20.2050	0.0000	0.000000	3.92823	1.84670	0.97654	1.91377	0.11884	0.000	-0.91930	1.57486	0.14911	0.000
RFCW	20.2050	0.0000	0.000000	3.92823	1.84670	0.97654	1.91377	0.11884	0.000	-0.91930	1.57486	0.14911	0.000
D4D	20.5542	0.0000	0.000000	3.97007	1.88659	1.84898	1.03564	0.17091	0.000	-1.57910	0.93984	0.14911	0.000
QFMH	20.6370	0.0000	-12.902180	3.97691	1.89990	1.94912	0.97784	0.17557	0.000	0.40557	-0.22132	-0.03734	0.000
BPMX	20.6370	0.0000	0.000000	3.97691	1.89990	1.94912	0.97784	0.17557	0.000	0.40557	-0.22132	-0.03734	0.000
BPMY	20.6370	0.0000	0.000000	3.97691	1.89990	1.94912	0.97784	0.17557	0.000	0.40557	-0.22132	-0.03734	0.000
QFMH	20.7198	0.0000	-12.902180	3.98400	1.91273	1.72244	1.11333	0.16482	0.000	2.25091	-1.46311	-0.22051	0.000
D5	20.8160	0.0000	0.000000	3.99415	1.92491	1.32196	1.42094	0.14360	0.000	1.91209	-1.73449	-0.22051	0.000
E	20.8160	-4.4452	0.000000	3.99415	1.92491	1.32196	1.42094	0.14360	0.000	1.96253	-1.78872	-0.22599	0.000
B	21.1360	0.1571	0.000000	4.06388	1.95025	0.42687	2.86836	0.09490	0.000	0.81158	-2.73446	-0.07780	0.000
E	21.1360	-4.4452	0.000000	4.06388	1.95025	0.42687	2.86836	0.09490	0.000	0.82787	-2.84391	-0.08142	0.000
DQD	21.2337	0.0000	0.000000	4.10768	1.95519	0.30279	3.45430	0.08694	0.000	0.44213	-3.15346	-0.08142	0.000
QDH	21.2830	0.0000	18.325650	4.13490	1.95739	0.28132	3.61209	0.08484	0.000	-0.00013	0.00067	-0.00411	0.000
BPMX	21.2830	0.0000	0.000000	4.13490	1.95739	0.28132	3.61209	0.08484	0.000	-0.00013	0.00067	-0.00411	0.000
BPMY	21.2830	0.0000	0.000000	4.13490	1.95739	0.28132	3.61209	0.08484	0.000	-0.00013	0.00067	-0.00411	0.000
YCOR	21.2830	0.0000	0.000000	4.13490	1.95739	0.28132	3.61209	0.08484	0.000	-0.00013	0.00067	-0.00411	0.000
QDH	21.3323	0.0000	18.325650	4.16211	1.95960	0.30282	3.45418	0.08653	0.000	-0.44241	3.15468	0.07302	0.000
DQD	21.4300	0.0000	0.000000	4.20591	1.96454	0.42695	2.86802	0.09367	0.000	-0.82820	2.84490	0.07302	0.000
EH	21.4300	-4.4452	0.000000	4.20591	1.96454	0.42695	2.86802	0.09367	0.000	-0.81191	2.73546	0.06944	0.000
BH	21.5900	0.0785	0.000000	4.25051	1.97500	0.78235	2.06839	0.11076	0.000	-1.40474	2.26223	0.14408	0.000
XCOR	21.5900	0.0000	0.000000	4.25051	1.97500	0.78235	2.06839	0.11076	0.000	-1.40474	2.26223	0.14408	0.000
BH	21.7500	0.0785	0.000000	4.27562	1.98988	1.32230	1.42019	0.13973	0.000	-1.96299	1.78900	0.21783	0.000
EH	21.7500	-4.4452	0.000000	4.27562	1.98988	1.32230	1.42019	0.13973	0.000	-1.91253	1.73480	0.21250	0.000
DQF	21.8462	0.0000	0.000000	4.28577	2.00207	1.72286	1.11254	0.16017	0.000	-2.25139	1.46321	0.21250	0.000
QFH	21.9290	0.0000	-15.525920	4.29290	2.01483	1.91613	0.99541	0.16900	0.000	0.00070	0.00131	-0.00098	0.000
QFH	22.0118	0.0000	-15.525920	4.30003	2.02760	1.72265	1.11208	0.16001	0.000	2.25250	-1.46002	-0.21436	0.000
DQF	22.1080	0.0000	0.000000	4.31018	2.03980	1.32190	1.41905	0.13939	0.000	1.91332	-1.73092	-0.21436	0.000
E	22.1080	-4.4452	0.000000	4.31018	2.03980	1.32190	1.41905	0.13939	0.000	1.96376	-1.78507	-0.21968	0.000
B	22.4280	0.1571	0.000000	4.37995	2.06517	0.42642	2.86360	0.09275	0.000	0.81154	-2.72914	-0.07124	0.000
E	22.4280	-4.4452	0.000000	4.37995	2.06517	0.42642	2.86360	0.09275	0.000	0.82781	-2.83842	-0.07478	0.000
DQD	22.5257	0.0000	0.000000	4.42380	2.07012	0.30239	3.44841	0.08544	0.000	0.44169	-3.14741	-0.07478	0.000
QDH	22.5750	0.0000	18.325650	4.45106	2.07233	0.28096	3.60586	0.08364	0.000	-0.00043	0.00129	0.00131	0.000
BPMX	22.5750	0.0000	0.000000	4.45106	2.07233	0.28096	3.60586	0.08364	0.000	-0.00043	0.00129	0.00131	0.000
BPMY	22.5750	0.0000	0.000000	4.45106	2.07233	0.28096	3.60586	0.08364	0.000	-0.00043	0.00129	0.00131	0.000
QDH	22.6243	0.0000	18.325650	4.47830	2.07453	0.30248	3.44816	0.08557	0.000	-0.44264	3.14976	0.07747	0.000
DQD	22.7220	0.0000	0.000000	4.52214	2.07948	0.42671	2.86293	0.09314	0.000	-0.82892	2.84033	0.07747	0.000
EH	22.7220	-4.4452	0.000000	4.52214	2.07948	0.42671	2.86293	0.09314	0.000	-0.81263	2.73108	0.07391	0.000
BH	22.8820	0.0785	0.000000	4.56674	2.08997	0.78247	2.06463	0.11094	0.000	-1.40626	2.25834	0.14856	0.000
XCOR	22.8820	0.0000	0.000000	4.56674	2.08997	0.78247	2.06463	0.11094	0.000	-1.40626	2.25834	0.14856	0.000
BH	23.0420	0.0785	0.000000	4.59185	2.10487	1.32302	1.41759	0.14063	0.000	-1.96526	1.78561	0.22228	0.000
EH	23.0420	-4.4452	0.000000	4.59185	2.10487	1.32302	1.41759	0.14063	0.000	-1.91478	1.73151	0.21692	0.000
DQF	23.1382	0.0000	0.000000	4.60199	2.11709	1.72407	1.11055	0.16150	0.000	-2.25408	1.46019	0.21692	0.000
QFH	23.2210	0.0000	-15.525920	4.60912	2.12987	1.91765	0.99371	0.17062	0.000	-0.00035	0.00063	0.00153	0.000
QFH	23.3038	0.0000	-15.525920	4.61624	2.14265	1.72418	1.11033	0.16174	0.000	2.25352	-1.45866	-0.21402	0.000
DQF	23.4000	0.0000	0.000000	4.62638	2.15487	1.32322	1.41704	0.14116	0.000	1.91438	-1.72965	-0.21402	0.000
E	23.4000	-4.4452	0.000000	4.62638	2.15487	1.32322	1.41704	0.14116	0.000	1.96488	-1.78372	-0.21941	0.000
B	23.7200	0.1571	0.000000	4.69606	2.18027	0.42698	2.86080	0.09458	0.000	0.81282	-2.72803	-0.07111	0.000
E	23.7200	-4.4452	0.000000	4.69606	2.18027	0.42698	2.86080	0.09458	0.000	0.82911	-2.83720	-0.07472	0.000
DQD	23.8177	0.0000	0.000000	4.73987	2.18523	0.30269	3.44539	0.08728	0.000	0.44300	-3.14626	-0.07472	0.000
QDH	23.8670	0.0000	18.325650	4.76710	2.18744	0.28114	3.60286	0.08552	0.000	0.00072	-0.00035	0.00305	0.000

BPMX	23.8670	0.0000	0.000000	4.76710	2.18744	0.28114	3.60286	0.08552	0.000	0.00072	-0.00035	0.00305	0.000
BPMY	23.8670	0.0000	0.000000	4.76710	2.18744	0.28114	3.60286	0.08552	0.000	0.00072	-0.00035	0.00305	0.000
YCOR	23.8670	0.0000	0.000000	4.76710	2.18744	0.28114	3.60286	0.08552	0.000	0.00072	-0.00035	0.00305	0.000
QDH	23.9163	0.0000	18.325650	4.79433	2.18965	0.30255	3.44545	0.08758	0.000	-0.44144	3.14563	0.08095	0.000
DQD	24.0140	0.0000	0.000000	4.83817	2.19460	0.42650	2.86098	0.09549	0.000	-0.82729	2.83669	0.08095	0.000
EH	24.0140	-4.4452	0.000000	4.83817	2.19460	0.42650	2.86098	0.09549	0.000	-0.81101	2.72751	0.07731	0.000
BH	24.1740	0.0785	0.000000	4.88282	2.20509	0.78163	2.06369	0.11383	0.000	-1.40399	2.25554	0.15185	0.000
XCOR	24.1740	0.0000	0.000000	4.88282	2.20509	0.78163	2.06369	0.11383	0.000	-1.40399	2.25554	0.15185	0.000
BH	24.3340	0.0785	0.000000	4.90795	2.22000	1.32136	1.41743	0.14403	0.000	-1.96240	1.78358	0.22546	0.000
EH	24.3340	-4.4452	0.000000	4.90795	2.22000	1.32136	1.41743	0.14403	0.000	-1.91198	1.72949	0.21996	0.000
DQF	24.4302	0.0000	0.000000	4.91811	2.23221	1.72184	1.11074	0.16519	0.000	-2.25092	1.45861	0.21996	0.000
QFH	24.5130	0.0000	-15.525920	4.92524	2.24499	1.91514	0.99417	0.17437	0.000	-0.00023	-0.00115	-0.00026	0.000
QFH	24.5958	0.0000	-15.525920	4.93237	2.25777	1.72191	1.11114	0.16515	0.000	2.25056	-1.46141	-0.22044	0.000
DQF	24.6920	0.0000	0.000000	4.94253	2.26998	1.32150	1.41844	0.14394	0.000	1.91172	-1.73290	-0.22044	0.000
E	24.6920	-4.4452	0.000000	4.94253	2.26998	1.32150	1.41844	0.14394	0.000	1.96214	-1.78702	-0.22594	0.000
B	25.0120	0.1571	0.000000	5.01229	2.29535	0.42668	2.86487	0.09525	0.000	0.81113	-2.73307	-0.07777	0.000
E	25.0120	-4.4452	0.000000	5.01229	2.29535	0.42668	2.86487	0.09525	0.000	0.82741	-2.84239	-0.08141	0.000
DQD	25.1097	0.0000	0.000000	5.05611	2.30029	0.30269	3.45052	0.08729	0.000	0.44167	-3.15202	-0.08141	0.000
QDH	25.1590	0.0000	18.325650	5.08333	2.30250	0.28125	3.60833	0.08520	0.000	-0.00053	-0.00138	-0.00378	0.000
BPMX	25.1590	0.0000	0.000000	5.08333	2.30250	0.28125	3.60833	0.08520	0.000	-0.00053	-0.00138	-0.00378	0.000
BPMY	25.1590	0.0000	0.000000	5.08333	2.30250	0.28125	3.60833	0.08520	0.000	-0.00053	-0.00138	-0.00378	0.000
QDH	25.2083	0.0000	18.325650	5.11055	2.30471	0.30279	3.45078	0.08692	0.000	-0.44283	3.14951	0.07369	0.000
DQD	25.3060	0.0000	0.000000	5.15434	2.30965	0.42703	2.86557	0.09412	0.000	-0.82877	2.84035	0.07369	0.000
EH	25.3060	-4.4452	0.000000	5.15434	2.30965	0.42703	2.86557	0.09412	0.000	-0.81247	2.73100	0.07010	0.000
BH	25.4660	0.0785	0.000000	5.19893	2.32012	0.78264	2.06722	0.11131	0.000	-1.40553	2.25873	0.14472	0.000
XCOR	25.4660	0.0000	0.000000	5.19893	2.32012	0.78264	2.06722	0.11131	0.000	-1.40553	2.25873	0.14472	0.000
BH	25.6260	0.0785	0.000000	5.22403	2.33501	1.32287	1.41999	0.14038	0.000	-1.96398	1.78645	0.21844	0.000
EH	25.6260	-4.4452	0.000000	5.22403	2.33501	1.32287	1.41999	0.14038	0.000	-1.91350	1.73227	0.21309	0.000
DQF	25.7222	0.0000	0.000000	5.23418	2.34720	1.72364	1.11277	0.16088	0.000	-2.25249	1.46123	0.21309	0.000
QFH	25.8050	0.0000	-15.525920	5.24130	2.35995	1.91700	0.99598	0.16973	0.000	0.00066	-0.00092	-0.00132	0.000
QFH	25.8878	0.0000	-15.525920	5.24843	2.37271	1.72344	1.11310	0.16066	0.000	2.25353	-1.46346	-0.21559	0.000
DQF	25.9840	0.0000	0.000000	5.25858	2.38489	1.32250	1.42079	0.13992	0.000	1.91425	-1.73499	-0.21559	0.000
E	25.9840	-4.4452	0.000000	5.25858	2.38489	1.32250	1.42079	0.13992	0.000	1.96471	-1.78921	-0.22093	0.000
B	26.3040	0.1571	0.000000	5.32832	2.41023	0.42653	2.86868	0.09287	0.000	0.81213	-2.73544	-0.07252	0.000
E	26.3040	-4.4452	0.000000	5.32832	2.41023	0.42653	2.86868	0.09287	0.000	0.82840	-2.84491	-0.07607	0.000
DQD	26.4017	0.0000	0.000000	5.37217	2.41517	0.30240	3.45483	0.08544	0.000	0.44215	-3.15461	-0.07607	0.000
QDH	26.4510	0.0000	18.325650	5.39942	2.41737	0.28092	3.61271	0.08357	0.000	0.00000	0.00000	0.00000	0.000
BPMX	26.4510	0.0000	0.000000	5.39942	2.41737	0.28092	3.61271	0.08357	0.000	0.00000	0.00000	0.00000	0.000
BPMY	26.4510	0.0000	0.000000	5.39942	2.41737	0.28092	3.61271	0.08357	0.000	0.00000	0.00000	0.00000	0.000
YCOR	26.4510	0.0000	0.000000	5.39942	2.41737	0.28092	3.61271	0.08357	0.000	0.00000	0.00000	0.00000	0.000
QDH	26.5003	0.0000	18.325650	5.42668	2.41958	0.30240	3.45483	0.08544	0.000	-0.44215	3.15461	0.07607	0.000
DQD	26.5980	0.0000	0.000000	5.47052	2.42452	0.42653	2.86868	0.09287	0.000	-0.82840	2.84491	0.07607	0.000
EH	26.5980	-4.4452	0.000000	5.47052	2.42452	0.42653	2.86868	0.09287	0.000	-0.81213	2.73544	0.07252	0.000
BH	26.7580	0.0785	0.000000	5.51515	2.43498	0.78212	2.06904	0.11046	0.000	-1.40573	2.26232	0.14718	0.000
XCOR	26.7580	0.0000	0.000000	5.51515	2.43498	0.78212	2.06904	0.11046	0.000	-1.40573	2.26232	0.14718	0.000
BH	26.9180	0.0785	0.000000	5.54027	2.44985	1.32250	1.42079	0.13992	0.000	-1.96471	1.78921	0.22093	0.000
EH	26.9180	-4.4452	0.000000	5.54027	2.44985	1.32250	1.42079	0.13992	0.000	-1.91425	1.73499	0.21559	0.000
DQF	27.0142	0.0000	0.000000	5.55042	2.46204	1.72344	1.11310	0.16066	0.000	-2.25353	1.46346	0.21559	0.000
QFH	27.0970	0.0000	-15.525920	5.55754	2.47479	1.91700	0.99598	0.16973	0.000	-0.00066	0.00092	0.00132	0.000
QFH	27.1798	0.0000	-15.525920	5.56466	2.48755	1.72364	1.11277	0.16088	0.000	2.25249	-1.46123	-0.21309	0.000
DQF	27.2760	0.0000	0.000000	5.57481	2.49974	1.32287	1.41999	0.14038	0.000	1.91350	-1.73227	-0.21309	0.000
E	27.2760	-4.4452	0.000000	5.57481	2.49974	1.32287	1.41999	0.14038	0.000	1.96398	-1.78645	-0.21844	0.000
B	27.5960	0.1571	0.000000	5.64450	2.52509	0.42703	2.86557	0.09412	0.000	0.81247	-2.73100	-0.07010	0.000
E	27.5960	-4.4452	0.000000	5.64450	2.52509	0.42703	2.86557	0.09412	0.000	0.82877	-2.84035	-0.07369	0.000
DQD	27.6937	0.0000	0.000000	5.68829	2.53004	0.30279	3.45078	0.08692	0.000	0.44283	-3.14951	-0.07369	0.000
QDH	27.7430	0.0000	18.325650	5.71551	2.53224	0.28125	3.60833	0.08520	0.000	0.00053	0.00138	0.00378	0.000
BPMX	27.7430	0.0000	0.000000	5.71551	2.53224	0.28125	3.60833	0.08520	0.000	0.00053	0.00138	0.00378	0.000
BPMY	27.7430	0.0000	0.000000	5.71551	2.53224	0.28125	3.60833	0.08520	0.000	0.00053	0.00138	0.00378	0.000
QDH	27.7923	0.0000	18.325650	5.74274	2.53445	0.30269	3.45052	0.08729	0.000	-0.44167	3.15202	0.08141	0.000
DQD	27.8900	0.0000	0.000000	5.78656	2.53940	0.42668	2.86487	0.09525	0.000	-0.82741	2.84239	0.08141	0.000

EH	27.5900	-4.4452	0.000000	5.78656	2.53940	0.42668	2.86487	0.09525	0.000	-0.81113	2.73307	0.07777	0.000
BH	28.0500	0.0785	0.000000	5.83118	2.54987	0.78181	2.06597	0.11367	0.000	-1.40392	2.26005	0.15233	0.000
XCOR	28.0500	0.0000	0.000000	5.83118	2.54987	0.78181	2.06597	0.11367	0.000	-1.40392	2.26005	0.15233	0.000
BH	28.2100	0.0785	0.000000	5.85632	2.56477	1.32150	1.41844	0.14394	0.000	-1.96214	1.78702	0.22594	0.000
EH	28.2100	-4.4452	0.000000	5.85632	2.56477	1.32150	1.41844	0.14394	0.000	-1.91172	1.73290	0.22044	0.000
DQF	28.3062	0.0000	0.000000	5.86647	2.57698	1.72191	1.11114	0.16515	0.000	-2.25056	1.46141	0.22044	0.000
QFH	28.3890	0.0000	-15.525920	5.87360	2.58975	1.91514	0.99417	0.17437	0.000	0.00023	0.00115	0.00026	0.000
QFH	28.4718	0.0000	-15.525920	5.88073	2.60253	1.72184	1.11074	0.16519	0.000	2.25092	-1.45861	-0.21996	0.000
DQF	28.5680	0.0000	0.000000	5.89089	2.61475	1.32136	1.41743	0.14403	0.000	1.91198	-1.72949	-0.21996	0.000
E	28.5680	-4.4452	0.000000	5.89089	2.61475	1.32136	1.41743	0.14403	0.000	1.96240	-1.78358	-0.22546	0.000
B	28.8880	0.1571	0.000000	5.96067	2.64014	0.42650	2.86098	0.09549	0.000	0.81101	-2.72751	-0.07731	0.000
E	28.8880	-4.4452	0.000000	5.96067	2.64014	0.42650	2.86098	0.09549	0.000	0.82729	-2.83669	-0.08095	0.000
DQD	28.9857	0.0000	0.000000	6.00451	2.64510	0.30255	3.44545	0.08758	0.000	0.44144	-3.14563	-0.08095	0.000
QDH	29.0350	0.0000	18.325650	6.03175	2.64731	0.28114	3.60286	0.08552	0.000	-0.00072	0.00035	-0.00305	0.000
BPMX	29.0350	0.0000	0.000000	6.03175	2.64731	0.28114	3.60286	0.08552	0.000	-0.00072	0.00035	-0.00305	0.000
BPMY	29.0350	0.0000	0.000000	6.03175	2.64731	0.28114	3.60286	0.08552	0.000	-0.00072	0.00035	-0.00305	0.000
YCOR	29.0350	0.0000	0.000000	6.03175	2.64731	0.28114	3.60286	0.08552	0.000	-0.00072	0.00035	-0.00305	0.000
QDH	29.0843	0.0000	18.325650	6.05898	2.64952	0.30269	3.44539	0.08728	0.000	-0.44300	3.14626	0.07472	0.000
DQD	29.1820	0.0000	0.000000	6.10278	2.65447	0.42698	2.86080	0.09458	0.000	-0.82911	2.83720	0.07472	0.000
EH	29.1820	-4.4452	0.000000	6.10278	2.65447	0.42698	2.86080	0.09458	0.000	-0.81282	2.72803	0.07111	0.000
BH	29.3420	0.0785	0.000000	6.14736	2.66496	0.78275	2.06338	0.11193	0.000	-1.40616	2.25588	0.14571	0.000
XCOR	29.3420	0.0000	0.000000	6.14736	2.66496	0.78275	2.06338	0.11193	0.000	-1.40616	2.25588	0.14571	0.000
BH	29.5020	0.0785	0.000000	6.17246	2.67987	1.32322	1.41704	0.14116	0.000	-1.96488	1.78372	0.21941	0.000
EH	29.5020	-4.4452	0.000000	6.17246	2.67987	1.32322	1.41704	0.14116	0.000	-1.91438	1.72965	0.21402	0.000
DQF	29.5982	0.0000	0.000000	6.18261	2.69209	1.72418	1.11033	0.16174	0.000	-2.25352	1.45866	0.21402	0.000
QFH	29.6810	0.0000	-15.525920	6.18973	2.70488	1.91765	0.99371	0.17062	0.000	0.00035	-0.00063	-0.00153	0.000
QFH	29.7638	0.0000	-15.525920	6.19685	2.71766	1.72407	1.11055	0.16150	0.000	2.25408	-1.46019	-0.21692	0.000
DQF	29.8600	0.0000	0.000000	6.20699	2.72987	1.32302	1.41759	0.14063	0.000	1.91478	-1.73151	-0.21692	0.000
E	29.8600	-4.4452	0.000000	6.20699	2.72987	1.32302	1.41759	0.14063	0.000	1.96526	-1.78561	-0.22228	0.000
B	30.1800	0.1571	0.000000	6.27671	2.75526	0.42671	2.86293	0.09314	0.000	0.81263	-2.73108	-0.07391	0.000
E	30.1800	-4.4452	0.000000	6.27671	2.75526	0.42671	2.86293	0.09314	0.000	0.82892	-2.84033	-0.07747	0.000
DQD	30.2777	0.0000	0.000000	6.32054	2.76021	0.30248	3.44816	0.08557	0.000	0.44264	-3.14976	-0.07747	0.000
QDH	30.3270	0.0000	18.325650	6.34779	2.76242	0.28096	3.60586	0.08364	0.000	0.00043	-0.00129	-0.00131	0.000
BPMX	30.3270	0.0000	0.000000	6.34779	2.76242	0.28096	3.60586	0.08364	0.000	0.00043	-0.00129	-0.00131	0.000
BPMY	30.3270	0.0000	0.000000	6.34779	2.76242	0.28096	3.60586	0.08364	0.000	0.00043	-0.00129	-0.00131	0.000
QDH	30.3763	0.0000	18.325650	6.37504	2.76463	0.30239	3.44841	0.08544	0.000	-0.44169	3.14741	0.07478	0.000
DQD	30.4740	0.0000	0.000000	6.41889	2.76958	0.42642	2.86360	0.09275	0.000	-0.82781	2.83842	0.07478	0.000
EH	30.4740	-4.4452	0.000000	6.41889	2.76958	0.42642	2.86360	0.09275	0.000	-0.81154	2.72914	0.07124	0.000
BH	30.6340	0.0785	0.000000	6.46354	2.78005	0.78179	2.06580	0.11013	0.000	-1.40495	2.25711	0.14591	0.000
XCOR	30.6340	0.0000	0.000000	6.46354	2.78005	0.78179	2.06580	0.11013	0.000	-1.40495	2.25711	0.14591	0.000
BH	30.7940	0.0785	0.000000	6.48866	2.79495	1.32190	1.41905	0.13939	0.000	-1.96376	1.78507	0.21968	0.000
EH	30.7940	-4.4452	0.000000	6.48866	2.79495	1.32190	1.41905	0.13939	0.000	-1.91332	1.73092	0.21436	0.000
DQF	30.8902	0.0000	0.000000	6.49882	2.80715	1.72265	1.11208	0.16001	0.000	-2.25250	1.46002	0.21436	0.000
QFH	30.9730	0.0000	-15.525920	6.50594	2.81991	1.91613	0.99541	0.16900	0.000	-0.00070	-0.00131	0.00098	0.000
QFH	31.0558	0.0000	-15.525920	6.51307	2.83267	1.72286	1.11254	0.16017	0.000	2.25139	-1.46321	-0.21250	0.000
DQF	31.1520	0.0000	0.000000	6.52322	2.84486	1.32230	1.42019	0.13973	0.000	1.91253	-1.73480	-0.21250	0.000
E	31.1520	-4.4452	0.000000	6.52322	2.84486	1.32230	1.42019	0.13973	0.000	1.96299	-1.78900	-0.21783	0.000
B	31.4720	0.1571	0.000000	6.59293	2.87021	0.42695	2.86802	0.09367	0.000	0.81191	-2.73546	-0.06944	0.000
E	31.4720	-4.4452	0.000000	6.59293	2.87021	0.42695	2.86802	0.09367	0.000	0.82820	-2.84490	-0.07302	0.000
DQD	31.5697	0.0000	0.000000	6.63673	2.87515	0.30282	3.45418	0.08653	0.000	0.44241	-3.15468	-0.07302	0.000
QDH	31.6190	0.0000	18.325650	6.66394	2.87735	0.28132	3.61209	0.08484	0.000	0.00013	-0.00067	0.00411	0.000
BPMX	31.6190	0.0000	0.000000	6.66394	2.87735	0.28132	3.61209	0.08484	0.000	0.00013	-0.00067	0.00411	0.000
BPMY	31.6190	0.0000	0.000000	6.66394	2.87735	0.28132	3.61209	0.08484	0.000	0.00013	-0.00067	0.00411	0.000
YCOR	31.6190	0.0000	0.000000	6.66394	2.87735	0.28132	3.61209	0.08484	0.000	0.00013	-0.00067	0.00411	0.000
QDH	31.6683	0.0000	18.325650	6.69116	2.87956	0.30279	3.45430	0.08694	0.000	-0.44213	3.15346	0.08142	0.000
DQD	31.7660	0.0000	0.000000	6.73496	2.88450	0.42687	2.86836	0.09490	0.000	-0.82787	2.84391	0.08142	0.000
EH	31.7660	-4.4452	0.000000	6.73496	2.88450	0.42687	2.86836	0.09490	0.000	-0.81158	2.73446	0.07780	0.000
BH	31.9260	0.0785	0.000000	6.77957	2.89496	0.78215	2.06899	0.11332	0.000	-1.40434	2.26159	0.15236	0.000
XCOR	31.9260	0.0000	0.000000	6.77957	2.89496	0.78215	2.06899	0.11332	0.000	-1.40434	2.26159	0.15236	0.000
BH	32.0860	0.0785	0.000000	6.80469	2.90983	1.32196	1.42094	0.14360	0.000	-1.96253	1.78872	0.22599	0.000

ELEM	S(M)	PHI(DEG)	K(1/M2)	NUX	NUY	BX(M)	BY(M)	EX(M)	EY(M)	AX	AY	EX'	EY'
EH	32.[illegible]860	-4.4452	0.000000	6.80469	2.90983	1.32196	1.42094	0.14360	0.000	-1.91209	1.73449	0.22051	0.000
D5	32.1822	0.0000	0.000000	6.81484	2.92202	1.72244	1.11333	0.16482	0.000	-2.25091	1.46311	0.22051	0.000
QFMH	32.2650	0.0000	-12.902180	6.82193	2.93485	1.94912	0.97784	0.17557	0.000	-0.40557	0.22132	0.03734	0.000
QFMH	32.3478	0.0000	-12.902180	6.82878	2.94815	1.84898	1.03564	0.17091	0.000	1.57910	-0.93984	-0.14911	0.000
D4D	32.6970	0.0000	0.000000	6.87062	2.98804	0.97654	1.91377	0.11884	0.000	0.91930	-1.57486	-0.14911	0.000
RFCW	32.6970	0.0000	0.000000	6.87062	2.98804	0.97654	1.91377	0.11884	0.000	0.91930	-1.57486	-0.14911	0.000
D4C	33.1117	0.0000	0.000000	6.96745	3.01354	0.53901	3.53270	0.05701	0.000	0.13575	-2.32899	-0.14911	0.000
SD	33.1117	0.0000	0.000000	6.96745	3.01354	0.53901	3.53270	0.05701	0.000	0.13575	-2.32899	-0.14911	0.000
QDMH	33.1610	0.0000	-0.743500	6.98216	3.01569	0.52926	3.77343	0.04961	0.000	0.06196	-2.55682	-0.15106	0.000
BPMX	33.1610	0.0000	0.000000	6.98216	3.01569	0.52926	3.77343	0.04961	0.000	0.06196	-2.55682	-0.15106	0.000
BPMY	33.1610	0.0000	0.000000	6.98216	3.01569	0.52926	3.77343	0.04961	0.000	0.06196	-2.55682	-0.15106	0.000
QDMH	33.2103	0.0000	-0.743500	6.99704	3.01770	0.52681	4.03751	0.04212	0.000	-0.01229	-2.80314	-0.15274	0.000
D3	33.3170	0.0000	0.000000	7.02877	3.02161	0.55104	4.66068	0.02582	0.000	-0.21486	-3.03722	-0.15274	0.000
EH	33.3170	-4.4452	0.000000	7.02877	3.02161	0.55104	4.66068	0.02582	0.000	-0.19383	-3.21508	-0.15373	0.000
BH	33.4770	0.0785	0.000000	7.07154	3.02653	0.65753	5.75177	0.00745	0.000	-0.47032	-3.60426	-0.07579	0.000
XCOR	33.4770	0.0000	0.000000	7.07154	3.02653	0.65753	5.75177	0.00745	0.000	-0.47032	-3.60426	-0.07579	0.000
BH	33.6370	0.0785	0.000000	7.10582	3.03056	0.85081	6.96741	0.00159	0.000	-0.73522	-3.99345	0.00262	0.000
EH	33.6370	-4.4452	0.000000	7.10582	3.03056	0.85081	6.96741	0.00159	0.000	-0.70276	-4.25932	0.00256	0.000
D2	33.7886	0.0000	0.000000	7.13081	3.03372	1.10424	8.32198	0.00198	0.000	-0.96894	-4.67582	0.00256	0.000
QDIH	33.8570	0.0000	15.393090	7.13990	3.03501	1.33311	8.35883	0.00223	0.000	-2.45710	4.15006	0.00476	0.000
YCOR	33.8570	0.0000	0.000000	7.13990	3.03501	1.33311	8.35883	0.00223	0.000	-2.45710	4.15006	0.00476	0.000
QDIH	33.9254	0.0000	15.393090	7.14699	3.03640	1.80924	7.24026	0.00264	0.000	-4.67023	11.80886	0.00730	0.000
D1	34.0727	0.0000	0.000000	7.15637	3.04066	3.45866	4.18226	0.00371	0.000	-6.52739	8.95148	0.00730	0.000
QFIH	34.1570	0.0000	-10.484290	7.15979	3.04446	4.34136	3.05768	0.00418	0.000	-3.68223	4.71835	0.00379	0.000
BPMX	34.1570	0.0000	0.000000	7.15979	3.04446	4.34136	3.05768	0.00418	0.000	-3.68223	4.71835	0.00379	0.000
BPMY	34.1570	0.0000	0.000000	7.15979	3.04446	4.34136	3.05768	0.00418	0.000	-3.68223	4.71835	0.00379	0.000
XCOR	34.1570	0.0000	0.000000	7.15979	3.04446	4.34136	3.05768	0.00418	0.000	-3.68223	4.71835	0.00379	0.000
QFIH	34.2413	0.0000	-10.484290	7.16274	3.04936	4.63954	2.51101	0.00434	0.000	0.23334	1.92669	0.00000	0.000
D0	35.2680	0.0000	0.000000	7.19923	3.22316	4.39997	0.53288	0.00434	0.000	0.00000	0.00000	0.00000	0.000

*ACCUMULATED TRANSFER MATRICES:

	VERTICAL			HORIZONTAL		
END (S= 35.2680)	0.16782	0.52533	0.00000	0.31362	4.17798	0.00298
	-1.84997	0.16782	0.00000	-0.21581	0.31362	0.00094
	0.00000	0.00000	1.00000	0.00000	0.00000	1.00000

*TUNE/QUADRUPOLE SENSITIVITIES:

QUAD	DNUY/(DQ/Q)	DNUX/(DQ/Q)
QFH	-3.38240	6.05957
QDH	9.20110	-0.74590
QFIH	-1.77414	2.38738
QDIH	5.47253	-0.92080
QFMH	-0.68673	1.28799
QDMH	-0.08815	0.01237

Figure 6.2.3

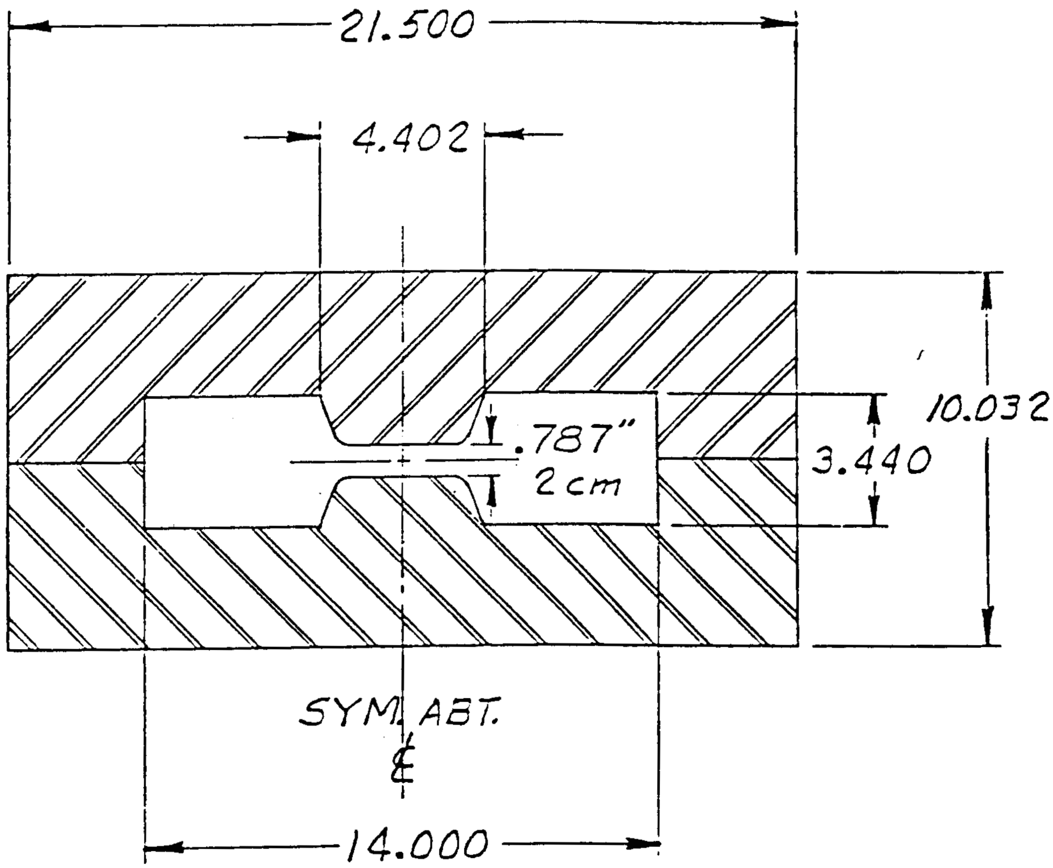

SECTION THRU 19.7 KG BEND MAGNET

Figure 6.2.4

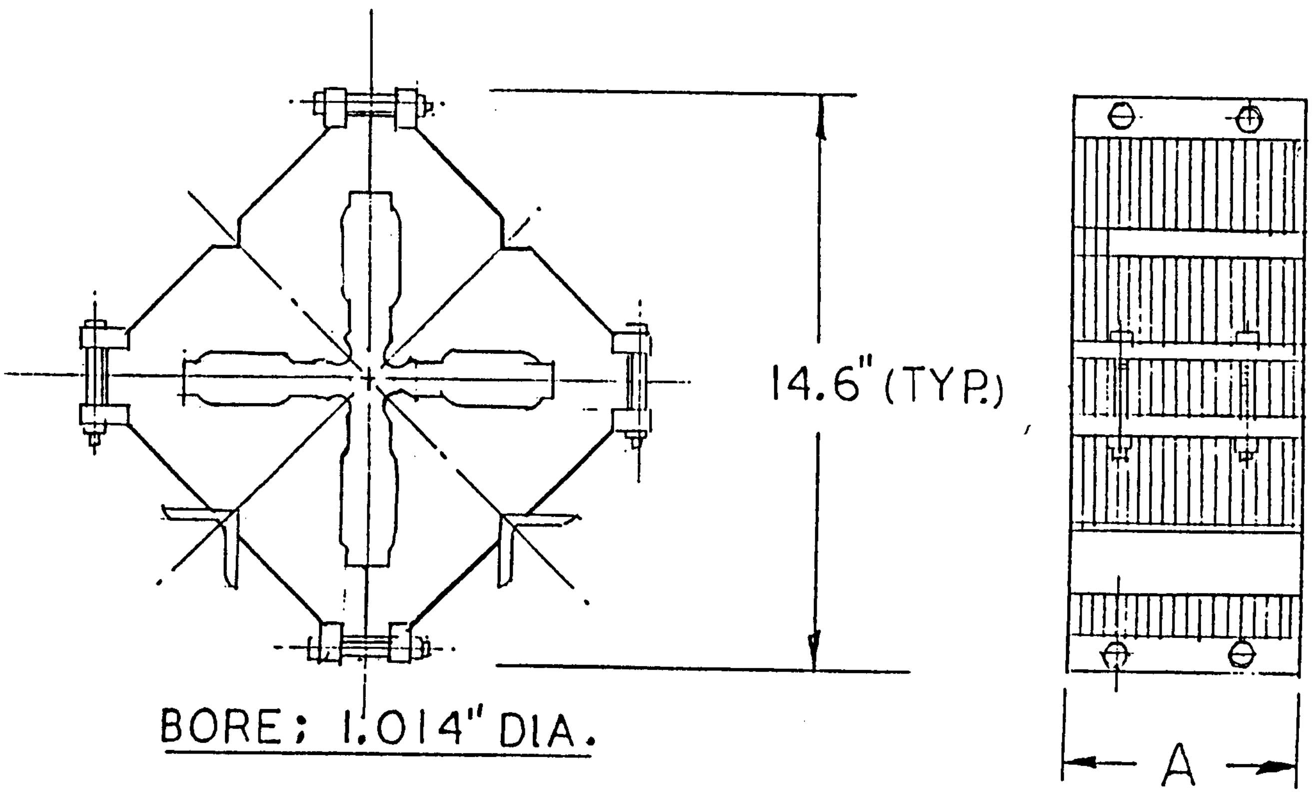

TYPICAL DAMPING RING QUAD

DIM.'A' { FOCUSING — 5.950" (16 TOTAL)
DEFOCUSING — 3.375" (18 TOTAL)

6.3 LINAC-TO-RING TRANSPORT LINE (LTR)

The unique geometry of the LTR transport line evolved early in the design of the damping ring complex, in response to the need for beam polarization control while simultaneously matching geometric constraints determined by 1) the choice to combine the extraction and injection region in the linac and 2) the optical requirements of the more sensitive designs of the ring (DR) and return line (RTL).

To preserve and manipulate the spin polarization of the electron beam, the optics and geometry of the transport lines are so chosen that solenoidal spin rotators ($B_z\ell \approx 6.3\,T - m$) can be inserted in regions of zero dispersion and at odd $\pi/2$ multiples of spin precession angle. At 1.21 GeV this occurs at bend angles of $(2n+1) \times 32.8°$. Thus in LTR after 164° of bend the longitudinally polarized beam extracted from the linac has precessed to become transversly polarized in the plane of bend. The solenoidal field then precesses the spin direction to be normal to the bend plane of the ring so that polarization will be preserved during damping. The transfer matrix for a solenoidal field can be represented by a focusing element nested between a rotation and inverse rotation about the beam axis, thus a requirement that the dispersion be zero at the rotator solenoid avoids mixing horizontal and vertical dispersion caused by rotation. The induced correlation in the $x-y$ projection of the beam phase space can be made transparent by causing $\beta_x = \beta_y$ and $\alpha_x = \alpha_y$ in the solenoid. Such a provision will be a minor future modification to LTR.

Having provided for polarization control, the need to match to a geometry prescribed by the RTL optics (where a smooth monotonic $\int(\eta/\rho)\delta s$ is desirable) and the ring resulted in the unusual geometry and optics of LTR.

A path length constraint was also applied to synchronize positron and electron beams.

Figures 6.3.1 and 6.3.2 show the betatron and dispersion functions for LTR. The future spin rotator solenoid will be located near the point where $s = 40$ m. Figure 6.3.3 shows the mechanical apertures superimposed on the envelope of a beam for which $\epsilon_x = \epsilon_y = 1.0$ mm–mr and $\delta = 1.0\%$.

The transport line contains 23 horizontal bend magnets identical in cross section to the ring bend magnets (see Fig. 6.2.3). These magnets are powered in series from a single source and provide 200.7° of bend. Three vertical bends also powered in series are used to bring the beam to the elevation of the level plane of the damping ring, 36 cm below the height of the extraction point. All of the LTR line outside of the linac housing also lies in this plane.

The main windings of the 45 quadrupoles are powered in series while the first eight and the last ten are equipped with trim windings for correction and tuning. In the two central straight sections the quadrupoles are arranged in a FODO array with 45° phase shift per cell. The β function is not now matched in these regions but this loss of elegance has not effected performance. The remaining quadrupoles ($\sim 1/2$) were used in the design to match to the linac and damping ring machine functions.

Extraction from the linac is achieved by pulsing a laminated core horizontal bending magnet (r.t. $\approx$ 3 ms, rate $\geq$ 20 Hz) which bends the electron(positron) beam south (north) by 7.0° (see Fig. 6.3.4). The beam after passing through a protection collimator and a ten port vacuum chamber then enters a field free aperture in the yoke of the downstream reinjection magnet. A small correcting dipole has been placed immediately upstream of this aperture to correct for any field leakage into the aperture. Vertical bending magnets not shown in the figure then deflect the beam into the level plane which is common to the remainder of LTR, the ring and most of RTL. When the upstream magnet is not pulsed the undeflected beam enters the good field region of the reinjection magnet, thus this magnet must remain off for straight ahead operation.

Diagnostics

The LTR transport line is equipped with diagnostic instrumentation for measuring the beam size, intensity, energy spread and orbit distortions. Control, status and appropriate output signals are interfaced through CAMAC to a microprocessor dedicated to LTR. The microprocessor is linked through SLCNET to the VAX residing at the Main Control Center (see I&C Section 7.).

The energy spectrum of the beam being delivered from Sector 1 is measured with a 20 foil spectrum monitor (see Fig. 6.3.5) placed 3 m downstream of the extraction point. The tungsten foils are 0.8 mm wide with 2.0 mm spacing giving a resolution of 0.4% ($\delta E/E$ per foil). In the axial direction the foils are thick ($\approx$ 3 r.l.) thus the unamplified signals are suitable input for a simple multichannel charge integrator with video graphics display. Charge integration and hold time are controllable through the VAX. During typical operation, the display is updated at 2 Hz for a 10 Hz beam of $< 10^{10}$ electrons per pulse. The spectrum monitor foils are supported on the front face of a movable water cooled collimator. The collimator has two positions. When in one position, all foils are in the beam and the collimator serves as a 4 kW dump for tuning Sector 1. When the collimator and its foils are moved to the alternate position the 8 central foils are removed from the beam which now passes through a 16 mm-diameter hole defining the energy spread to be $\pm 1\%$, matching the acceptance of the ring.

Three beam current measuring toroids are located in LTR. The first is placed upstream of the energy defining aperture and measures the intensity of the beam delivered from Sector 1. The second toroid, downstream of the collimator measures the beam intensity within the energy acceptance of the ring. A third toroid at the end of LTR measures the transmission efficiency of the beam line. Signals from these last two toroids are to be integrated and compared during each machine pulse providing a means of limiting component damaging beam loss to an acceptable level (100–200 W).

A Faraday cup can be remotely inserted into the beam downstream of the last toroid as an independent measurement of the charge delivered to the ring.

The beam orbit is measured by 19 beam position monitors (BPM) placed at intervals of approximately one-quarter of a betatron wavelength. Each beam position monitor has four strip line detectors, one in each quadrant. The four signals (one from each electrode) are electronically summed then digitized for processing by the SLC VAX computer (see Fig. 6.3.6). Beam position information is then presented in either numeric or graphic form. All beam position monitors are not read out during the passage of a single beam pulse. Instead, a system of CAMAC-controlled solid state one pole-ten throw relays sequentially switch signals to the processor during the inter-pulse period. Three of these relays with three processors presently allow a sequential scan of the beam position monitors in sets of three. The scan rate is limited by software processing time and it requires approximately 3 seconds for a scan of all LTR BPM's. This slow scan rate has not presented any operational difficulty however, since orbit correction is usually done with low intensity beams having good pulse to pulse stability. The measured orbits reproduce with rms deviations of $\approx 100\,\mu m$.

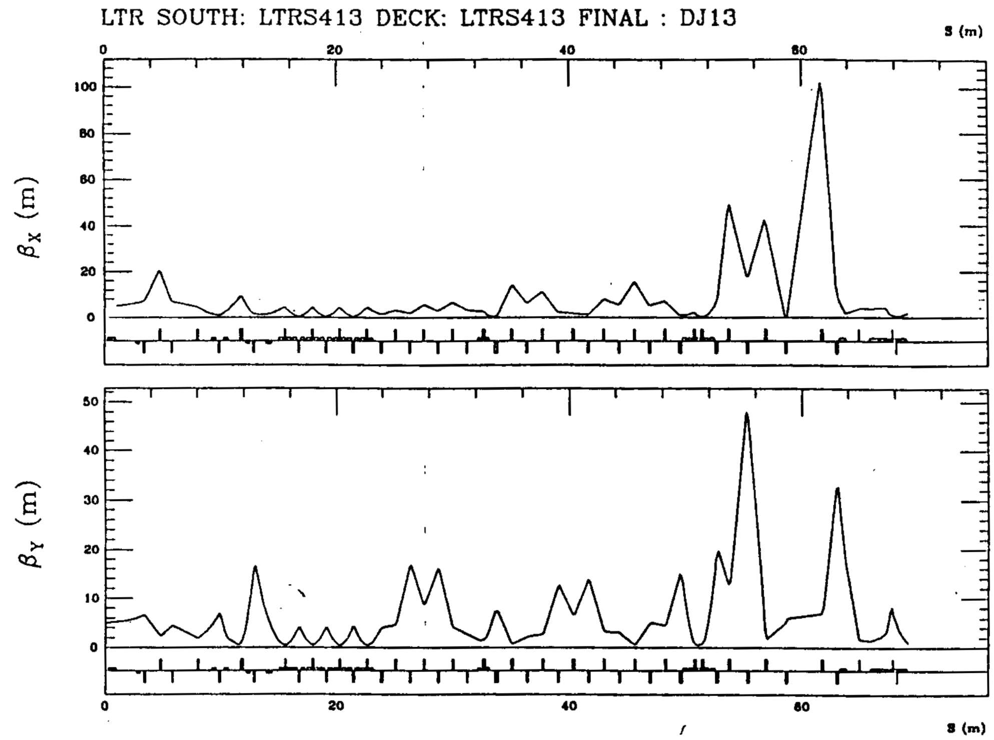

Figure 6.3.1
LTR Betatron Functions

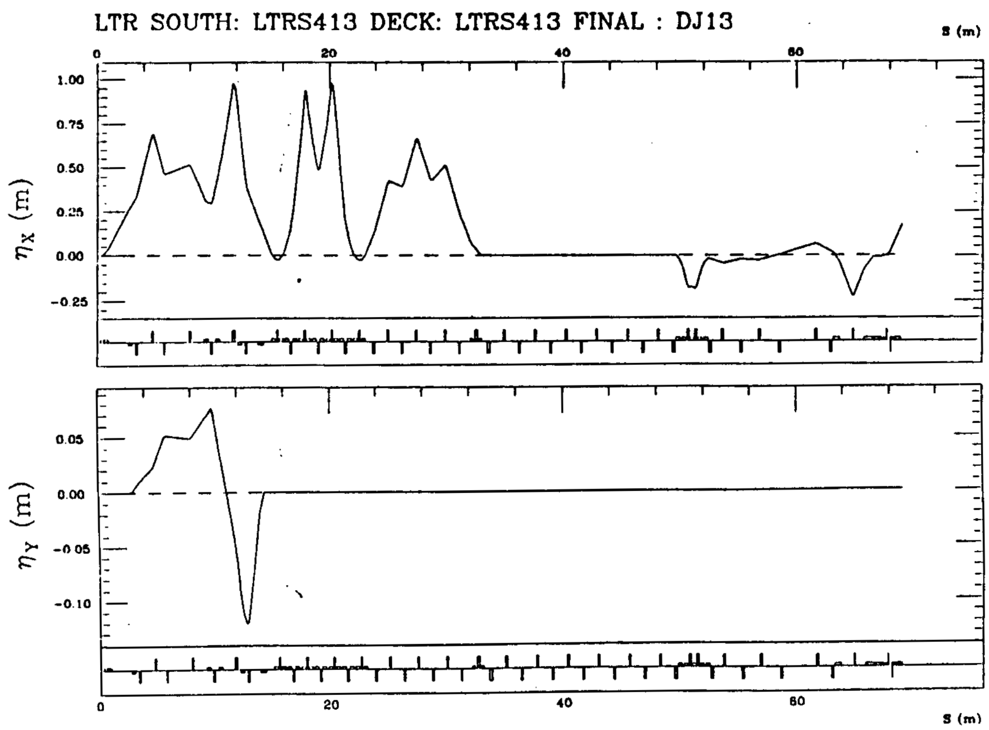

Figure 6.3.2
LTR Eta Functions

Figure 6.3.3 LTR Beam and Vacuum Chamber Clearance

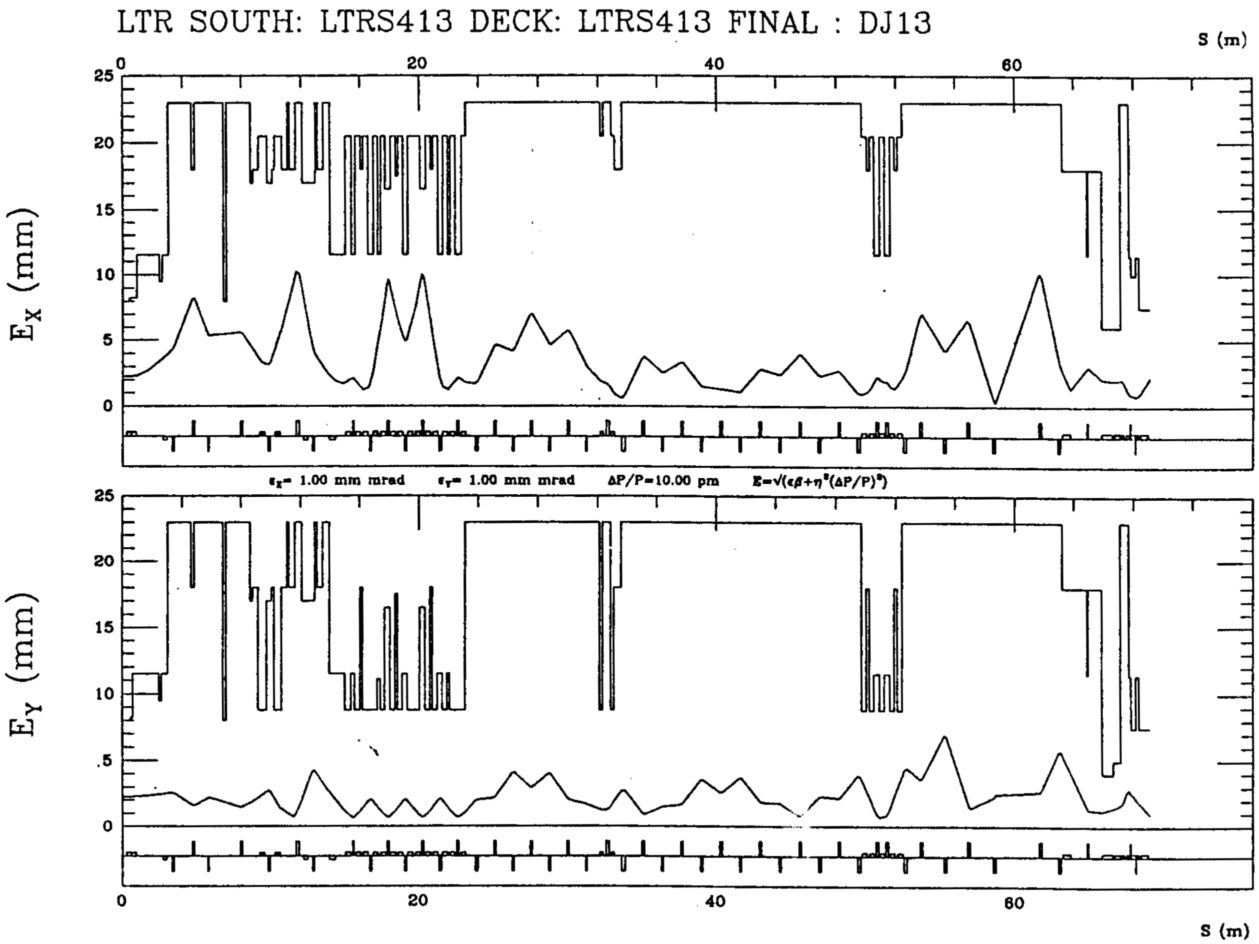

Figure 6.3.4 Extraction and Re-Injection at Girder 1–9

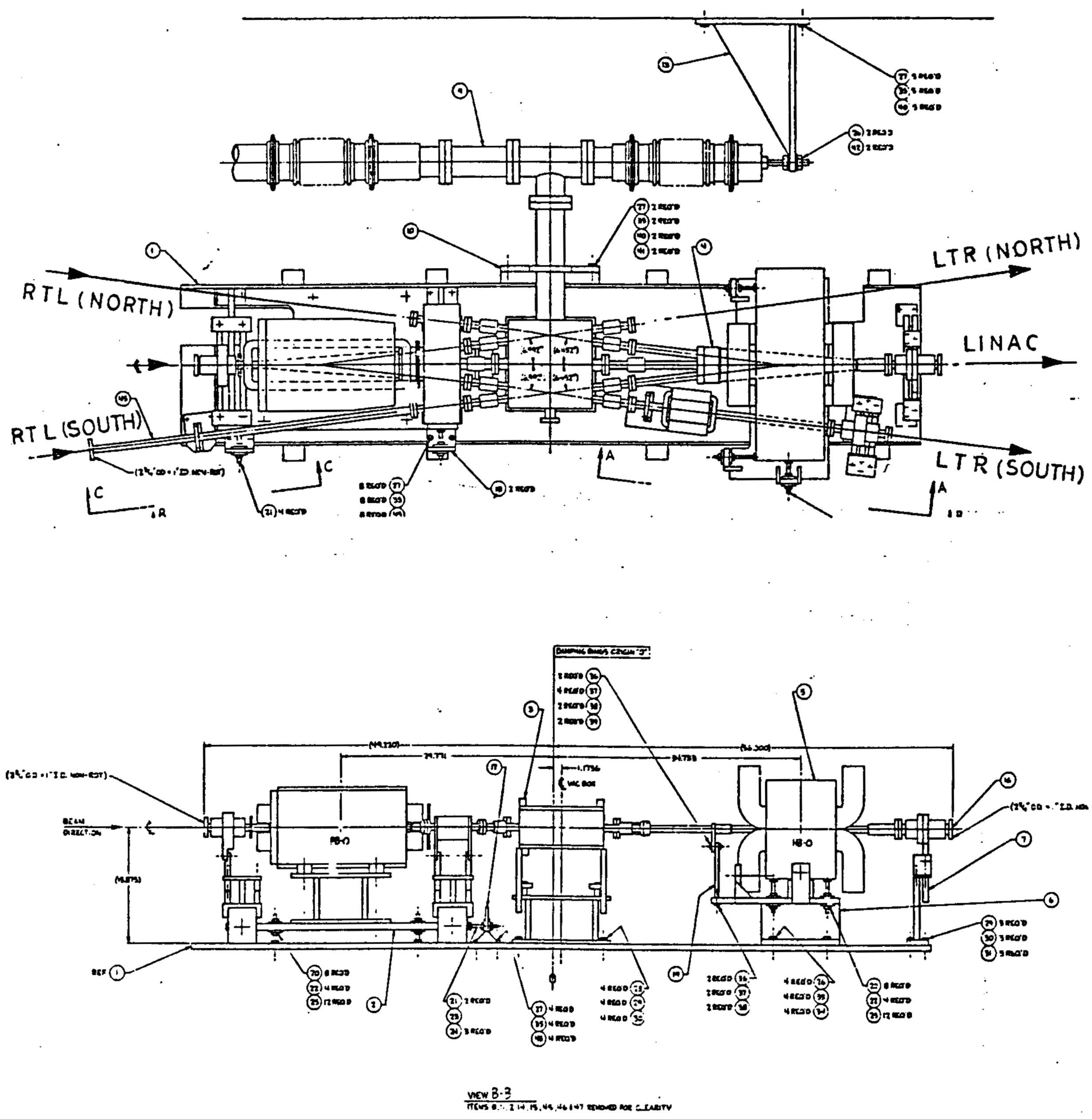

Figure 6.3.5 Spectrum Monitor Foils and Collimator

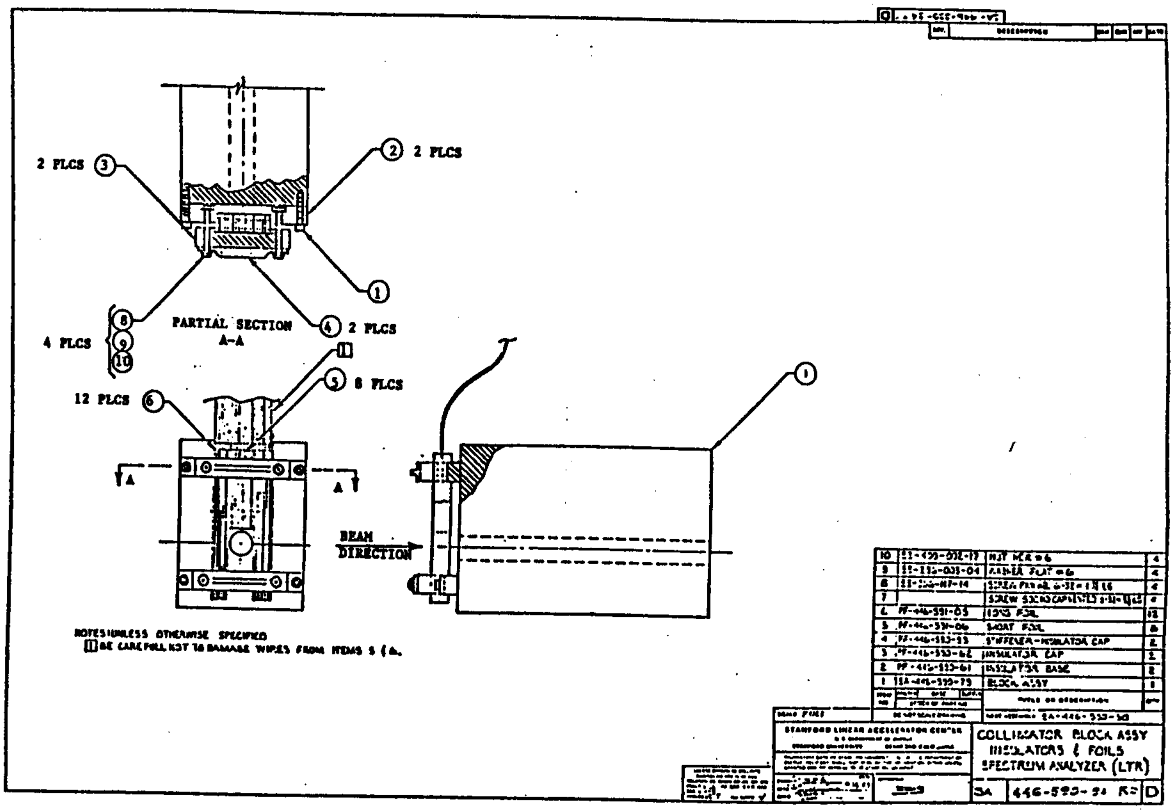

Figure 6.3.6 Beam Position Monitor Signal Processing

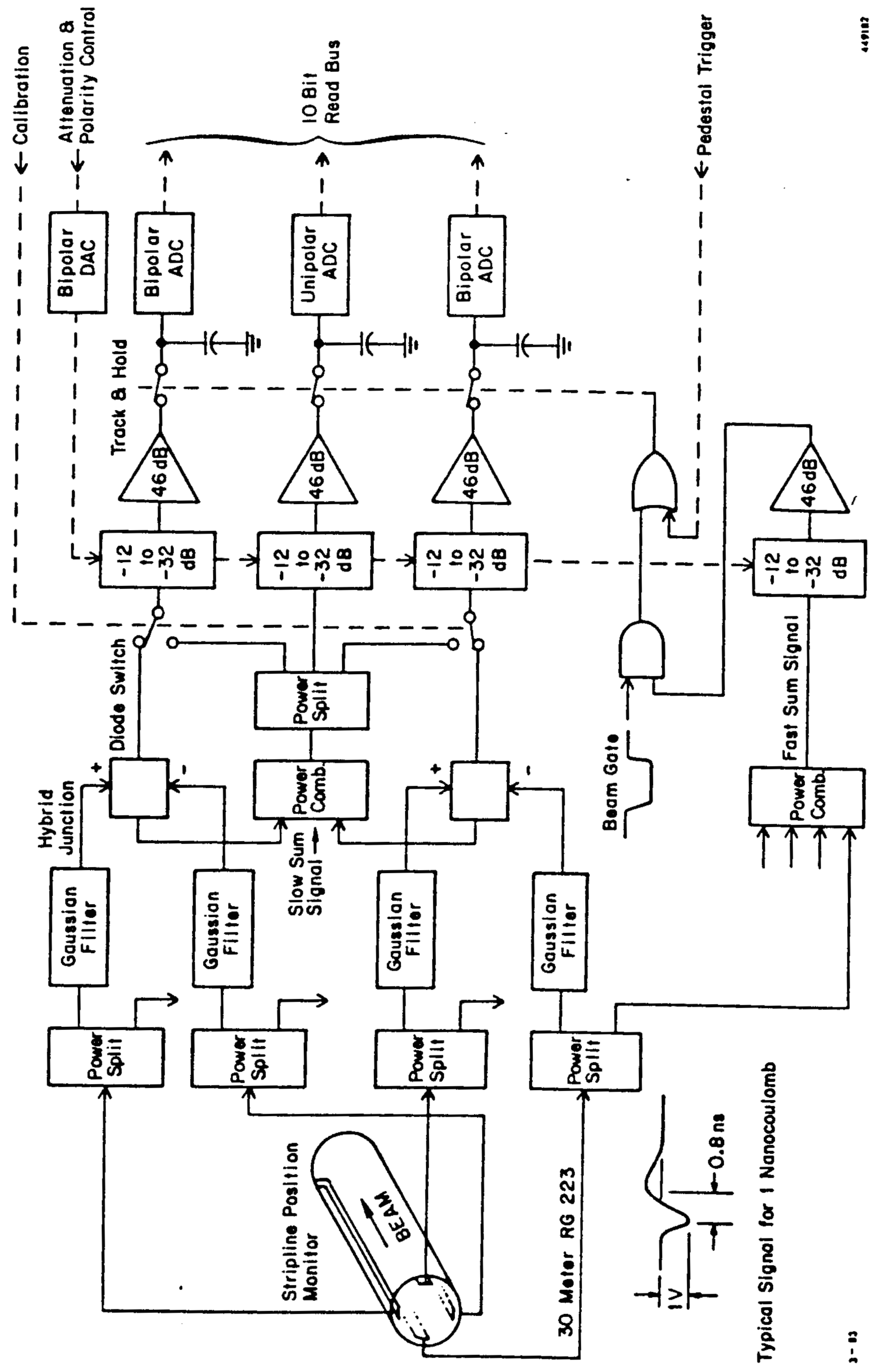

6.4 RING-TO-LINAC TRANSPORT LINE (RTL)

The first and second order optics for the damping ring to linac transport line are designed[7] to preserve the damped transverse emittance while simultaneously compressing the bunch length of the beam to that length required for reinjection into the linac. This design, including provisions for future control of beam polarization, is described here.

The design parameters for the SLC damping ring (DR) have been described elsewhere.[8] Those parameters important to the description of the RTL transport line are listed in Table 6.4.1 and were taken as given input conditions for the transport line. At the output of the transport line it is important to have control of the bunch length to reduce both the transverse emittance growth and the energy spread due to transverse and longitudinal wake fields as the particle bunches are accelerated through the linac. A delicate balance must be maintained to minimize these effects since the transverse emittance growth decreases with shorter bunch length while the opposite is true for the energy spread. Calculation of the effects of these fields[9] have shown that an rms bunch length on the order of 1.0 mm is suitable for the acceleration of 5×10^{10} particles/bunch. To ensure that adequate control of this parameter can be provided the choice was made to design the RTL beam line such that compression of the 6.0 mm rms DR bunch length to a minimum rms length of 0.5 mm will be achieved.

Table 6.4.1 Damping Ring Parameters	
Energy	1.21 GeV
Equilibrium emittance	$9.1 \times 10^{-9}\pi$ rad-m
Extracted beam emittance	$1.2 \times 10^{-8}\pi$ rad-m
Equilibrium-related energy spread	7.4×10^{-4}
Equilibrium bunch length	5.9 mm

Compression

The bunch length compression in RTL is accomplished by first passing the particle bunches through an S-band accelerating section at 0° central phase angle immediately after extraction from the damping ring. This maneuver introduces a correlation between the position of a particle in the bunch and its energy (see Fig. 6.4.1). Compression then occurs due to energy dependent path length differences proportional to the momentum compaction factor α (see Fig. 6.4.2).

It can be seen from Fig. 6.4.1 that the slope of the required correlation between energy and bunch length is very nearly defined by the damping ring energy spread $\delta(0)$ and the chosen rms bunch length $\ell(1)$ of 0.5 mm after compression. Hence the energy spread at the end of RTL will be given by $\delta(1) \approx [\delta(0)/\ell(1)]\,\ell(0) \approx 0.009$. The required peak accelerating voltage V_{RF} then follows from $\delta(1) = (V_{\mathrm{RF}}/E_R)\sin(2\pi\ell(0)/\lambda)$ where E_R is the ring operating energy of 1210 MeV and λ is the S-band wavelength of 0.105 m. Thus, V_{RF} is $\approx$ 30 MeV which in practice can be easily supplied by a single 3-m disc loaded waveguide identical to those used in the linac. The momentum compaction factor given by $\ell(1)/L\delta(0) = \alpha \approx 1/\nu^2$ can be used to estimate that the RTL should span approximately two betatron wavelengths.

Optical Design

The RTL transport line will be required to have an energy acceptance greater than $\pm 2\delta(1)$. For such a large energy spread control of chromatic aberrations becomes a primary concern. The concept of the second-order magnetic optical achromat[10] was used as a design guide though strict adherence to its principles

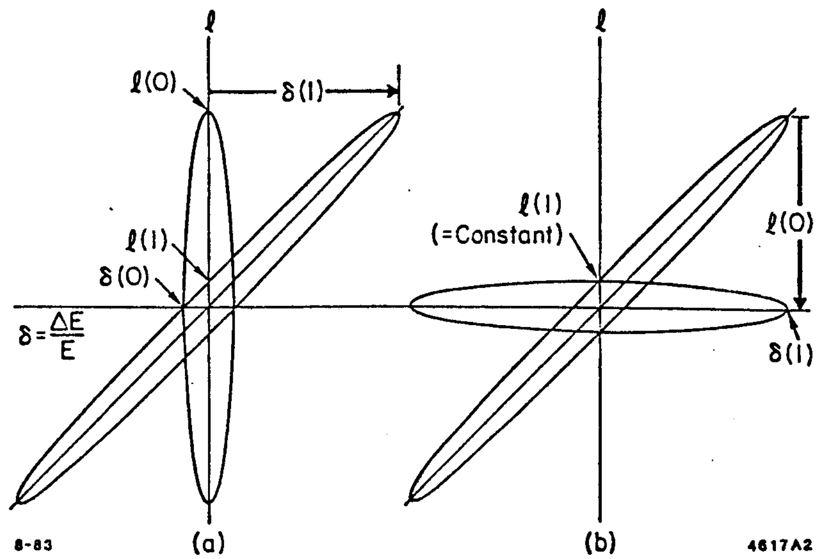

Figure 6.4.1

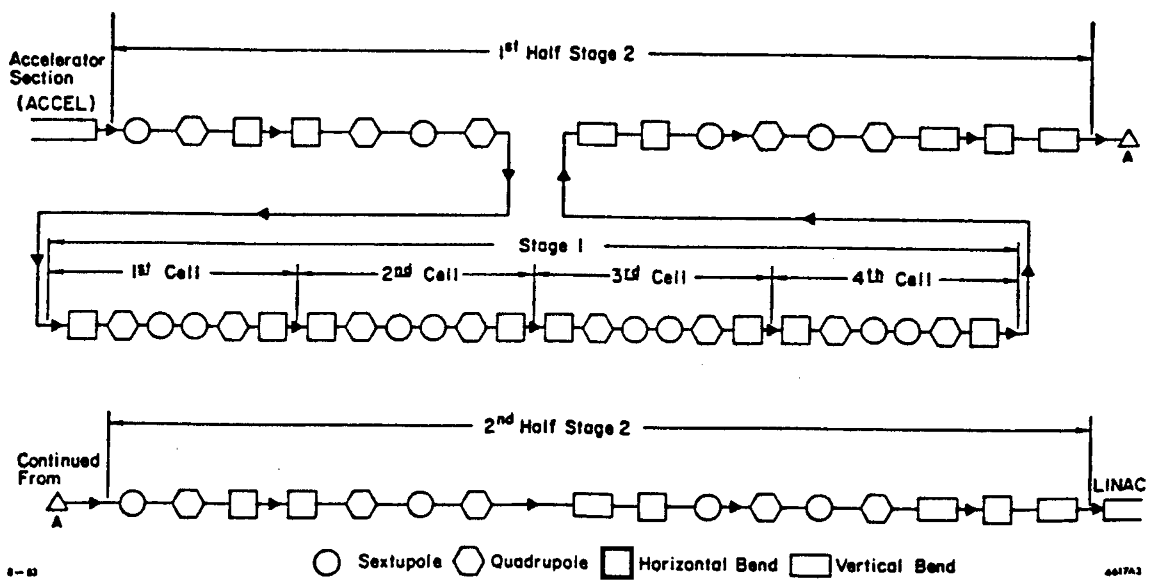

Figure 6.4.2

was precluded because of the need to fit the transport line into an existing linac housing. The theoretical principles of the second-order achromat are described elsewhere.[11] Here we describe its application to the RTL design. The beam line consists of two stages (see Fig. 6.4.2) each characterized by a transformation matrix equal to the identity matrix. Stage one consists of four identical cells, each cell containing two bending magnets, two quadrupoles, and two sextupoles. The strength of the two quadrupoles and two drift distances are determined by the constraint that the overall transformation be the identity with a total phase shift of 2π. Then, since there are four identical cells the second-order geometric terms vanish due to symmetry. And, as shown by K. Brown, all second-order chromatic terms can be removed by properly setting the strength of the two sextupoles.

Stage two is not so neatly characterized. The placement of the bending magnets in this stage is dominated by the geometry of the RTL tunnel and the linac housing. With needed reverse bends and vertical as well as horizontal bends n-fold symmetry could not be maintained for $n > 2$. Instead, the stage is composed of two identical "cells" giving "half wave symmetry." All components in this stage, including those special magnets used to re-inject into the linac are imaged by the negative of the identity matrix onto an identical component in the other "cell," assuring that overall dispersion and second-order geometric aberrations vanish. Thus, stage two consists of six independent pairs of bend magnets, five independent pairs of quadrupoles and four independent pairs of sextupoles.

Another unusual feature of stage two can be observed in Fig. 6.4.2. It will be noted that the first half of this stage has been split and stage one has been inserted, a maneuver that was made possible by the stage one transformation being the identity. This "nested achromat" was introduced to take advantage of the large horizontal bend angle in the first two bending magnets of stage two to obtain a practical fit to the existing housing.

With the bend magnet strengths thus constrained by the geometry, six parameters, namely four of the quadrupole strengths and two pairs of intervening drifts, are determined by the constraint that the overall transformation of stage two be the identity. One pair of imaged quadrupoles are used to match to a periodic η-function in the nested stage one, providing a smooth bunch length compression in this section.

Matching the Linac Lattice

Figures 6.4.3a–c illustrate the resulting matching functions after completion of the first-order fitting described above and a match has been made to the linac lattice. This latter matching is achieved by inserting four quadrupoles between the damping ring extraction optics and the upstream end of the compressor waveguide. These quadrupoles are used to match to the desired linac lattice at the beginning of the two achromats just downstream of the compressor waveguide where there is an identical image of the linac entry point. Second-order effects in the region before the compressor waveguide are negligible because of the small momentum spread of the extracted beam.

Second-Order Correction in Stage Two

The mixture of horizontal and vertical bends in stage two results in mixed x, y dispersion at the sextupole sites. In order to avoid the introduction of cross-plane chromatic aberrations, this means that the four sextupole pairs must be rotated axially with respect to the beam coordinate system. That was done in conjunction with variation of the strengths of the four sextupole pairs to zero the T_{i66}, $i = 1,2,3,4$ and the T_{ij6}, $i = 1,2$, $j = 3,4$, elements of the second-order transfer matrix.

It was found empirically that the foregoing prescription reduced all chromatic aberrations in stage two to insignificant levels. It may not, however, be generally applicable because we are not dealing with a theoretically perfect second-order achromat.

Bunch Length

The progressive compression of a bunch as it moves through the RTL beam line is shown in Fig. 6.4.4a. Most of the compression occurs relatively smoothly in stage one. There is some unwanted but unavoidable fluctuation of the length

Figure 6.4.3: (a) β vs. s(m); (b) η vs. s(m); (c) Envelope vs. s(m); where $E = \sqrt{\epsilon\beta + (\eta\delta)^2}$, for $\epsilon_x = \epsilon_y = 0.01$ mm-mrad and $\delta = 2\%$

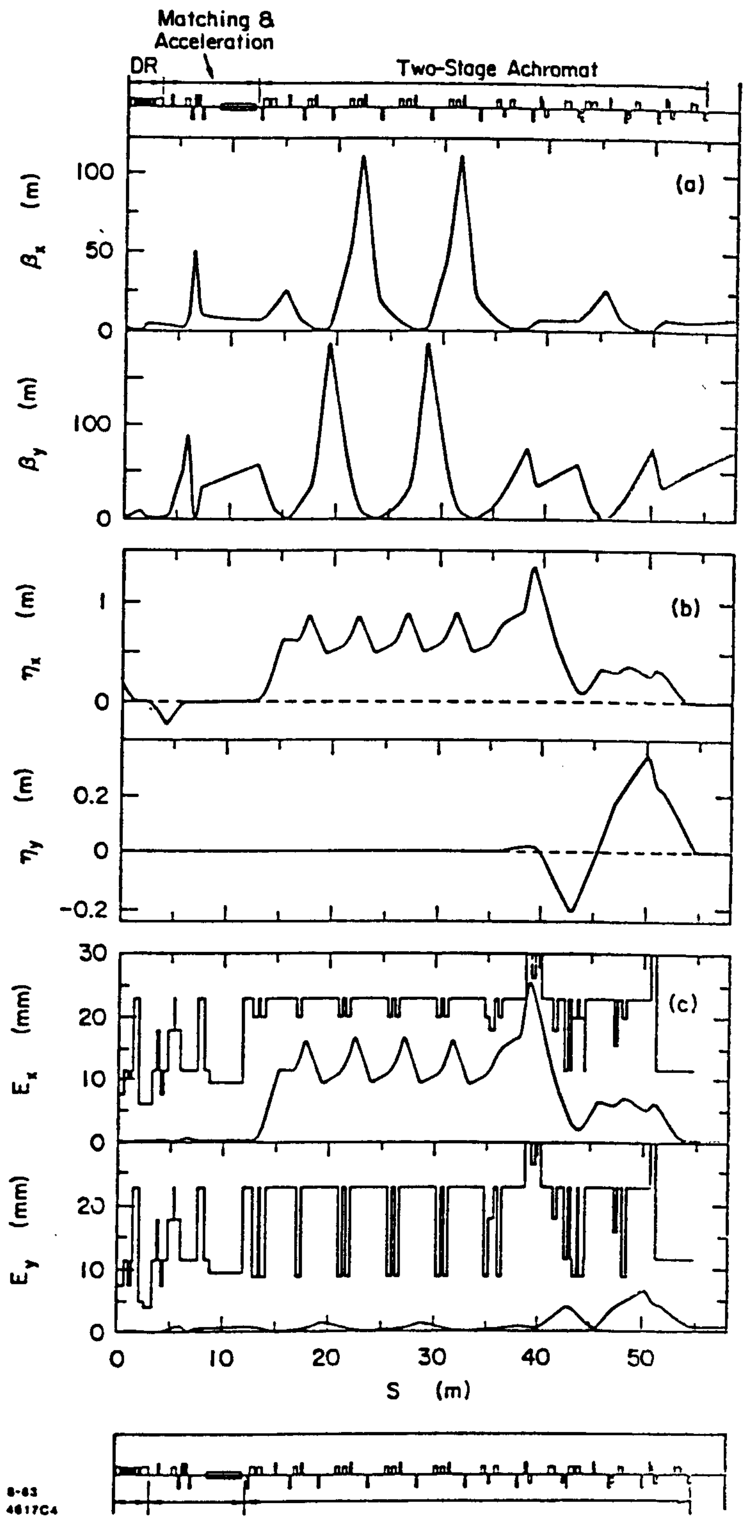

of the fully compressed bunch in stage two. Figure 6.4.4b shows the correlation of the bunch length and the momentum spread as given by the r_{56} correlation term of the TRANSPORT sigma matrix. The locations in the second stage where this term is less than zero correspond to over-compression. At the point of injection into the linac this term is equal to zero as intended.

Bunch Lengthening Effects

Figure 6.4.1a–b indicate a linear correlation for the particle position and its energy. This would only be true for $2\pi\ell(0) \ll 1$. Antisymmetric bunch lengthening occurs when the small angle approximation is not satisfied. A second effect which is symmetric about the bunch center is also introduced by the second order momentum dependent path length differences. Both these effects have been examined[12] for this design and can be adequately compensated by trimming the compressor waveguide voltage and phase angle.

Coherent bunch lengthening due to the longitudinal wake field of the bunch has also been examined and shown to be negligible.

Spin Polarization of the Electron Beam

It is expected that an electron beam from a polarized source will be injected into the DR with transverse spin polarization perpendicular to the plane of the DR. One of the design goals for the RTL electron beam is to be able to rotate the spin polarization to any arbitrary direction.[13] This will be done with the aid of suitably disposed solenoid magnets. In order to avoid disruption of the basic optics of the RTL beam, solenoids can only be located in places where there is no dispersion and where the beam is "round," (i.e., $\beta_x = \beta_y; \alpha_x = \alpha_y = 0$). Two solenoids are needed, and for arbitrary control the spin precession angle in the RTL-bends between them should be an odd multiple of 90°. There are only two possible locations which satisfy these criteria, one just before entry into the achromats and the other just after reinjection into the linac. The spin precession angle in the intervening beam line, the whole RTL beam, is almost exactly 270° at 1.2 GeV.

Figure 6.4.4: (a) Bunch length vs. s(m) for $V_{RF} = 33$ MeV; final rms length is 0.5 mm. (b) r_{56} $\ell - \delta$ correlation) vs. s(m).

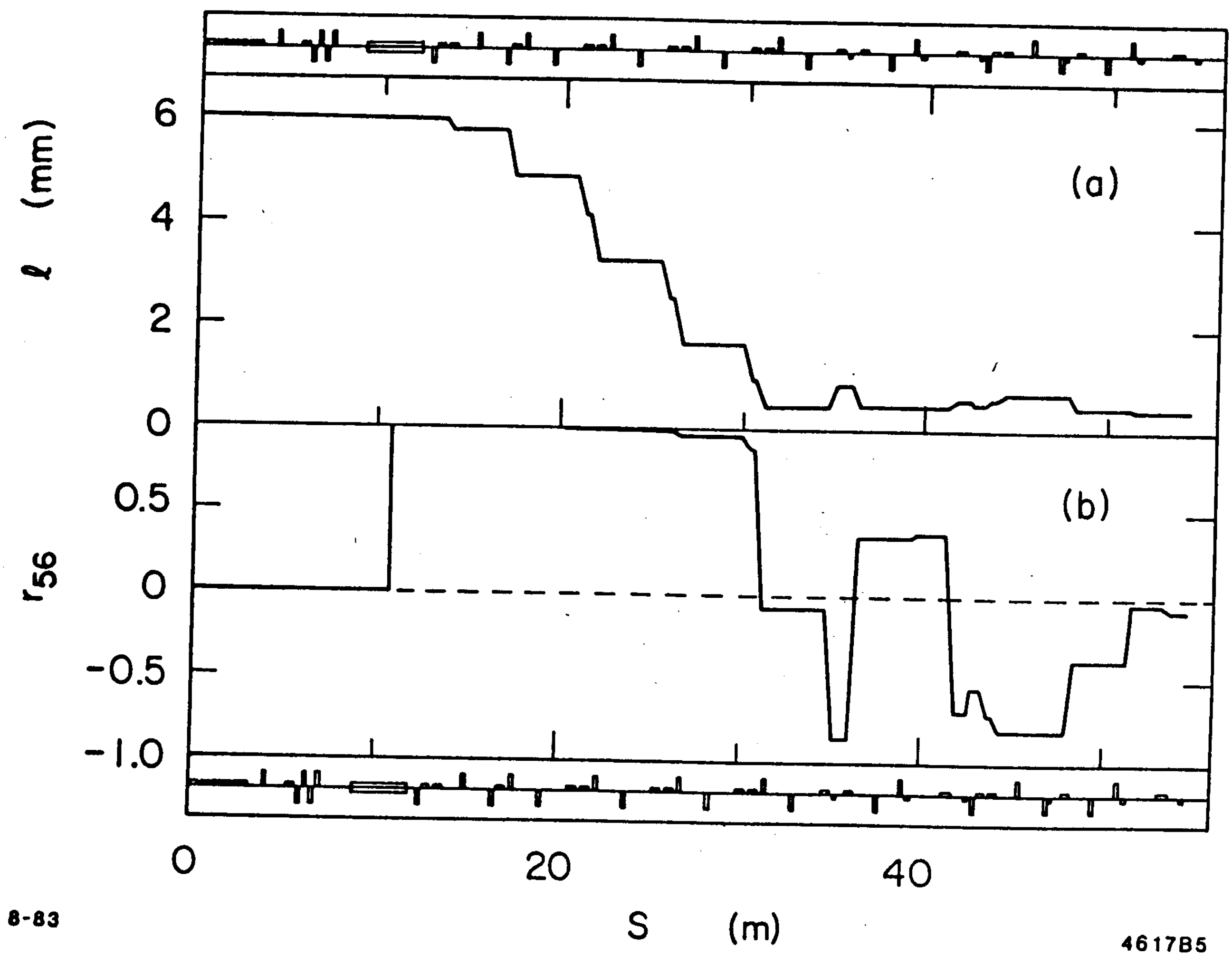

Orbit Correction

The placement of beam position monitors and orbit correcting magnets in RTL was determined by the same method[14] used for the LTR beam line.

The construction of ten beam lines, each with randomly displaced components were simulated and the efficacy of various correction schemes were tested. The criteria for judging performance included a one milliradian bend as a practical upper limit for the strength of the correctors. Each component including the beam position monitors themselves were independently misaligned using untruncated gaussian distributions. It is expected that in practice such errors would not be truly gaussian but would be truncated, thus this estimate is conservative.

The alignment tolerances used for these simulations and construction specifications were:

for all (mm)	for quads (mr)	for bends (mr)
$\delta x = 0.2$	$\delta x' = 0.5$	$\delta x' = 0.1$
$\delta y = 0.2$	$\delta y' = 1.0$	$\delta y' = 0.1$
$\delta z = 2.0$	$\delta z' = 0.5$	$\delta z' = 0.1$

The results of this study are shown in Figures 6.4.5–6.4.7.

Figure 6.4.5a

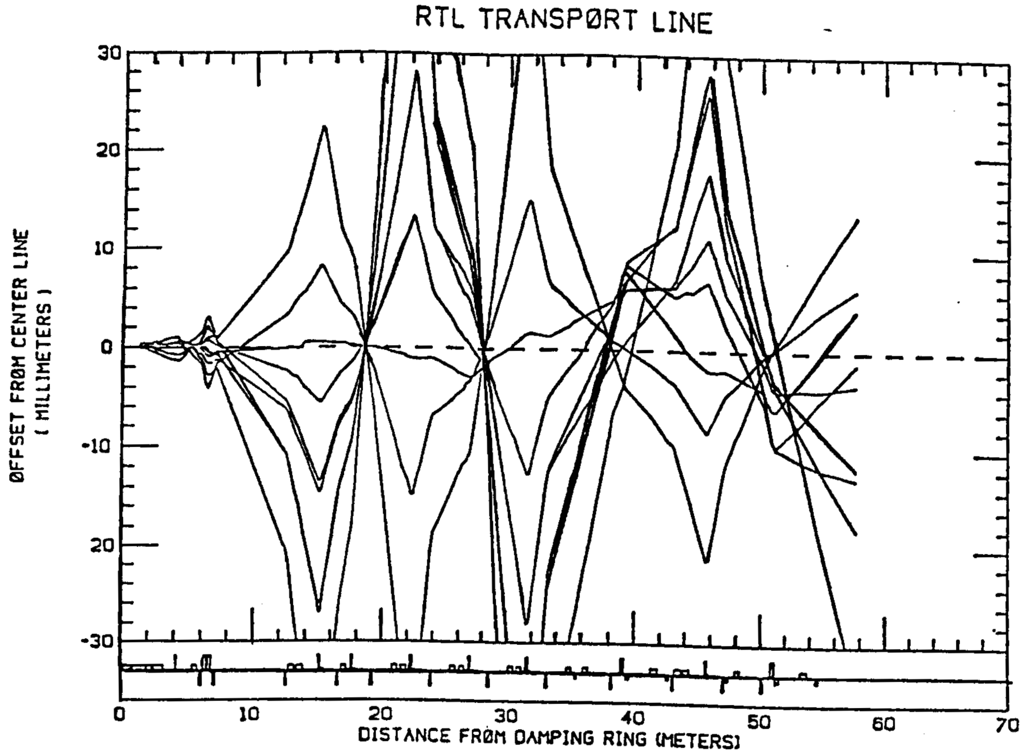

UNCØRRECTED HØRIZØNTAL TRAJECTØRIES

Figure 6.4.5b

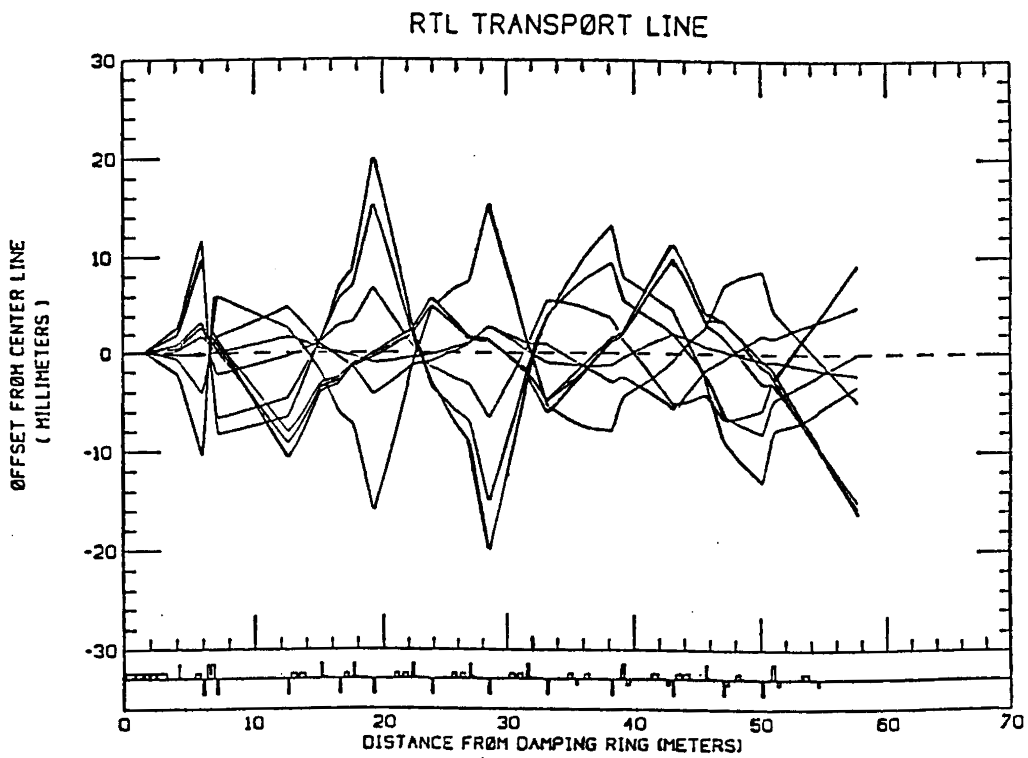

UNCØRRECTED VERTICAL TRAJECTØRIES

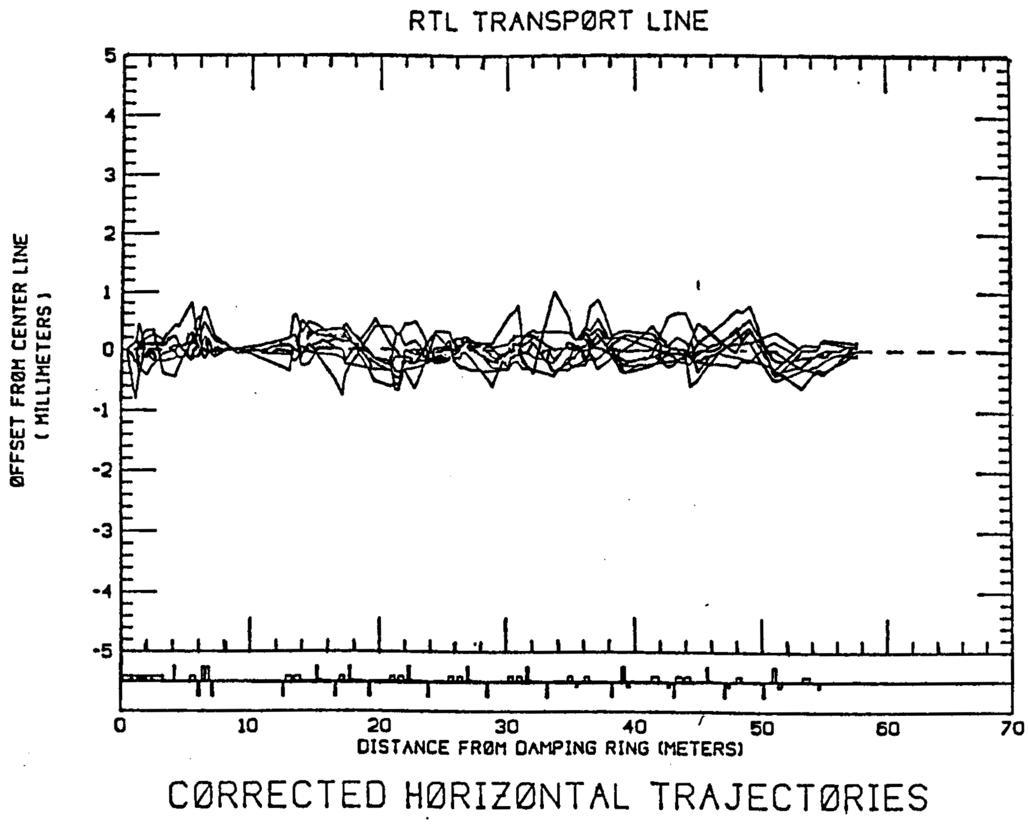

Figure 6.4.6a

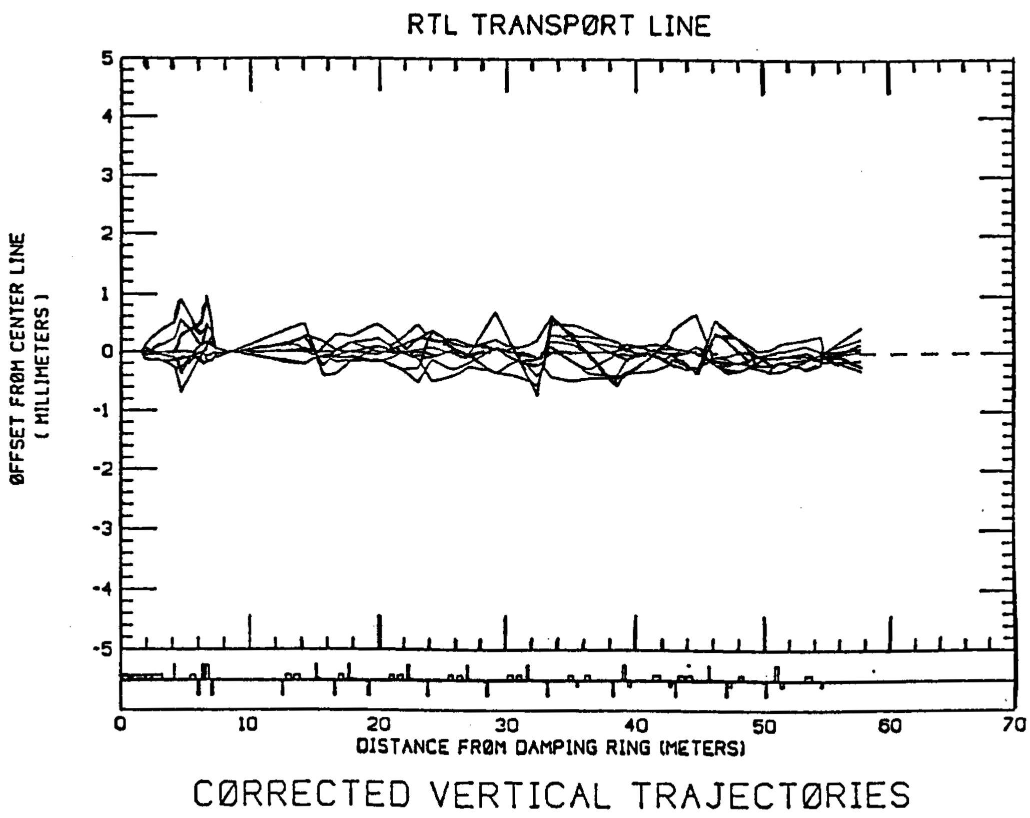

Figure 6.4.6b

Figure 6.4.7a

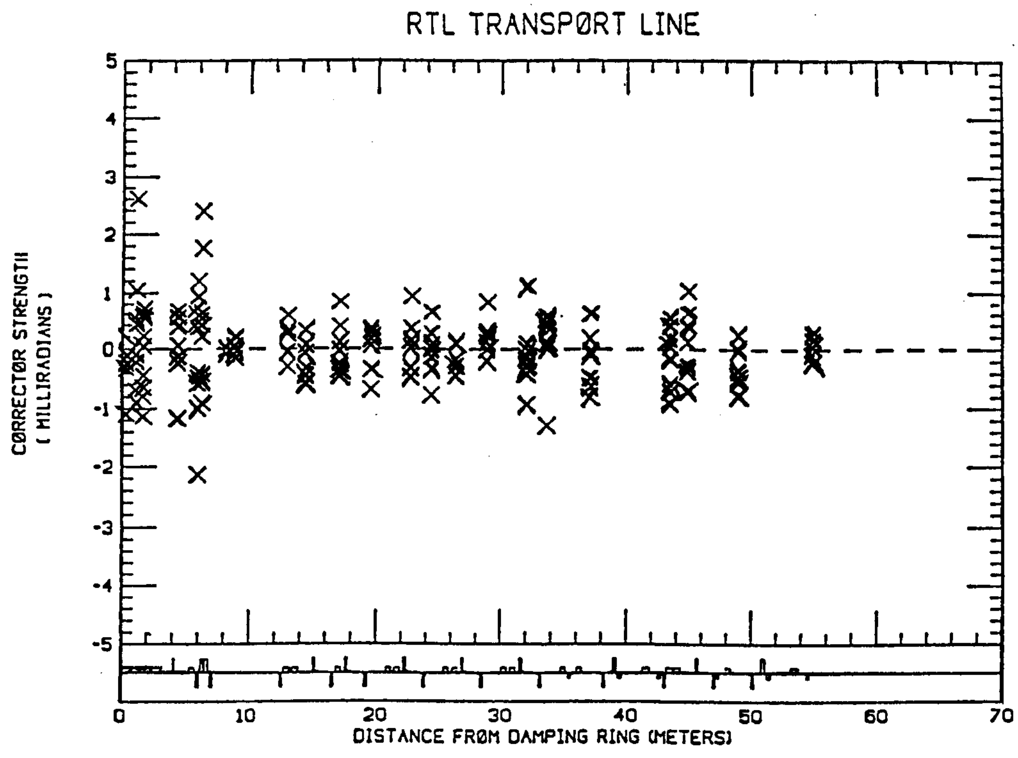

HØRIZØNTAL CØRRECTØR STRENGTHS

Figure 6.4.7b

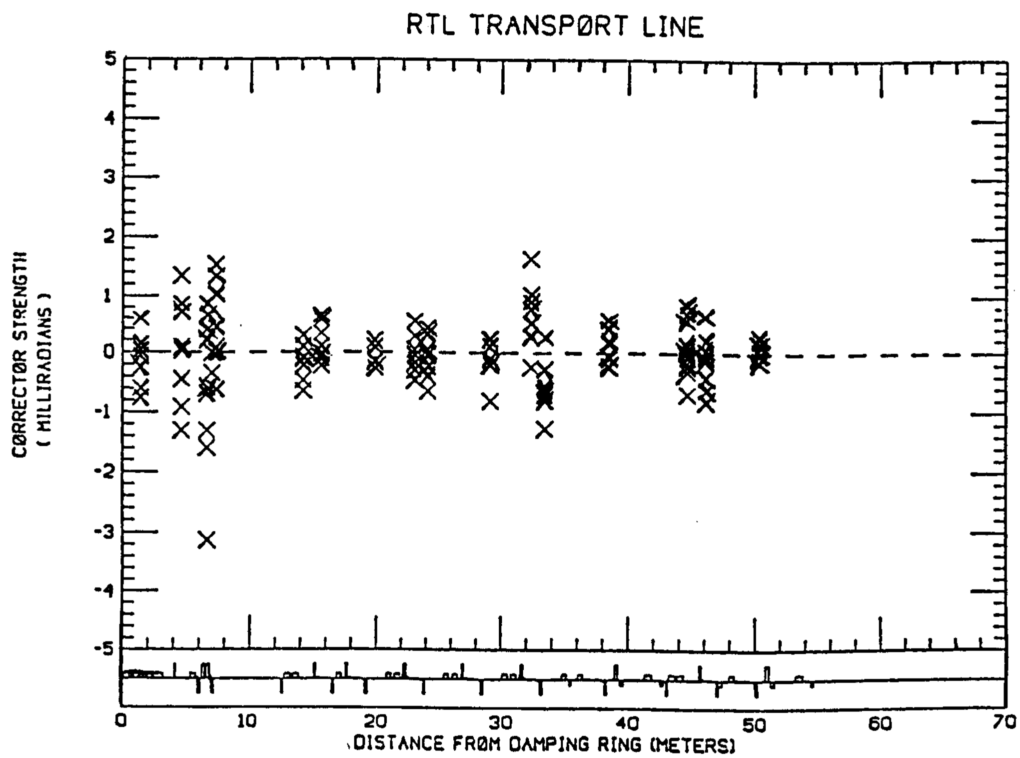

VERTICAL CØRRECTØR STRENGTHS

6.5 SUBSYSTEMS AND COMPONENTS

6.5.1 Damping Ring RF System[15]

The linear collider project at SLAC contains two damping rings to reduce the emittance of short electron or positron bunches which contain 5×10^{10} particles per bunch. Two of these bunches are stored at a time and then extracted for acceleration in the collider. The RF system is subject to strong transients in beam loading. A computer model is used to optimize capture while minimizing RF power. The introduction of phase jump in the RF drive at injection time together with offsets in the tuning loops of the RF cavities when no beam is stored allows optimum performance under heavy beam load conditions. The RF system (800 kV at 714 MHz) for the electron damping ring has been built, tested and installed, and is being tested with beam.

Introduction

The linear collider project at SLAC (SLC) contains two damping rings to reduce the emittance of the e^+ and e^- bunches. This is necessary to attain high luminosity at collision. The bunches of each charge type are stored in separate damping rings. Each ring is a small high-field storage ring in which radiation damping takes place. The RF system is required to replace the energy lost by synchrotron radiation. The parameters of the RF system are given in Table 6.5.1.1. At the 1.21 GeV energy of the stored beams the radiation per turn is a modest 93 keV. However, each injected bunch contains 5×10^{10} particles and this induces parasitic mode losses and strong transient beam loading. A theoretical treatment of beam loading effects indicates that optimum performance can be obtained by introducing a phase jump at injection together with an offset in the tuning of the cavity under no beam conditions. All particles which arrive with an energy spread of $\pm 1\%$ will be captured with the RF system preset in such a fashion. No rapid tuning is necessary, which greatly simplifies the system, but the offset in the tuning loop has to be applied during the time when no beam is stored to keep the cavities in the proper tune condition.

Table 6.5.1.1 RF System Parameters		
RF Frequency	714	MHz
Harmonic Number	84	
Available Klystron Power	50	kW
Total Cavity Shunt Impedance	35	MΩ
Unloaded Q	24000	
Cavity Coupling Coefficient	2.5	
Cavity Tuning Angle	−64°	
Injection Phase Angle	78°	
Phase Jump at Injection	−50°	
Energy of Stored Beam	1.21.	GeV
Energy Loss per Turn	93	keV
Parasitic Mode Loss per Turn (full current)	48	keV
Circulating Current per Bunch	70	mA
Storage Time Between Pulses (electrons)	5.56	msec
Storage Time Between Pulses (positrons)	11.11	msec

Two RF cavities with two cells each provide the required gap voltage. Amplitude and phase feedback loops stabilize the RF fields in the cavities and thus give the beams a precise timing when they are ejected into the linear accelerator.

To date the damping ring for e^- particles has been constructed and is being commissioned.

Parasitic Mode Losses

A bunch of charged particles circulating in a storage ring excites electromagnetic fields in the neighborhood of discontinuities in the vacuum chamber walls. In the damping ring there are discontinuities and transitions between vacuum chamber components. The bunch can, in addition, excite higher-order modes in the RF cavities. Field and modes excited by the bunch represent an energy loss which is in addition to the synchrotron radiation loss per turn. By adding together losses for all the individual components plus the higher-order mode losses in the RF cavities, an estimate can be made for the total loss voltage, $V_1 = Z_1 I_0$, where I_0 is the circulating current per bunch and Z_1 is the loss impedance. For the damping ring

$$Z_1(\mathrm{M}\Omega) \approx 1.9 \exp[-0.17\, \sigma_z(\mathrm{mm})]$$

Note that the loss impedance depends strongly on the bunch length. At the design current of 70 mA per bunch, the loss voltage is $V_1 \approx 48$ kV for the damped bunch length of 6 mm. This must be added to the synchrotron radiation loss of 93 kV to obtain the total voltage per turn that must be supplied by the RF system.

Transient Beam Loading

In the damping ring the total stored charge is injected in one or two bunches on a single turn, rather than over many turns lasting many cavity filling times, as is usually the case for a storage ring. Thus transient beam loading effect might affect the RF voltage required to capture the injected bunches. It is not simple to write analytic expressions taking into account transient beam loading effects because of the large injected energy spread ($\pm1\%$), and the resulting large-amplitude phase oscillations for particles at the extremes of this spread. It is straightforward, however, to write turn-by-turn expressions for the energy and phase deviations from the synchronous energy and phase for a relatively small number of superparticles distributed over the injected phase space. The recurrence relations expressing the energy deviation ϵ and phase deviation θ of the ith particle on the nth turn in terms of quantities on the previous turn are:

$$\theta_n^{(i)} = \theta_{n-1}^{(i)} + A\epsilon_n^{(i)}$$

$$\epsilon_n^{(i)} = \epsilon_{n-1}^{(i)} + V_{g\,n-1}^{(i)} - V_{B_{n-1}}^{(i)} - V_s$$

Here $A = 2\pi\alpha h/E_0$ where α is the momentum compaction factor, h is the harmonic number and eE_0 is the beam energy; eV_s is the synchrotron energy loss per turn, V_g is the generator voltage component $V_g = V_{gR} \cos\psi \cos(\theta + \psi)$, where ψ is the tuning angle and V_{gR} is the generator voltage component at resonance; and V_B is the beam loading voltage component given by an appropriate sum over the beam induced voltages of all of the individual super particles. In calculating this sum, the decay of the beam induced voltages between turns due to the finite cavity filling time, and the phase shifts due to phase oscillations, must be taken into account. The program DAMP[16] has been written at SLAC to perform this calculation.[17]

Initial results indicated that a minimum klystron power of 44 kW would be required to capture uniform injected energy distribution with $\delta\epsilon_{\max} = \pm 12$ MeV, $\sigma_\epsilon = \pm 7$ MeV. This minimum power was obtained by adjusting the cavity coupling and tuning, and the injection phase and energy deviation of the central superparticle in a distribution which is uniform in energy up to $\delta\epsilon_{max}$ with zero phase width. It was soon realized that the required klystron power could be reduced by making a jump in the generator phase at the moment of injection such that the transient in the generator voltage roughly cancels the transient beam induced voltage. A more precise cancellation of all transient beam loading effects could be obtained by jumping both the phase and amplitude of the generator voltage component, but a phase jump alone gives good results and the hardware and control problems are simpler.

Figures 6.5.1.1 and 6.5.1.2 give a typical example of the oscillations in energy and phase for 500 turns after injection for a phase jump in VG at injection of $-40°$.

Details of the other RF and ring parameters are given in Ref. 18. Fig. 6.5.1.3 shows the distribution in phase and energy for the injected bunch and for the superparticles after 500 turns ($\approx 60\,\mu s$). Also shown is the damped distribution after several damping times ($\tau_d = 1.5$ ms for phase oscillations). Note that the rms energy spread has been reduced by damping by about a factor of six.

By adjusting the magnitude of the phase jump, the cavity coupling coefficient, the cavity tuning angle and the injection phase angle, it is possible to reduce the klystron power required to about 30 kW and still capture the complete injected energy spread. Without a phase jump, the minimum klystron power is 44 kW. The maximum energy excursion is also reduced slightly, from

±15 MeV to ±13 MeV.

RF System Description

The block diagram of the RF system is shown in Fig. 6.5.1.4. The design of the RF accelerator structure was optimized to achieve a peak accelerating potential in excess of 1 MV with the available 50 kW of RF power. Calculations with the LALA program yielded a cavity design using four re-entrant copper cells with slot coupling between cells. Due to limited straight section space in the storage ring the four cells were split into two assemblies (see Fig. 6.5.1.5) with two cells each, installed almost opposite each other in the ring. Each structure includes a ceramic window in the input waveguide and a slot coupling from the waveguide into one cell as well as a fixed and a moveable tuner. Two ports are provided for vacuum pumps. A shunt impedance of $R = V^2/P = 17.4$ MΩ was measured for each two-cell RF structure.

A waveguide magic tee is used to split the power feed to the two RF cavities. Since no counter rotating particles are stored in the damping rings the waveguide lengths and position of the cavities in the ring can be arranged such that reflected power from each cavity is combined in the magic tee's terminated port. Thus the requirement for a costly isolator to protect the klystron is eliminated. The klystron is a commercially-available TV tube with 50 kW CW output.

The RF system is stabilized by a total of four feedback loops to assure accurate ejection of the stored and damped beams back into the linear accelerator at the correct phase of the fields in the linear accelerator.

Each cavity is tuned by a feedback loop which compares the RF phase of the field in the cavity to the phase of the driving signal and uses the resulting error to operate the tuner via a stepping motor. Since the intermitantly stored beam is a strong detuning element to the cavity, the tuning loop is adjusted to provide optimum tuning, i.e., minimizing reflected power from the cavity with the beam stored. A pulsed offset is introduced when no beam is in the ring. This offset counteracts the large error which would otherwise be detected when the beam is not present and thus keeps the cavity in a state ready for the next injected beam.

In a similar fashion a pulsed offset is introduced in the main phase feedback loop during the "beam-off" time to rotate the phase of the field in the two cavities to a position where it can best capture the injected beam. The offset is removed at beam injection, and produces the phase jump discussed earlier in this paper.[18] Immediately after injection the rapidly rising beam induced fields rotate the cavity fields to the desired phase. The main function of the phase feedback loop is to lock the vector sum of the field vectors in the two RF cavities to the input signal of the RF system. Long cable runs in this loop are temperature stabilized with the coax cable surrounded by a coaxial water jacket operating at $+45°C \pm 0.1°C$. Phase stable coax cables with ± 9 ppm/°C temperature coefficient and foam dielectric are used.

The gap voltage feedback loop sums the field amplitudes detected from samples of each cell and compares it to a fixed reference voltage. The resulting error signal is applied to a variable attenuator in the drive line to the klystron.

The amplitude and phase detectors, electronic attenuators and phase shifters used in the drive and feedback circuits had been developed for the PEP storage ring RF systems and are described in an earlier paper.[18]

Present Status

The RF system as described is operational and the damping ring has stored current of $\approx$10 mA with a lifetime of close to one hour. The synchrotron frequency has been measured as a function of gap voltage and the "cold tested" parameter of the cavities have been verified with the beam. The heavy beam loading tests await the production of intense bunches from the linac.

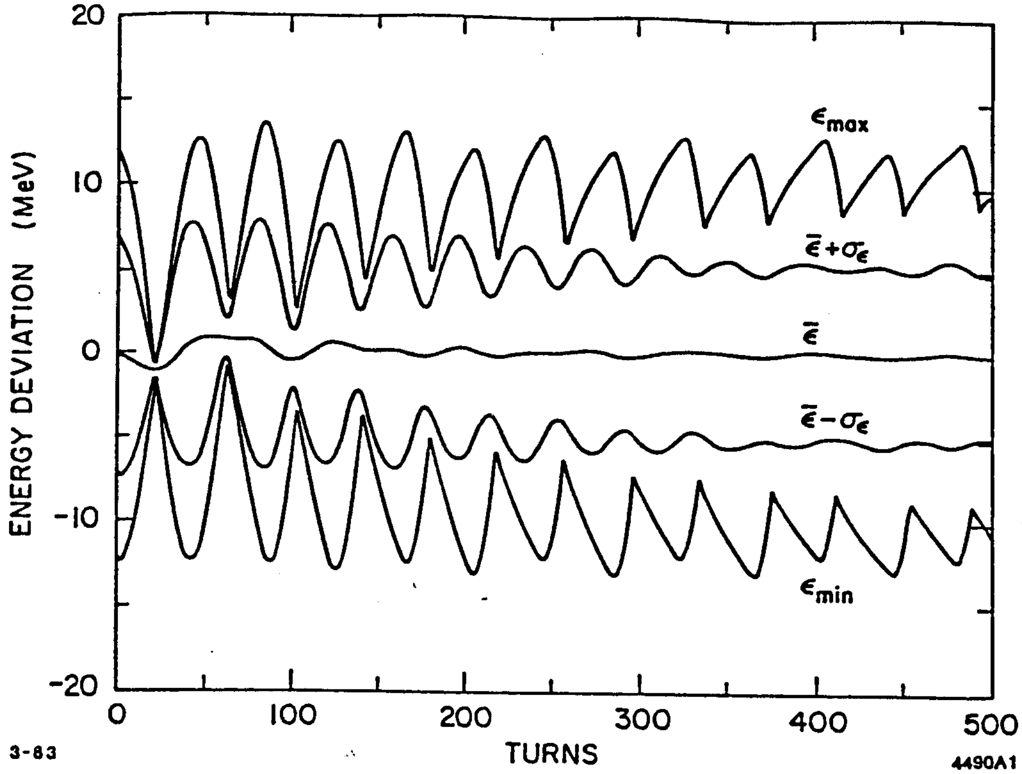

Figure 6.5.1.2 Variations in the mean energy deviation, the rms energy deviations and the extreme energy deviations for 500 turns.

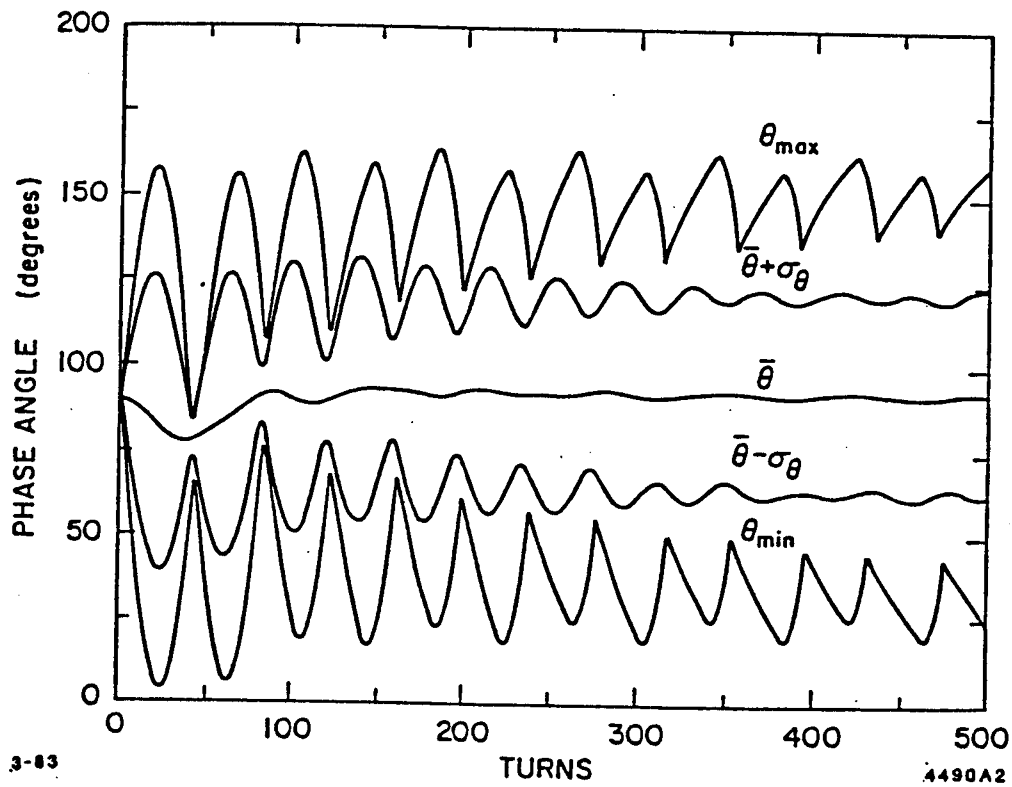

Figure 6.5.1.1 Variations in the mean phase, the rms phase and the extreme phase excursions for 500 turns.

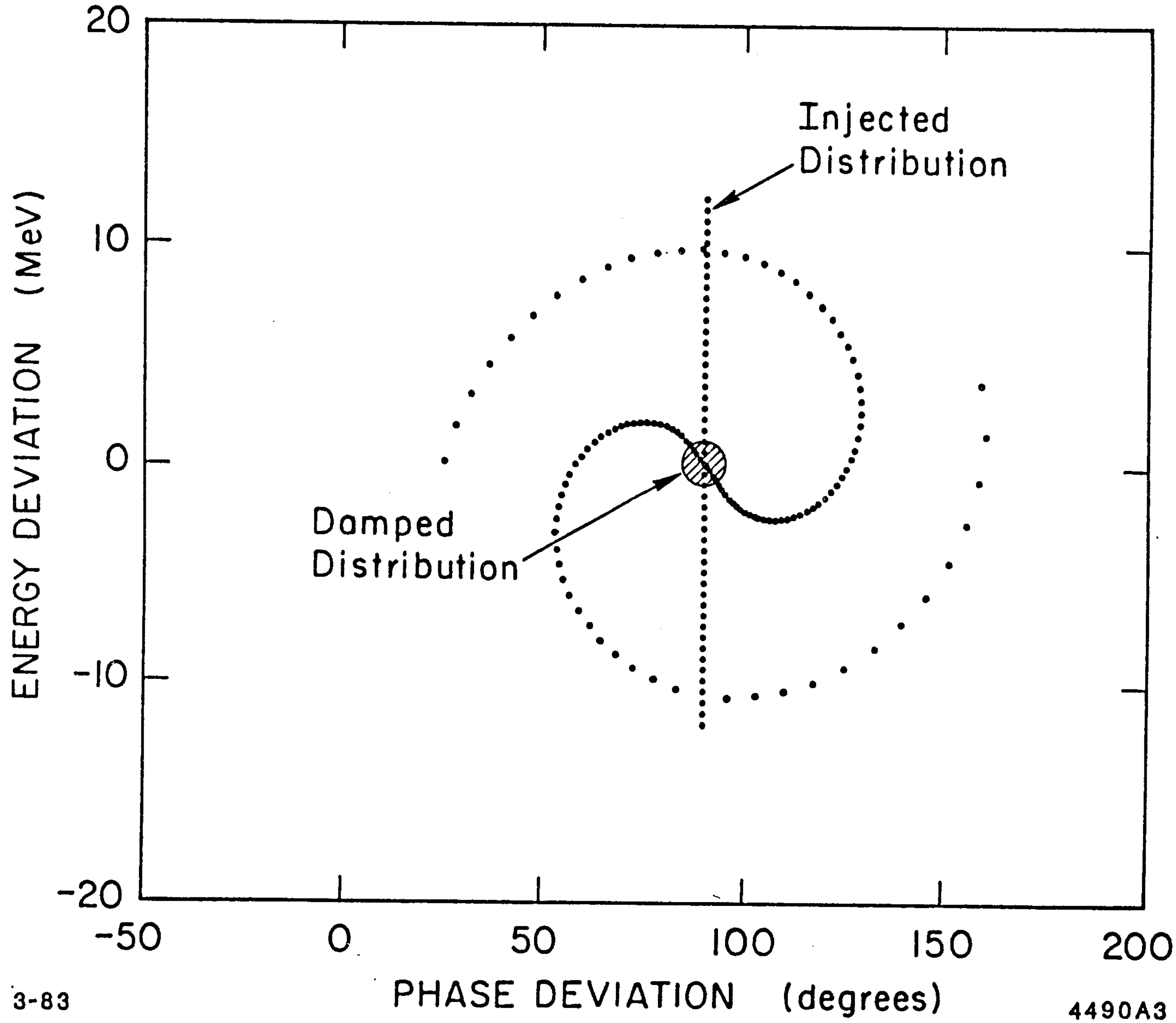

Figure 6.5.1.3 The injected distribution, the distribution after 500 turns and the damped distribution after 50,000 turns in phase space for 121 superparticles (injected distribution shows for only every third superparticle).

Figure 6.5.1.4 Block diagram of damping ring RF system

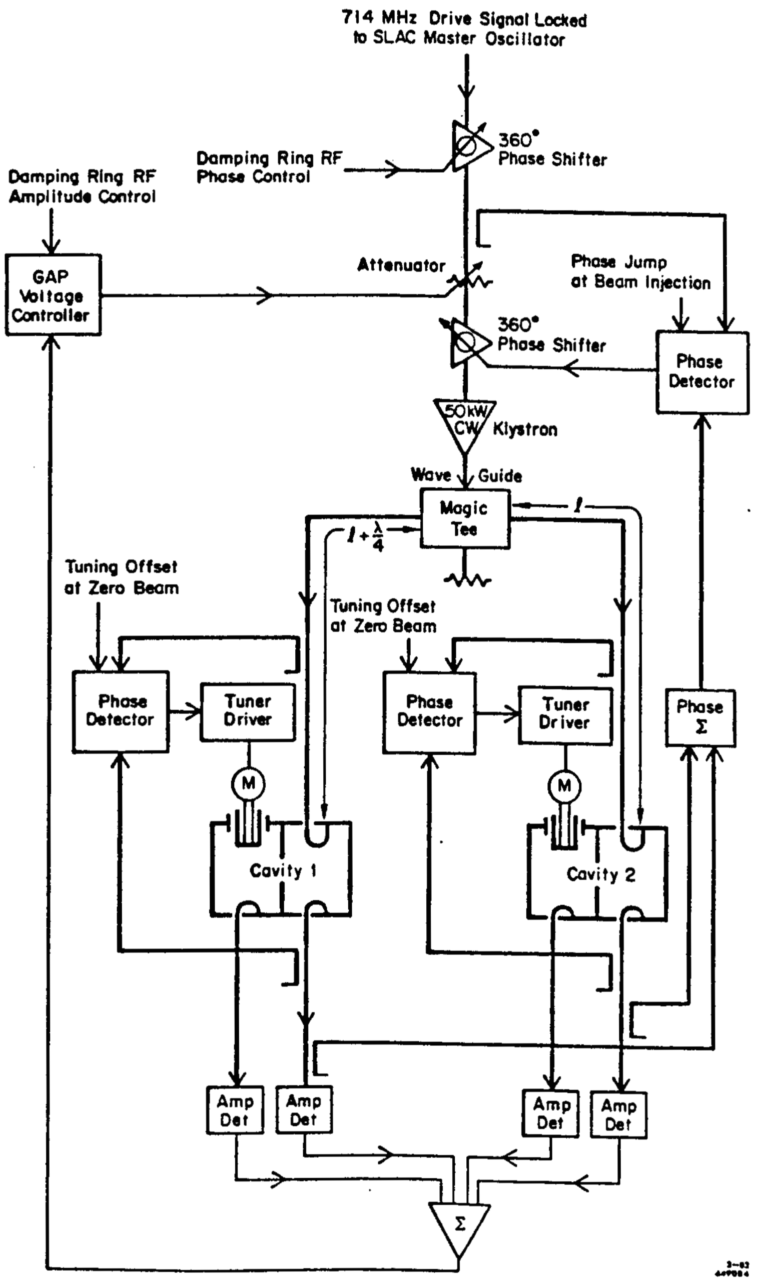

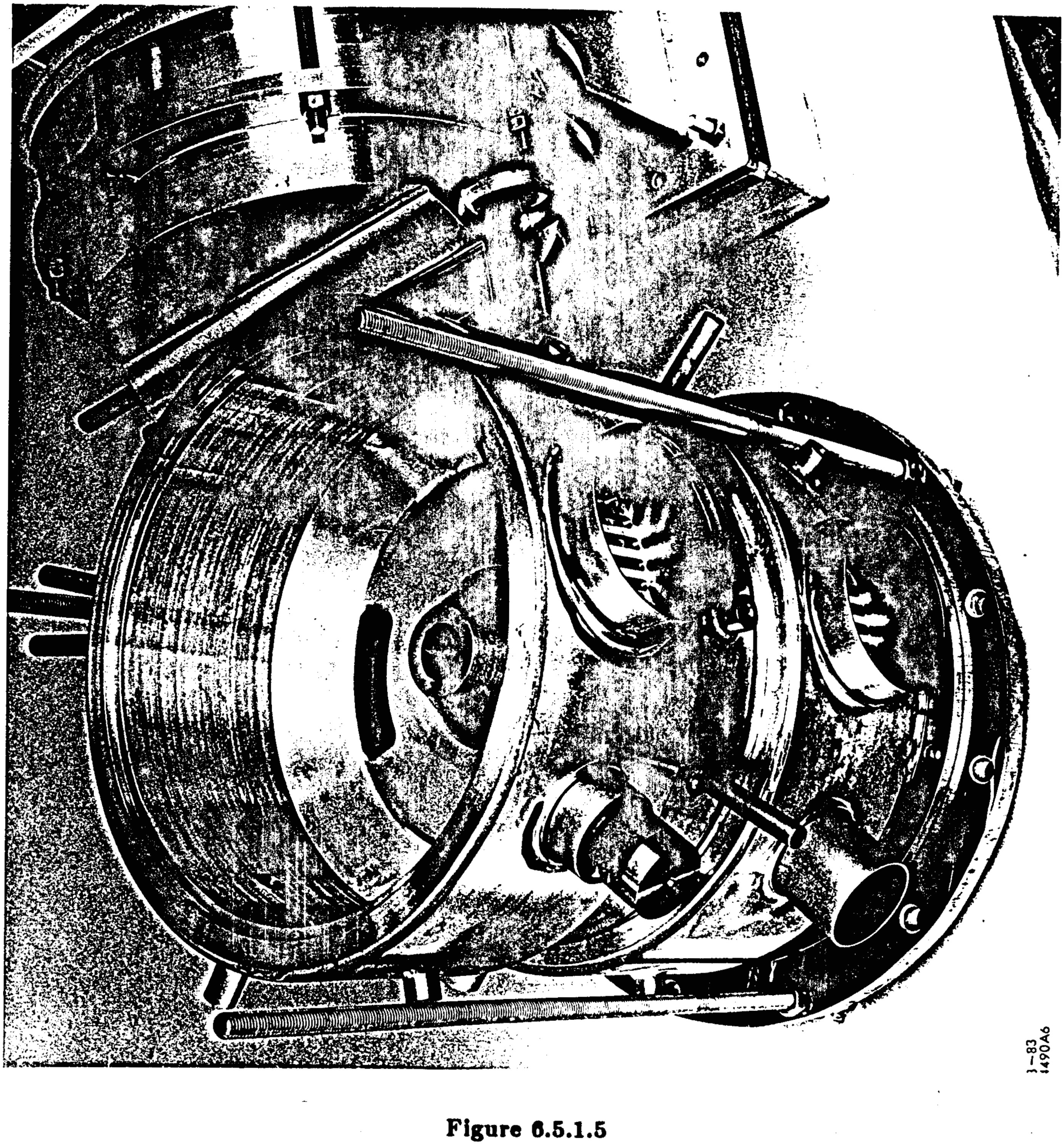

Figure 6.5.1.5

6.5.2 Vacuum System

The vacuum system for the first damping ring has designed[19] requirements to 1) provide sufficient cooling capability to absorb 13 kW of synchrotron radiation power; 2) provide beam position monitor electrodes shielded from synchrotron radiation; 3) include ion clearing electric fields, while; 4) providing a base pressure of $\approx 5 \times 10^{-8}$ Torr in a low conductance system. The small size and close packed construction of the ring made meeting the requirement a unique engineering challenge.

Ion effects, if not dealt with, can be expected to affect the phase space of the beams in the electron ring.[20] A two step attack on the problem is employed. Distributed ion pumps (150 l/sec) are located in each of the 40 bending magnets to reduce pressure (after clean-up) into the 10^{-8} Torr range. Further, the partitioned vacuum chamber is designed to let the electric field of the pump electrodes leak into the beam region to cause the ions to migrate and be cleared. Clearing in the remaining circumference is provided by clearing electrodes and by biasing the beam position monitor strips with voltages up to ± 1 kV.

Damping Ring (DR)

The ring is oval in shape with short straight sections near the end of each arc and two longer straight sections separating the arcs. Forty bend magnets with alternating focusing and defocusing quadrupoles define the arcs, while the straight sections are delineated by quadrupoles, sextupoles, kickers, septa and RF cavities.

The vacuum system consists of 34 metal chambers joined by conflat-type flanges with metal gaskets. The arcs are composed of sixteen standard cells which are, in many respects, similar to the standard bend chambers of SPEAR and PEP. Each arc chamber is contained within two bend magnets and focusing and defocusing quads. Sections through the bend magnets are aluminum extrusions containing distributed ion pumps. Sections through the quads are stainless steel tubing which contain clearing field electrodes, beam position monitors (BPM), water cooling and synchrotron masks. Each standard aluminum arc chamber also has stainless steel welded bellows at one end. At the ends of each straight section are matching chambers (eight total) which are contained within a single bend magnet and various combinations of sextupole and quad magnets. The components of the matching chambers represent slight variations of the standard chamber to accommodate the matching cells lattice. The short straight sections near the ends of one (north) arc are formed by the RF cavities. The cavities are oxygen-free, electronic (OFE) copper assemblies, brazed in a hydrogen furnace. Near the ends of the other (south) arc are straight sections composed of alumina (Al_2O_3) ceramic vacuum chambers clamped with the pulsed kicker magnets. Both long straight sections contain the septa, drift chambers, and instrumentation chambers: the optical monitor and horizontal and vertical beam scrapers. The septum magnets are contained with the vacuum chamber.

Distributed Ion Pumps

The distributed pump for the damping ring is a diode sputter ion pump which operates in the 19.8 kG magnetic field of each bend magnet. The pump structure shown in Figure 6.5.2.1 consists of a stainless steel anode array sandwiched between two titanium cathode plates. The anode array is an assembly of 728, 3 mm dia $\times$ 6 mm long stainless steel tubes. The cells are spot welded together to form an array of 91 rows of 8 cells each. The array structure is bent to conform to the bend radius of the vacuum chamber. The anode array is held at a potential of 3.5 kV which can be increased up to a maximum of 7 kV. The pump evacuates the beam chamber through a slot 6 mm wide. The slot limits the effective speed of the pump to $\approx$ 2 l/sec per cm of length. The stray electric field from the anode array combined with the magnetic field of the bending magnet produces a clearing field which removes ionized gas molecules from the bend magnet chamber.

Figures 6.5.2.2–6.5.2.4 show the performance of a prototype structure consisting of 207, 3 mm dia × 5.7 mm cells. The solid curves were calculated from the empirical formulae of Malev and Trachtenberg.[21]

Transport Lines

The transport lines are named the linac-to-Ring (LTR) line and the Ring-to-linac (RTL) line. The LTR consists of 81 vacuum chambers interconnected with various off-the-shelf bellows and fittings. The system is primarily aluminum (tubing and extrusions) to distribute the thermal effects of a miss-steered beam striking the wall. Various diameters of tubing are used to match the bores of magnets and size of the beams through each section of the line. Rectangular extrusions form the beampipe through bending magnets. Diagnostic instruments (profile monitors, spectrum analyzers, Faraday cups, beam stoppers, etc.) are mounted in standardized instrument containers and distributed along the LTR. The line is ion-pumped and pressure is monitored with nude Bayard-Alpert-type ionization gauges. The line is isolated from the linac and damping ring by Viton™ o-rings sealed, electropneumatically operated gate valves. Magnets and vacuum components are mounted and prealigned on concrete rafts prior to installation in the tunnel.

The RTL is similar to the LTR except for a compressor section which shortens the bunch length of beams removed from the damping ring. The compressor is a standard linac accelerator section with its own waveguide and klystron station. The RTL is ion-pumped and isolated from the linac and damping ring by gate valves.

In operation, the LTR and RTL maintain pressures better than the design criteria of 5×10^{-8} Torr. The damping ring has a base pressure of 5×10^{-9} Torr. Normal operation with high current beams may cause some degradation of the vacuum.

Figure 6.5.2.1

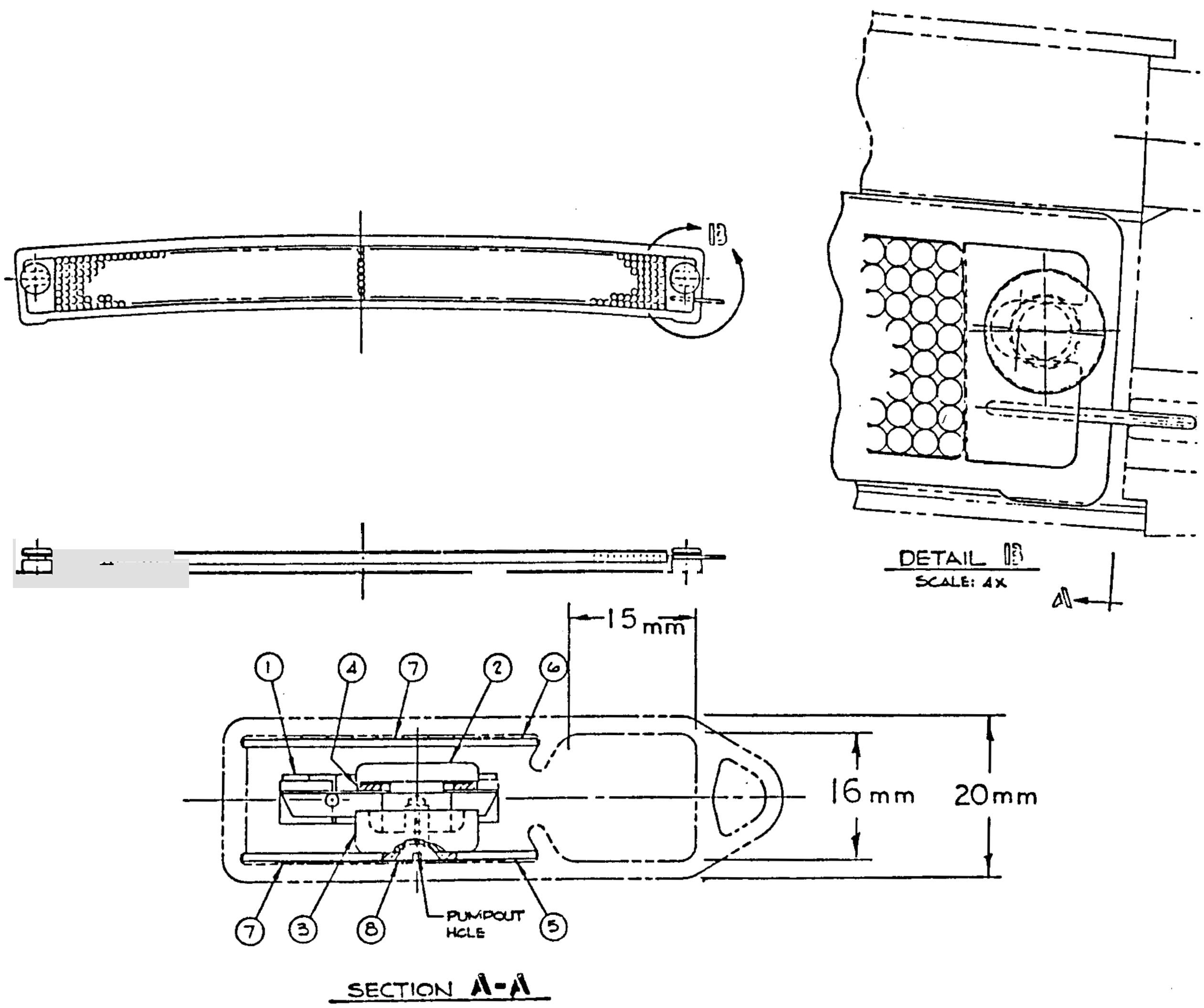

B
DETAIL B
SCALE: 4X
A
15 mm
16 mm
20mm
1
4
7
2
6
7
3
8
PUMPOUT HOLE
5
SECTION A-A

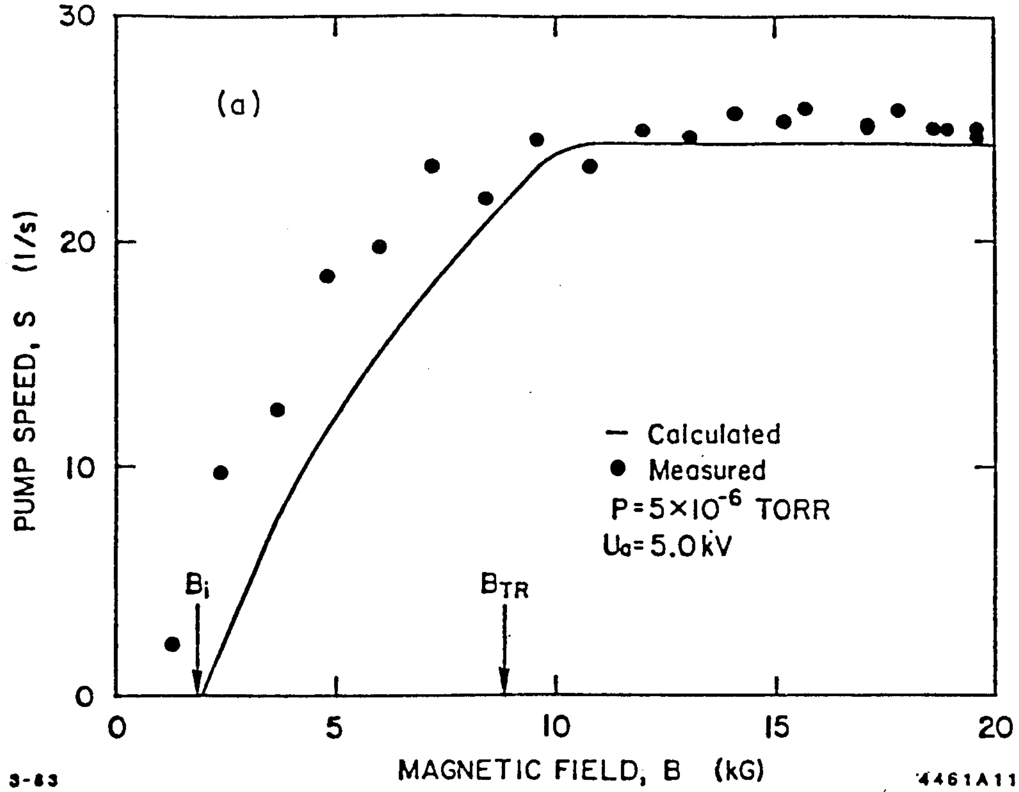

Figure 6.5.2.2

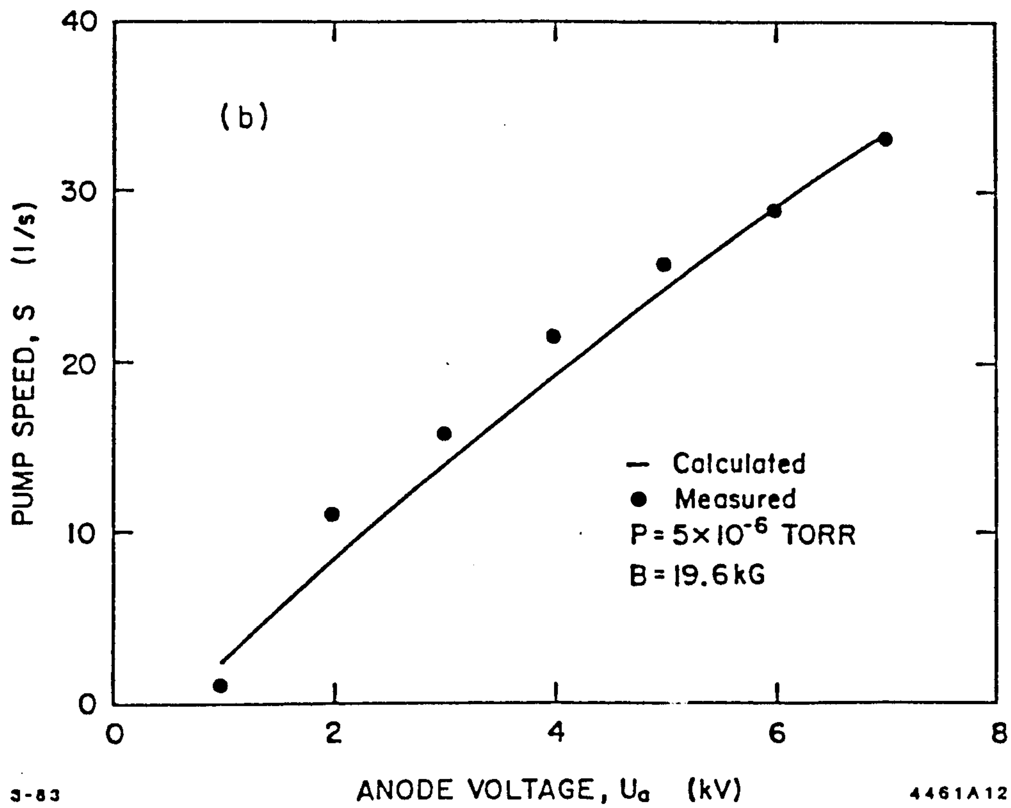

Figure 6.5.2.3

Figure 6.5.2.4

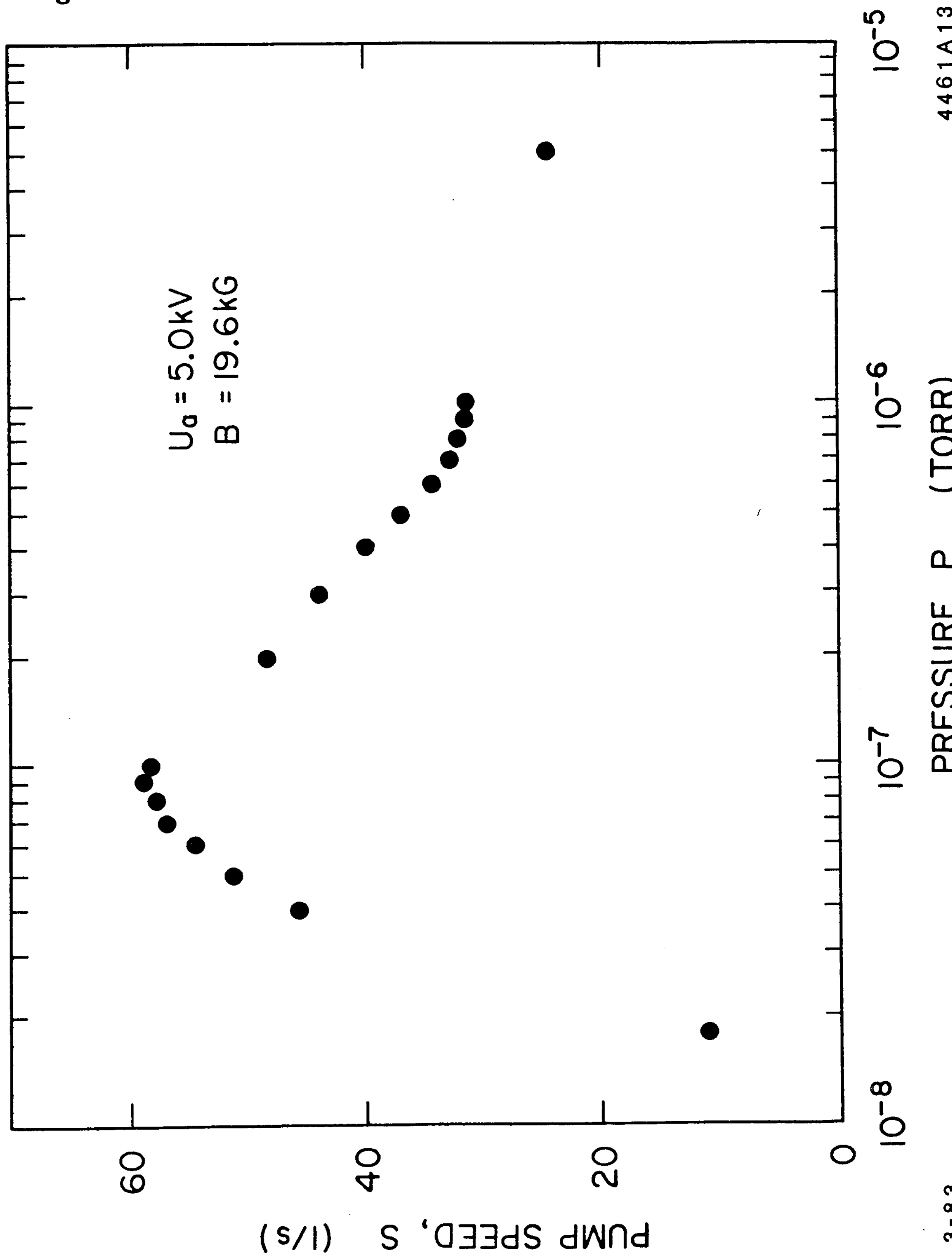
U_a = 5.0kV
B = 19.6kG
PUMP SPEED, S (l/s)
PRESSURE, P (TORR)
0
20
40
60
10^{-8}
10^{-7}
10^{-6}
10^{-5}
4461A13
3-83

6.5.3 Magnets and Power Supplies

The following lists (not yet completed) of magnets are in order as seen by the beam. The identification number in the leftmost column is that used in the engineering drawings. Power supplies are identified by the magnet string that they power. Further documentation is being prepared.

DAMPING RING

(System)

Table 6.5.3

Date 01/18/84

Sheet 1 of 1

QUADRUPOLE MAGNETS
Location (L.T.R)

Listing by W.A.D-W /G.F.C

Tran Mag# Q/...	Pos Mag	Kg	Grad Kg/cm	Eff.L in cms	Number of Lams	Bore in ins	Steel Length ins	No Turns	Current Amps Approx	Conductor Size Gauge or ins	Inside Coil Length ins	Outside Coil Length ins	/pole coil Length ft	/Mag total Volts	Mag trim coil turns	%age trim of main
d53b	1	11.840	1.231	9.618	15	2.026	2.774	22	155.0	0.188	3.399	4.274	30.9	7.67	76	8.9
f53b	2	29.000	4.000	7.250	12	1.432	2.138	34	155.0	0.188	2.763	3.638	42.5	10.55	76	5.8
d53a	3	26.920	4.000	6.730	11	1.432	1.934	34	155.0	0.188	2.559	3.434	41.4	10.26	76	5.8
f53a	4	11.840	1.000	11.840	20	2.026	3.648	17	155.0	0.188	4.273	5.148	26.4	6.55	38	5.8
d49	5	34.920	4.000	8.730	15	1.432	2.721	34	155.0	0.188	3.346	4.221	45.8	11.37	76	5.8
f47	6	31.520	4.000	7.880	13	1.432	2.386	34	155.0	0.188	3.011	3.886	44.0	10.90	76	5.8
d45	7	31.120	4.000	7.780	14	1.013	2.556	17	155.0	0.188	3.181	4.056	21.9	5.42	38	5.8
f43	8	57.440	4.000	14.360	28	1.013	5.147	17	155.0	0.188	5.772	6.647	29.2	7.24	38	5.8
d39	9	56.800	4.000	14.200	27	1.013	5.084	17	155.0	0.188	5.709	6.584	29.0	7.20	0	0.0
f35	10	56.800	4.000	14.200	26	1.432	4.875	34	155.0	0.188	5.500	6.375	58.0	14.40	0	0.0
d31	11	56.800	4.000	14.200	27	1.013	5.084	17	155.0	0.188	5.709	6.584	29.0	7.20	0	0.0
f27	12	56.800	4.000	14.200	26	1.432	4.875	34	155.0	0.188	5.500	6.375	58.0	14.40	0	0.0
d23	13	56.800	4.000	14.200	27	1.013	5.084	17	155.0	0.188	5.709	6.584	29.0	7.20	0	0.0
f19	14	42.000	4.000	10.500	20	1.013	3.627	17	155.0	0.188	4.252	5.127	24.9	6.17	0	0.0
d17d	15	26.440	2.000	13.220	23	2.026	4.192	34	155.0	0.188	4.817	5.692	55.9	13.85	0	0.0
f17c	16	26.440	2.000	13.220	23	2.026	4.192	34	155.0	0.188	4.817	5.692	55.9	13.85	0	0.0
d17c	17	26.440	2.000	13.220	23	2.026	4.192	34	155.0	0.188	4.817	5.692	55.9	13.85	0	0.0
f17b	18	26.440	2.000	13.220	23	2.026	4.192	34	155.0	0.188	4.817	5.692	55.9	13.85	0	0.0
d17b	19	26.440	2.000	13.220	23	2.026	4.192	34	155.0	0.188	4.817	5.692	55.9	13.85	0	0.0
f17a	20	23.800	2.000	11.900	20	2.026	3.672	34	155.0	0.188	4.297	5.172	52.9	13.12	0	0.0
d17a	21	8.340	0.934	10.600	17	2.026	3.160	14	155.0	0.188	3.785	4.660	20.6	5.11	0	0.0
f15	22	42.000	2.000	21.000	38	2.026	7.255	34	155.0	0.188	7.880	8.755	73.2	18.16	0	0.0
d13g	23	46.500	2.000	23.250	43	2.026	8.141	34	155.0	0.188	8.766	9.641	78.2	19.40	0	0.0
f13f	24	38.040	2.000	19.020	34	2.026	6.475	34	155.0	0.188	7.100	7.975	68.8	17.06	0	0.0
d13f	25	26.440	2.000	13.220	23	2.026	4.192	34	155.0	0.188	4.817	5.692	55.9	13.85	0	0.0
f13b	26	26.440	2.000	13.220	23	2.026	4.192	34	155.0	0.188	4.817	5.692	55.9	13.85	0	0.0
d13b	27	26.440	2.000	13.220	23	2.026	4.192	34	155.0	0.188	4.817	5.692	55.9	13.85	0	0.0
f13d	28	26.440	2.000	13.220	23	2.026	4.192	34	155.0	0.188	4.817	5.692	55.9	13.85	0	0.0
d13d	29	26.440	2.000	13.220	23	2.026	4.192	34	155.0	0.188	4.817	5.692	55.9	13.85	0	0.0
f13c	30	26.440	2.000	13.220	23	2.026	4.192	34	155.0	0.188	4.817	5.692	55.9	13.85	0	0.0
d13c	31	26.440	2.000	13.220	23	2.026	4.192	34	155.0	0.188	4.817	5.692	55.9	13.85	0	0.0
f13b	32	26.440	2.000	13.220	23	2.026	4.192	34	155.0	0.188	4.817	5.692	55.9	13.85	0	0.0
d13b	33	26.440	2.000	13.220	23	2.026	4.192	34	155.0	0.188	4.817	5.692	55.9	13.85	0	0.0
f13a	34	27.380	2.000	13.690	24	2.026	4.377	34	155.0	0.188	5.002	5.877	56.9	14.11	0	0.0
d13a	35	43.300	2.000	21.650	40	2.026	7.511	34	155.0	0.188	8.136	9.011	74.7	18.52	0	0.0
f9	36	86.503	5.149	16.800	32	1.013	6.108	22	155.0	0.188	6.733	7.608	41.3	10.25	0	0.0
f7	37	86.503	5.149	16.800	32	1.013	6.108	22	155.0	0.188	6.733	7.608	41.3	10.25	0	0.0
d3d	38	34.754	2.000	17.377	31	2.026	5.828	34	155.0	0.188	6.453	7.328	65.1	16.15	76	5.8
f3c	39	36.390	2.000	18.195	33	2.026	6.150	34	155.0	0.188	6.775	7.650	67.0	16.61	76	5.8
d3c	40	33.430	2.000	16.715	30	2.026	5.568	34	155.0	0.188	6.193	7.068	63.7	15.79	76	5.8
f3b	41	32.786	2.000	16.393	29	2.026	5.441	34	155.0	0.188	6.066	6.941	62.9	15.61	76	5.8
d3b	42	38.108	2.000	19.054	34	2.026	6.489	34	155.0	0.188	7.114	7.989	68.9	17.08	76	5.8
3a	43	35.564	2.000	17.782	32	2.026	5.988	34	155.0	0.188	6.613	7.488	66.0	16.38	76	5.8
d3a	44	36.276	2.000	18.138	33	2.026	6.128	34	155.0	0.188	6.753	7.628	66.8	16.58	76	5.8
f-1	45	58.332	5.851	9.973	19	1.013	3.420	29	155.0	0.188	4.045	4.920	41.5	10.28	60	5.3
														570.9 V		

Table 6.5.3 Continued

DAMPING RING

(System)

QUADRUPOLE MAGNETS
Location (R.T.L)

Date 01/18/84

Sheet 1 of 1

Listing by W.A.D-W

Tran Mag# Q/...	Pos Mag	Kg	Grad Kg/cm	Eff.L in cms	Number of Lams	Bore in ins	Steel Length ins	No Turns	Current Amps Approx	Conductor Size Gauge or ins	Inside Coil Length ins	Outside Coil Length ins	/pole coil Length ft	/Mag total Volts	Mag trim coil turns	%age trim of main
f202	1	58.181	7.953	7.316	solid	0.760	2.500	25	127.0	0.188	2.687	4.500	31.4	6.38	54	6.8
dm204a	2	116.000	5.800	20.000	39	1.013	7.368	34	125.0	0.188	7.993	8.868	71.0	14.20	76	7.2
fm204a	3	116.000	5.800	20.000	39	1.013	7.368	34	125.0	0.188	7.993	8.868	71.0	14.20	76	7.2
dm204b	4	116.000	5.800	20.000	39	1.013	7.368	34	125.0	0.188	7.993	8.868	71.0	14.20	76	7.2
fm204b	5	116.000	5.800	20.000	39	1.013	7.368	34	125.0	0.188	7.993	8.868	71.0	14.20	76	7.2
d204	6	14.808	1.600	9.255	15	2.026	2.631	34	127.0	0.188	3.256	4.131	47.0	9.55	76	7.0
f208	7	22.770	1.600	14.231	25	2.026	4.590	34	127.0	0.188	5.215	6.090	58.1	11.81	76	7.0
d208	8	12.568	0.800	15.710	28	2.026	5.172	17	127.0	0.188	5.797	6.672	30.7	6.24	76	14.1
f210	9	26.600	1.600	16.625	30	2.026	5.532	34	127.0	0.188	6.157	7.032	63.5	12.90	76	7.0
d210	10	25.715	1.600	16.072	28	2.026	5.315	34	127.0	0.188	5.940	6.815	62.2	12.64	76	7.0
f214	11	26.600	1.600	16.625	30	2.026	5.532	34	127.0	0.188	6.157	7.032	63.5	12.90	76	7.0
d214	12	25.715	1.600	16.072	28	2.026	5.315	34	127.0	0.188	5.940	6.815	62.2	12.64	76	7.0
f218	13	26.600	1.600	16.625	30	2.026	5.532	34	127.0	0.188	6.157	7.032	63.5	12.90	76	7.0
d218	14	25.715	1.600	16.072	28	2.026	5.315	34	127.0	0.188	5.940	6.815	62.2	12.64	76	7.0
f222	15	26.600	1.600	16.625	30	2.026	5.532	34	127.0	0.188	6.157	7.032	63.5	12.90	76	7.0
d222	16	25.715	1.600	16.072	28	2.026	5.315	34	127.0	0.188	5.940	6.815	62.2	12.64	76	7.0
d228	17	23.434	1.600	14.646	26	2.026	4.753	34	127.0	0.188	5.378	6.253	59.0	12.00	76	7.0
f228	18	27.571	1.024	26.935	49	2.533	9.338	34	127.0	0.188	9.963	10.838	86.5	17.57	76	7.0
d234	19	14.808	1.600	9.255	15	2.026	2.631	34	127.0	0.188	3.256	4.131	47.0	9.55	76	7.0
f238	20	22.770	1.600	14.231	25	2.026	4.590	34	127.0	0.188	5.215	6.090	58.1	11.81	76	7.0
d238	21	12.568	0.800	15.710	28	2.026	5.172	17	127.0	0.188	5.797	6.672	30.7	6.24	76	14.1
d242	22	23.434	1.600	14.646	26	2.026	4.753	34	127.0	0.188	5.378	6.253	59.0	12.00	76	7.0
f242	23	27.571	1.024	26.935	49	2.533	9.338	34	127.0	0.188	9.963	10.838	86.5	17.57	76	7.0

Table 6.5.3 Continued

DAMPING RING SUPPLY SYSTEM
OUTPUT VOLTAGE/OUTPUT CURRENT VALUES

Beam Line Section	P.S. Id.	Rating	Run val. 950 Mev	Loop Ohms	Run val. 1.21 Gev
LTR	PB-0	300V/200A	210V/10A	21.0	273V/13A
LTR	LTR-VB	45V/400A	16V/255A	.063	21V/326A
LTR	LTR-BEND	600V/450A	310V/268A	1.16	453V/392A
LTR	LTR-QUAD	600V/450A	410V/120A	3.41	530V/155A
LTR	SB-0(ACME)	100V/450A	45V/255A	1.76	58V/326A
LTR	QE13	20V/120A	N/A		N/A
RING	RING BEND	850V/450A	540V/271A	2.00	827V/415A
RING	R QD	300V/200A	170V/124A	1.37	214V/156A
RING	R QF	300V/200A	150V/98A	1.53	195V/127A
RING	R QDI	300V/200A	80V/74A	1.08	118V/109A
RING	R QFI	300V/200A	120V/100A	1.20	178V/148A
RING	R QFM	45V/400A	30V/79A	.380	40V/104A
RING	K1-INS	20 KV	16.3 KV	N/A	20400V
RING	K2-EXT	20 KV	18 KV	N/A	23130V
RING	SEPT-INS	30V/2500A	10V/2003A	.005	13V/2600A
RING	SEPT-EXT	30V/2500A	10V/2038A	.005	13V/2600A
RING	SEPT-INS(BL)	36V/80A	11V/48A	.230	N/A
RING	SEPT-EXT(BL)	60V/50A	11V/48A	.230	N/A
RING	B1 BYPASS	9V/1000A	8V/100A	.080	N/A
RING	B2 BYPASS	9V/1000A	7.5V/250A	.030	N/A
RTL	RTL BEND	600V/450A	178V/249A	.720	233V/326A
RTL	RTL VB	150V/350A	32V/214A	.150	44V/294A
RTL	RTL QUAD	300V/200A	155V/96A	1.614	N/A
RTL	RTL QD4A	20V/125A	12V/91A	.130	15V/116A
RTL	RTL QF4A	20V/125A	11V/82A	.130	14V/104A
RTL	RTL QD4B	20V/125A	1V/8A	.130	1.3V/10A
RTL	RTL QF4B	20V/125A	8V/58A	.130	10V/74A
RTL	VB42-VB0	95V/220A	N/A		/288A

6.5.3.1 Septa: The ring injection and extraction septa are of the current sheet type and can operate, in the high vacuum environment of the ring, since there are no vacuum windows. The pre-septum is 3 mm thick and carries 2400 Amps to produce 3 kG in a 1 cm gap. The post-septa are of two-turn construction to produce 8 kG in a 0.7 cm gap. Total deflection is $\approx 10°$.

6.5.3.2 Kickers: The injection and extraction kickers are 33 cm long, 2.2 cm gap, ferrite loaded (Ferrox-cube 4C4) transmission lines of characteristic impedance 16.6 Ω. They transmit their field through ceramic vacuum tubes, the inside of which have been coated with a conducting layer (1.2 Ω/□ of Kovar) to carry the high image currents of the beam. The time to establish peak fields of 1 kG is about 45 nsec, short enough to not disturb the second, circulating bunch. This time is a combination of the natural rise time of the pulser, the filling time of the ferrite and the shift introduced by eddy currents in the coating of the vacuum chamber. The 40 kV pulser (see Fig. 6.5.3.2.1) consists of a resonantly-charged Blumlein discharged by means of a thyratron firing at rates up to 180 pps. Since the launch angle and position into the linac, which controls wake field effects, is related to the angle of the extraction kick, the pulse-to-pulse amplitude jitter must be held to better than 0.03%. This tolerance has been met!

Figure 6.5.3.2.1 Kicker Magnet Pulser

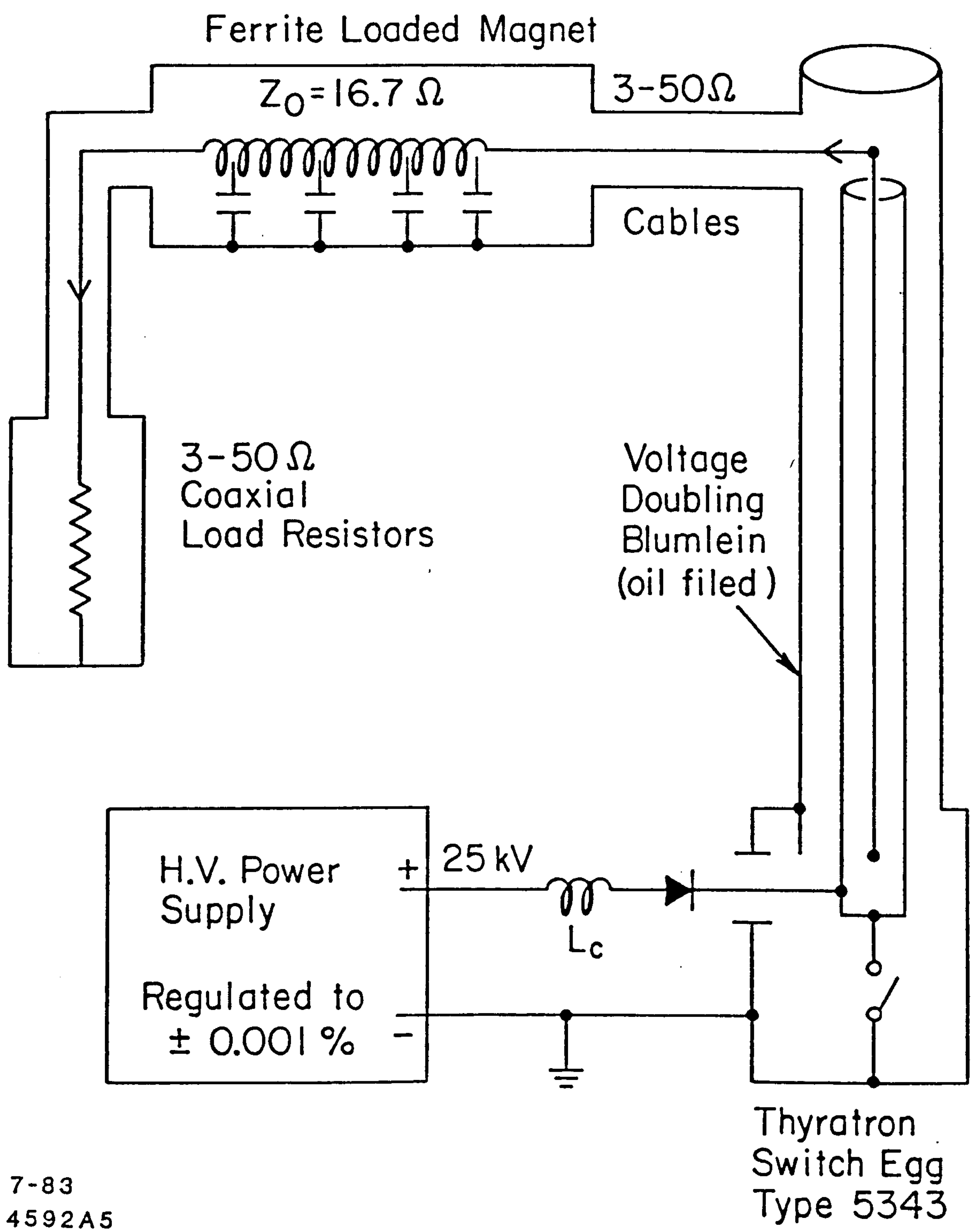

Inventory of Components

With the exception of those items common to both beams in the linac and the fact that the positron ring will not require clearing electrodes, the construction of the second ring and its transport will entail the duplication of the components listed in the following Tables:

Table 6.5.4.1 Magnet and Power Supply Inventory						
LOCATION TYPE	RING	LINAC TO RING	RING TO LINAC	LINAC	TOTAL	NO. OF POWER SUPPLIES
BANDS (dc)	40	24	16	1	81′	3
QUADS (dc)	50	45	23	1	119	8
SEXTUPOLES (dc)	4	0	16	0	20	6
KICKERS (100 ns)	2	0	0	0	2	2
PULSED MAGN. (8 MS)	0	0	0	1	1	1
SEPTA (dc)	4	0	0	0	4	1
VERTICAL BENDS (dc)	0	3	4	1	8	2
MAGNET TOTALS	100	72	59	4	235	23
BIPOLAR CORRECTORS	0	25	35	0	60	64
UNIPOLAR CORRECTORS	40	24	16	1	80	64
CORRECTOR TOTALS	40	49	52	1	140	128

Table 6.5.4.2 RF, Vacuum, I&C Component Inventories

LOCATION	RING	LINAC TO RING	RING TO LINAC	LINAC	TOTALS
RF Transmitter 50 kW	1	0	0	0	0
RF Cavities 714 MHz	2	0	0	0	
S. Band Acc. Section			10 ft/	0	10/
& Waveguide	0	0	200 ft	0	200
Low Level Instrumentation	1	0	1	0	2
Length of Vac. Chamber	111 ft	229 ft	180 ft	0	520
Number of Pumps	40 DIP	9 HIP	9 HIP	0	78
	20 HIP	9 HIP	9 HIP		
Number of Ion Gauges	4	3	3	0	10
Number of Valves	0	3	3	0	6
Beam Position Monitors	26	19	22	0	67
Clearing Electrodes	28	0	0	0	28
Moveable Scrapers, H.V.	1	0	0	0	1
Profile Monitors	0	4	5	1	9
Spectrum Monitors	0	1	1	0	2
Toroids	0	3	3	1	7
Gap Monitores	0	3	3	0	6
Synchrotron Light Monitor	1	0	0	0	0
Faraday Cups	0	1	1	0	2

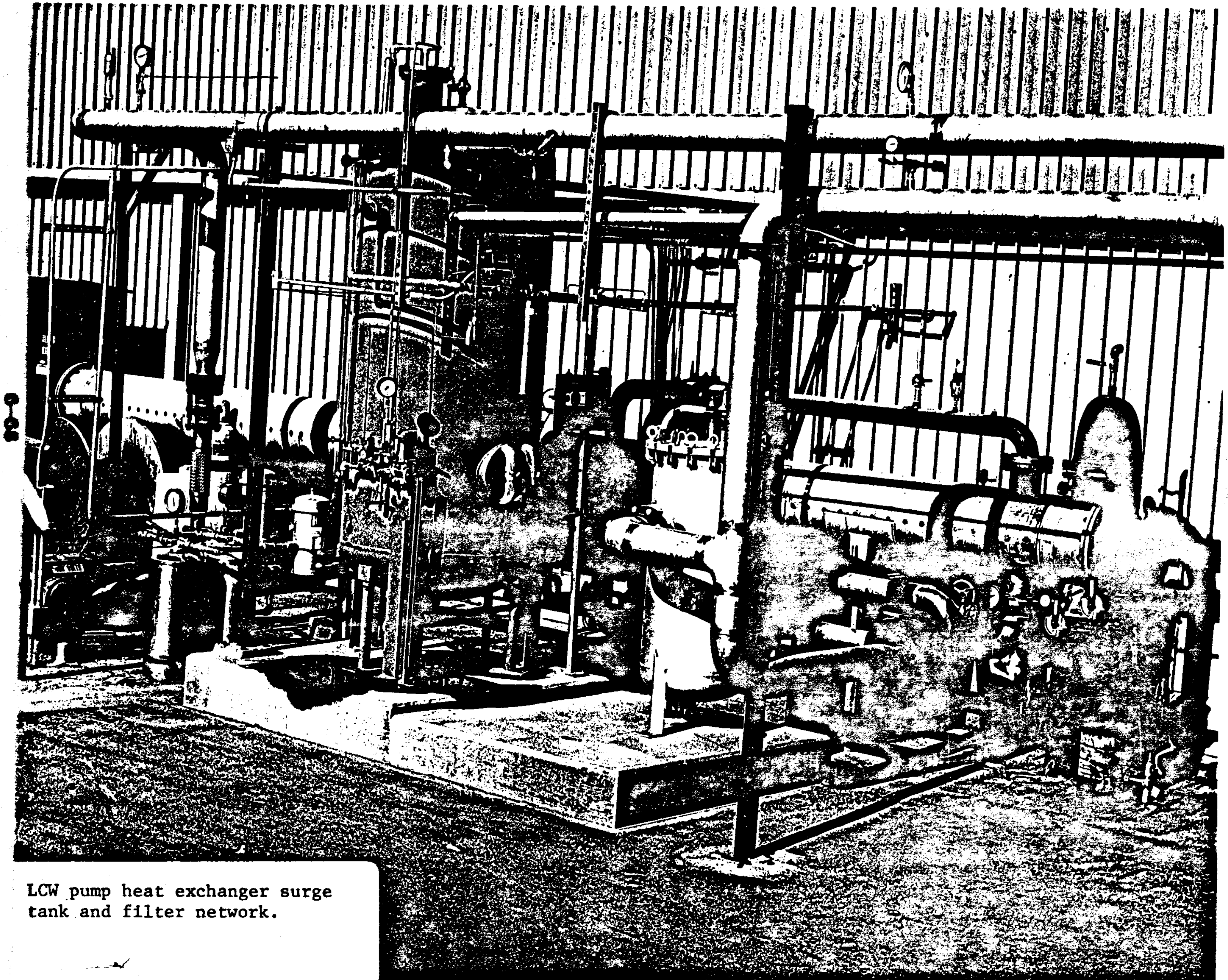

LCW pump heat exchanger surge tank and filter network.

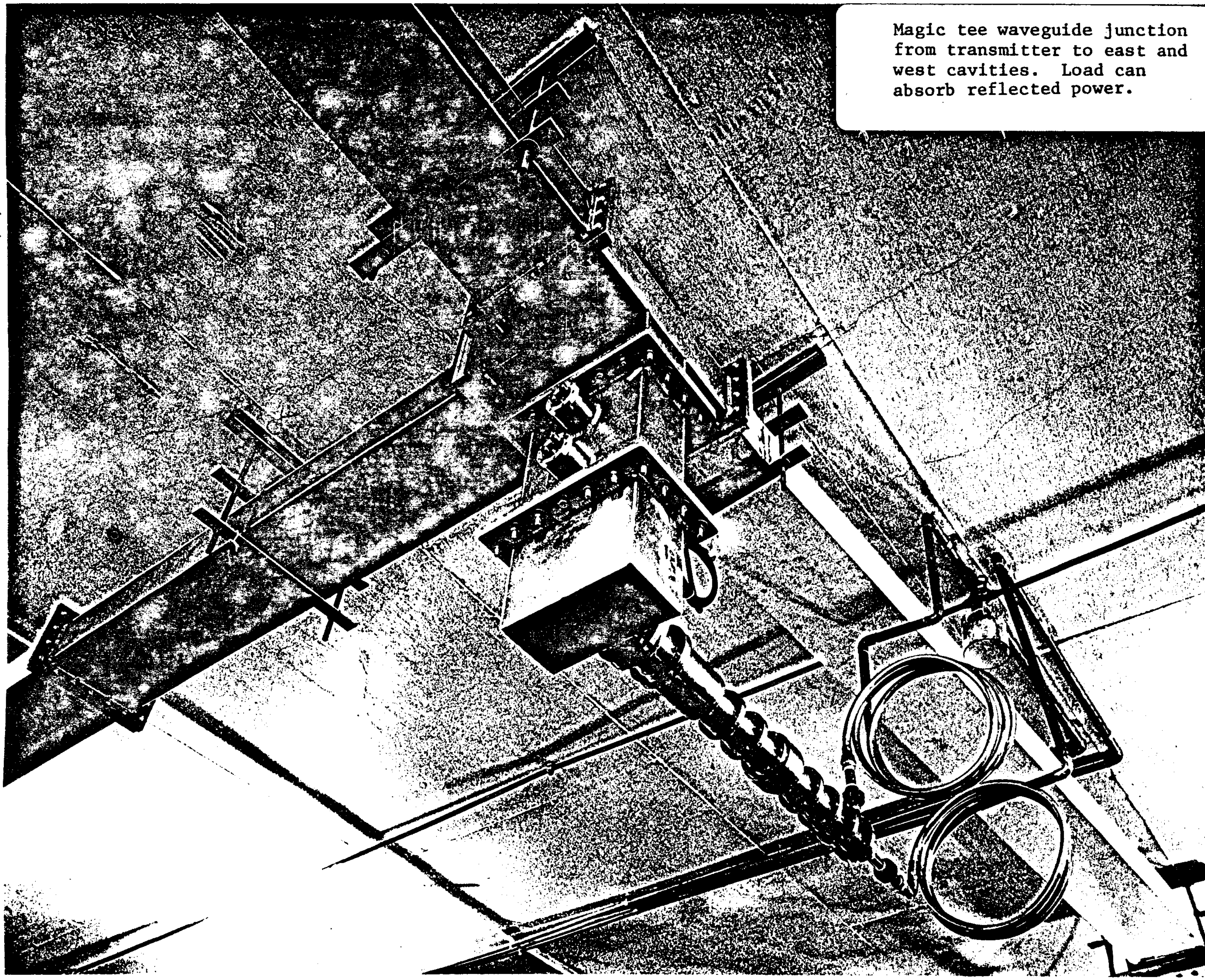

Magic tee waveguide junction from transmitter to east and west cavities. Load can absorb reflected power.

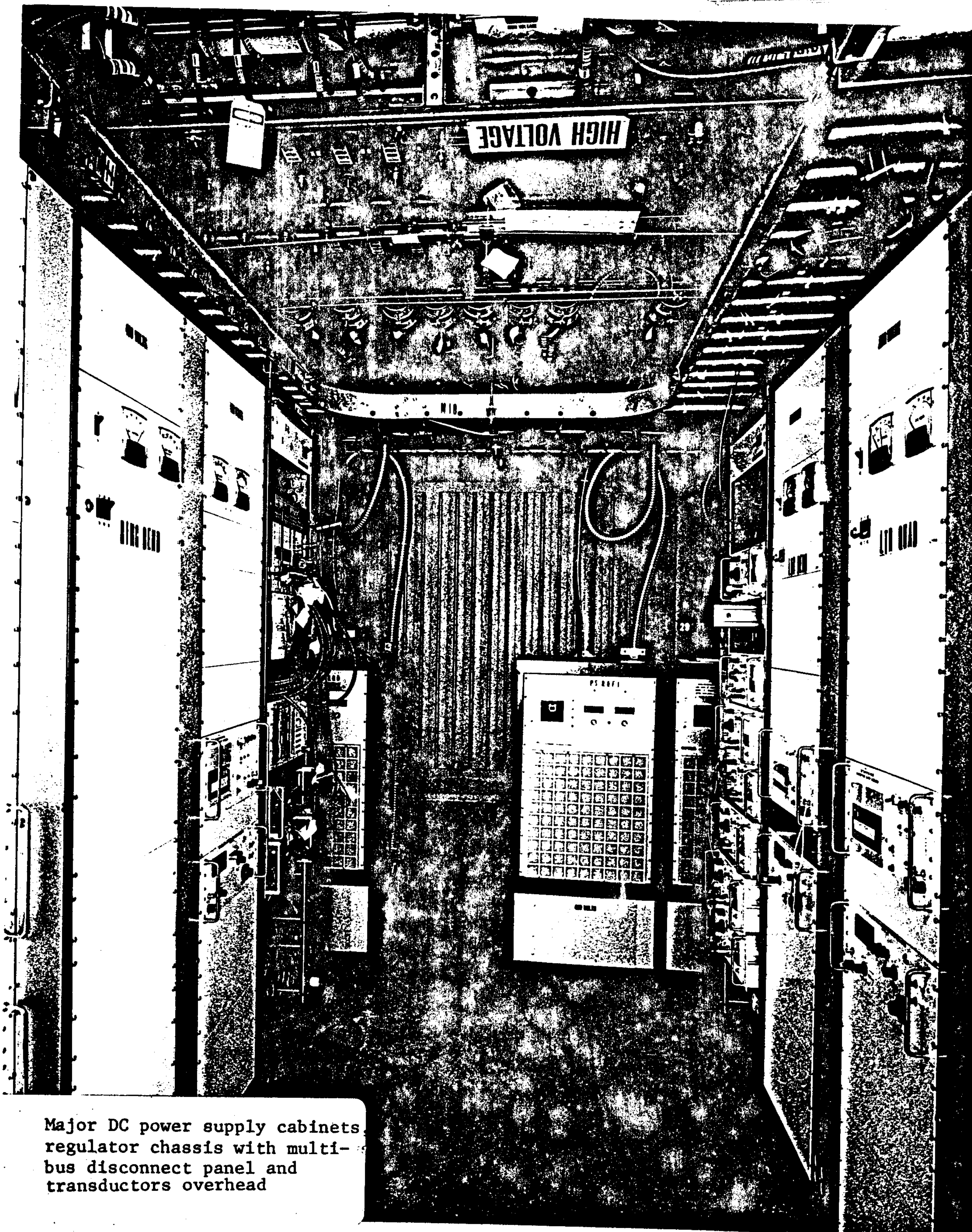

Major DC power supply cabinets, regulator chassis with multi-bus disconnect panel and transductors overhead

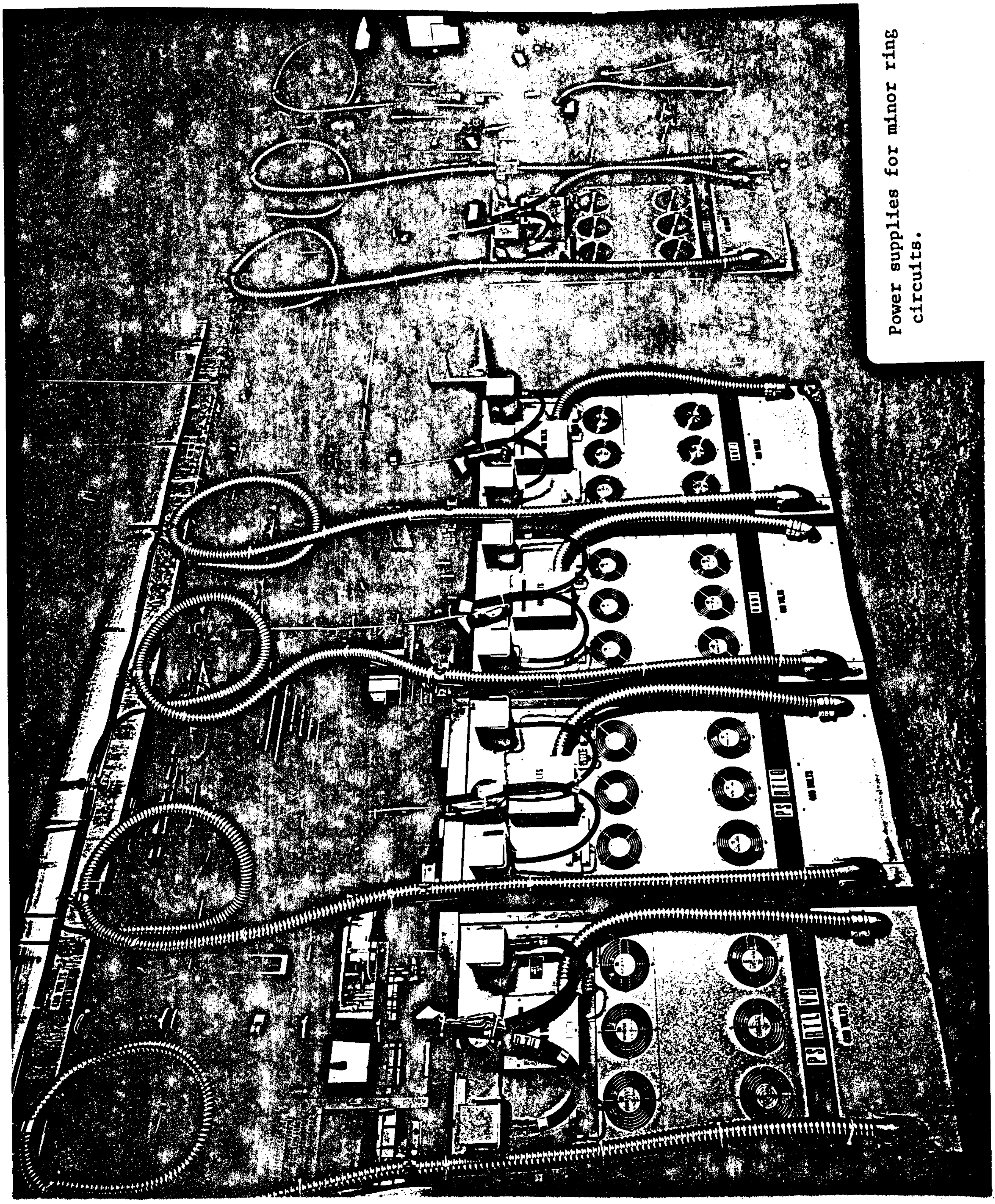

Power supplies for minor ring circuits.

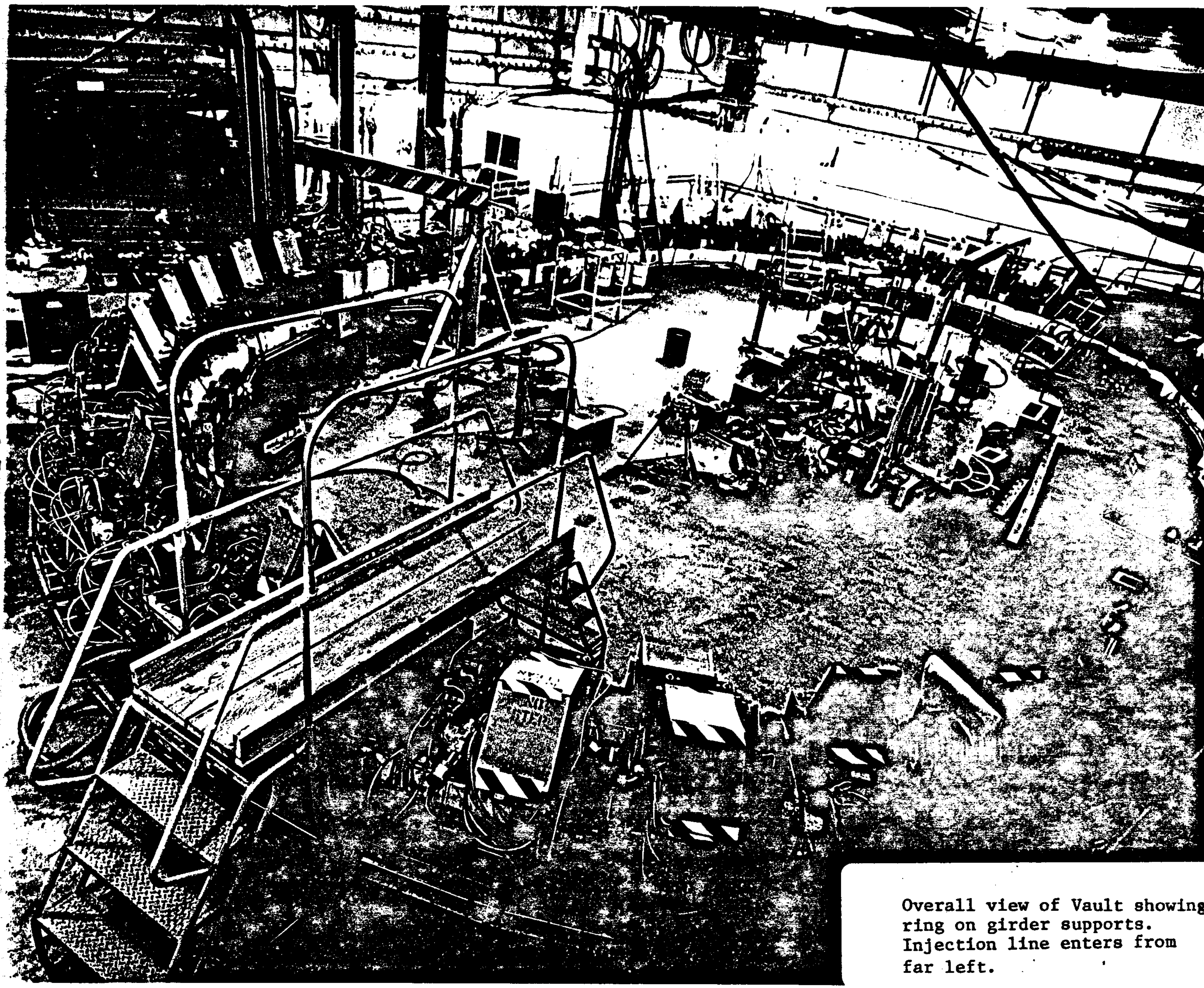

Overall view of Vault showing ring on girder supports. Injection line enters from far left.

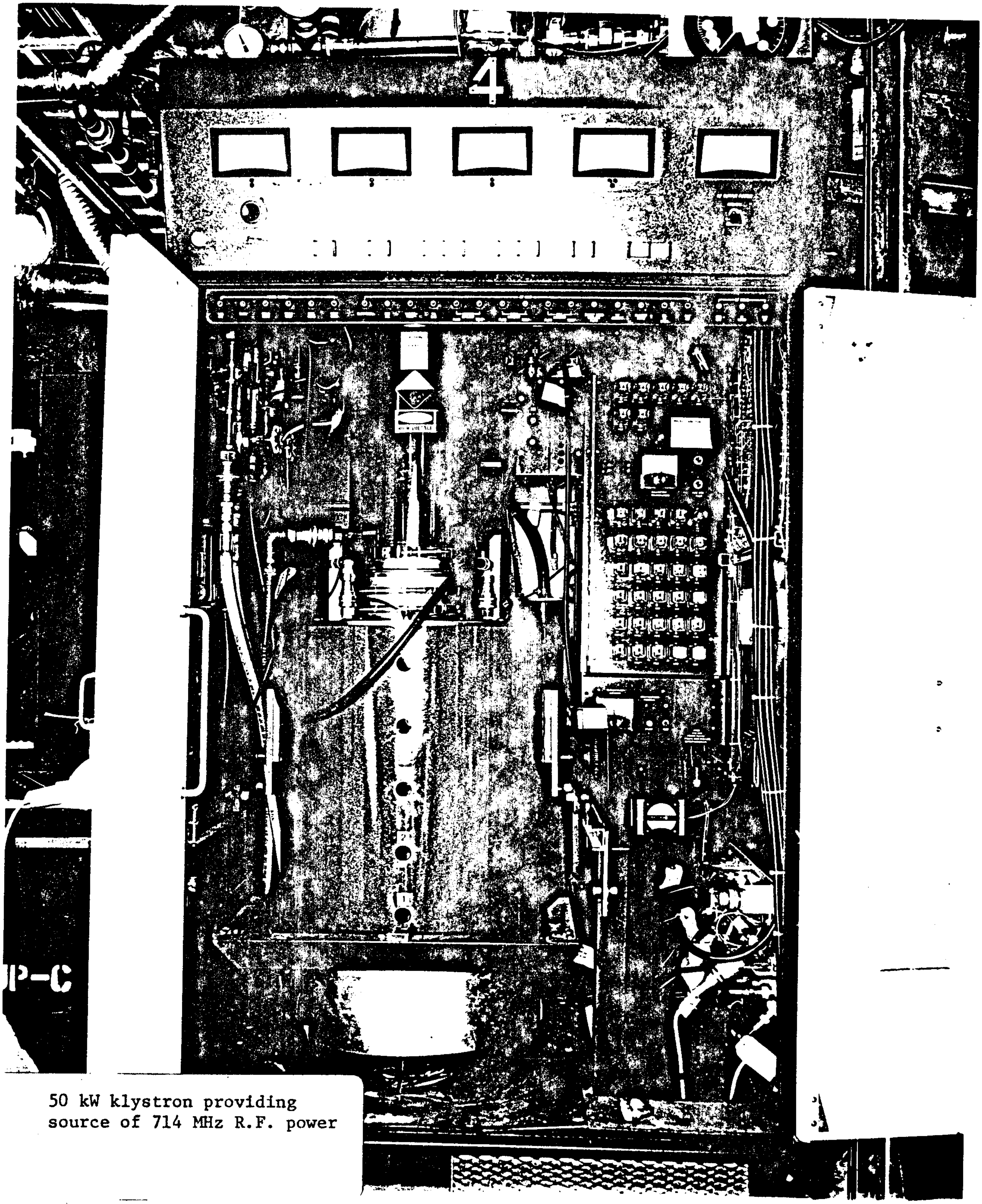

50 kW klystron providing
source of 714 MHz R.F. power

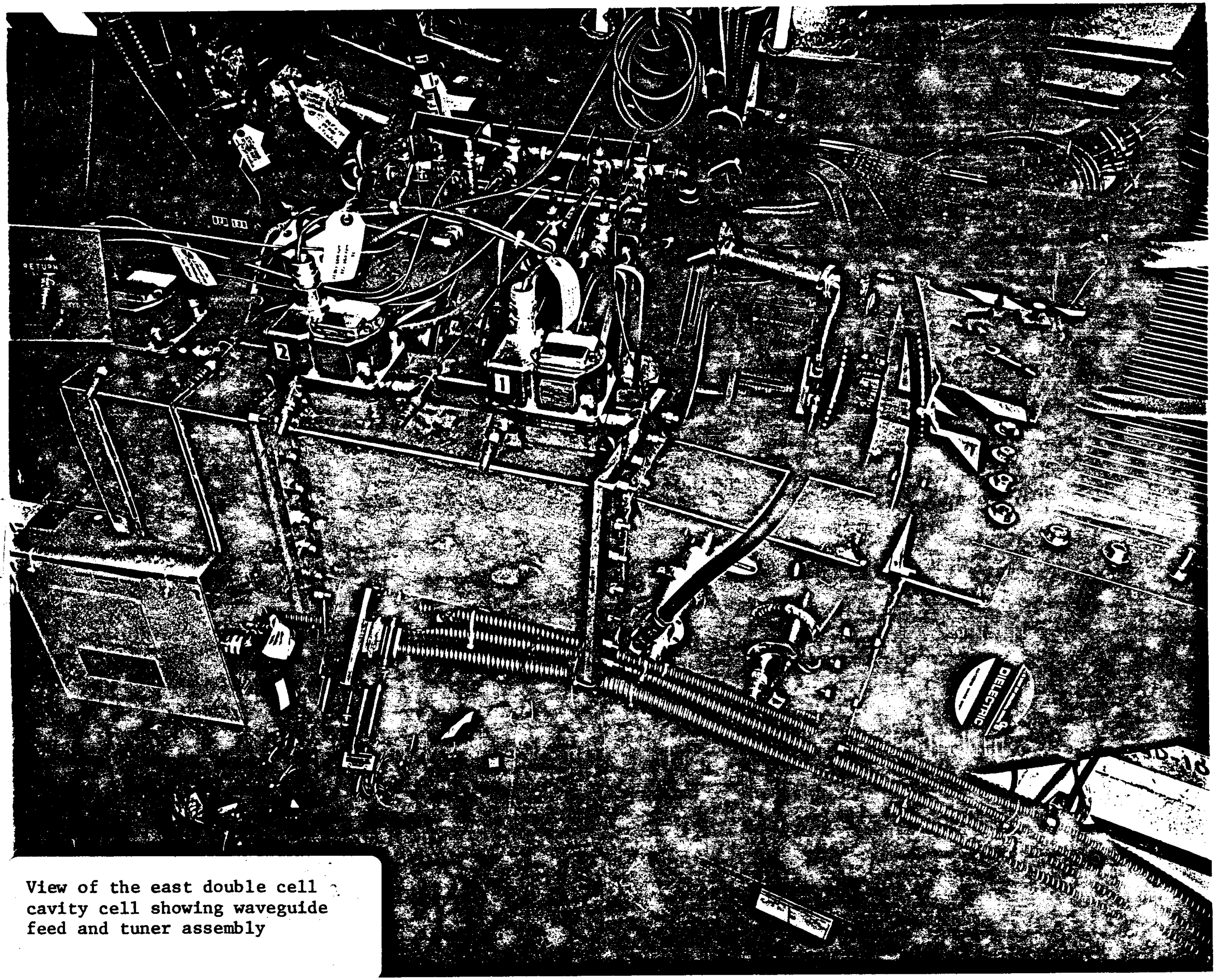

View of the east double cell cavity cell showing waveguide feed and tuner assembly

View of injection kicker - high voltage charging equipment - Blumlein in the background, matching resistor in the foreground.

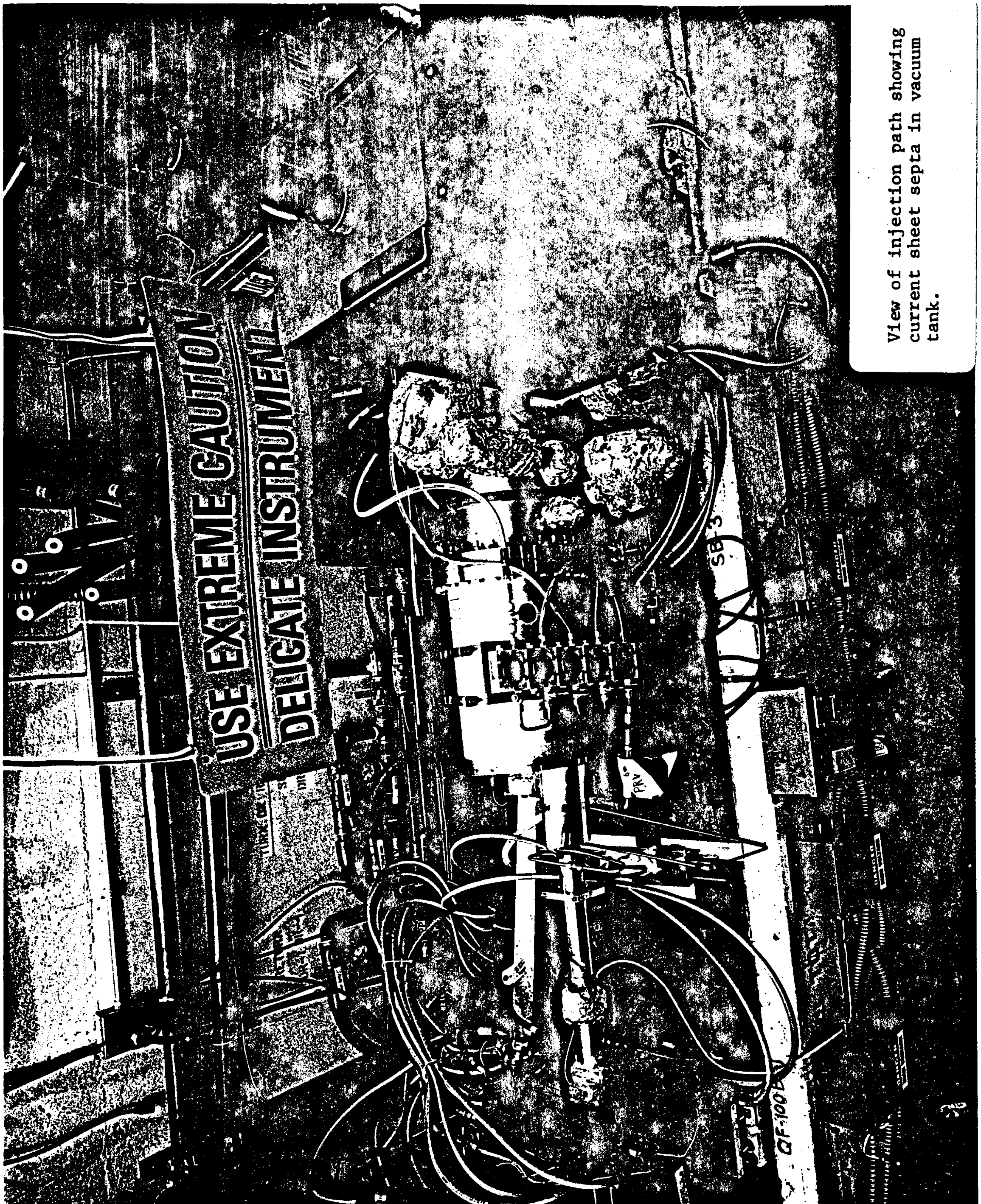

View of injection path showing current sheet septa in vacuum tank.

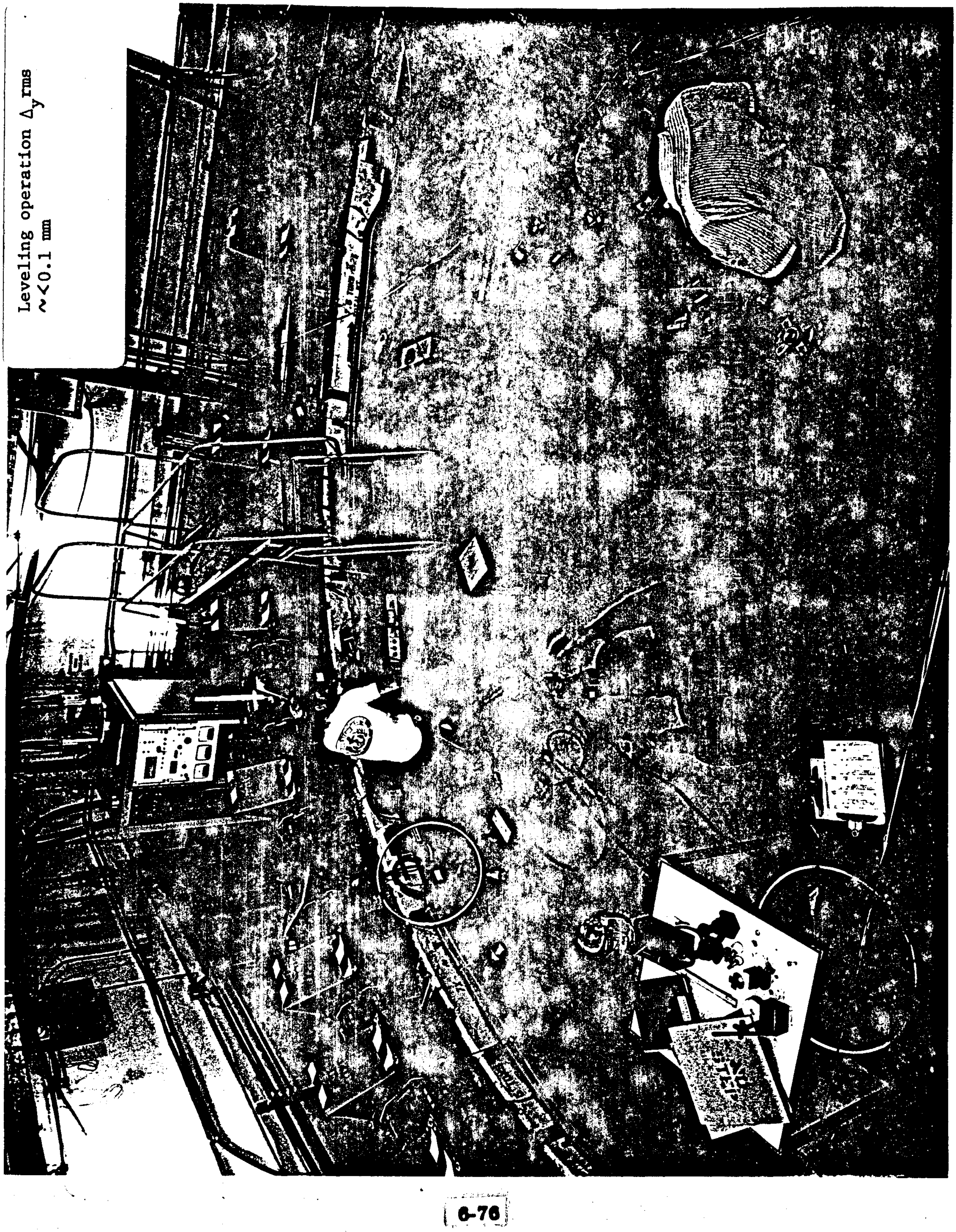

Leveling operation Δ_y rms
~<0.1 mm

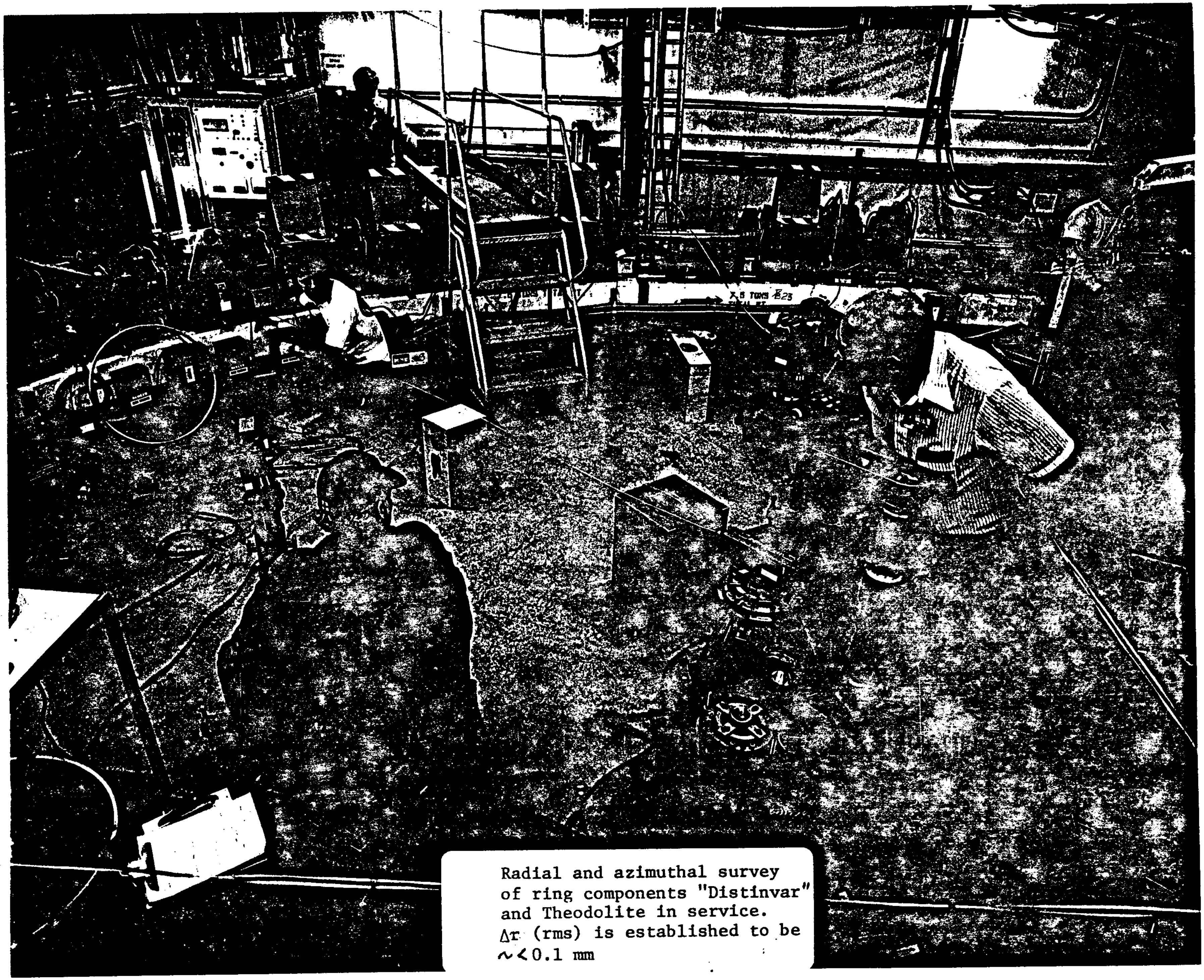

Radial and azimuthal survey of ring components "Distinvar" and Theodolite in service. Δr (rms) is established to be $\sim < 0.1$ mm

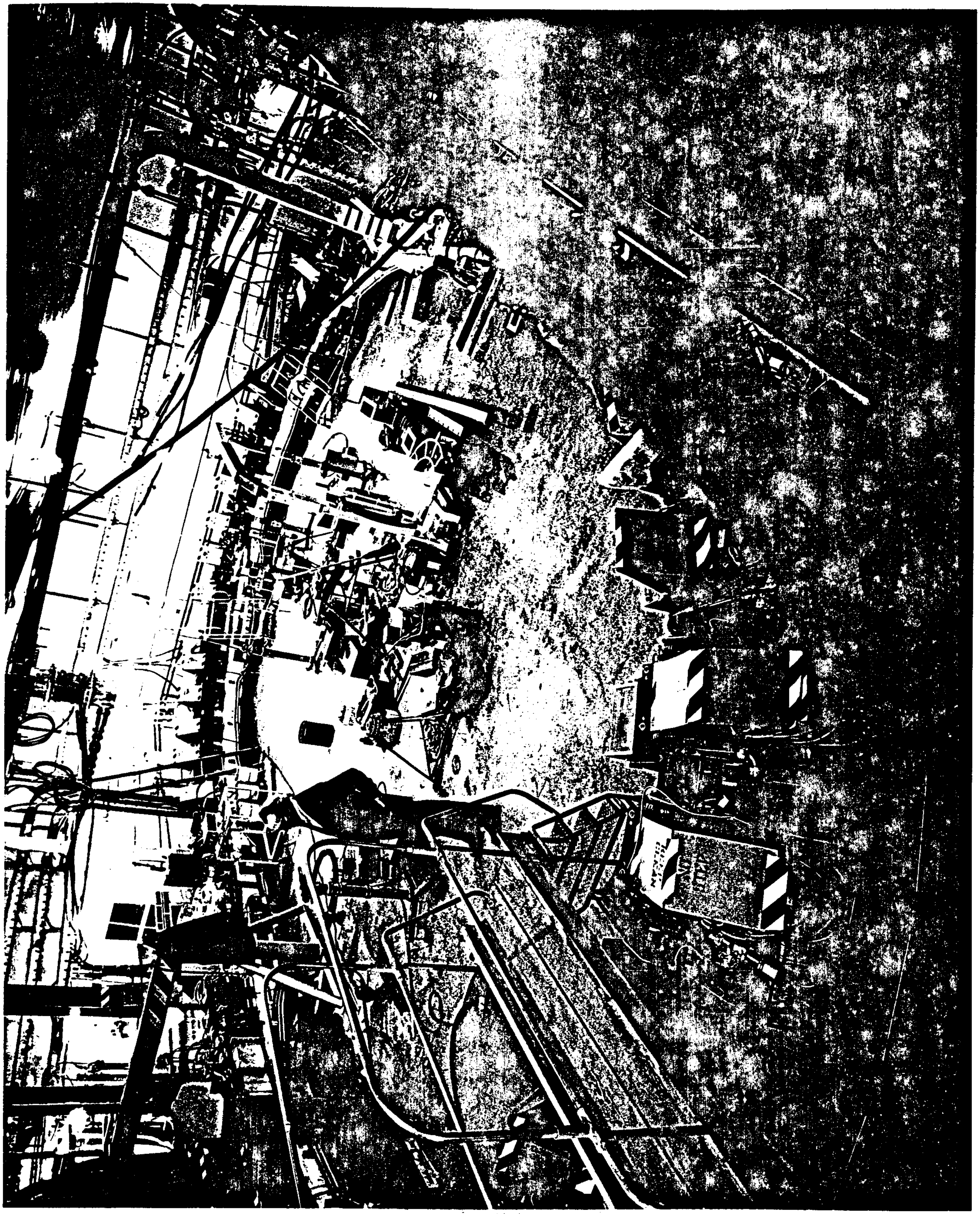

REFERENCES

1. G.E. Fischer, W. Davies-White, T. Fieguth, H. Wiedemann, SLAC-PUB-3170, July. 1983. (cont. paper XII Int. Conf. on High Energy Acc., Fermilab, 1983, to be published).
2. G.A. Loew, SLAC Report, CN-33, Feb. 1980.
3. H. Wiedemann, Proc. XI Int. Conf. on High Energy Acc., Geneva, 1980, p.693 and SLAC Report AATF/79/8, Sept. 1979.
4. M.J. Lee, J.C. Sheppard, M. Sullenberger, M.D. Woodley, SLAC-PUB-3217, Sept.,1983.
5. G. Fischer, SLAC Report, CN-98, July, 1980
6. F. Fischer and S. Kheifets, SLAC Report, CN-122, Sept., 1981
7. T.H. Fieguth and J.J. Murray, SLAC-PUB-3174, July 1983 (cont. paper XIIth Int. Conf. on High Energy Acc., Fermilab, 1983, to be published).
8. G. Fischer et al, SLAC-PUB-3170, July 1983
9. SLAC Linear Collider Conceptual Design Report, SLAC Report 229, Appendix A.
10. K.L. Brown, SLAC-PUB-2257.
11. D.C. Carey, Nucl, Instrum. and Meth., 189 (1981), p.365.
12. T.H. Fieguth, SLAC Report CN-79, June 1981.
13. R.H. Stiening, SLAC Report AATF/80/28. August 1980.
14. T.H. Fieguth, SLAC Report CN-141, January 1982.
15. M.A. Allen, H.D. Schwarz, P.B. Wilson, (cont. to Part. Acc. Conf., Santa Fe, NM, March 1983), SLAC-PUB-3084.
16. T. Knight, author of the computer code DAMP, 1980.
17. T. Knight and P. Wilson, SLAC internal reports CN-38 (Dec. 1980), CN-43 (Feb. 1981), CN-74 (June 1981), and CN-86 (June 1981).
18. J.L. Pellegrin, H. Schwarz, "Control Electronics of the PEP RF System," 1981 Particle Accelerator Conf., March 1981, SLAC-PUB-2664.

19. D. Wright, N. Dean (to be published.)

20. P. Morton, SLAC Report, CN-89, July 1981.

21. E. Garwin, (Review, Particle Acc. Conf., Santa Fe, NM, March 1983), SLAC-PUB-3033.

6.7 COLLIDER NOTE REFERENCES BY SUBJECT

Emittance

CN-25	Considerations with Respect to e^+ Emittance	S. Ecklund	9-80
CN-33	SLC Emittance	G.A. Loew	1-81

General Theory

CN-26	Head Tail in the Damping Ring	J. LeDuff	8-80
CN-35	Parasitic Mode Losses in the Damping	P.B. Wilson	12-80
CN-37	Beam Size and Beam Stay Clear (BSC) in the Damping Ring	H. Wiedemann	12-80
CN-38	Transient Energy and Phase Oscillations in the Damping Ring	P. Wilson T. Knight	12-80
CN-43	Results of a Tracking Program for Computing the Transient Energy and Phase Oscillations in the Damping Ring.	P. Wilson T. Knight	2-81
CN-62	Touschek Effect and Multiple Coulomb in the Damping Ring	H. Wiedemann	5-81
CN-71	Threshold for Tubulent Bunch Lengthening in the Damping Ring	P. Wilson	5-81

Orbit Correction

CN-80	Some Beam Positron Monitor Considerations for Damping Ring Complex	G. Fischer J.-L. Pellegrin	6-81 6-81
CN-98	Some More Orbit Correction Considerations for the Damping Ring	G. Fischer	7-81
CN-116	Beam Position Monitor Signal Processors	J. Pellegrin S. Williams	12-81
CN-122	Damping Ring Beam Position Correcting System	G. Fischer S. Kheiffets	10-81
CN-126	Low Cost Electronics for Beam Position Monitoring on the Damping Ring and Its Beam Lines	J. Denard	10-81

CN-141	Effects of Misaligning LRT Optical Components and a Possible Correction Scheme	T. Fieguth	1-82
CN-185	MUX System for the Damping Ring BPMs	J. Denard G. Oxoby	6-82
Geometry			
CN-41	Location and Geometry of the Damping Ring	H. Wiedemann	1-81
CN-44	Additional Path Length Constraints	T. Fieguth	2-81
Magnets			
CN-56	Magnet Parameters for the Damping Ring	H. Wiedemann	5-81
CN-133	A Configuration for the VB-53 Vertical Bend Magnet	R. Early	12-81
CN-134	Pandira Calculations for the Damping Ring Bend Magnet	R. Early	12-81
Injection			
CN-46	The Injection and Extraction Systems of the Damping Ring	J.M. Peterson	4-81
CN-49	Requirements for Resistive Coating on Ceramic Tubes in Kicker Magnets	J.M. Peterson	4-81
Pulse Magnets			
CN-59	SLC linac Vertical Pulse Magnet Power Supply	B.T. Tomlin	5-81
Kickers			
CN-60	Specification for the Damping Ring Kicker Modulator High Voltage dc Power Supply	B.T. Tomlin	5-81
CN-72	Kicker Magnet and Pulser	F. Bulos	5-81
CN-166	Damping Ring Kickers	F. Bulos	3-82

		B. Tomlin J. Weaver	
Septa			
CN-125	Specification for Septum Magnets S-1 and S-2 in SLC Damping Ring	G. Fischer J. Peterson	10-81
Ion Effects			
CN-89	Ion Effects in the Damping Ring	P. Morton	7-81
CN-123	More on Ions in the Damping Ring	A. Chao	10-81
R.F.			
CN-27	Energy Acceptance of the Damping Ring	M. Allen	9-80
CN-32	SLC Frequencies and Associated	G.A. Loew	1-81
CN-44	Additional Path Length Constraints	T. Fieguth	2-81
CN-54	Time Requirement in the Damping Ring	M. Allen	4-81
CN-74	Transient Energy Oscillations in the Damping Ring with an RF Phase Jump at Injection	P. Wilson T. Knight	6-81
CN-86	Minimum Klystron Power Required for Capture in the Damping Ring	P. Wilson T. Knight	6-81
Compressor			
CN-13	Compressor-Parameter (Use for Budget Only)	H. Wiedemann	2-80
CN-57	Parameters for the Positron Compressor	H. Wiedemann	5-81
CN-63	Compressor RF System Stability	R. Stiening	5-81
CN-79	Notes on Compressor I&C and Length of Injected Bunch	T. Fieguth	6081
CN-117	Bunch length as a Function of the Compressor Voltage	H. Wiedemann	9-81
CN-147	Some Effects in the Compressor	A. Chao H. Wiedemann	1-82
I & C			
CN-47	Timing for Damping Ring Injection and	T. Fieguth	4-81